Higher-Point Correlation Functions in $\mathcal{N} = 4$ Supersymmetric Yang–Mills Theory

Dissertation

zur Erlangung des Doktorgrades an der Fakultät für Mathematik, Informatik und Naturwissenschaften

Fachbereich Physik der Universität Hamburg

vorgelegt von

Albert Bekov

Hamburg

2026

Gutachter der Dissertation:

Dr. Till Bargheer
Prof. Dr. Gleb E. Arutyunov

Zusammensetzung der Prüfungskommission:

Prof. Dr. Sven-Olaf Moch
Dr. Till Bargheer
Prof. Dr. Gleb E. Arutyunov
Prof. Dr. Elisabetta Gallo-Voss
Dr. Aditya Pathak

Vorsitzender der Prüfungskommission:

Prof. Dr. Sven-Olaf Moch

Datum der Disputation:

01.07.2026

Vorsitzender des Fach-Promotionsausschusses Physik:

Prof. Dr. Johannes Haller

Leiter des Fachbereichs Physik:

Prof. Dr. Markus Drescher

Dekan der Fakultät MIN:

Prof. Dr.-Ing. Norbert Ritter

Higher-Point Correlation Functions in $\mathcal{N} = 4$ Supersymmetric Yang–Mills Theory

This thesis investigates loop integrands of correlation functions of scalar half-BPS operators in four-dimensional $\mathcal{N} = 4$ supersymmetric Yang–Mills (SYM) theory. $\mathcal{N} = 4$ SYM provides a central "theoretical laboratory" due to its high degree of symmetry, its role in the AdS/CFT correspondence, and the emergence of integrability in the planar limit.

First, we study planar higher-point generating functions, which combine infinitely many fixed-charge correlators into unified expressions using ten-dimensional coordinates that merge spacetime and R-symmetry variables. We compute the five-point generating function at one and two loops, and the six-point function at one loop. The results exhibit a recursive nesting structure in which higher-order ten-dimensional poles are controlled by lower-point correlators.

Second, we analyze ten-dimensional null polygons, obtained as a specific kinematic limit of the generating functions, where these factorize into simpler polygon functions with disc topology. We present a twistor-based direct computation of the polygon integrands, and determine the two-loop integrands for any number of external operators. By imposing soft and collinear bootstrap constraints in off-shell kinematics, we uniquely fix the five-point pentagon integrand up to five loops. This provides a useful setting for testing dualities between correlation functions and massive scattering amplitudes.

Finally, we go beyond the planar limit and compute the full non-planar five-loop four-point integrand for the lightest scalar operators. This is achieved using a GPU-accelerated algorithm for evaluating Grassmann multiplications in the twistor Feynman rules. The result shows that the integrand can be expressed purely in terms of genus-one contributions. Furthermore, it allows us to extract the non-planar five-loop correction to the Konishi anomalous dimension.

These results provide new insight into the structure of higher-point correlation functions in $\mathcal{N} = 4$ SYM and open avenues for further investigations of both planar and non-planar dynamics.

Mehrpunkt-Korrelationsfunktionen in der
$\mathcal{N} = 4$ Supersymmetrischen Yang–Mills Theorie

Diese Arbeit untersucht Schleifenintegranden von Korrelationsfunktionen skalarer Half-BPS-Operatoren in der vierdimensionalen $\mathcal{N} = 4$ supersymmetrischen Yang–Mills Theorie (SYM). Die $\mathcal{N} = 4$ SYM stellt aufgrund ihres hohen Symmetriegrades, ihrer Rolle in der AdS/CFT-Korrespondenz und dem Auftreten von Integrabilität im planaren Limes ein zentrales „theoretisches Labor“ dar.

Zunächst untersuchen wir planare generierende Funktionen mehrerer Punkte, die unendlich viele Korrelatoren mit fester Ladung zu einheitlichen Ausdrücken kombinieren, wobei zehndimensionale Koordinaten verwendet werden, die Raumzeit- und R-Symmetrie-Variablen zusammenführen. Wir berechnen die generierenden Funktionen bei fünf Punkten für eine und zwei Schleifen, sowie die generierende Funktion bei sechs Punkten für eine Schleife. Die Ergebnisse zeigen eine rekursive Verschachtelungsstruktur, in der zehndimensionale Pole höherer Ordnung durch Korrelatoren geringerer Punkte gesteuert werden.

Als Nächstes analysieren wir zehndimensionale Nullpolygone, die als spezifischer kinematischer Limes der generierenden Funktionen erhalten werden, indem diese in einfachere Polygonfunktionen mit Scheibentopologie faktorisiert werden. Wir präsentieren eine Twistor-basierte direkte Berechnung der Polygonintegranden und bestimmen die Integranden bei zwei Schleifen für eine beliebige Anzahl externer Operatoren. Durch Nutzen von weichen und kollinearen Bootstrap-Bedingungen in der Off-Shell-Kinematik legen wir den Fünfpunkt-Pentagonintegranden bis zu fünf Schleifen eindeutig fest. Dies bietet einen nützlichen Rahmen zum Testen von Dualitäten zwischen Korrelationsfunktionen und massiven Streuamplituden.

Schließlich gehen wir über den planaren Limes hinaus und berechnen den vollständigen nicht-planaren Vierpunkt-Integranden bei fünf Schleifen für die leichtesten Skalaroperatoren. Dies wird mithilfe eines GPU-beschleunigten Algorithmus zur Berechnung von Grassmann-Multiplikationen in den Twistor-Feynman-Regeln erreicht. Das Ergebnis zeigt, dass sich der Integrand ausschließlich als Summe von Beiträgen vom Genus 1 ausdrücken lässt. Darüber hinaus ermöglicht es uns, die nicht-planare Fünf-Schleifen-Korrektur zur anomalen Dimension des Konishi-Operators zu ermitteln.

Diese Ergebnisse liefern neue Einblicke in die Struktur der Mehrpunkt-Korrelationsfunktionen in der $\mathcal{N} = 4$ SYM und eröffnen neue Wege für weitere Untersuchungen sowohl der planaren als auch der nicht-planaren Dynamik.

Statement of Originality

This thesis is based on the following publications:

- T. Bargheer, A. Bekov, C. Bercini and F. Coronado, *Higher-point correlators in $\mathcal{N}=4$ SYM: generating functions*, *JHEP* **02** (2026) 161 [2509.14332] [1]
- T. Bargheer, A. Bekov, C. Bercini and F. Coronado, *Higher-Point Correlators in N=4 SYM: Ten-Dimensional Null Polygons*, 2512.19780 [2]
- T. Bargheer and A. Bekov, *The Non-Planar Four-Point Integrand and Konishi Dimension in N=4 Super Yang-Mills Theory at Five Loops*, 2511.21807 [3]
- T. Bargheer and A. Bekov, *The Higher-Loop Pentagon Integrand in N=4 SYM*, to appear, (2026) [4]

All authors contributed equally to the above publications.

Contents

1. Introduction

In the last century, high-energy experiments have reached an unprecedented level of precision. Collider experiments have enabled detailed analyses of scattering processes, the discovery of heavy particles, and deep insights into the structure of matter, thereby testing theoretical predictions with remarkable accuracy. At the microscopic level, these phenomena are described by quantum field theories (QFTs), among which Quantum Chromodynamics (QCD) governs the strong interaction between quarks and gluons. A key property of QCD is asymptotic freedom, which implies that at high momentum transfer the effective coupling becomes small, allowing for perturbative computations. In this regime, theoretical predictions can be matched to experimental data with high precision. However, at low energies the coupling constant increases, and perturbation theory breaks down. As a result, many fundamental phenomena, such as color confinement, still lack a complete analytical understanding.

This limitation is not unique to QCD, but rather reflects a general challenge in quantum field theory: our computational control is largely restricted to weakly coupled regimes. Yet, QFTs provide the microscopic description of all known fundamental interactions, as well as a wide range of condensed matter systems. Developing methods that extend beyond perturbation theory is therefore a central goal in theoretical physics. A fruitful strategy has been to focus on theories with enhanced symmetry or special limits, where exact or non-perturbative results can be obtained and later used to guide our understanding of more general systems.

In this spirit, the main setting of this thesis is provided by a highly symmetric and well-controlled quantum field theory, namely *four-dimensional* $\mathcal{N}=4$ *supersymmetric Yang–Mills theory* (SYM). Due to its exceptional degree of symmetry, it has long served as a theoretical laboratory in which new methods can be developed and computations can be pushed to unprecedented precision. Before outlining the specific questions addressed in this thesis, we first review the relevant background and motivate the problems under consideration, and then summarize the main results and structure of the thesis in the final introductory section.

1.1. Motivation and Background

Four-dimensional $\mathcal{N} = 4$ SYM with gauge group SU(N_c) [5,6] plays a distinguished role among quantum field theories. It is maximally supersymmetric and conformally invariant, implying that its Lagrangian is completely fixed by symmetry. It is the most symmetric interacting QFT without gravity in four dimensions. Importantly, its conformal symmetry persists even at the quantum level, since the coupling of the theory does not run with the energy scale. As a conformal field theory (CFT), its observables are highly constrained: correlation functions can be decomposed using the operator product expansion (OPE), such that all dynamical information is encoded in the spectrum of local operators and their three-point structure constants. In this sense, complete knowledge of all two- and three-point functions would amount to solving the theory. Despite its high degree of symmetry, $\mathcal{N} = 4$ SYM remains a rich and interacting theory, providing a controlled setting in which to explore strongly coupled gauge dynamics. It therefore serves as an ideal theoretical laboratory for developing and testing non-perturbative methods.

An additional motivation for studying $\mathcal{N} = 4$ SYM arises from its role in holography. The *holographic principle* posits that quantum field theories can be equivalently described by theories of gravity in higher-dimensional spacetimes [7]. A concrete realization of this idea is the AdS/CFT correspondence, proposed by Maldacena [8] and subsequently formulated more precisely in [9,10], which conjectures a duality between $\mathcal{N} = 4$ SYM and type IIB string theory on $\mathrm{AdS}_5 \times S^5$. A remarkable feature of this duality is its strong/weak nature: when the gauge theory is strongly coupled, the dual gravitational description becomes weakly coupled, and vice versa. This provides a powerful framework to access strongly coupled regimes with common perturbative techniques or even trough classical gravity.

A further simplification arises in the limit where the number of colors N_c becomes large. In this regime, it is natural to reorganize perturbation theory in terms of the 't Hooft coupling $a \sim g_{\mathrm{YM}}^2 N_c$ [11], with g_{YM} denoting the Yang–Mills coupling. Keeping a fixed as $N_c \to \infty$, the N_c-dependence of Feynman diagrams acquires a topological description when expressed in double-line notation, such that each diagram can be associated with a discretized two-dimensional surface. The contribution of a diagram then scales as N_c^{2-2g}, where g denotes the genus of the corresponding surface. Perturbation theory is thus organized as a double expansion in the coupling a and in powers of $1/N_c^2$, with planar diagrams ($g = 0$) providing the leading

contribution, while higher-genus corrections are suppressed by successive powers of $1/N_c^2$. In the planar limit, only planar diagrams contribute, leading to a significant simplification of the combinatorial structure of perturbation theory.
Beyond this organizational principle, the full power of the planar limit only unfolded after the discovery of the AdS/CFT correspondence, where it acquires a direct physical interpretation. In this context, the two-dimensional surfaces associated with planar Feynman diagrams are identified with string worldsheets endowed with their own dynamics, describing in particular the scattering of gravitons. From this perspective, the genus expansion of the large-N_c limit is naturally interpreted as the loop expansion in quantum gravity.

One of the most remarkable properties of planar $\mathcal{N} = 4$ SYM is the emergence of *integrability* (see [12] for a review). Integrability implies the existence of an infinite number of conserved charges, allowing for the exact solution of certain observables. A first concrete manifestation of this structure was found in the study of the dilatation operator, which governs the scaling dimensions of local operators. At one loop, it can be mapped to the Hamiltonian of an integrable Heisenberg spin chain [13], and this picture was subsequently extended to higher loops, leading to the asymptotic Bethe ansatz for the full spectral problem [14]. In this framework, the infinite set of conserved charges arises from the underlying integrable structure of the spin chain. In particular, the spectrum of local operators has been determined non-perturbatively through the quantum spectral curve [15,16]. Beyond spectral quantities, integrability also manifests itself in scattering amplitudes, where a hidden dual conformal symmetry emerges in the planar limit and, together with the ordinary conformal symmetry, generates an infinite-dimensional Yangian algebra [17, 18]. This extended symmetry severely constrains the form of amplitudes and underlies powerful on-shell methods. In particular, it enables the formulation of recursion relations at loop level, generalizing the tree-level BCFW construction [19] and allowing for the systematic construction of scattering amplitudes [20, 21].
For three- and higher-point correlation functions, the state-of-the-art integrability-based method is hexagonalization [22, 23], which decomposes correlation functions into fundamental building blocks associated with integrable excitations. This approach is particularly effective for operators with large charges, but remains challenging to apply at small charges. As a result, despite these developments, significantly less is known about structure constants than about the spectrum in $\mathcal{N} = 4$ SYM.

An alternative route to accessing dynamical information in the theory is to consider higher-point correlation functions of suitably chosen operators, rather than attempting to determine all three-point functions directly. In particular, correlators of protected operators, which are simpler due to their symmetry properties, provide a controlled setting in which non-trivial dynamics can be studied. By analyzing their operator product expansion, one can extract information about the spectrum and structure constants of more general, non-protected operators. In this way, higher-point functions serve as a powerful probe of the full dynamical content of the theory.

Before going into detail on the correlators of these protected operators, let us introduce another remarkable feature of $\mathcal{N} = 4$ SYM, namely that it admits a formulation in twistor space. Twistor theory, originally introduced by Penrose in the late 1960s [24], provides a geometric framework in which space-time physics is reformulated in terms of complex geometry on twistor space. Early developments established a number of profound correspondences, such as the Penrose transform [25], relating zero-rest-mass fields on space-time to cohomological data on twistor space, and the Ward correspondence [26] between self-dual Yang–Mills instantons and holomorphic vector bundles.
While these constructions revealed deep connections between geometry and classical field theory, the full impact of twistor methods on quantum field theory only emerged much later. A major breakthrough was achieved by Witten in [27], where a description of scattering amplitudes in planar $\mathcal{N} = 4$ SYM in terms of a topological string theory in twistor space was provided. This proposal further motivated the search for a more complete twistor-based formulation of QFT beyond tree level, leading to the twistor action approach [28], which provides a formulation of gauge theory directly on twistor space and allows for the study of perturbative observables to all orders. Together, these developments firmly established twistor methods as a powerful tool in the study of $\mathcal{N} = 4$ SYM, where a reformulation of the action was given in [29]. Specifically, this has led to the formulation of twistor Feynman rules for protected operators, which will be reviewed in Chapter 3.

In $\mathcal{N} = 4$ SYM, particular attention has been devoted to correlators of *half-BPS operators*, whose scaling dimensions are fixed by symmetry. While their two- and three-point functions are protected from quantum corrections, their four- and higher-point functions are highly non-trivial and encode a wealth of dynamical information. In special kinematic limits, these correlators are related to Wilson loops and scattering amplitudes [30–38], and via holography, they encode graviton scattering in $\mathrm{AdS}_5 \times S^5$. They also give rise to physically relevant observables such as event shapes and detector correlators through light-ray transforms [39, 40].

The simplest non-trivial example is provided by the four-point correlator of the lightest scalar operators, so-called $\mathbf{20'}$ operators, which has been computed to high orders in both weak-coupling perturbation theory and at strong coupling [41–45]. At finite coupling, additional approaches such as localization and the conformal bootstrap have provided complementary insights [46–49]. Beyond the lightest operators, correlators of scalar half-BPS operators with higher R-charge have also been extensively studied. At weak coupling, their four-point functions are known up to three-loop order [50], and in certain kinematic limits up to five loops [51].
In perturbation theory, performing computations to higher-loop order or to higher-point functions is a difficult task. First, the complexity grows dramatically as one increases the number of loops or external points. Second, the integrals that arise become increasingly difficult to evaluate. To address the latter issue, it is useful to consider the loop integrand, which is defined via the *Lagrangian insertion procedure* [41,52]. The loop integrand is given by the tree-level correlator with ℓ insertions of the chiral on-shell Lagrangian. Upon integrating over the insertion points, one recovers the ℓ-loop corrections to the correlator. In terms of this loop integrand, the four-point correlator of $\mathbf{20'}$ operators is known to much higher-loop order in the planar limit, namely up to twelve loops [41, 53–58].

In the full theory, including non-planar corrections, determining the loop integrand becomes significantly more challenging, as the allowed underlying topologies increase. For correlation functions of $\mathbf{20'}$ operators, non-planar contributions first appear at four loops. The corresponding four-point loop integrand can be obtained by constructing a constrained ansatz and fixing the remaining freedom using the twistor reformulation of $\mathcal{N} = 4$ SYM [53, 59]. In this thesis, we extend this program and determine the five-loop integrand including non-planar corrections using similar methods, as described in Chapter 7. This is the only part of the thesis in which we consider the full theory. Throughout the rest, we restrict to the planar limit.

Beyond four points, significant progress has also been achieved. Higher-point correlators of the lightest protected operators have been studied at weak coupling at the level of the loop integrand [60], as well as at strong coupling [61, 62]. At five points, correlators of higher-charged operators have also been computed at one-loop order [63].

A remarkable structural feature that has emerged in the study of planar $\mathcal{N} = 4$ SYM is the appearance of a hidden *ten-dimensional symmetry*. In particular, the four-point correlators of half-BPS operators with arbitrary R-charge can be organized into a single generating function that exhibits a ten-dimensional conformal invariance. This symmetry group, $\mathrm{SO}(10, 2)$, combines the four-dimensional spacetime conformal symmetry $\mathrm{SO}(4, 2)$ with the internal $\mathrm{SO}(6)$ R-symmetry, acting on unified ten-dimensional coordinates $X = (x, y)$, where x denotes spacetime coordinates and y parametrizes the R-symmetry polarization.
Evidence for this symmetry has been identified in two distinct regimes in the planar limit. At strong coupling, it arises in the tree-level supergravity approximation of the holographic dual [64], while at weak coupling it appears at the level of loop integrands in perturbation theory [65]. However, this symmetry does not persist in full generality. On the gravitational side, it is broken by stringy α' corrections, while on the gauge theory side, it is lost once the spacetime integrations over the insertion points are carried out. At present, no derivation from first principles is known, and both the origin of the symmetry and the mechanism underlying its breaking remain poorly understood. Already at four points, the ten-dimensional invariance only becomes visible at the level of a reduced correlator, that arises after factoring out a universal superconformal prefactor [66] from the full generating function. It is therefore not clear how such a symmetry, if present, should manifest itself for higher-point functions, as there are more superconformal invariants for higher points and a unique decomposition into them does not seem to exist [67, 68].

Some progress towards understanding these structures has been made by considering correlators of generalized operators that combine the lightest half-BPS operators with their higher R-charge counterparts [65]. Such correlators can be viewed as *generating functions* that encode all correlators of half-BPS operators with fixed R-charge configurations. These generalized operators admit a natural realization in the twistor space formulation of $\mathcal{N} = 4$ SYM [69]. In this framework, one obtains a set of effective Feynman rules in the self-dual sector of the theory, where the relevant correlators appear as particular supercomponents. The construction involves an effective scalar propagator carrying a ten-dimensional pole in $X = (x, y)$, together with additional interaction vertices encoding Grassmann degrees of freedom.

While this formalism makes the ten-dimensional pole structure of the loop integrands manifest at arbitrary multiplicity and loop order, it does not render the underlying $\mathrm{SO}(10,2)$ symmetry manifest. Even at four points, establishing this symmetry requires summing over all contributing diagrams, and the situation becomes even more intricate at higher points. In this thesis, we employ these rules to extend the computation of generating functions beyond four points, as presented in Chapter 4.

The generating functions exhibit poles in ten-dimensional distances, which allow for interesting limits to be taken. In this context, the so-called ten-dimensional null polygon limit plays a central role. In this limit, correlators of large-charge operators factorize into simpler building blocks, known as polygon correlators, which capture essential dynamical information. These objects exhibit remarkable factorization properties and admit efficient perturbative computations. Moreover, they are conjectured to be related to massive scattering amplitudes on the Coulomb branch of the theory [65]. Their loop integrands can be obtained either from generating functions, as described above, or directly via twistor methods, as explained in Chapter 5.
Up to six points, the scalar fields of the theory allow one to construct large-charge correlation functions with suitable polarizations such that they are equivalent to the polygon correlators. In particular, the operators must be polarized in such a way that adjacent operators are connected by large bundles of propagators, which factorize the color surface into an "inside" and an "outside". This is precisely the limit in which such objects were first studied at four points, where the resulting correlator is known as the "octagon". It has been computed to all orders in perturbation theory [70–73] and even at finite coupling [74,75]. This was possible since the disk topology of this object makes it particularly amenable to efficient computations using integrability-based hexagonalization. Its extension to five points has also been studied [76, 77]. Chapter 5 and Chapter 6 are devoted to extend the study of the polygon correlators by considering their loop integrands and pushing the computations to higher multiplicity and higher-loop order.

To conclude, a variety of remarkable structures have emerged in $\mathcal{N} = 4$ SYM in recent years. While these developments have provided important insights into the theory in specific regimes, extending them systematically to higher-loop orders and higher-point functions remains a challenging task. The complexity increases rapidly, and it is often unclear to what extent the observed structures persist in more general settings.

In this thesis, we take several steps in this direction by studying higher-point correlators of half-BPS operators and their associated loop integrands. We analyze their organization in terms of generating functions and investigate their behavior in certain limits. In addition, we consider non-planar contributions to four-point functions at high loop order. The main results of this work are summarized in the following overview section.

1.2. Overview

To conclude this introduction, let us give a brief overview of the main results obtained in this thesis, which are summarized schematically in Fig. 1.1. The common theme underlying all chapters is the explicit computation of correlation functions of scalar half-BPS operators in $\mathcal{N} = 4$ SYM, with a particular emphasis on pushing the frontier of what is currently accessible at the level of the loop integrand. The results are grouped into three closely related directions. Taken together, they probe the interplay between multiplicity, loop order, R-charge, and topology, and provide new perturbative data for a broad range of correlators.

We begin by reviewing the most important theoretical foundations underlying this thesis. In Chapter 2, we review key aspects of $\mathcal{N} = 4$ SYM. In particular, we present its field content, discuss the symmetry algebra and the resulting representations. We introduce half-BPS protected operators, which can be formulated conveniently in analytic superspace. Subsequently, we discuss their correlation functions, with an emphasis on four-point functions, as these provide the basic examples of the correlators studied throughout this thesis. We conclude this chapter by reviewing the appearance of the ten-dimensional symmetry.
In Chapter 3, we continue this review by introducing the basic features of twistor space and the twistor reformulation of $\mathcal{N} = 4$ SYM. We further review how the corresponding Feynman rules for the operators under consideration are drastically simplified in this setting. We conclude by presenting these twistor Feynman rules, as they will be used throughout this thesis to compute and verify the results obtained.

Moving on to the result chapters, the starting point is the generating function for planar correlators of scalar half-BPS operators with arbitrary R-charge configurations. This object unifies infinitely many correlators into a single function and is therefore particularly well suited for investigating structural properties that are difficult to recognize in fixed-charge observables. In this thesis, we compute the five-point generating functions at one and two loops, as well as the six-point generating function at one loop, as described in Chapter 4. These results provide new data for higher-point correlators with arbitrarily high R-charges and allow one to investigate to which extent the ten-dimensional structures known from four points persist at higher multiplicity.

A second major direction is obtained by taking a polygonal ten-dimensional null limit, which reduces the generating functions to a product of polygon functions. In this regime, the correlators simplify considerably while at the same time exhibiting a rich factorization structure. Up to six points, this limit can be interpreted as selecting correlators of large-charge operators with suitable polarizations, which give rise to polygon functions. The corresponding observables are planar polygon functions of large-charge operators with disk topology. In this thesis, they are studied in two complementary ways. First, in Chapter 5, polygon functions of arbitrary multiplicity are determined up to two loops. Second, in Chapter 6, the five-point polygon function, or pentagon function, is pushed to five loops, providing access to a higher-point observable at high-loop order.

The third direction of the thesis departs from the planar limit. While the previous chapters focus on planar correlators, the final part addresses the full non-planar four-point correlator of the lightest scalar half-BPS operators at five loops, presented in Chapter 7. In particular, the computation establishes a non-vanishing genus-one contribution, while higher-genus corrections vanish, and allows for the extraction of the Konishi anomalous dimension at five loops.

From this perspective, the structure of the thesis may be understood as an exploration of the space of half-BPS correlators along several different directions. One direction is the generalization in external R-charge, captured by the generating functions. Another is the large-charge limit, which leads to polygon functions and gives access to new all-multiplicity structures. A third is the extension to very high loop order in special cases, represented here by the pentagon function. Finally, the non-planar four-point correlator probes the theory beyond the planar limit.

We conclude this thesis in Chapter 8 by summarizing our findings and outlining possible directions for future research based on the results obtained in this work.

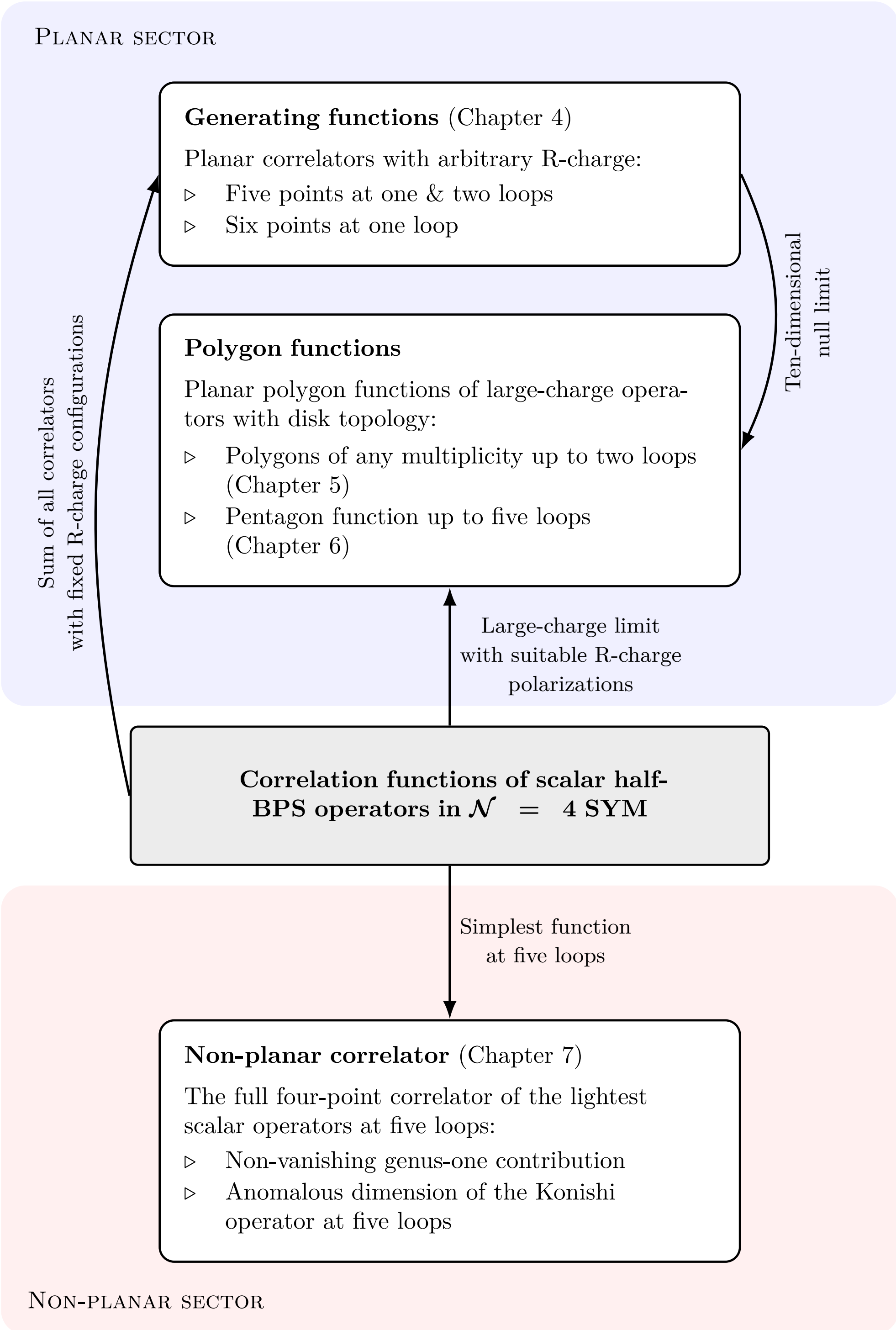

Figure 1.1.: Overview of the main computations performed in this thesis.

Part I.

Review

2. $\mathcal{N} = 4$ Supersymmetric Yang–Mills Theory

We begin by introducing the theory on which this thesis is based, namely $\mathcal{N} = 4$ supersymmetric Yang–Mills theory (SYM). This is the maximally supersymmetric interacting gauge theory in four spacetime dimensions that does not include gravity. For this reason, it provides an especially valuable theoretical laboratory for the study of quantum field theory in a highly constrained and yet nontrivial setting.

$\mathcal{N} = 4$ SYM exhibits a number of remarkable properties and occupies a central position in modern theoretical physics. As already mentioned in the introduction, it furnishes the canonical example of holography through the AdS/CFT correspondence and, at least in the planar limit, appears to be an integrable quantum field theory. In the present chapter, however, our emphasis will be on those structural features of $\mathcal{N} = 4$ SYM that are directly relevant for the analysis of higher-point correlation functions studied in this thesis.

In Section 2.1, we introduce the field content and the Lagrangian of $\mathcal{N} = 4$ SYM, and subsequently discuss its supersymmetry algebra and the resulting representations in Section 2.2. In particular, we introduce half-BPS supermultiplets and review analytic superspace in Section 2.3, which provides a convenient framework to describe these multiplets. In Section 2.4, we discuss the main features of correlation functions of these operators up to four points. Finally, in Section 2.5, we review the emergence of an unexpected ten-dimensional symmetry of correlation functions of half-BPS operators, which combines their space-time and internal variables in a unified way.

All contents of this chapter review existing results from the literature. Much of this material has already been discussed extensively, and we do not aim to provide a complete presentation here. Instead, we focus on introducing the most relevant aspects needed for the following chapter and for presenting our results. For general properties of $\mathcal{N} = 4$ SYM, we mostly follow [78, 79]. For the discussion of analytic superspace and the properties of correlation functions, we follow the presentation in [41, 80], as well as the review [67].

2.1. Fields and Lagrangian

$\mathcal{N} = 4$ SYM with gauge group $\mathrm{SU}(N_c)$ in four dimensions consists of a gauge field A_μ, four Weyl fermions $\Psi_{B\alpha}$ as well as their conjugates $\bar{\Psi}^B_{\dot{\alpha}}$ (with $B = 1, \ldots, 4$ and $\alpha, \dot{\alpha} = 1, 2$), and six scalar fields Φ^I (with $I = 1, \ldots, 6$). All fields are gathered in a single supermultiplet and transform in the adjoint representation of the gauge group.

The dynamics of these fields are given by the Lagrangian which reads [81]

$$\begin{aligned}
\mathcal{L}_{\mathcal{N}=4}(x) \;=\; \mathrm{tr}\Bigg(&- \frac{1}{2g^2_{\mathrm{YM}}} F_{\mu\nu}F^{\mu\nu} + \frac{\theta}{8\pi^2} F_{\mu\nu}\tilde{F}^{\mu\nu} - \bar{\Psi}^B_{\dot{\alpha}} (\sigma_\mu)^{\dot{\alpha}\beta} D^\mu \Psi_{B\beta} \\
&+ g_{\mathrm{YM}}\, (\bar{\Sigma}^I)^{BC} \Psi_{B\alpha} \epsilon^{\alpha\beta} [\Phi^I, \Psi_{C\beta}] + g_{\mathrm{YM}}\, (\Sigma^I)_{BC} \bar{\Psi}^B_{\dot{\alpha}} \epsilon^{\dot{\alpha}\dot{\beta}} [\Phi^I, \bar{\Psi}^C_{\dot{\beta}}] \\
&- D_\mu \Phi^I D^\mu \Phi^I + \frac{g^2_{\mathrm{YM}}}{2} [\Phi^I, \Phi^J][\Phi^I, \Phi^J] \Bigg)
\end{aligned} \tag{2.1}$$

The gauge field is encoded in the gauge-covariant derivative $D_\mu = \partial_\mu \cdot + i[A_\mu, \cdot]$, the field strength tensor and its dual

$$F_{\mu\nu} \;=\; \partial_\mu A_\nu - \partial_\nu A_\mu + i[A_\mu, A_\nu] \quad \text{and} \quad \tilde{F}_{\mu\nu} \;=\; \frac{1}{2} \epsilon_{\mu\nu\rho\sigma} F^{\rho\sigma} \,. \tag{2.2}$$

Moreover, $\epsilon_{\alpha\beta}$ denotes the antisymmetric invariant tensor of SU(2), the matrices σ^μ are Pauli matrices, and the coefficients Σ are sigma matrices relating the fundamental representation of $\mathrm{SO}(6)_R$ to the antisymmetric of $\mathrm{SU}(4)_R$. Finally, the Yang–Mills coupling is denoted by g_{YM}.

The Lagrangian contains the usual kinetic terms for all fields, together with quartic scalar interactions and Yukawa couplings between scalars and fermions. The theory is invariant under the $\mathcal{N} = 4$ super-Poincaré group, which extends the Poincaré symmetry by supersymmetry transformations.

At the classical level, $\mathcal{L}$ is scale invariant. This follows upon assigning the standard mass dimensions to the fields and couplings,

$$[\Phi] = [D_\mu] = 1, \qquad [\Psi_\alpha] = \frac{3}{2}, \qquad [F_{\mu\nu}] = 2. \tag{2.3}$$

Consequently, the Lagrangian has dimension $[\mathcal{L}] = 4$, and the action is classically scale invariant. In local unitary relativistic field theories, scale invariance is expected to enhance to full conformal invariance under mild assumptions, and this holds in particular in two dimensions and in all known four-dimensional examples [82, 83]. Combining conformal symmetry with $\mathcal{N} = 4$ supersymmetry leads to $\mathcal{N} = 4$ superconformal symmetry, whose algebra is $\mathfrak{psu}(2,2|4)$. A remarkable feature of perturbatively quantized $\mathcal{N} = 4$ SYM is the absence of ultraviolet divergences in correlation functions of the canonical fields. Consequently, the renormalization-group β-function vanishes identically, since the renormalization procedure introduces no dependence on a renormalization scale. The theory therefore remains exactly scale invariant, and the superconformal symmetry persists at the quantum level.
The $\mathcal{N} = 4$ SYM Lagrangian contains two parameters: the Yang–Mills coupling constant $_{\mathrm{YM}}$ and the topological θ-angle multiplying the term $F_{\mu\nu}\tilde{F}^{\mu\nu}$. These combine into the complex coupling

$$\tau \equiv \frac{\theta_I}{2\pi} + \frac{4\pi i}{g^2_{\mathrm{YM}}} \,. \tag{2.4}$$

Since the θ-term contributes only through non-perturbative effects such as instanton-corrections, and we will set henceforth to zero $\theta = 0$.

2.2. Superconformal Symmetry

As described, $\mathcal{N} = 4$ SYM is characterized by its high degree of symmetry encoded in the superalgebra $\mathfrak{psu}(2,2|4)$, which provides a maximal extension of both space-time and internal symmetry structures. The study of this algebra is central for the classification of local, gauge-invariant operators, which are organized into unitary representations labeled by their scaling dimensions, Lorentz spin, and $SU(4)_R$ quantum numbers. Within this framework, a distinguished role is played by shortened BPS representations, which we review in this section.

2.2.1. Superconformal Algebra $\mathfrak{psu}(2,2|4)$

The superconformal algebra $\mathfrak{psu}(2,2|4)$ contains the following symmetry generators:

- *Conformal symmetry*, forming the algebra $\mathfrak{so}(2,4) \sim \mathfrak{su}(2,2)$, generated by translations P^μ, Lorentz transformations $M_{\mu\nu}$, dilatations D, and special conformal transformations K^μ.

- *R-symmetry*, which is a bosonic subalgebra representing the internal symmetry transformations, forming the algebra $\mathfrak{so}(6)_R \sim \mathfrak{su}(4)_R$, generated by $R^i{}_j$, with $i, j = 1, \ldots, \mathcal{N} = 4$.

- *Poincaré supersymmetries*, generated by the supercharges $Q^A{}_\alpha$ and their complex conjugates $\bar{Q}_{A\dot{\alpha}}$, with $A = 1, \cdots, 4$ and $\alpha, \dot{\alpha} = 1, 2$. These symmetries are present by virtue of the $\mathcal{N} = 4$ Poincaré supersymmetry of the theory.

- *Conformal supersymmetries*, generated by the supercharges $S_A{}^\alpha$ and their complex conjugates $\bar{S}^{A\dot{\alpha}}$, where the indices run over the same numbers as before. These arise because the Poincaré supercharges and the special conformal generators K_μ do not commute. Since both are symmetries of the theory, their commutator must again generate a symmetry, namely the S-type generators.

The (anti-)commutation relations between these generators are standard within conformal and supersymmetric theories, and we refer to [78] for their explicit form.
The structure of the algebra is organized by a natural grading defined by the scaling dimension of its generators. The bosonic generators of the Lorentz group ($M_{\mu\nu}$), the R-symmetry group ($R^i{}_j$), and the dilatation operator (D) all carry dimension 0. In contrast, the translations P^μ carry dimension $+1$, while the special conformal transformations K^μ carry dimension -1. The fermionic supercharges follow a parallel logic: the Poincaré supercharges Q have dimension $+1/2$, while the conformal supercharges S have dimension $-1/2$.

2.2.2. Superconformal Representations

The classification of states is fundamentally a problem of characterizing the irreducible representations of the superalgebra $\mathfrak{psu}(2, 2|4)$. These representations are organized into supermultiplets, which are generated by the action of the fermionic supercharges on a specific starting state known as the superconformal primary.
A representation is uniquely identified by the quantum numbers of its superconformal primary state, denoted as $|\Delta; k, p, q; j, \bar{j}\rangle$. These labels correspond to the eigenvalues of the Cartan generators of the maximal bosonic subalgebra $\mathfrak{su}(2, 2) \times \mathfrak{su}(4)_R$:

- Scaling dimension (Δ): The eigenvalue of the dilatation operator D, which represents the energy of the state in radial quantization.

- R-symmetry Labels $[k, p, q]$: The Dynkin labels are three integers that characterize the irreducible representation under the internal $\mathfrak{su}(4)_R$ symmetry.

- Lorentz spins $(j, \bar{j})$: The labels for the representation under the Lorentz group $\mathfrak{so}(4) = \mathfrak{su}(2) \oplus \mathfrak{su}(2)$. A state with $(0,0)$ is a scalar, for example.

A state is called a *superconformal primary* if it is a conformal primary (i.e. annihilated by $K_{\alpha\dot{\alpha}}$), and is, in addition, annihilated by all superconformal generators $S_{A\alpha}$ and $\bar{S}^A_{\dot{\alpha}}$. As mentioned, the conformal supercharges are of dimension $-1/2$, implying that repeated action of S on any operator of definite dimension must eventually terminate: otherwise, one would generate operators of negative dimension, which is impossible in a unitary representation. Furthermore, it is required to be a highest weight state with respect to both the internal $\mathfrak{su}(4)_R$ symmetry and the four-dimensional Lorentz algebra $\mathfrak{su}(2) \oplus \mathfrak{su}(2)$.
Let H_i, $i = 1, 2, 3$, denote the Cartan generators of the R-symmetry algebra, and J_3, $\bar{J}_3$ the Cartan generators of the left and right $\mathfrak{su}(2)$, respectively. Correspondingly, we denote by E_i, $i = 1, 2, 3$, and J_+, $\bar{J}_+$ the associated raising operators. The superconformal primary then satisfies

$$\begin{aligned} (K_{\alpha\dot{\alpha}}, S_{A\alpha}, \bar{S}^A_{\dot{\alpha}}, E_i, J_+, \bar{J}_+) \, |\Delta; k, p, q; j, \bar{j}\rangle = 0, \quad i = 1, 2, 3, \quad A = 1, \ldots, 4\,, \\ (D; H_1, H_2, H_3; J_3, \bar{J}_3) \, |\Delta; k, p, q; j, \bar{j}\rangle = (\Delta; k, p, q; j, \bar{j}) \, |\Delta; k, p, q; j, \bar{j}\rangle\,. \end{aligned} \tag{2.5}$$

A commonly used shorthand notation for such a state is $[k, p, q]^{(j,\bar{j})}_{\Delta}$. The full supermultiplet is then generated by the successive action of the 16 supersymmetry generators, ${Q^A}_\beta$ and $\bar{Q}_{B\dot{\beta}}$

$$\prod_{A,B=1}^{4} \prod_{\beta,\dot{\beta}=1}^{2} (Q^A_\beta)^{n_{A\beta}} (\bar{Q}_{B\dot{\beta}})^{\bar{n}_{B\dot{\beta}}} \, |\Delta; k, p, q; j, \bar{j}\rangle\,, \quad \text{for} \quad n_{A\beta}, \bar{n}_{B\dot{\beta}} = 0, 1\,. \tag{2.6}$$

Each application of the supersymmetric creates a distinct module under $\mathfrak{su}(2,2) \times \mathfrak{su}(4)_R$, identified by this highest weight primary state. Since the supercharges have scaling dimension $1/2$, their action on a superconformal primary state increases its dimension by $1/2$. Consequently, the superconformal primary is the state of lowest dimension within a given multiplet.
It is useful to construct explicit forms of superconformal primary operators. Their construction becomes most transparent upon using the fact that the action of the supercharges increases the scaling dimension by $1/2$. Consequently, a superconformal primary operator cannot be written as a Q-commutator of another operator. The essential input is therefore the schematic form of the Q-transformations of the

canonical fields in the theory,

$$\begin{aligned}
[Q, \Phi] &= \Psi\,, \\
\{Q, \Psi\} &= F + [\Phi, \Phi]\,, \\
\{Q, \bar{\Psi}\} &= D\Phi\,, \\
[Q, F] &= D\Psi\,.
\end{aligned} \tag{2.7}$$

Any local polynomial operator containing one of the structures appearing on the right-hand side of these relations cannot be primary. It follows that chiral primary operators cannot contain the Weyl fermions Ψ or the field strengths F. Since they are therefore functions solely of the scalars Φ, they can involve neither derivatives nor commutators of Φ. Hence, superconformal primary operators are gauge-invariant scalar operators constructed from symmetrized products of the scalar fields only.

The simplest examples are the single-trace operators, of the form

$$\mathrm{str}\left(\Phi^{I_1}\Phi^{I_2}\cdots\Phi^{I_n}\right) \tag{2.8}$$

where the indices I_j, $j = 1, \cdots, n$, transform in the fundamental representation of $SO(6)_R$, and the "str" stands for a symmetrized trace over the gauge group. As a consequence, the operator is totally symmetric in the $SO(6)_R$ indices I_j. In general, these operators transform in a reducible representation, namely the symmetrized tensor product of n fundamentals. Irreducible components are obtained by subtracting traces over the $SO(6)_R$ indices. Since we are considering the gauge group $\mathrm{SU}(N_\mathrm{c})$ and thus $\mathrm{tr}\,\Phi^I = 0$, the simplest such operators are

$$\begin{aligned}
\sum_I \mathrm{tr}\,\Phi^I\Phi^I \quad &\sim \quad \text{Konishi multiplet}\,, \\
\mathrm{tr}\,\Phi^{\{I}\Phi^{J\}} \quad &\sim \quad \text{stress-tensor multiplet}\,,
\end{aligned}$$

where the curly brackets denote the $\mathfrak{su}(4)_R$ traceless symmetric combination. The Konishi multiplet [84] is the simplest operator with an unprotected scaling dimension, i.e. it receives quantum corrections. We will return to this operator in Section 7.5, where we determine the perturbative corrections to its dimension at five-loop order. The stress-tensor multiplet, on the other hand, is the lowest-dimension representative of a class of multiplets known as half-BPS multiplets. We will discuss these in more detail in the next subsection.

2.2.3. Shortened Multiplets and BPS States

In the classification of representations of the superconformal algebra $\mathfrak{psu}(2,2|4)$, a fundamental distinction arises between long multiplets and shortened (or BPS) multiplets. While long multiplets possess a full set of 2^{16} states, shortened multiplets occur when the superprimary state is annihilated by a subset of the Poincaré supercharges Q and $\bar{Q}$. These BPS states are characterized by "protected" scaling dimensions Δ, which are determined by their R-symmetry quantum numbers and remain invariant under quantum corrections [85, 86].

Within this thesis, we will be concerned with shortened representations known as half-BPS multiplets, denoted by $[0,p,0]^{\Delta=p}_{(0,0)}$. These representations are invariant under half of the 16 supercharges and satisfy the shortening condition $\Delta = p$, where p is the R-charge. In the last subsection, we saw how these are realized on the field-theoretic side by gauge-invariant single-trace operators constructed from the six scalar fields Φ^I transforming in the $\mathbf{6}$ of $\mathfrak{su}(4)_R$. The general half-BPS operator of charge $p \geq 2$ is defined as the symmetrized traceless product

$$\mathcal{O}_p^{I_1 \dots I_p}(x) = \operatorname{str}\left(\Phi^{\{I_1}(x)\Phi^{I_2}(x)\dots\Phi^{I_p\}}(x)\right) , \tag{2.9}$$

where "str" denotes again the symmetrized trace over the $\mathrm{SU}(N_\mathrm{c})$ gauge indices, and again, the curly brackets denote the $\mathfrak{su}(4)_R$ traceless symmetric combination.

The $p = 2$ half-BPS representation is known as the stress-tensor supermultiplet $\mathbb{O}_2$. The stress-tensor supermultiplet is the simplest non-trivial gauge-invariant multiplet in $\mathcal{N} = 4$ SYM. Its superprimary is the scalar operator in the $\mathbf{20'}$ representation of $SU(4)_R$, hence often just called $\mathbf{20'}$ operator. It takes the explicit form:

$$\mathcal{O}_2^{IJ}(x) = \operatorname{tr}\left(\Phi^{\{I}\Phi^{J\}}\right) = \operatorname{tr}\left(\Phi^I\Phi^J\right) - \frac{1}{6}\delta^{IJ}\operatorname{tr}\left(\Phi^K\Phi^K\right) . \tag{2.10}$$

The full multiplet is generated by successive action of the eight remaining supercharges, namely four chiral charges Q^A_α, $i = 3, 4$, and four anti-chiral charges $\bar{Q}_{B\dot{\alpha}}$, $i = 1, 2$, on the primary operator $\mathcal{O}_2$, under which it is not invariant. Acting with the four chiral supercharges yields the chiral on-shell Lagrangian of $\mathcal{N} = 4$ SYM,

$$\mathcal{L} \sim [0,0,0]^{\Delta=4}_{(0,0)} .$$

Its conjugate $\bar{\mathcal{L}}$ is obtained analogously by acting with the four $\bar{Q}$-charges. The stress-tensor supermultiplet furthermore contains the conserved currents of the theory. These include the $SU(4)_R$ current

$$J_{\alpha\dot{\alpha}}(x) \sim [1,0,1]^{\Delta=3}_{(\frac{1}{2},\frac{1}{2})} ,$$

as well as spinor currents transforming in the $[0,0,1]_{(\frac{1}{2},1)}$ and $[1,0,0]_{(1,\frac{1}{2})}$ representations. Finally, the multiplet also contains the energy-momentum tensor

$$T_{\mu\nu} \sim [0,0,0]^{\Delta=4}_{(1,1)} ,$$

which arises from the action of two chiral and two anti-chiral supercharges. We will return to the explicit expansion of the (chiral) stress-tensor multiplet in Section 2.3.2.
As introduced above, half-BPS operators of charge p carry p indices transforming in the $\mathbf{6}$ of $\mathfrak{su}(4)_R$. When considering correlation functions of such operators, it is convenient to introduce polarization vectors in order to contract these indices. Concretely, we consider six-dimensional vectors y^I, with $I = 1, \ldots, 6$, satisfying the null condition $y^I y^I = 0$. The superconformal primaries of half-BPS multiplets of general charge p can then be defined as

$$\mathcal{O}_p(x,y) = y^{I_1} \cdots y^{I_p}\, \mathcal{O}_p^{I_1 \ldots I_p}(x) = \mathrm{tr}\left(Y^I \Phi^I(x)\right)^p . \tag{2.11}$$

The null condition on the polarization vectors ensures that the operator transforms in the traceless symmetric representation of the internal symmetry group. In the next section, we will see how these polarization vectors arise naturally within the analytic superspace formulation of half-BPS multiplets.

2.3. Analytic Superspace

In the previous section, we introduced the algebra $\mathfrak{psu}(2,2|4)$ and its representations, with particular emphasis on the half-BPS shortened operators and the stress-tensor multiplet. To study their kinematic realization, it is useful to formulate these representations on an appropriate superspace. The natural framework for this purpose is analytic superspace, a special form of harmonic superspace.
Harmonic superspace, originally developed in the context of $\mathcal{N} = 2$ theories [87], extends ordinary superspace by an internal manifold associated with the R-symmetry group. This construction makes superconformal symmetry manifest and allows the field content of the theory to be packaged into superfields defined on the extended space.

$\mathcal{N} = 4$ analytic superspace provides a particularly convenient framework for the description of half-BPS operators in $\mathcal{N} = 4$ SYM [88–93]. In contrast to the standard superspace formulation, where shortening conditions are imposed as differential constraints, analytic superspace implements these constraints geometrically. As a result, half-BPS multiplets can be described as unconstrained superfields.

In the following, we introduce the analytic superspace relevant for $\mathcal{N} = 4$ SYM and discuss its main properties, with a focus on its role in the description of half-BPS multiplets. We closely follow the notation of [41], as well as the results and presentations in [67, 80].

2.3.1. $\mathcal{N} = 4$ Harmonic Variables

In this construction, we introduce auxiliary bosonic variables, known as harmonic variables, which facilitate the covariant breaking of the R-symmetry group $SU(4)$. Specifically, the chiral and anti-chiral Grassmann coordinates θ^A_α and $\bar{\theta}^{\dot{\alpha}}_A$ (where $A = 1, \ldots, 4$ and $\alpha, \dot{\alpha} = 1, 2$) are decomposed by splitting the index as $A = (a, a')$, with $a, a' = 1, 2$. We define the projected odd variables as

$$\theta^A_\alpha \quad \longrightarrow \quad \theta^{+a}_\alpha = \theta^A_\alpha u^{+a}_A \,, \quad \theta^{-a'}_\alpha = \theta^A_\alpha u^{-a'}_A \,, \tag{2.12}$$

and similarly for the anti-chiral variables $\bar{\theta}^{\dot{\alpha}}_A$. Here, we introduced bosonic harmonic variables taking values in $SU(4)$

$$(u^{+a}_A, u^{-a'}_A) \in SU(4) \,. \tag{2.13}$$

The index $A = 1, 2, 3, 4$ transforms in the anti-fundamental representation of $SU(4)$. The second index splits according to the subgroup $SU(2) \times SU(2)' \times U(1) \subset SU(4)$ with indices $a, a' = 1, 2$ corresponding to the fundamental representations of $SU(2)$ and $SU(2)'$, respectively. The $U(1)$ factor assigns definite charges to these variables: u^{+a}_A carries charge $(+1)$, while $u^{-a'}_A$ carries charge (-1). This is reflected in the $\pm$ superscripts of the variables. In the following, we adopt the same notation for projected fields and Grassmann numbers, as is standard in the literature.

The harmonic variables satisfy the unitarity condition $u^\dagger u = \mathbb{I}$, which implies the orthogonality and normalization relations

$$\begin{aligned} &\bar{u}^A_{-a'}\, u^{+b}_A = 0 \,, && \bar{u}^A_{+a}\, u^{-b'}_A = 0 \,, \\ &\bar{u}^A_{+a}\, u^{+b}_A = \delta^b_a \,, && \bar{u}^A_{-a'}\, u^{-b'}_A = \delta^{b'}_{a'} \,. \end{aligned} \tag{2.14}$$

This allows one to reconstruct the original Grassmann coordinates θ^A from their harmonic projections

$$\theta^A = \theta^{+a}\,\bar{u}^A_{+a} + \theta^{-a'}\,\bar{u}^A_{-a'}\,. \tag{2.15}$$

The harmonic variables parameterize the coset

$$Gr(4,2) = \frac{SU(4)}{SU(2)\times SU(2)'\times U(1)}\,, \tag{2.16}$$

which is the Grassmannian manifold $Gr(4,2)$, i.e. the space of two-dimensional complex planes in $\mathbb{C}^4$. Introducing these variables allows one to reformulate supermultiplets in a way that makes $SU(4)$ invariance manifest, while the fields transform covariantly under the subgroup $SU(2)\times SU(2)'\times U(1)$. In this framework, the shortening condition of half-BPS multiplets is implemented in a particularly simple way: such multiplets are characterized by their independence of half of the Grassmann coordinates, namely $\theta^{-a'}$ (and similarly $\bar{\theta}_{+a}$).

2.3.2. The Stress-Tensor Multiplet in Analytic Superspace

In this subsection, we formulate the stress-tensor multiplet using the harmonic variables introduced above. Let us start by considering its bottom component, the $\mathbf{20'}$ operator. The introduction of harmonic variables allows one to parameterize the scalar fields in the theory in the following way

$$\Phi^{++}(x,u) = u^{+a}_A \epsilon_{ab} u^{+b}_B\,\Phi^{AB}\,, \tag{2.17}$$

The scalar fields $\Phi^{AB} = -\Phi^{BA}$ transform in the antisymmetric tensor representation of $SU(4)_R$, which is the $\mathbf{6}$ and is equivalent to the vector representation of $SO(6)$. This description therefore contains the same information as the six real scalars Φ^I. They can be related to each other by

$$\Phi^{AB} = \frac{1}{\sqrt{2}}(\Sigma_I)^{AB}\,\Phi^I\,, \tag{2.18}$$

where Σ^I denote the sigma matrices, already encountered in the Lagrangian (2.1). They satisfy the identity

$$(\Sigma^I)_{AB}(\Sigma^I)_{CD} = \frac{1}{2}\,\epsilon_{ABCD}\,. \tag{2.19}$$

The operator in the $\mathbf{20'}$ representation can be constructed from the scalar fields as

$$\mathcal{O}_2(x,u) = \operatorname{tr}\left(\Phi^{++}(x,u)\,\Phi^{++}(x,u)\right). \tag{2.20}$$

At this stage, it becomes apparent that the harmonic variables introduced here are closely related to the polarization vectors y^I defined in (2.11). Indeed, upon identifying

$$y_I = \frac{1}{\sqrt{2}}(\Sigma_I)^{AB}\,\epsilon_{ab}\,u_A^{+a}\,u_B^{+b}\,, \tag{2.21}$$

one obtains

$$\Phi^{++}(x,u) = y^I(u)\Phi^I(x)\,. \tag{2.22}$$

Starting from the $\mathbf{20'}$ operator, the full stress-tensor multiplet is obtained by the action of the supercharges Q and $\bar{Q}$. Upon decomposing the $SU(4)$ indices, one can distinguish the subset of supercharges that annihilate the primary operator, reflecting the half-BPS condition. Acting with the remaining eight supercharges, Q_a^α and $\bar{Q}_{\dot{\alpha}}^a$, generates the full multiplet

$$\mathbb{O}_2(x,\theta^+,\bar{\theta}_-,u) = \exp\left(\theta_\alpha^{+a}Q_a^\alpha + \bar{\theta}^{\dot{\alpha}}_{-a'}\bar{Q}^{a'}_{\dot{\alpha}}\right)O_2(x,u)\,. \tag{2.23}$$

In the following, we make an important simplification and restrict to the chiral sector by setting the anti-chiral Grassmann variables to zero, $\bar{\theta} = 0$. While the full multiplet contains additional structure, the chiral sector is sufficient for our purposes, as will become clear in the discussion of correlation functions. In particular, loop corrections can be computed using the Lagrangian insertion procedure (see Section 2.4.1), in which the chiral Lagrangian is inserted into the correlator. Since the chiral Lagrangian appears as the top component of the chiral stress-tensor multiplet, this sector captures the relevant information for our analysis.

The expansion of the chiral stress-tensor multiplet takes the form [80]

$$\begin{aligned}
\mathbb{O}_2(x,\theta^+,0,u) = {}&\operatorname{tr}(\Phi^{++}\Phi^{++}) + 2\sqrt{2}i\,\theta_\alpha^{+a}\ \operatorname{tr}(\Psi_a^{+\alpha}\Phi^{++})\\
&+ (\theta^{+2})_{\alpha\beta}\ \operatorname{tr}(\Psi^{+c\{\alpha}\Psi_c^{+\beta\}} - i\sqrt{2}\,F^{\alpha\beta}\,\Phi^{++})\\
&- (\theta^{+2})^{ab}\ \operatorname{tr}(\Psi^{+\gamma}_{\{a}\Psi^{+}_{b\}\gamma} - g_{\mathrm{YM}}\sqrt{2}[\Phi^{+C}_{\{a},\bar{\Phi}_{+Cb\}}]\Phi^{++})\\
&- \frac{4}{3}(\theta^{+3})^a_\alpha\ \operatorname{tr}(F^\alpha_\beta\Psi^{+\beta}_a + ig_{\mathrm{YM}}\,[\Phi^{+B}_a,\bar{\Phi}_{BC}]\Psi^{C\alpha})
\end{aligned}$$

$$+\frac{1}{3}(\theta^{+4})\,\mathcal{L}(x)\,, \tag{2.24}$$

where we defined the projected fields $\Psi_a^{+\alpha} = \epsilon_{ab} u_B^{+b} \Psi^{\alpha B}$ and $\Phi_a^{+C} = \epsilon_{ab} u_B^{+b} \Phi^{BC}$. For the Grassmann numbers we uses the following shorthand notation

$$\begin{aligned} (\theta^{+2})_{\alpha\beta} &= \theta_\alpha^{+a}\epsilon_{ab}\theta_\beta^{+b}\,, & (\theta^{+2})^{ab} &= \theta_\alpha^{+a}\epsilon^{\alpha\beta}\theta_\beta^{+b}\,, \\ (\theta^{+3})_\alpha^a &= \theta_\alpha^{+b}\,\theta_b^{+\beta}\,\theta_\beta^{+a}\,, & (\theta^{+4}) &= \theta_\alpha^{+b}\,\theta_b^{+\beta}\,\theta_\beta^{+c}\,\theta_c^{+\alpha}\,. \end{aligned} \tag{2.25}$$

Finally, $\mathcal{L}(x)$ denotes the chiral $\mathcal{N}=4$ SYM Lagrangian. Since $(\theta^+)^4$ is proportional to the Grassmann delta function, $(\theta^+)^4 = 12\,\delta^{0|4}(\theta^+)$, one obtains

$$\mathcal{L}(x) = \frac{1}{4}\int d^4\theta^+\,\mathbb{O}_2(x,\theta^+,0,u)\,. \tag{2.26}$$

As the chiral Lagrangian is the top component of the multiplet, it is annihilated by the chiral supercharges,

$$Q_\alpha^A\,\mathcal{L}(x) = 0\,. \tag{2.27}$$

so that it is supersymmetric. It carries no $U(1)$ charge and is therefore an $SU(4)$ singlet, i.e. independent of the harmonic variables. Explicitly, the chiral $\mathcal{N}=4$ SYM Lagrangian is given by

$$\mathcal{L}(x) = \mathrm{tr}\Big(-\frac{1}{2}F_{\alpha\beta}F^{\alpha\beta} + \sqrt{2}\,g_{\mathrm{YM}}\,\Psi^{\alpha A}[\Phi_{AB},\Psi_\alpha^B] - \frac{g_{\mathrm{YM}}^2}{8}[\Phi^{AB},\Phi^{CD}][\Phi_{AB},\Phi_{CD}]\Big)\,. \tag{2.28}$$

2.3.3. General Half-BPS Multiplets in Analytic Superspace

The construction of the stress-tensor multiplet can be straightforwardly generalized to arbitrary half-BPS multiplets. Starting from the $\mathbf{20'}$ operator, one defines the superconformal primary of charge p as

$$\mathcal{O}_p(x,u) = \mathrm{tr}\left((\phi^{++}(x,u))^p\right)\,. \tag{2.29}$$

Acting with the supercharges, as described in (2.23), generates the full supermultiplet

$$\mathbb{O}_p(x,\theta^+,\bar\theta_-,u) \;=\; \exp\left(\theta_\alpha^{+a}Q_a^\alpha + \bar\theta_{-a'}^{\dot\alpha}\bar Q_{\dot\alpha}^{a'}\right)O_p(x,u)$$

$$= \operatorname{tr}\Big((\phi^{++}(x,u))^p\Big) + \cdots + \frac{1}{3}(\theta^+)^4 \mathcal{L}_p(x,u)\Big|_{\bar{\theta}_- \to 0} . \tag{2.30}$$

Considering only the chiral half of the supermultiplet, its component expansion terminates at order $(\theta^+)^4$. The top component $\mathcal{L}_p(x,u)$ can be viewed as a generalization of the chiral Lagrangian, carrying $U(1)$ charge $(p-2)$. In the context of the AdS/CFT correspondence, these operators are dual to Kaluza–Klein modes of type IIB supergravity on $AdS_5 \times S^5$, with the case $p=2$ corresponding to the supergravity multiplet containing the graviton [94]. Therefore, we refer to $\mathcal{L}_p(x,u)$, (or equivalently $\mathcal{L}_p(x,y)$) as higher-KK modes of the chiral Lagrangian.

2.4. Correlation Functions of Half-BPS Operators

In $\mathcal{N}=4$ SYM, a central class of observables is given by correlation functions of half-BPS operators. Computing these functions at higher-loop order, for higher-point configurations, and for operators with larger R-charges is the main focus of this thesis. In this review section, we discuss the basic properties of these correlators, mostly focusing on their simplest example: four-point correlation functions of the stress-tensor multiplet. In the previous section, we reviewed how these objects are conveniently described in analytic superspace. Now, we adopt this description to formulate their correlation functions. We emphasize once more that we restrict our attention to the chiral half of the supermultiplet.

2.4.1. The Lagrangian Insertion Procedure

The n-point correlation function of chiral stress-tensor multiplets is defined as the vacuum expectation value of n such operators

$$\begin{aligned} \mathcal{G}_n(1,\ldots,n) &= \langle \mathbb{O}_2(1)\mathbb{O}_2(2)\ldots\mathbb{O}_2(n)\rangle \\ &= \int \mathcal{D}A\,\mathcal{D}\Psi\,\mathcal{D}\bar{\Psi}\,\mathcal{D}\Phi\, e^{i\int \mathrm{d}^4x\, \mathcal{L}_{\mathcal{N}=4}(x)}\, \mathbb{O}_2(1)\mathbb{O}_2(2)\ldots\mathbb{O}_2(n)\,, \end{aligned} \tag{2.31}$$

where the operators are labeled by their values in analytic superspace (x_i, θ_i^+, u_i), and in the second line we have written the path integral over the fundamental fields of the theory. Moreover, $\mathcal{L}_{\mathcal{N}=4}(x)$ denotes the Lagrangian (2.1). The correlator admits a perturbative expansion

$$\mathcal{G}_n = \sum_{\ell\geq 0} a^\ell\, G_n^{(\ell)}\,, \tag{2.32}$$

where a is the 't Hooft coupling $a = g^2_{\rm YM} N_{\rm c}/(4\pi^2)$. It is often more convenient to reorganize the perturbative expansion in terms of a instead of the Yang–Mills coupling $g_{\rm YM}$, since in the large-$N_{\rm c}$ limit ($g_{\rm YM} \to 0$, $N_{\rm c} \to \infty$ with a fixed) the dependence on the gauge group is captured by powers of N_c, while the dynamics is governed by a. In particular, loop corrections come with powers of $g^2_{\rm YM} N_{\rm c}$, so that each loop order effectively contributes one power of a, making it the natural expansion parameter.

The evaluation of the loop-corrections $\mathcal{G}_n^{(\ell)}$ is significantly streamlined by utilizing the so-called Lagrangian insertion procedure [41, 95]. It involves considering the derivative of the correlation function $\mathcal{G}_n$ with respect to the coupling constant a. Such an operation generates an insertion of the $\mathcal{N}=4$ SYM action integral into the vacuum expectation value

$$a \frac{\partial}{\partial a} \mathcal{G}_n = -i \int \mathrm{d}^4 x_{n+1} \, \langle \mathbb{O}_2(1) \mathbb{O}_2(2) \ldots \mathbb{O}_2(n) \mathcal{L}_{N=4}(x_{n+1}) \rangle \,. \tag{2.33}$$

Prior to differentiating, one rescales all fields in the Lagrangian by a factor of $g^{-1}_{\rm YM}$. As a consequence, the coupling g is removed from the interaction terms in $\mathcal{L}_{\mathcal{N}=4}$ and instead reappears as an overall prefactor multiplying the action.

In deriving this relation, the rescaling of the operators, and thus of the correlator itself, are neglected. Acting with the derivative $\partial/\partial a$ on the resulting overall factor produces an additional contribution proportional to the correlator itself. However, this contribution is spurious: it is exactly canceled by contact terms arising in the $(n+1)$-point correlator under the integral in (2.33) (see [37,66]). These contact terms originate from the kinetic terms of the fields in the inserted Lagrangian. Discarding such contact terms, as we have implicitly done in (2.33), allows us to replace the full Lagrangian by its on-shell form (2.28). In other words, up to contact terms, the insertion under the space-time integral in (2.33) can be written as

$$\int \mathrm{d}^4 x_{n+1} \; \mathcal{L}_{\mathcal{N}=4}(x_{n+1}) \; \to \; \int \mathrm{d}^4 x_{n+1} \; \mathcal{L}(x_{n+1}) \,. \tag{2.34}$$

An important feature of the stress-tensor correlators is that the chiral on-shell Lagrangian $\mathcal{L}(x)$ is the top component of the multiplet itself (2.26). Thus, we can write the on-shell action integral as

$$S_{\text{on-shell}} = \int \mathrm{d}^4 x \, \mathcal{L}(x) = \frac{1}{4} \int d^4 x \, d^4 \theta^+ \, \mathbb{O}_2(x, \theta^+, u) \tag{2.35}$$

Iterative application of this procedure allows the ℓ-loop correction to be recovered from $(n+\ell)$-point tree-level correlation functions of the supermultiplet

$$\mathcal{G}_n^{(\ell)} = \frac{(-i/4)^\ell}{\ell!} \int \prod_{j=1}^{\ell} \mathrm{d}^4 x_{n+j}\, \mathrm{d}^4\theta_{n+j}^+ \; G_{n+\ell}^{(0)}(1,\dots,n+\ell) \tag{2.36}$$

where the integral over the ℓ additional superspace coordinates (x_{n+j},θ^+_{n+j}) effectively picks out the Lagrangian component of the multiplets at the insertion points. Importantly, while this last manipulation holds only for correlation functions of the stress-tensor multiplet, since the chiral on-shell Lagrangian appears as its top component, the Lagrangian insertion procedure (2.33) with (2.34) itself is more general and applies to all correlators of half-BPS operators.

2.4.2. Grassmann Structure

The n-point correlation function of stress-tensor supermultiplets (2.31) cannot only be expanded in a perturbative way, but also in terms of its Grassmann dependency. Thereby, the Grassmann structure of $\mathcal{G}_n$ is constrained by $\mathfrak{psu}(2,2|4)$ superconformal invariance. Each superfield $\mathbb{O}_2$ admits a finite expansion in the projected Grassmann variables θ^{+a}_α, and the full supercorrelator can be decomposed accordingly. Consequently, the supercorrelator admits a double expansion in the 't Hooft coupling a and the Grassmann degree,

$$\begin{aligned}\mathcal{G}_n &= \sum_{k=0}^{n-4}\sum_{\ell=0}^{\infty} a^{\ell+k}\mathcal{G}_{n;k}^{(\ell)}\,,\\ &= \sum_{\ell=0}^{\infty} a^\ell \mathcal{G}_{n;0}^{(\ell)} + a^{\ell+1}\mathcal{G}_{n;1}^{(\ell)} + \dots + a^{n+\ell-4}\mathcal{G}_{n;n-4}^{(\ell)}\end{aligned} \tag{2.37}$$

where $\mathcal{G}_{n;k}^{(\ell)}$ is a homogeneous polynomial of degree $4k$ in the Grassmann variables θ_i^+ and the top component of the correlator goes at most with $(\theta^+)^{4(n-4)}$.

We note the following features about the above expansion: first, the restriction to Grassmann degrees $4k$ follows from the underlying R-symmetry. In harmonic superspace, the superfields $\mathbb{O}_2(x,\theta^+,u)$ carry definite $U(1)$ charges, and invariance under the center $\mathbb{Z}_4 \subset SU(4)$, acting as $\theta^+ \to \omega\theta^+$ with $\omega^4=1$, implies that only powers of the chiral measure $(\theta^+)^4$ can appear. As a result, the supercorrelator decomposes into sectors of Grassmann degree $4k$. Second, by utilizing the 16 chiral generators of the theory (eight Poincaré supersymmetry generators Q and eight conformal supersymmetry generators $\bar{S}$) one can eliminate 16 Grassmann variables, leaving $4(n-4)$ independent ones. This leads to a decomposition into components $\mathcal{G}_{n;k}$ with $k=0,\ldots,n-4$.

The fact that these components start at different orders in perturbation theory can be understood from the operator content of the multiplet. Expanding in θ_i^+ produces correlators of component operators corresponding to the different Grassmann degrees in (2.23), where higher Grassmann degree corresponds to higher components. In particular, already at $k=1$ one encounters terms where one insertion is the on-shell Lagrangian $\mathcal{L}$, while the remaining ones are scalar operators. Such correlators necessarily involve interaction vertices even at tree level, and are therefore proportional to at least one power of the coupling, implying $\mathcal{G}_{n;1}^{(0)}=\mathcal{O}(a)$. More generally, increasing the Grassmann degree introduces additional insertions of $\mathcal{L}$, each bringing an extra power of a. This explains why $\mathcal{G}_{n;k}$ starts at order a^k.

2.4.3. Two- and Three-Point Correlation Function

The Grassmann structure allows us to draw an important conclusion for the Lagrangian insertion procedure. Given a tree-level n-point correlator $\mathcal{G}_n^{(0)}$, the maximal Grassmann degree is $4(n-4)$. Consequently, using the Lagrangian insertion procedure (2.36), we can at most recover the $(n-4)$-loop correction to the four-point correlator,

$$\mathcal{G}_4^{(n-4)}(1,2,3,4)=\frac{(-i/4)^{(n-4)}}{(n-4)!}\int\prod_{k=5}^{n}\mathrm{d}^4x_k\,\mathrm{d}^4\theta_k^+\;\mathcal{G}_n^{(0)}(1,\ldots,n)\,, \tag{2.38}$$

since beyond this point there are no remaining Grassmann variables to integrate over. This simple observation reproduces the well-known result that two- and three-point functions of the stress-tensor multiplet are protected from quantum corrections [52, 85, 86, 95–98]. Importantly, as the same Grassmann structure persists for general half-BPS multiplets with $p>2$, their two- and three-point functions are equally protected. For the same reason, their tree-level correlation function cannot depend on the Grassmann variables. Hence, the two- and three-point correlators of stress-tensor multiplets coincide with their tree-level, lowest (bosonic) component,

$$\mathcal{G}_n=\mathcal{G}_{n;0}^{(0)}\,,\quad\text{for}\quad n=2,3\,. \tag{2.39}$$

To evaluate these functions, let us consider the propagator of two scalar fields Φ^{++} (2.17),

$$\begin{aligned}\langle \Phi^{++}(1)\Phi^{++}(2)\rangle^{(0)} &= \frac{1}{4}(u_1^+)^a_A\epsilon_{ab}(u_1^+)^b_B\,(u_2^+)^c_C\epsilon_{cd}(u_2^+)^d_D\,\langle \Phi^{AB}(x_1)\Phi^{CD}(x_2)\rangle^{(0)} \\ &= \frac{1}{4}(u_1^+)^a_A\epsilon_{ab}(u_1^+)^b_B\,(u_2^+)^c_C\epsilon_{cd}(u_2^+)^d_D\,\frac{\epsilon^{ABCD}}{4\pi^2 x_{12}^2} \\ &= \frac{y_1^I y_2^I}{4\pi^2 x_{12}^2} = \frac{y_{12}^2}{4\pi^2 x_{12}^2}\,,\end{aligned} \tag{2.40}$$

where in the second step we used the appropriately normalized scalar propagator, and in the last step we employed (2.19) and (2.21) to rewrite the harmonic variables in terms of polarization vectors. Here, we defined $y_{12}^2 = y_1^I y_2^I$ and $x_{12}^2 = (x_1 - x_2)^2$. We do not display the color structure of the Φ fields in order not to clutter the notation.

For $n = 2$ and $n = 3$, the tree-level correlators are obtained by forming cyclic chains of free propagators. The two-point function is given by

$$\mathcal{G}_2^{(0)} = \frac{N_c^2 - 1}{2(4\pi^2)^2}\left(\frac{y_{12}^2}{x_{12}^2}\right)^2 . \tag{2.41}$$

The three-point function similarly takes the form of a cyclic chain of propagators,

$$\mathcal{G}_3^{(0)} = \frac{N_c^2 - 1}{(4\pi^2)^3}\frac{y_{12}^2 y_{23}^2 y_{31}^2}{x_{12}^2 x_{23}^2 x_{31}^2}\,, \tag{2.42}$$

where in both cases the prefactor arises from a combination of combinatorial factors and the $SU(N_\text{c})$ color structure.

2.4.4. Four-Point Correlation Function

The simplest correlator that receives non-trivial quantum corrections is the four-point function. Its loop corrections can be computed via (2.38), which we rewrite in a slightly different form

$$\mathcal{G}_4^{(\ell)}(1,2,3,4) = \frac{(-i/4)^\ell}{\ell!}\int\prod_{k=1}^{\ell}\mathrm{d}^4x_{4+k}\,\mathrm{d}^4\theta_{4+k}^+\;\mathcal{G}_{4+\ell;\ell}^{(0)}(1,\ldots,4+\ell)\,. \tag{2.43}$$

Thus, the integrand of the ℓ-loop correction is given by the tree-level correlator $\mathcal{G}^{(0)}_{4+\ell;\ell}$. Here, we have indicated that only the Grassmann component of degree 4ℓ contributes.

The total number of chiral Grassmann variables in an n-point correlator is $4n$. However, the superconformal algebra contains 16 chiral generators, namely the eight Poincaré supersymmetries Q^α_A and the eight special conformal supersymmetries $\bar{S}^{\dot\alpha}_A$, which act as shifts in analytic superspace. These can be used to gauge away 16 Grassmann variables, so that $\mathcal{G}^{(0)}_{4+\ell;\ell}$ corresponds to the top Grassmann component.

As a consequence, the integrand can be written in terms of a unique superconformal invariant. This invariant can be constructed as an integral over the parameters of Q and $\bar{S}$ supersymmetries [41],

$$I_n(x_i, \theta^+_i, u_i) = \int \mathrm{d}^8\epsilon \, \mathrm{d}^8\bar{\xi} \prod_{i=1}^{n} \delta^{(4)}\Big((\theta^+_i)^a_\alpha - \epsilon^A_\alpha \, (u^+_i)^a_A - (x_i)^{\dot\alpha}_\alpha \, \bar{\xi}^A_{\dot\alpha} \, (u^+_i)^a_A\Big) \,, \tag{2.44}$$

which is a homogeneous polynomial of degree $4(n-4)$ in the variables θ^+_i. It carries conformal weight -2 and $U(1)$ charge $+4$ at each point. Comparing these properties with those of $\mathcal{G}^{(0)}_{4+\ell;\ell}$, we find agreement except for the conformal weight: the correlator has weight $+2$ at each point. Therefore, the invariant $I_{4+\ell}$ must be multiplied by a conformally covariant function of x_i with weight $+4$ at each point.

Using this invariant, the loop integrand of the four-point function can thus be written as

$$\mathcal{G}^{(0)}_{4+\ell;\ell} = \frac{2(N_\mathrm{c}^2-1)}{(4\pi^2)^{4+\ell}} \, I_{4+\ell}(x_i, \theta^+_i, u_i) \, F^{(\ell)}(x_i) \,, \tag{2.45}$$

where $F^{(\ell)}(x_i)$ depends only on the space-time coordinates and carries conformal weight $+4$ at each point. It is known as the reduced correlator. Importantly, since both $\mathcal{G}^{(0)}_{4+\ell;\ell}$ and $I_{4+\ell}$ are fully symmetric under permutations of all $4+\ell$ points, the same must hold for $F^{(\ell)}$. This reveals a hidden $S_{4+\ell}$ symmetry of the loop integrand, extending beyond the naively expected $S_4 \times S_\ell$ symmetry [41].

When evaluating the loop correction in (2.43), it is useful to focus on the component of the integrand with maximal Grassmann degree at the insertion points, since this is the only contribution that survives the Grassmann integration. By setting the Grassmann coordinates at four points to zero,

$$\theta^+_1 = \theta^+_2 = \theta^+_3 = \theta^+_4 = 0 \,, \tag{2.46}$$

the invariant in (2.44) can be computed explicitly, yielding [41]

$$I_{4+\ell}\big|_{\theta_1^+=\cdots=\theta_4^+=0} = \left(x_{12}^2 x_{13}^2 x_{14}^2 x_{23}^2 x_{24}^2 x_{34}^2\right) \mathcal{R}_{1234} \prod_{k=5}^{4+\ell} \delta^{(4)}(\theta_k^+)\,, \tag{2.47}$$

where we defined

$$\mathcal{R}_{1234} = \frac{1}{8} x_{12}^2 x_{34}^2 \left(\frac{y_{12}^2 y_{34}^2}{x_{12}^2 x_{34}^2} - \frac{y_{13}^2 y_{24}^2}{x_{13}^2 x_{24}^2}\right)\left(\frac{y_{12}^2 y_{34}^2}{x_{12}^2 x_{34}^2} - \frac{y_{14}^2 y_{23}^2}{x_{14}^2 x_{23}^2}\right) + (\mathrm{S}_4 \text{ perms})\,. \tag{2.48}$$

The decomposition of the four-point correlator in terms of this invariant was already observed in [66].

The representation of the loop integrand of the four-point correlator in this form, together with the full permutation symmetry of $F^{(\ell)}$, provides a powerful framework for determining the integrand at higher-loop orders. By exploiting various limits, such as Euclidean and Minkowskian OPE limits, different loop orders can be related recursively, allowing for a bootstrap of the integrand. In the planar sector, this program has been carried out very successfully up to twelve loops [41, 53–58]. In Chapter 6, we review several methods used to construct the four-point loop integrand and adapt them for our purposes. These are largely based on a duality relating correlation functions to massless scattering amplitudes in the theory (see Section 2.4.5).

In the full theory, including non-planar corrections, determining the integrand becomes significantly more involved, as the reduced correlator $F^{(\ell)}$ is much less constrained. Non-planar contributions first appear at four loops. The corresponding integrand was obtained by combining constraints from OPE limits [53] with a direct twistor-space computation to fix the remaining freedom [59]. In Chapter 7, we discuss these constructions in more detail and explain how to adapt these methods in order to compute the full integrand at five-loop order.

Considering four-point correlators of general half-BPS operators is more involved, since one loses the full permutation symmetry of $F^{(\ell)}$, and the function acquires a dependence on the polarization vectors. Nevertheless, the decomposition into a unique four-point superconformal invariant and the reduced correlator persists. Exploiting this structure, together with constraints from OPE limits and hexagonalization, allowed the determination of four-point functions of half-BPS operators with arbitrary charges p_i, $i = 1, 2, 3, 4$, up to five loops [50, 51].

Building on these results, an even stronger property was uncovered. Summing the four-point integrands of half-BPS operators with arbitrary charges into a single generating function reveals a hidden ten-dimensional symmetry. This symmetry allows one to reconstruct the full result from the $\mathbf{20}'$ four-point integrand [65]. We will discuss this symmetry in Section 2.5.

2.4.5. Correlator/Amplitude Duality

To conclude this section, we discuss an interesting limit of the correlation function of stress-tensor multiplets that relates them to scattering amplitudes. This limit arises when the operator insertion points are taken to be consecutively light-like separated. Applying this limit, it was first found, that the correlators are related to Wilson loop in the adjoint representation, defined along a light-like polygon whose vertices coincide with the insertion points [30]. At the same time, the amplitude/Wilson loop duality [31, 34, 35, 37, 99, 100] identifies polygonal Wilson loops in the fundamental representation of planar $\mathcal{N} = 4$ SYM with scattering amplitudes. In the planar limit, Wilson loops in the adjoint representation factorize into the square of those in the fundamental representation. Taken together, these observations imply that, in the light-like limit, correlators reduce to the square of scattering amplitudes. This correspondence has been confirmed in various works [30, 38, 101, 102]. Notably, the duality holds already at the level of the integrand, establishing a direct relation between rational functions and thus bypassing any subtleties associated with regularization.

We briefly summarize the basic aspects of this duality. In particular, we present the supercorrelator/superamplitude duality proposed in [80, 103], which relates the chiral supercorrelator of stress-tensor multiplets to scattering superamplitudes in planar $\mathcal{N} = 4$ SYM. It states that, in the light-like limit where consecutive insertion points become null-separated, the normalized correlator reduces to the square of the superamplitude,

$$\lim_{\substack{x^2_{i,i+1}\to 0\\ i=1,\ldots,n}} \sum_{\ell\geq 0} a^\ell \frac{\mathcal{G}_n^{(\ell)}}{\mathcal{G}_{n;0}^{(0)}} = \left(\sum_{\ell\geq 0} a^\ell \frac{\mathcal{A}_n^{(\ell)}}{\mathcal{A}_n^{(0),\mathrm{MHV}}}\right)^2 . \tag{2.49}$$

Here, $\mathcal{G}_n^{(\ell)}$ denotes the integrand of the ℓ-loop correction to the supercorrelator, normalized by its lowest (bosonic) component $\mathcal{G}_{n;0}^{(0)}$. On the amplitude side, $\mathcal{A}_n^{(\ell)}$ is the planar ℓ-loop superamplitude divided by the tree-level MHV amplitude $\mathcal{A}_n^{(0),\mathrm{MHV}}$.

Both objects admit an expansion in Grassmann variables. On the correlator side, this corresponds to the decomposition into components of definite Grassmann degree $4k$, as discussed previously. On the amplitude side, the Grassmann expansion is organized according to the MHV degree,

$$\mathcal{A}_n = \mathcal{A}_n^{\mathrm{MHV}} + \mathcal{A}_n^{\mathrm{NMHV}} + \mathcal{A}_n^{\mathrm{N^2MHV}} + \cdots + \mathcal{A}_n^{\mathrm{N}^{n-4}\mathrm{MHV}}\,, \tag{2.50}$$

where the N^kMHV component has Grassmann degree $4k$ relative to the MHV sector. The quantity $\mathcal{A}_n^{\mathrm{N}^k\mathrm{MHV}}$ describes n-particle scattering amplitudes of total helicity $4-n+2k$, with $k=0,\ldots,n-4$. In this way, the Grassmann expansion on both sides of the duality matches sector by sector.

2.5. Ten-Dimensional Symmetry

The four-point correlation functions of protected half-BPS operators exhibit structural constraints that exceed those imposed by four-dimensional superconformal symmetry. Summing them into a generating function that encode all correlators of four scalar half-BPS operators with arbitrary R-charges reveals a ten-dimensional symmetry that combine the four-dimensional spacetime vectors x^μ with the six-dimensional polarization vectors y^I [65]. In this section, we briefly review the occurrence of this symmetry and discuss the ten-dimensional null limit under which this generating function factorizes into a product of two functions with disc topology.

2.5.1. Fixed R-Charge Four-Point Correlators

Before introducing the notion of generating functions, let us briefly discuss four-point functions of scalar half-BPS operators with higher R-charges. This will mainly serve to introduce slight changes in notation compared to the previous sections. Throughout this section, we restrict ourselves to the planar limit, i.e. we keep only the leading terms in the $1/N_\mathrm{c} \to 0$ expansion.

The four-point function of half-BPS operators with arbitrary charges can be expanded perturbatively using the Lagrangian insertion procedure (2.36),

$$\begin{aligned}&\langle \mathcal{O}_{p_1}(x_1,y_1)\mathcal{O}_{p_2}(x_2,y_2)\mathcal{O}_{p_3}(x_3,y_3)\mathcal{O}_{p_4}(x_4,y_4)\rangle \\ &\qquad\qquad = \sum_{\ell=0}^{\infty} \frac{(i\,a)^\ell}{\ell!} \int \frac{\mathrm{d}^4 x_5}{4\pi^2} \cdots \frac{\mathrm{d}^4 x_{4+\ell}}{4\pi^2}\, G_{(p_1,p_2,p_3,p_4),\ell}\,.\end{aligned} \tag{2.51}$$

The loop integrand is obtained by inserting ℓ copies of the chiral on-shell Lagrangian $\mathcal{L}(x)$ into the correlator, as discussed in Section 2.4.4,

$$G_{(p_1,p_2,p_3,p_4),\ell} = \langle \mathcal{O}_{p_1}(x_1,y_1)\mathcal{O}_{p_2}(x_2,y_2)\mathcal{O}_{p_3}(x_3,y_3)\mathcal{O}_{p_4}(x_4,y_4)\mathcal{L}(x_5)\dots\mathcal{L}(x_{4+\ell})\rangle_{\text{tree}} \,. \tag{2.52}$$

Since all four-point correlators of half-BPS operators factorize into the universal superconformal invariant [66] (see Section 2.4.4), we can write

$$G_{(p_1,p_2,p_3,p_4),\ell} = C_{p_1p_2p_3p_4}\,\left(2x_{12}^2x_{13}^2x_{14}^2x_{23}^2x_{24}^2x_{34}^2\right)\mathcal{R}_{1234}\,F^{(\ell)}_{p_1,p_2,p_3,p_4}(x_i,y_i)\,, \tag{2.53}$$

where the normalization factor is given by [50]

$$C_{p_1p_2p_3p_4} = \frac{1}{2}\left(\frac{N_\text{c}}{2}\right)^{\frac{1}{2}\sum_i p_i - 2}\frac{p_1p_2p_3p_4}{(4\pi^2)^{\frac{1}{2}\sum_i p_i}}\,. \tag{2.54}$$

To make contact with the previous notation, let us note that for equal charges $p_i = 2$ one recovers the four-point correlator of $\mathbf{20'}$ operators. In this case,

$$G_{(2,2,2,2),\ell} = (4\pi^2)^\ell \int \prod_{k=1}^{\ell} \mathrm{d}^4\theta^+_{4+k}\;\mathcal{G}^{(0)}_{4+\ell;\ell}\,. \tag{2.55}$$

2.5.2. Generating Operators and Two- and Three-Point Functions

To make the hidden symmetry manifest, it is necessary to sum correlators with fixed R-charge configurations into a single generating function. To this end, we introduce a generating operator $\mathcal{O}(x,y)$ that packages the full tower of single-trace half-BPS scalar operators $\mathcal{O}_p(x,y)$ (2.29). It is defined as

$$\mathcal{O}(x,y) \equiv \sum_{p=1}^{\infty}\mathcal{O}_p(x,y)\,,\qquad \mathcal{O}_p(x,y) = \frac{1}{p}\left(\frac{8\pi^2}{N_\text{c}}\right)^{p/2}\operatorname{tr}[(y\cdot\Phi(x))^p]\,. \tag{2.56}$$

For the gauge group $\mathrm{SU}(N_\text{c})$, the sum effectively starts at $p=2$, corresponding to the $\mathbf{20'}$ operator. The normalization in (2.56) is chosen such that the prefactor $C_{p_1p_2p_3p_4}$ appearing in the four-point function is absorbed into the definition of the generating operators, thereby simplifying the resummation of correlators.

The two-point function of the generating operators is then given by

$$\langle \mathcal{O}(x_1,y_1)\mathcal{O}(x_2,y_2)\rangle = \sum_{p\geq 2}\frac{1}{p}\,(d_{12})^p\,, \qquad d_{ij} = \frac{-y_{ij}^2}{x_{ij}^2}\,. \tag{2.57}$$

Here, we slightly modified the definition of the polarization distance to

$$y_{ij}^2 = (y_i - y_j)^2 = -2\, y_i^I y_j^I\,, \tag{2.58}$$

so that it is directly analogous to the space-time distance $x_{ij}^2 = (x_i - x_j)^2$. This convention follows [65] and is adopted for convenience.

The three-point function of the generating operators takes the form [65]

$$\langle \mathcal{O}(x_1,y_1)\mathcal{O}(x_2,y_2)\mathcal{O}(x_3,y_3)\rangle = \frac{1}{N_\mathrm{c}}\, D_{12}D_{23}D_{31} + G_3^{\text{extremal}}\,, \tag{2.59}$$

where D_{ij} denotes the so-called fat propagator,

$$D_{ij} = \frac{d_{ij}}{1-d_{ij}} = d_{ij} + (d_{ij})^2 + \cdots = \frac{-y_{ij}^2}{X_{ij}^2}\,, \tag{2.60}$$

with the ten-dimensional distance defined as $X_{ij}^2 = (x_i - x_j)^2 + (y_i - y_j)^2$. The fat propagator thus resums an arbitrary number of standard propagators d_{ij} between the two operators.

The term G_3^{extremal} denotes an additional contribution beyond the triangle-like structure of the first term. Such contributions typically depend on the choice of gauge group and also appear in four- and higher-point correlators. They can be removed by passing from the single-trace basis to a single-particle basis [104]

$$\mathcal{O}_p(x,y) \;\to\; \mathcal{O}_p^{\text{sp}}(x,y) = \operatorname{tr}[(y\cdot\Phi(x))^p] + \text{multi-traces}\,. \tag{2.61}$$

In this basis, the operators are orthogonal to all pure multi-trace operators. We will work with these single-particle operators throughout this Section and Chapter 4. In the ten-dimensional null polygon limit, the extremal contributions vanish in any case, so for the subsequent Chapters this distinction will not play a role.

2.5.3. Four-Point Generating Function and Ten-Dimensional Symmetry

We now consider the planar four-point correlator of the generating operators,

$$\begin{aligned} G_4 &= \langle \mathcal{O}(x_1,y_1)\mathcal{O}(x_2,y_2)\mathcal{O}(x_3,y_3)\mathcal{O}(x_4,y_4)\rangle \\ &= \sum_{\ell=0}^{\infty} \frac{(i\,a)^\ell}{\ell!} \int \frac{\mathrm{d}^4 x_5}{4\pi^2} \dots \frac{\mathrm{d}^4 x_{4+\ell}}{4\pi^2}\, G_{4,\ell}\,. \end{aligned} \tag{2.62}$$

Using the Lagrangian insertion procedure (2.36), the loop corrections are expressed in terms of the loop integrand

$$G_{4,\ell} = \langle \mathcal{O}(x_1,y_1)\mathcal{O}(x_2,y_2)\mathcal{O}(x_3,y_3)\mathcal{O}(x_4,y_4)\mathcal{L}(x_5)\dots\mathcal{L}(x_{4+\ell})\rangle_{\text{tree}}\,, \tag{2.63}$$

where the insertions are given by the chiral on-shell Lagrangian (2.28). This object plays the role of a generating function, as it encodes all fixed R-charge correlators upon expanding in the polarization vectors y_i.

Since all four-point correlators of half-BPS operators decompose into the universal superconformal invariant, as discussed in Section 2.4.4, we can write

$$G_{4,\ell} = \left(2x_{12}^2 x_{13}^2 x_{14}^2 x_{23}^2 x_{24}^2 x_{34}^2\right) \mathcal{R}_{1234}\, \mathcal{F}^{(\ell)}(x_i,y_i)\,. \tag{2.64}$$

Here, $\mathcal{F}^{(\ell)}(x_i,y_i)$ is the natural generalization of the reduced correlator $F^{(\ell)}(x_i)$, which now also depends on the polarization vectors y_i. Expanding the generating operators in (2.56) into fixed charges then implies

$$\mathcal{F}^{(\ell)}(x_i,y_i) = \sum_{p_i\geq 2} F^{(\ell)}_{p_1p_2p_3p_4}(x_i,y_i)\,, \tag{2.65}$$

where, in particular, $F^{(\ell)}_{2222}(x_i,y_i) = F^{(\ell)}(x_i)$ is the reduced correlator of four $\mathbf{20'}$ operators.

The main proposal of [65] is that the reduced correlator of the generating function is given by

$$\mathcal{F}^{(\ell)}(x_i,y_i) = F^{(\ell)}(X_i)\,, \qquad X_i = x_i + y_i\,, \tag{2.66}$$

where it is understood that $y_i = 0$ for $i \geq 5$. In other words, all higher R-charge four-point loop integrands can be obtained from the $\mathbf{20'}$ correlator by promoting the four-dimensional distances to ten-dimensional ones. This is in agreement with the available data up to five loops [50, 51], and is conjectured to hold more generally.

Moreover, if one includes higher Kaluza–Klein modes of the Lagrangian in the loop integrand (2.63),

$$\mathcal{L}(x) \;\to\; \mathcal{L}(x,y) = \sum_{p\geq 2} \mathcal{L}_p(x,y)\,, \tag{2.67}$$

the relation (2.66) is conjectured to become exact without setting the polarization vectors of the Lagrangian insertions to zero. This has been explicitly verified up to three loops [69].

One of the questions that can be probed via the results of this work is to what extent this ten-dimensional symmetry persists for higher-point generating functions. It is important to note, however, that already at four points the symmetry is only manifest at the level of the reduced correlator, after factoring out the unique superconformal invariant. Since for five and higher points such a unique decomposition is no longer available, it will not be possible to draw a definitive conclusion about the persistence of the ten-dimensional symmetry.

2.5.4. The Ten-Dimensional Null Limit and Octagon Factorization

A particularly powerful application of the formulation of correlators in terms of a single generating function arises in the ten-dimensional null-square limit. This limit is defined by requiring the ten-dimensional distances between adjacent points to vanish, $X_{i,i+1}^2 \to 0$, such that the operators form a light-like polygon in ten dimensions.

In this limit, the generating function G_4 factorizes into the square of a fundamental building block known as the *octagon* $\mathbb{O}$ [70, 71]. The octagon captures the large R-charge limit of the four-point function, in which adjacent operators are connected by large bundles of propagators. As a result, planar Feynman diagrams are suppressed unless they are constrained by the perimeter of the square.

At the level of the loop integrand, this factorization can be made precise using the generating function (2.63). Taking the residue in the limit $d_{i,i+1} \to 1$, one finds

$$\operatorname*{Res}_{d_{i,i+1}=1} G_{4,\ell} = \sum_{\ell_1+\ell_2=\ell} M_{4,\ell_1}\, M_{4,\ell_2}\,, \tag{2.68}$$

where the sum reflects the fact that the Lagrangian insertions can be distributed between the inside and the outside of the null ten-dimensional square in all possible ways. The full octagon is then obtained by resumming these contributions perturbatively

$$\mathbb{O} = \sum_{\ell=0}^{\infty} \frac{(i\,a)^{\ell}}{\ell!} \int \frac{\mathrm{d}^4 x_5}{4\pi^2} \dots \frac{\mathrm{d}^4 x_{4+\ell}}{4\pi^2}\, M_{4,\ell}\,. \tag{2.69}$$

The ten-dimensional null limit provides a natural generalization of the bosonic correlator/amplitude duality discussed in Section 2.4.5. In four dimensions, the light-like limit of the correlator of $\mathbf{20'}$ operators is dual to the square of the massless MHV amplitude. In the present case, performing the ten-dimensional null limit on the generating function yields a polygonal object. It is conjectured that this object is related to scattering amplitudes on the Coulomb branch of the theory [65].

In Chapter 5 and Chapter 6, we will generalize the construction of polygon functions to higher-point configurations. In particular, we determine the loop integrand of general n-gons up to two loops and study the five-point case in detail, by using bootstrap methods to compute the pentagon loop integrand up to five-loop order.

3. Twistor Space

Correlation functions of local operators are central observables in $\mathcal{N} = 4$ SYM, capturing a wealth of dynamical information. Among these, protected half-BPS operators are of particular interest due to them being the simplest operators in the theory. Yet, dynamical information of other operators are still encoded in their correlation functions via the operator product expansion. However, computing weak coupling corrections using conventional spacetime Feynman diagrams is a notoriously difficult task, as the number and complexity of diagrams increase rapidly with the number of points.

To circumvent these difficulties, it is useful to consider the reformulation of $\mathcal{N} = 4$ SYM in twistor space. In this twistor formulation, individual diagrammatic contributions transform covariantly under supersymmetry, thereby making the symmetry much more transparent than in a conventional spacetime Feynman diagram expansion. In particular, supersymmetry is effectively built into the formalism at the level of the fundamental building blocks. Moreover, the enlarged gauge freedom inherent in this description allows correlation functions to be computed as sums of twistor graphs involving only propagators, without the need for interaction vertices at tree level.

A key development in this framework is the introduction of determinant operators, which serve as generating functions for all single-trace half-BPS operators [69]. In the following, we review how these operators can be realized in twistor space (Section 3.2) and how the associated twistor Feynman rules for correlation functions are obtained (Section 3.3). We further explain how these rules reduce to the Feynman rules used for computing correlation functions of the chiral stress-tensor supermultiplet, as introduced in [105], in Section 3.4. We start by explaining the basic twistor space geometry and its relation to ordinary spacetime in Section 3.1.

Our presentation follows closely [69,105], while for the fundamental aspects of twistor space we refer to [106].

3.1. Foundations of Twistor Space

The calculation of correlation functions in $\mathcal{N} = 4$ SYM is significantly streamlined by moving from Minkowski spacetime to twistor space. This transition is motivated by the fact that the self-dual sector of SYM is free in an appropriate gauge on twistor space, allowing multi-point correlators to be computed using a simplified set of Feynman rules that involve only propagators and no integration vertices. In this section, we establish the geometric correspondence between chiral Minkowski superspace and super-twistor space.

3.1.1. Bosonic Twistor Space

We begin by considering complexified Minkowski space $\mathbb{M}_{\mathbb{C}} \cong \mathbb{C}^4$, which admits a natural description in spinor notation. A point in space-time is represented by a bispinor $x^{\alpha\dot{\alpha}}$, where $\alpha, \dot{\alpha} = 1, 2$ are spinor indices associated with the two $SL(2, \mathbb{C})$ factors of the complexified Lorentz group. It is related to the usual vector notation using the 2×2 Pauli matrices by

$$x^{\alpha\dot{\alpha}} = (\sigma_\mu)^{\alpha\dot{\alpha}}\, x^\mu\,. \tag{3.1}$$

Bosonic twistor space is defined as the complex projective space $\mathbb{CP}^3$, i.e. the space of complex lines through the origin in $\mathbb{C}^4$. This means that its points are equivalence classes of non-zero vectors $Z^I \in \mathbb{C}^4$ under the identification $Z^I \sim c\, Z^I$ with $c \in \mathbb{C}^*$. A point in twistor space is described by homogeneous coordinates, which we decompose into two spinors as

$$Z^I = (\lambda_\alpha, \mu^{\dot{\alpha}}) = (\lambda_1, \lambda_2, \mu^1, \mu^2)\,. \tag{3.2}$$

The fundamental relation between space-time and twistor space is the *incidence relation*

$$\mu^{\dot{\alpha}} = x^{\alpha\dot{\alpha}}\lambda_\alpha\,. \tag{3.3}$$

For fixed x, this equation defines a line, i.e. a linearly embedded $\mathbb{CP}^1$, inside $\mathbb{CP}^3$, with λ_α serving as homogeneous coordinates on that line. Conversely, a point Z in twistor space does not correspond to a single point in space-time, but rather to a whole two-dimensional surface: it picks out all space-time points that share a common null direction encoded in Z. These points form a totally null plane (an α-plane), meaning that any two of them are connected by light-like separations.

Given two twistors Z_1 and Z_2 satisfying the incidence relation (3.3) for the same point $x^{\alpha\dot{\alpha}}$, this point can be reconstructed from their skew product

$$X^{IJ} = Z_1^I Z_2^J - Z_2^I Z_1^J = \langle\lambda_1\lambda_2\rangle \begin{pmatrix} \epsilon_{\alpha\beta} & -ix_{\alpha}^{\dot{\beta}} \\ ix^{\dot{\alpha}}_{\beta} & -\frac{1}{2}x^2\epsilon^{\dot{\alpha}\dot{\beta}} \end{pmatrix}, \tag{3.4}$$

where $\langle\lambda_1\lambda_2\rangle = \epsilon^{\alpha\beta}\lambda_{1\alpha}\lambda_{2\beta}$ and $x^2 = 2\det x = x^{\alpha\dot{\alpha}}x_{\alpha\dot{\alpha}}$. Thus, the pair of twistors determines the space-time point x, up to an overall normalization.

This correspondence implies that two space-time points x_i and x_j are null-separated if and only if the corresponding twistor lines intersect. This provides a particularly simple geometric characterization of light-like separation. Consider two points x_1 and x_2 in space-time, described by the twistor pairs $Z_{i,1}$ and $Z_{i,2}$ for $i = 1, 2$, such that

$$X_i^{IJ} = Z_{i,1}^I Z_{i,2}^J - Z_{i,2}^I Z_{i,1}^J\,. \tag{3.5}$$

Their space-time distance can then be written as

$$\begin{aligned} x_{ij}^2 = (x_i - x_j)^2 \propto{}& \frac{1}{4}\epsilon_{IJKL}X_i^{IJ}X_j^{KL} \\ ={}& \frac{1}{4}\epsilon_{IJKL}\epsilon^{ab}Z_{i,a}^I Z_{i,b}^J \epsilon^{cd}Z_{j,c}^K Z_{j,d}^L \equiv \langle Z_{i,1}Z_{i,2}Z_{j,1}Z_{j,2}\rangle\,, \end{aligned} \tag{3.6}$$

where the four-bracket denotes the determinant of the four twistors appearing in it. More precisely, the distance is obtained by dividing this four-bracket by the product of the two-brackets $\langle\lambda_{i,1}\lambda_{i,2}\rangle\langle\lambda_{j,1}\lambda_{j,2}\rangle$. Hence, two space-time points are light-like separated precisely when the corresponding twistor lines intersect, and vice versa (cf. Figure 3.1).

3.1.2. Super-Twistor Space

To describe chiral $\mathcal{N} = 4$ supermultiplets, the bosonic twistor space must be extended to include anti-commuting Grassmann coordinates η^A ($A = 1, \ldots, 4$), which transform in the fundamental representation of the $SU(4)$ R-symmetry group. This results in the projective super-twistor space $\mathbb{CP}^{3|4}$, given by the homogeneous coor-

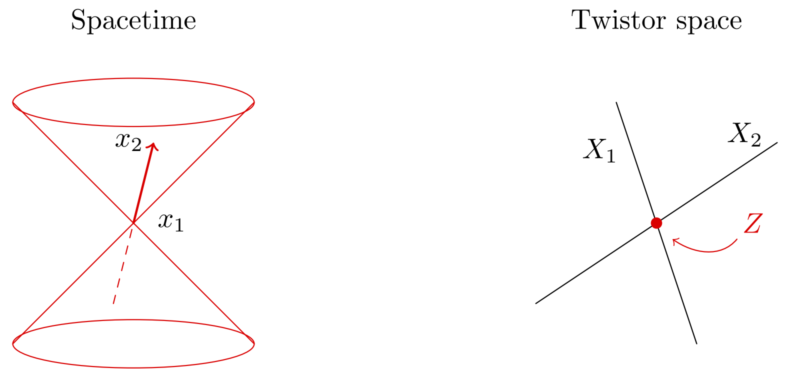

Figure 3.1.: Depiction of points in Minkowski space-time and twistor space. Points in space-time correspond to lines in twistor space, and null-separated points correspond to intersecting lines. Figure inspired by [106].

dinates:

$$\mathcal{Z}^I = (Z^I, \eta^A) = (\lambda_\alpha, \mu^{\dot{\alpha}}, \eta^A) \tag{3.7}$$

subject to the projective identification $\mathcal{Z} \sim c\mathcal{Z}$ for $c \in \mathbb{C}^*$.
A point in chiral Minkowski superspace $(x^{\alpha\dot{\alpha}}, \theta^{A\alpha})$ is mapped to a super-line in $\mathbb{CP}^{3|4}$ via the incidence relations:

$$\mu^{\dot{\alpha}} = x^{\alpha\dot{\alpha}}\lambda_\alpha, \quad \eta^A = \theta^{A\alpha}\lambda_\alpha \tag{3.8}$$

where $\theta^{A\alpha}$ are the chiral odd coordinates of the superspace. This identifies chiral Minkowski superspace with the space of lines in projective super-twistor space.

3.2. Twistor Reformulation of $\mathcal{N} = 4$ SYM

In this section, we describe the formulation of $\mathcal{N} = 4$ SYM as an expansion around its self-dual sector, both in space-time and in twistor space. In this framework, loop integrands can be interpreted as tree-level correlators in the self-dual theory, involving the operators of interest together with insertions of the non-self-dual part of the Lagrangian. Moreover, in twistor space the self-dual sector can be made manifestly Gaussian due to the enhanced gauge freedom, in particular upon choosing the axial gauge. This provides the main motivation for uplifting the theory to twistor space.

In this chapter, we make a few important changes in conventions. The main reason is to align our notation with the existing literature on generating functions [65, 69]. We stick to this change in notation in Chapter 4, Chapter 5 and Chapter 6.

First, concerning the gauge group, we now consider $U(N_\mathrm{c})$ instead of $SU(N_\mathrm{c})$. Passing from $SU(N_c)$ to $U(N_c)$ effectively amounts to adding a decoupled $U(1)$ sector. As a result, for correlation functions of single-trace operators the only modification is a change in the number of generators from N_c^2-1 to N_c^2, affecting overall normalization factors, which appear, for example, in (2.41) and (2.42). This choice will later be convenient when summing propagator contributions into a geometric series. For the same reason, we also rescale the scalar fields as

$$\Phi^{AB}(x) \to \frac{2\pi}{\sqrt{N_\mathrm{c}}}\,\Phi^{AB}(x)\,. \tag{3.9}$$

With this rescaling, the two-point function of two scalar fields in (2.40) becomes

$$\langle \Phi^{++}(1)\Phi^{++}(2)\rangle^{(0)} = \frac{1}{N_\mathrm{c}}\frac{y_{12}^2}{x_{12}^2}\,, \tag{3.10}$$

so that, in particular, the two-point function (2.41) is free of additional factors of N_c.

3.2.1. The Chalmers–Siegel Procedure

Standard $\mathcal{N}=4$ SYM can be viewed as an expansion around its self-dual part through the Chalmers-Siegel procedure [107]. In this formulation, the action is split into a self-dual (SD) part and an interaction term:

$$S_{\mathcal{N}=4} = S_{\mathrm{SD}} + a\int \frac{\mathrm{d}^4x}{4\pi^2}\,\mathcal{L}_{\mathrm{int}}(x), \tag{3.11}$$

where a is the 't Hooft coupling and the self-dual action is given by

$$\begin{aligned} S_{\mathrm{SD}} = \frac{N_\mathrm{c}}{4\pi^2}\int \mathrm{d}^4x\ \mathrm{tr}\Big(&G_{\alpha\beta}F^{\alpha\beta} - \tilde{\Psi}^{\dot{\alpha}}_A D_{\alpha\dot{\alpha}}\Psi^{\alpha A} - \frac{1}{4}D_\mu\Phi_{AB}D^\mu\Phi^{AB} \\ &+ \frac{1}{2}\Phi^{AB}[\tilde{\Psi}_{\dot{\alpha}A},\tilde{\Psi}^{\dot{\alpha}}_B]\Big)\,. \end{aligned} \tag{3.12}$$

Here, $G_{\alpha\beta}$ is a Lagrange multiplier field that enforces the on-shell condition of the field strength $F_{\alpha\beta}=0$ in the self-dual theory. To obtain the full $\mathcal{N}=4$ SYM action, one has to include the non-self-dual interaction given by

$$\mathcal{L}_{\rm int}(x) = -N_{\rm c}\,{\rm tr}\left(\frac{1}{2}G_{\alpha\beta}G^{\alpha\beta} - \frac{1}{2}\phi_{AB}[\psi^{\alpha A},\psi^{B}_{\alpha}] - \frac{1}{32}[\phi_{AB},\phi_{CD}][\phi^{AB},\phi^{CD}]\right)\,. \tag{3.13}$$

This additional term enforces the equation of motion $G_{\alpha\beta} = F_{\alpha\beta}/a$, thereby recovering the usual $\mathcal{N} = 4$ SYM action (2.1). Moreover, the interaction Lagrangian then coincides with the on-shell chiral Lagrangian (2.28), which appears as the top component of the chiral stress-tensor multiplet.

The Chalmers–Siegel procedure thus provides a reorganization of perturbation theory in which the self-dual sector serves as the starting point, while the non-self-dual part is treated perturbatively. As a consequence, correlation functions evaluated with respect to $S_{\rm SD}$ reproduce the tree-level correlator of the full theory. The reason is that the self-dual action already contains the propagators and interaction vertices required at leading order, whereas each insertion of the non-self-dual part is accompanied by an additional power of a and therefore generates higher-order corrections. Including the non-self-dual interaction thus restores the full correlator order by order in the coupling.

3.2.2. $\mathcal{N} = 4$ SYM in Twistor Space

The Penrose transform [24] provides a correspondence between fields defined on space-time and on twistor space. In the case of $\mathcal{N} = 4$ SYM, all component fields can be assembled into a single $(0,1)$-form connection $\mathcal{A}$ on twistor space, which admits a Grassmann expansion of the form

$$\begin{aligned}\mathcal{A}(Z,\bar{Z},\eta) =& A(Z,\bar{Z}) + \eta^{A}\Psi_{A}(Z,\bar{Z}) + \frac{1}{2!}\eta^{A}\eta^{B}\Phi_{AB}(Z,\bar{Z}) \\ &+ \frac{1}{3!}\epsilon_{ABCD}\eta^{A}\eta^{B}\eta^{C}\tilde{\Psi}^{D}(Z,\bar{Z}) + \frac{1}{4!}\epsilon_{ABCD}\eta^{A}\eta^{B}\eta^{C}\eta^{D}G(Z,\bar{Z})\,.\end{aligned} \tag{3.14}$$

Here, Z^{I} denote homogeneous twistor coordinates and η^{A} are fermionic variables. The Penrose transform provides a one-to-one mapping between these Grassmann components and physical fields on spacetime: the components A and G map to the anti-self-dual and self-dual parts of the field strength tensor, Ψ_{A} and $\tilde{\Psi}^{D}$ correspond to the Weyl fermions, and finally The scalar component ϕ_{AB} produces the six scalar fields of the theory.

As reviewed in [27, 29], this correspondence can be formulated off shell such that the self-dual sector of the theory maps to a holomorphic Chern–Simons action on twistor space,

$$S_{\text{SD}} = N_{\text{c}} \int \Omega_{3|4} \,\text{tr} \left(\mathcal{A} \bar{\partial} \mathcal{A} + \frac{2}{3} \mathcal{A}^3 \right), \tag{3.15}$$

where the integration is over $\mathbb{CP}^{3|4}$ and $\Omega_{3|4}$ denotes the canonical holomorphic measure

$$\Omega_{3|4} = \frac{1}{(2\pi i)^3 4!} \epsilon_{IJKL} Z^I dZ^J dZ^K dZ^L \, d^4\eta \,, \tag{3.16}$$

making the self-dual part of the action local in twistor space. The non-self-dual interaction term, on the other hand, is non-local on twistor space and is written as an integral over the moduli space of lines $\mathbb{CP}^1 \subset \mathbb{CP}^{3|4}$ corresponding to space-time points x as in (3.11). The interacting Langragian is given by

$$\mathcal{L}_{\text{int}}(x) = N_{\text{c}} \int d^8\theta \, \log\det \left(\bar{\partial} + \mathcal{A} \right)\big|_{\mathbb{CP}^1} . \tag{3.17}$$

In practice, this expression is understood through its formal expansion,

$$\log\det(\bar{\partial} + \mathcal{A}) - \log\det \bar{\partial}\big|_{\mathbb{CP}^1} = \sum_{m=1}^{\infty} \frac{(-1)^{m+1}}{m} \,\text{tr} \left(\bar{\partial}^{-1} \mathcal{A}_1 \cdots \bar{\partial}^{-1} \mathcal{A}_m \right), \tag{3.18}$$

which generates the interaction vertices.

A key feature of the twistor formulation is the presence of an enlarged gauge symmetry. In particular, one has the freedom to fix a reference twistor $\mathcal{Z}_*$ and impose that the connection vanishes along this direction [108]. In this so-called axial gauge, the cubic interaction term in the holomorphic Chern–Simons action drops out, so that the self-dual sector becomes Gaussian. The propagator is then given by [36]

$$\langle \mathcal{A}^a(Z_1) \mathcal{A}^b(Z_2) \rangle = \frac{1}{N_{\text{c}}} \bar{\delta}^{2|4}(\mathcal{Z}_1, \mathcal{Z}_2, \mathcal{Z}_*) \, \delta^{ab}, \tag{3.19}$$

where $\bar{\delta}^{2|4}(\mathcal{Z}_1, \mathcal{Z}_2, \mathcal{Z}_*)$ is a projective delta function defined by

$$\bar{\delta}^{2|4}(\mathcal{Z}_1, \mathcal{Z}_2, \mathcal{Z}_*) = \frac{1}{(2\pi i)^2} \int_{\mathbb{C}^2} \frac{\text{d}s \,\text{d}t}{s\, t} \, \bar{\delta}^{4|4}(s\mathcal{Z}_1 + t\mathcal{Z}_2 + \mathcal{Z}_*) \,. \tag{3.20}$$

It is a homogeneous $(0,2)$-form on twistor space that enforces the three super-twistors, that are its arguments, to be collinear in the projective space. We explicitly displayed the color indices of the fields by $\mathcal{A} = \mathcal{A}^a T^a$, where T^a are the generators of $\mathrm{U}(N_\mathrm{c})$ in the fundamental representation. The localization of the propagator on such configurations greatly simplifies perturbative computations in this formulation.

3.3. Superoperators and Twistor Feynman Rules

In this section, we explain how to compute correlators of the generalized operators (2.56) in the twistor reformulation of $\mathcal{N} = 4$ SYM, following [69]. As a reminder, these operators combine the $\mathbf{20'}$ operators with all their higher R-charge counterparts into a single object[1]

$$\mathcal{O}(x,y) \equiv \sum_{p=1}^{\infty} \mathcal{O}_p(x,y)\,, \qquad \mathcal{O}_p(x,y) = \frac{1}{p}\,\mathrm{tr}\left[(y\cdot\Phi(x))^p\right] + \text{multi-traces}\,. \tag{3.21}$$

Here, we work in the single-particle basis [104], as discussed around (2.61). By adding suitable multi-trace contributions, the operators become orthogonal to all pure multi-trace states.
We now consider the chiral supermultiplet associated with this generalized operator. Acting with the supercharges (cf. (2.30)), we obtain

$$\mathbb{O}(x,\theta^+,y) = e^{\theta^{+a}_{\alpha} Q^{\alpha}_{a}}\,\mathcal{O}(x,y) = \mathcal{O}(x,y) + \cdots + \frac{(\theta^+)^4}{N_\mathrm{c}}\,\mathcal{L}_\mathrm{int}(x,y)\,. \tag{3.22}$$

Here, $\mathcal{L}_\mathrm{int}(x,y)$ denotes the extension of the chiral on-shell Lagrangian including all higher Kaluza–Klein modes. The normalization is chosen such that in the limit $y \to 0$ one recovers the chiral, on-shell interaction Lagrangian,

$$\mathcal{L}_\mathrm{int}(x,y)\big|_{y\to 0} = \mathcal{L}_\mathrm{int}(x)\,, \tag{3.23}$$

in agreement with (3.13).

3.3.1. Half-BPS Operators in Twistor Space

In twistor space, the Grassmann variables η^A are related to the chiral Grassmann coordinates $\theta^{A\alpha}$ in Minkowski space via the incidence relation (3.8). Using the

[1] Compared to (2.56), we drop the N_c-dependent normalization, as it is already absorbed into the field normalization in (3.9), which is used throughout this chapter.

decomposition (2.15), one finds

$$\eta^A = \theta^A_\alpha \lambda^\alpha = \left(\theta^{+a}_\alpha\, \bar{u}^A_{+a} + \theta^{-a'}_\alpha\, \bar{u}^A_{-a'}\right) \lambda^\alpha = \theta^{+a}_\alpha\, \bar{u}^A_{+a}\, \lambda^\alpha + \psi^{a'}\, \bar{u}^A_{-a'}\,, \tag{3.24}$$

where we introduced $\psi^{a'} = \theta^{-a'}_\alpha \lambda^\alpha$. In analytic superspace, the half-BPS condition corresponds to independence of the variables θ^-. In twistor space, this translates into the condition

$$\frac{\partial}{\partial \psi^{a'}} \mathbb{O}(x, \theta^+, y) = \bar{u}^A_{-a'} \frac{\partial}{\partial \eta^A} \mathbb{O}(x, \theta^+, y) = 0\,, \tag{3.25}$$

i.e. the supermultiplet depends only on the projected variables (λ, ψ) associated with the chiral sector.

This condition admits a natural geometric interpretation: each operator is supported on a superline $\mathbb{CP}^{1|2} \subset \mathbb{CP}^{3|4}$ parametrized by (λ, ψ) and corresponding to a point (x, y, θ^+) in superspace. The main proposal of [69] is that this leads to the following representation of the operator in twistor space,

$$\mathbb{O}(x, \theta^+, y) = -\log \int \mathcal{D}\alpha\, \mathcal{D}\beta\; \exp\left(\int_{\mathbb{CP}^{1|2}} \frac{\langle \lambda\, d\lambda \rangle\, d^2\psi}{2\pi i}\; \alpha(\lambda, \psi)\, (\bar{\partial} + \mathcal{A} + \bar{\delta}^{1|2}_{\mu,\lambda})\, \beta(\lambda, \psi) \right), \tag{3.26}$$

where α and β are fermionic superfields transforming in the anti-fundamental and fundamental representations of $\mathrm{U}(N_\mathrm{c})$. This defines a Gaussian model supported on the superline $\mathbb{CP}^{1|2}$ associated with the point (x, y, θ^+). The term $\bar{\delta}^{1|2}_{\mu,\lambda}$ serves to localize the fields to a reference point μ on the line, removing zero modes, while the final correlators are independent of this choice.

The fields α and β can be integrated out explicitly by determining their superpropagator. It takes the simple form [69]

$$\langle \beta(\lambda_i, \psi_i)\, \alpha(\lambda_j, \psi_j) \rangle = 1 + R(\lambda_i, \lambda_j, \mu) \;\equiv\; \Delta(\lambda_i, \lambda_j, \mu)\,. \tag{3.27}$$

Here we use the shorthand $\langle \lambda_i \lambda_j \rangle = \epsilon_{ab} \lambda_i^a \lambda_j^b$, and the R-invariant is defined as

$$R(\lambda_i, \lambda_j, \lambda_k) = \frac{\delta^{0|2}(\langle \lambda_i \lambda_j \rangle \psi_k + \langle \lambda_j \lambda_k \rangle \psi_i + \langle \lambda_k \lambda_i \rangle \psi_j)}{\langle \lambda_i \lambda_j \rangle \langle \lambda_j \lambda_k \rangle \langle \lambda_k \lambda_i \rangle}\,. \tag{3.28}$$

This object is a natural superconformal invariant, enforcing the fermionic constraint that three points in $\mathbb{CP}^{1|2}$ lie on the same line. It has appeared in earlier twistor-space constructions [105].

Using the propagator Δ, the fields α and β can be integrated out, yielding a representation of the operator as a sum over single-trace vertices,

$$\mathbb{O}(x,\theta^+,y) = \sum_{n=1}^{\infty} \frac{1}{n} \int_{\mathbb{CP}^{1|2}} \prod_{a=1}^{n} \Omega_a^{1|2}\, \Delta(\lambda_a,\lambda_{a+1},\mu)\ \mathrm{tr}\left(\prod_{a=1}^{n} \mathcal{A}(Z(\lambda_a,\psi_a,\theta^+))\right)\,, \tag{3.29}$$

with cyclic identification $\lambda_{n+1}=\lambda_1$. The measure is given by

$$\Omega_a^{1|2} = \frac{\langle \lambda_a\, d\lambda_a\rangle}{2\pi i}\, d^2\psi_a\,. \tag{3.30}$$

Using this representation of the supermultiplet, one obtains a set of twistor Feynman rules for computing correlators with respect to the self-dual sector of the twistor action. As discussed previously, evaluating correlators in the self-dual theory corresponds to computing tree-level correlators of the full theory. In axial gauge, the self-dual action becomes purely quadratic, which significantly simplifies the computation.

3.3.2. Twistor Feynman Rules for the Supercorrelator

Using the representation of the superoperators in (3.29), the tree-level correlator of n such operators can be computed as

$$\begin{aligned}\left\langle \prod_{i=1}^{n} \mathbb{O}(x_i,\theta_i^+,y_i)\right\rangle_{\text{tree}} &= \int \mathcal{D}\mathcal{A}\, \exp\left[N_{\mathrm{c}} \int \Omega_{3|4}\ \mathrm{tr}\left(\frac{1}{2}\,\mathcal{A}\,\bar\partial\mathcal{A}\right)\right] \\ &\times \left[\prod_{i=1}^{n}\sum_{m=1}^{\infty} \frac{1}{m}\int_{\mathbb{CP}^{1|2}} \prod_{a=1}^{m} \Omega_{ia}^{1|2}\, \Delta(\lambda_{ia},\lambda_{i,a+1},\mu_i)\ \mathrm{tr}\left(\prod_{a=1}^{m}\mathcal{A}(\mathcal{Z}_{ia})\right)\right]\,. \end{aligned} \tag{3.31}$$

Here, the self-dual twistor action in axial gauge has been inserted. Using the propagator of twistor superfields (3.19), the vertices in the above expression, represented by the traces, are connected. The delta functions in the propagator localize the integrals over $\mathbb{CP}^{1|2}$, which leads to a set of twistor Feynman rules, that can be used to compute the correlator efficiently. We summarize the essential steps here and refer to Section 3 in [69] for a detailed derivation.

Each supermultiplet $\mathbb{O}_i = \mathbb{O}(x_i, y_i, \theta_i)$ is associated with a superline $\mathbb{CP}^{1|2}$ in twistor space, parameterized by (λ, ψ) as

$$Z_i(\lambda) = \lambda^1 Z_{i,1} + \lambda^2 Z_{i,2} = \lambda^\beta Z_{i,\beta}\,, \tag{3.32}$$

$$\eta_i(\lambda, \psi) = \lambda^\alpha (\theta_i)^a_\alpha W_{i,a} + \psi^{a'} Y_{i,a'}\,. \tag{3.33}$$

Here, $Z_{i,\beta}$ denote two bosonic twistors spanning the $\mathbb{CP}^1$ line corresponding to the point x_i. We introduced the notation $(\bar{u}_+)^A_{i,a} = W^A_{i,a}$ and $(\bar{u}_-)^A_{i,a'} = Y^A_{i,a'}$ for the harmonic variables. The bosonic twistors and Grassmann decomposition can be chosen as (with $B = (b, b')$)

$$(Z_{i,\beta})_{\alpha\dot{\alpha}} = (\epsilon_{\alpha\beta},\, x_{i,\beta\dot{\alpha}})\,, \qquad W^B_{i,a} = \left(\delta^b_a,\, 0\right)\,, \qquad Y^B_{i,a'} = \left(y^b_{i,a'},\, \delta^{b'}_{a'}\right)\,. \tag{3.34}$$

With this parametrization, the basic invariants are given by

$$\langle Z_{i,1} Z_{i,2} Z_{j,1} Z_{j,2} \rangle = x^2_{ij}\,, \tag{3.35}$$

$$\langle Y_{i,1} Y_{i,2} Y_{j,1} Y_{j,2} \rangle = -y^2_{ij}\,. \tag{3.36}$$

Performing the $\mathbb{CP}^{1|2}$ integrations in (3.31) localizes the parameters (λ, ψ) to

$$\lambda^\alpha_{ij} = \epsilon^{\alpha\beta} \frac{\langle Z_{i,\beta} Z_\star Z_{j,1} Z_{j,2} \rangle}{\langle Z_{i,1} Z_{i,2} Z_{j,1} Z_{j,2} \rangle}\,, \qquad \psi^{a'}_{ij} = \epsilon^{a'b'} \frac{\langle Y_{i,b'} E_{ij} Y_{j,1} Y_{j,2} \rangle}{\langle Y_{i,1} Y_{i,2} Y_{j,1} Y_{j,2} \rangle}\,, \tag{3.37}$$

where $Z_\star$ is the reference twistor introduced by the axial gauge. E_{ij} is given by

$$E^A_{ij} = \lambda^\alpha_{ij} (\theta_i)^a_\alpha W^A_{i,a} + \lambda^\alpha_{ji} (\theta_j)^a_\alpha W^A_{j,a}\,. \tag{3.38}$$

After stripping out the localizing delta functions from the bulk propagators (3.19), one is left with the ordinary propagator

$$d_{ij} = \frac{-y^2_{ij}}{x^2_{ij}} = \frac{\langle Y_{i,1} Y_{i,2} Y_{j,1} Y_{j,2} \rangle}{\langle Z_{i,1} Z_{i,2} Z_{j,1} Z_{j,2} \rangle}\,. \tag{3.39}$$

Since the superoperators contain contributions from arbitrarily high R-charges, these propagators appear as a geometric series, leading to an effective "fat" propagator

$$D_{ij} = d_{ij} + d^2_{ij} + \cdots = \frac{1}{1 - d_{ij}} = \frac{x^2_{ij}}{x^2_{ij} + y^2_{ij}}\,, \tag{3.40}$$

where the ten-dimensional distance naturally appears in the denominator.

Finally, the remaining building blocks are the Δ-functions evaluated on the localized solutions (3.37). For convenience, we introduce the shorthand notation

$$\Delta^i_{jk\mu} \equiv \Delta(\lambda_{ij}, \lambda_{ik}, \mu_i)\,. \tag{3.41}$$

These factors appear at each vertex i, between very two adjacent bulk propagators that connects it to other vertices j and k. For a vertex i connected to k vertices $j_1, \ldots, j_k$, we can therefore introduce the vertex factor

$$V^i_{j_1 j_2 \cdots j_k} \equiv \Delta^i_{j_1 j_2 \mu}\, \Delta^i_{j_2 j_3 \mu} \cdots \Delta^i_{j_k j_1 \mu}\,. \tag{3.42}$$

Using the properties of the R-invariant (3.28), this cyclic expression can be simplified [69]. In particular, for a vertex of valency two one finds

$$V^i_{j_1 j_2} = \Delta^i_{j_1 j_2 \mu}\, \Delta^i_{j_2 j_1 \mu} = 1\,, \tag{3.43}$$

while for higher valency $k \geq 3$ the vertex factor reduces to

$$V^i_{j_1 j_2 \cdots j_k} = \Delta^i_{j_1 j_2 j_3}\, \Delta^i_{j_1 j_3 j_4} \cdots \Delta^i_{j_1 j_{k-1} j_k}\,. \tag{3.44}$$

Let us summarize the outlined rules in the following box:

In order to compute the tree-level correlator of the superoperators $\mathbb{O}$ (cf. (3.31)), the following twistor Feynman rules Φ have to be applied to all relevant graphs:

- For each edge connecting two vertices i and j, one inserts a fat propagator,

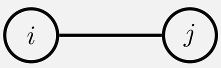

$$D_{ij} = \frac{d_{ij}}{1 - d_{ij}}\,. \tag{3.45}$$

- Each vertex i with outgoing lines $j_1, j_2, \ldots, j_k$, with $k \geq 3$, is dressed by a vertex factor,

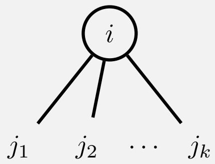

$$V^i_{j_1 j_2 \cdots j_k} = \Delta^i_{j_1 j_2 j_3} \Delta^i_{j_1 j_3 j_4} \ldots \Delta^i_{j_1 j_{k-1} j_k} \,. \tag{3.46}$$

  Here, each factor Δ is given by

$$\Delta^i_{jkl} = 1 + R^i_{jkl} \,, \qquad R^i_{jkl} = R(\lambda_{ij}, \lambda_{ik}, \lambda_{il}) \,, \tag{3.47}$$

  where the R-invariant is defined in (3.28), and the on-shell twistor variables in (3.37).

3.3.3. Twistor Graphs for the Supercorrelator

The final ingredient required for the computation of the super-correlator is the specification of the class of graphs that must be summed over. Working in the large-N_c limit, this sum runs over all inequivalent ribbon graphs (also referred to as fat graphs). In addition to the set of vertices and edges, such graphs encode a cyclic ordering of the edges at each vertex. This ordering captures the color structure of the underlying Feynman diagrams in the planar limit. As a consequence of this additional structure, the faces of the graph are well-defined and form disks. Together with the vertices and edges, they define a punctured compact surface on which the graph is embedded. These surfaces are precisely those appearing in the genus expansion introduced by 't Hooft [11]. In the sum over graphs, one must include configurations with multiple edges connecting the same pair of vertices, provided that these edges are homotopically distinct. Edges that are homotopically equivalent, on the other hand, are to be identified. In order to compute the planar, connected super-correlator $\mathbb{G}_{n+\ell}$, one therefore has to consider all planar, connected ribbon graphs with $(n+\ell)$ vertices and an arbitrary number of edges. In the single-particle basis, only graphs with vertices of valency at least two contribute (see Table 3.1).

In practice, there exist several ways to generate the complete set of ribbon graphs for fixed genus and number of vertices. One algorithm that we employ is described

genus\\n	3	4	5	6	7	8	9
0	1	4	21	216	3318	62767	1313096
1	21	584	20186	712862	24870531		
2	3910	542735					
3	2902406						

Table 3.1.: Numbers of graphs that contribute to the planar, connected super-correlator $\mathbb{G}_n$ for various numbers of points n and different genera, in the single-particle basis [1]. These are all planar, connected ribbon graphs with n vertices, where all vertices have valency at least two. The numbers were obtained by explicit graph construction.

in Appendix B of [109]. It constructs all inequivalent graphs by successively adding bridges to a given set of ribbon graphs in all possible ways, starting from the "empty" graph containing only vertices and no edges. Graphs whose genus exceeds the desired value are discarded. In this approach, the cyclic ordering of edges at each vertex is fixed from the outset. An alternative method is described around Table 1 of [69]. One begins by generating all ordinary graphs with the required number of vertices. Each such graph is then promoted to a set of ribbon graphs by assigning all possible cyclic orderings of edges at each vertex. Finally, each edge is split into all homotopically distinct configurations, subject to the constraint that the genus is not increased.

3.4. The Stress-Tensor Multiplet in Twistor Space

We conclude this chapter by reviewing the computation of correlators of the chiral stress-tensor multiplet in the twistor reformulation of $\mathcal{N}=4$ SYM. The corresponding twistor Feynman rules were derived in [105].

The starting point is to obtain a representation of the stress-tensor multiplet $\mathbb{O}_2$ in twistor space. The chiral Lagrangian is given by (3.17) as an integral over all eight chiral Grassmann variables. Since it corresponds to the top component of the multiplet, it can be written as

$$\mathcal{L}_{\text{int}}(x) = N_{\text{c}} \int \mathrm{d}^8\theta \, \log\det\left(\bar{\partial}+\mathcal{A}\right)\big|_{\mathbb{CP}^1} = N_{\text{c}} \int \mathrm{d}^4\theta^+ \, \mathbb{O}_2(x,\theta^+,y) \,. \tag{3.48}$$

This naturally suggests the representation

$$\mathbb{O}_2(x,\theta^+,y) = \int \mathrm{d}^4\theta^- \, \log\det\left(\bar{\partial}+\mathcal{A}\right)\big|_{\mathbb{CP}^1} \,, \tag{3.49}$$

which is precisely the proposal of [105]. Starting from this expression, the corresponding twistor Feynman rules were derived in that work.

Rather than reproducing this derivation, we instead recover the same result by taking an appropriate limit of the rules obtained in the previous section. Since the stress-tensor multiplet $\mathbb{O}_2$ appears as the lowest-charge component of the generalized operator $\mathbb{O}$, the corresponding correlators can be extracted directly from the generating function. In particular, we consider the tree-level correlator of n stress-tensor multiplets,

$$\mathcal{G}_n^{(0)}(1,\ldots,n) = \langle \mathbb{O}_2(1)\, \mathbb{O}_2(2)\, \ldots\, \mathbb{O}_2(n)\rangle_{\text{tree}}\,. \tag{3.50}$$

According to (2.37), this correlator admits an expansion in Grassmann degree of the form

$$\mathcal{G}_n^{(0)} = \mathcal{G}_{n;0}^{(0)} + a\, \mathcal{G}_{n;1}^{(0)} + \cdots + a^{n-4}\, \mathcal{G}_{n;n-4}^{(0)}\,. \tag{3.51}$$

Each component $\mathcal{G}_{n;k}^{(0)}$ has Grassmann degree $4k$. In addition, one can determine its total conformal weight summed over all n points, which is given by $2(n+k)$.

We now explain how this component can be efficiently extracted from the corresponding tree-level correlator of the superfields $\mathbb{O}$. As discussed in the previous section, such correlators are computed from graphs in which each edge contributes a fat propagator D_{ij}, while each vertex is dressed by factors generating the R-invariants. The latter carry conformal weight zero and Grassmann degree two (cf. (3.28)), whereas each fat propagator contributes at least conformal weight two, as follows from its expansion as a geometric series (3.40).

From this, we can deduce the following constraints for the computation of $\mathcal{G}_{n;k}^{(0)}$:

- Only graphs with at most $(n+k)$ edges can contribute, since otherwise the total conformal weight would exceed $2(n+k)$.

- Only graphs with at least $(n+k)$ edges can contribute, as otherwise the Grassmann degree would be too low. To see this, consider a graph with n vertices and n propagators. If all vertices have valency at least two, no vertex of valency three appears, and hence no vertex factor Δ is generated. As a result, the graph has no Grassmann dependence. Adding one additional edge produces two vertices of valency three, each contributing a factor Δ^i_{jkl}, and hence at most two R-invariants, corresponding to Grassmann degree four. Repeating this procedure shows that obtaining Grassmann degree $4k$ requires the addition of k extra edges.

In summary, the only contributing graphs are those with exactly $(n + k)$ edges. In this case, the fat propagators can be truncated to the ordinary propagators, $D_{ij} \to d_{ij}$, and the vertex factors can be replaced by their highest Grassmann component, $\Delta \to R$. Furthermore, no splitting of edges, as discussed in Section 3.3.3, needs to be considered, since such operations would lower the Grassmann degree and therefore cannot contribute to $\mathcal{G}^{(0)}_{n;k}$.

Let us summarize the outlined rules in the following box:

In order to compute the tree-level correlator of stress-tensor multiplets $\mathbb{O}_2$ (cf. (3.50)), the following twistor Feynman rules $\Phi_{\mathbf{20'}}$ have to be applied to all relevant graphs:

- For each edge connecting two vertices i and j, one inserts a standard propagator,

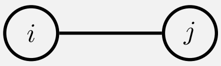

$$d_{ij}\,\delta^{a_{ij}a_{ji}}\,. \tag{3.52}$$

- Each vertex i with outgoing lines $j_1, j_2, \ldots, j_k$ is dressed by a vertex factor,

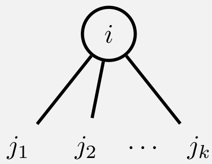

$$V^i_{j_1 j_2 \cdots j_k}\,\mathrm{tr}\left(T^{a_{ij_1}} \ldots T^{a_{ij_k}}\right)\,, \tag{3.53}$$

where T^a are the fundamental generators of the gauge group and

$$V^i_{j_1 j_2} = 1\,, \quad V^i_{j_1 j_2 \cdots j_k} = R^i_{j_1 j_2 j_3} R^i_{j_1 j_3 j_4} \ldots R^i_{j_1 j_{k-1} j_k}\,. \tag{3.54}$$

The R-invariant is defined in (3.28), and the on-shell twistor variables in (3.37).

Since we will make use of these rules in Chapter 7 to derive the non-planar corrections to the four-point integrand of $\mathbf{20'}$ operators at five loops, we have made the color factors in the above rules explicit. These follow the standard color Feynman rules when applied to ribbon graphs. For a derivation in which this is carried out explicitly, we refer to [105].

Importantly, the relevant graphs contributing to $\mathcal{G}_{n;k}^{(0)}$ now also include non-planar configurations. They are given by all inequivalent ribbon graphs with n vertices, each of at least valency two, and exactly $(n+k)$ edges.

Part II.

Higher-Point Correlation Functions

4. Generating Functions

In this chapter, we present our results on the computation of loop integrands of correlation functions of scalar half-BPS operators with arbitrary fixed R-charge. These correlators can be efficiently organized into generating functions, as discussed in Section 3.3. We follow this construction and employ the twistor Feynman rules for the supercorrelator [69] in order to find explicit expressions for particular generating functions.

Applying the method as described in [60], where higher-point $\mathbf{20'}$ integrands were computed, we use a suitable ansatz in terms of the basic Lorentz and internal invariants x_{ij}^2 and y_{ij}^2 to determine the five-point generating function at one- and two-loop order (see Section 4.5), as well as the six-point function at one loop (see Section 4.6). We begin by reviewing the definition of generating functions and fixed-charge correlators in Section 4.1. This is followed by a discussion of how the twistor Feynman rules for the supercorrelator can be projected onto loop integrands in Section 4.2. In Section 4.3 and Section 4.4, we discuss the tree-level generating functions and review the known results for the four-point case, respectively. We conclude the chapter by analyzing the ten-dimensional pole structure of the generating function in Section 4.7.

This chapter is based on the work presented in [1].

4.1. Supercorrelator and Loop Integrands

We study correlation functions of the half-BPS operator as defined in (3.21). Let us state them again for convenience

$$\mathcal{O}(x,y) = \sum_{k=2}^{\infty} \mathcal{O}_k(x,y)\,, \qquad \mathcal{O}_k(x,y) = \frac{1}{k}\,\mathrm{tr}\,[y\cdot\phi(x)]^k + \text{multi-traces}\,. \tag{4.1}$$

This operator resums the tower of scalar protected operators $\mathcal{O}_k$ with integer scaling dimension k. In its definition, the trace is taken on the adjoint matrices $\mathrm{U}(N_\mathrm{c})$. Besides the single-trace term, we include additional multi-trace terms to make these operators orthogonal to all other pure multi-trace operators. This is the single-particle basis introduced in [104].[1]

The two- and three-point correlators of these operators are tree-level exact due to supersymmetry [52, 95]. On the other hand, the four- and higher-point correlators receive quantum corrections in general kinematics. These perturbative corrections can be computed by means of the Lagrangian insertion method as [41, 95] (cf. Section 2.4.1):

$$\left\langle \prod_{i=1}^{n} \mathcal{O}(x_i, y_i) \right\rangle = \sum_{\ell=0}^{\infty} \frac{(-a)^\ell}{\ell!} \int \left[\prod_{k=1}^{\ell} \frac{\mathrm{d}^4 x_{n+k}}{4\pi^2} \right] G_{n,\ell} \,, \tag{4.2}$$

where the integral is written after Wick rotating to Euclidean signature. In contrast, the ℓ-loop integrand $G_{n,\ell}$ is a correlator of the n original operators with ℓ extra insertions of the chiral Lagrangian $\mathcal{L}_{\text{int}}$ (see (3.13)) computed at tree-level

$$G_{n,\ell} \equiv \left\langle \prod_{i=1}^{n} \mathcal{O}(x_i, y_i) \prod_{i=1}^{\ell} \mathcal{L}_{\text{int}}(x_i) \right\rangle_{\text{tree}} \,. \tag{4.3}$$

At large N_{c}, the connected part of the correlator scales as:

$$G_{n,\ell} \sim N_{\mathrm{c}}^{2-n} \,. \tag{4.4}$$

The correlator $G_{n,\ell}$ is in general a rational function of the spacetime and R-charge distances: $x_{ij}^2 \equiv (x_i - x_j)^2$ and $y_{ij}^2 \equiv (y_i - y_j)^2$, and it can also depend on other Lorentz and R-charge invariants that appear for $n \geq 5$ (see for instance the odd part of the integrand in (4.60), and the R-structure in (4.61)). The loop integrand $G_{n,\ell}$ of $\mathcal{O}$ serves as a generating function for the loop integrands of operators $\mathcal{O}_k$ with fixed but arbitrary R-charge.

The best studied are the four-point loop integrands $G_{4,\ell}$, as we reviewed in Section 2.5.3. As we have seen it deocmposes into a unique superconformal invariant and a remaining function, namely the reduced correlator. The latter enjoys a full ten-dimensional symmetry [65]. We review the explicit three-loop results in Section 4.4.

On the other hand, higher-point integrands are less constrained by supersymmetry. In particular, there is no known generalization of the factorization for five- and

[1] The conceptual motivation for these single-particle operators is that they are natural duals to single-particle scalar supergravity states on $\mathrm{AdS}_5 \times \mathrm{S}^5$. See [110] for a first study that fixed the double-trace admixture.

higher-point integrands, and hence also the generalization of the ten-dimensional symmetry is unclear. In this chapter, we explore the structure of the simplest non-trivial five- and six-point integrands:

$$G_{5,1} \text{ in Section 4.5.2}, \quad G_{5,2} \text{ in Section 4.5.3}, \quad \text{and} \quad G_{6,1} \text{ in Section 4.6.1}. \tag{4.5}$$

In order to compute these correlators, we follow the method put forward in [69]. In that paper, the loop integrand in (4.3) was generalized in two ways, by adding all (chiral) superdescendants, and the higher R-charge partners of the chiral Lagrangian. In Section 3.3, we reviewed this construction defining the superoperator

$$\mathbb{O}(x,\theta^+,y) = e^{\theta^a_\alpha Q^\alpha_a}\,\mathcal{O}(x,y) = \mathcal{O}(x,y) + \cdots + \frac{\theta^4}{N_\mathrm{c}}\,\mathcal{L}_\mathrm{int}(x,y)\,. \tag{4.6}$$

From now on, we write θ instead of θ^+ and implicitly understand it to denote the chiral Grassmann variables. The truncation at order θ^4 is due to the half-BPS condition. The top component, proportional to θ^4, is a generalization of the chiral Lagrangian $\mathcal{L}_\mathrm{int}(x)$ (3.13), which can be extracted in the limit $y \to 0$ as:[2]

$$\mathcal{L}_\mathrm{int}(x,y) \xrightarrow{y\to 0} \mathcal{L}_\mathrm{int}(x)\,. \tag{4.7}$$

We define the tree-level expectation value of the supercorrelator as:

$$\mathbb{G}_n \equiv \left\langle \prod_{i=1}^{n} \mathbb{O}(x_i,y_i,\theta_i) \right\rangle_\mathrm{tree}\,. \tag{4.8}$$

It is then evident that this supersymmetric correlator contains the loop integrand $G_{n,\ell}$ as a component that can be obtained by performing projections in the Grassmann (θ) and R-charge (y) variables. We state these projections in detail at the end of this section in (4.17). Before, we review some of the basic properties of the supercorrelator.

The free scalar propagator is normalized to:

$$\big\langle (y_1\cdot\phi(x_1))(y_2\cdot\phi(x_2))\big\rangle_\mathrm{free} = \frac{d_{12}}{N_\mathrm{c}} \qquad \text{with} \qquad d_{ij} \equiv \frac{2\,y_i\cdot y_j}{x_{ij}^2} \equiv \frac{-y_{ij}^2}{x_{ij}^2}\,. \tag{4.9}$$

[2]This definition includes an overall N_c factor, which explains why the ℓ-loop integrand has the large N_c scaling in eq. (4.4). In this normalization, the top component of $\mathbb{O}$ gives $\mathcal{L}_\mathrm{int}/N_\mathrm{c}$ as in (4.6).

Under this normalization, we have the large-N_c scaling:

$$\mathbb{G}_n \sim N_\mathrm{c}^{2-n}\,. \tag{4.10}$$

Thanks to non-renormalization theorems, the two-, three- and four-point supercorrelators just evaluate to their scalar bottom components:

$$\mathbb{G}_n = G_{n,0} \quad \text{for } n = 1,2,3,4\,. \tag{4.11}$$

These correlators can be computed by Wick contractions using the scalar propagator (4.9):

$$\begin{aligned}
\mathbb{G}_2 &= \log(1+D_{12}) + \mathcal{O}(N_\mathrm{c}^{-1}) \overset{y\to 0}{=} \left(d_{12} + \frac{d_{12}^2}{2} + \frac{d_{12}^3}{3} + \cdots\right) + \mathcal{O}(N_\mathrm{c}^{-1})\,,\\
\mathbb{G}_3 &= \frac{1}{N_\mathrm{c}}\, D_{12}D_{23}D_{31} + \mathcal{O}(N_\mathrm{c}^{-2})\,,\\
\mathbb{G}_4 &= \frac{1}{N_\mathrm{c}^2}\big[D_{12}D_{23}D_{34}D_{14}(1+2D_{13}+D_{13}^2+2D_{24}+D_{24}^2) + (1\leftrightarrow 2) + (1\leftrightarrow 4)\\
&\qquad\quad + 2D_{12}D_{13}D_{14}D_{23}D_{24}D_{34}\big] + \mathcal{O}(N_\mathrm{c}^{-3})\,,
\end{aligned} \tag{4.12}$$

with the effective propagator given by $D_{ij} \equiv d_{ij}/(1-d_{ij})$ as well as the four-, six- and ten-dimensional distances:

$$D_{ij} \equiv \frac{-y_{ij}^2}{X_{ij}^2}\,, \quad x_{ij}^2 \equiv (x_i - x_j)^2\,, \quad y_{ij}^2 \equiv (y_i - y_j)^2 = -2\, y_i\cdot y_j\,, \quad X_{ij}^2 \equiv x_{ij}^2 + y_{ij}^2 \tag{4.13}$$

The three-point function is given by a single term, thanks to our choice of basis. In the single-particle basis, extremal correlators vanish (compare the discussion at the end of Section 2.5.2).

Starting at five points, we have a non-trivial Grassmann dependence on the supercorrelator, which can be organized as:

$$\mathbb{G}_n = G_{n,0} + \sum_{k=1}^{n-4} \mathbb{G}_n^{\mathrm{N}^k\mathrm{MHV}} \quad \text{for } n \geq 5\,. \tag{4.14}$$

The "MHV" or bottom component $G_{n,0}$ is Grassmann independent (we collect further results on $G_{n,0}$ for $n \geq 5$ in Section 4.3). The N^kMHV component has Grassmann degree $4k$, and should be decomposable into a basis of superconformal invariants.[3] This Grassmann expansion follows the one for the correlator of stress-tensor multiplets (cf. (2.37)). For the top component $\mathbb{G}_{k+4}^{\mathrm{N}^k\mathrm{MHV}}$, there is a single superconformal invariant [66], whose coefficient is proportional to the reduced correlator $F^{(k)}$ in (2.45). However, other, lower components are expected to have a larger basis of susy invariants, see for instance the three invariants for $\mathbb{G}_6^{\mathrm{NMHV}}$ in eq. (4.57). There is no classification of these susy invariants in general, see however [69] for the NMHV case. In this chapter, our main focus is on the NMHV and N^{2}MHV components of seven-point supercorrelator, which contain the loop integrands we are studying.

The supersymmetric correlator contains the loop integrand as a component that is obtained by performing Grassmann (θ) and R-charge (y) projections as:

$$\mathbb{G}_{n+\ell} \equiv \left\langle \prod_{i=1}^{n+\ell} \mathbb{O}(x_i, y_i, \theta_i) \right\rangle_{\text{tree}} , \tag{4.15}$$

$$\begin{aligned} \tilde{G}_{n,\ell} &\equiv N_{\mathrm{c}}^{\ell} \int \mathrm{d}^4\theta_{n+1} \dots \mathrm{d}^4\theta_{n+\ell}\, \mathbb{G}_{n+\ell}^{\mathrm{N}^\ell\mathrm{MHV}} \Big|_{\theta_i \to 0} \\ &= \left\langle \prod_{i=1}^{n} \mathcal{O}(x_i, y_i) \prod_{i=1}^{\ell} \mathcal{L}_{\text{int}}(x_i, y_i) \right\rangle_{\text{tree}} , \end{aligned} \tag{4.16}$$

$$G_{n,\ell} \equiv \tilde{G}_{n,\ell} \Big|_{y_{n+1},\dots,y_{n+\ell} \to 0} . \tag{4.17}$$

These projections are also summarized in Figure 4.1. For our targets in (4.5), we need the supercorrelators

$$\mathbb{G}_6^{\mathrm{NMHV}} \to G_{5,1} , \quad \mathbb{G}_7^{\mathrm{N}^2\mathrm{MHV}} \to G_{5,2} \quad \text{and} \quad \mathbb{G}_7^{\mathrm{NMHV}} \to G_{6,1} . \tag{4.18}$$

Finally, following the definition (4.1) of the operator $\mathcal{O}$, its correlators $G_{n,\ell}$ serve as generating functions of correlators of fixed-charge operators $\mathcal{O}_k$ at each point:

$$G_{n,\ell} = \sum_{k_1,\dots,k_n=2}^{\infty} \langle k_1 \dots k_n \rangle_{\ell} . \tag{4.19}$$

These correlators can be extracted by performing the rescaling $y_i \to t_i y_i$ and picking the coefficient of $t_1^{k_1} t_2^{k_2} \cdots t_n^{k_n}$ in the series of $t_i \to 0$. This can be effectively

[3]This N^{k}MHV-nomenclature was used in [69] in the same supercorrelator context, and is inspired by the Grassmann decomposition of the gluon super-amplitude [17]. Furthermore, from the correlator-amplitude duality, the light-like limit of the stress-tensor supercorrelator is identical to the (square of) the gluon superamplitude [80, 103].

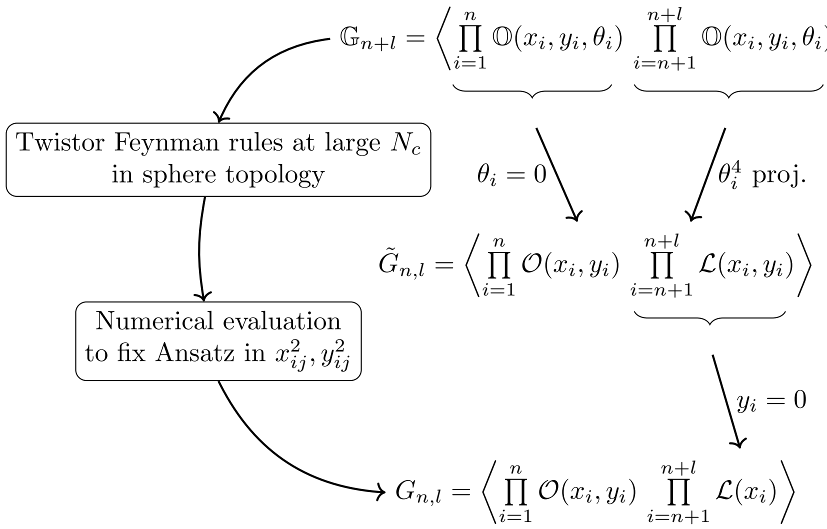

Figure 4.1.: Tree-level correlators in $\mathcal{N} = 4$ SYM and the methods to compute them [1]. The supercorrelator is computed by using twistor Feynman rules, as reviewed in Section 3.3.2. And the loop integrands $G_{n,l}$ are extracted by performing Grassmann θ-projections and R-charge y-projections. We obtain explicit results in terms of conformal integrands by matching a numerical evaluation of the supercorrelator with an ansatz in x-y kinematic space.

performed by using differential operations accompanied by some factorials:

$$\begin{aligned} \langle k_1 k_2 \cdots k_n \rangle_\ell &\equiv \left\langle \prod_{i=1}^{n} \mathcal{O}_{k_i}(x_i, y_i) \prod_{i=1}^{\ell} \mathcal{L}_{\text{int}}(x_i) \right\rangle_{\text{tree}} \\ &= \frac{1}{k_1!} \frac{\partial^{k_1}}{\partial t_1^{k_1}} \cdots \frac{1}{k_n!} \frac{\partial^{k_n}}{\partial t_n^{k_n}} G_{n,\ell}(x_i, t_i\, y_i) \Big|_{t_i \to 0} . \end{aligned} \tag{4.20}$$

4.2. From Twistors Rules to Loop Integrands

In this section, we explain how we obtain our expressions for the correlators (4.17) from the twistor rules that were derived in [69] (reviewed in Section 3.3.2).

These rules efficiently integrate out the self-dual quantum corrections to the correlators $\mathbb{G}_{n+\ell}$. However, the usual caveat inherent to the twistor formulation of $\mathcal{N} = 4$ SYM theory applies: All intermediate expressions depend on the choice of an arbitrary but fixed reference twistor $Z_\star$. This gauge dependency makes it virtually impossible to analytically convert the result generated by the twistor rules to a manifestly invariant expression. As was done in past computations [59, 60, 69], we therefore resort to creating a suitable ansatz in terms of spacetime and internal invariants x_{ij}^2, y_{ij}^2, and fix all freedom in the ansatz by numerical comparison to the twistor result. To make this process feasible, we restrict the super-correlator $\mathbb{G}_{n+\ell}$ to its bosonic integrand component $G_{n,\ell}$ by performing a projection in the variables θ_i and y_i on the twistor side. We can construct a finite rational ansatz for the generating function $G_{n,\ell}$, based on its pole structure. However, due to the large size of this ansatz, we found it practical to further extract fixed-charge component integrands $\langle k_1 k_2 \dots k_n \rangle_\ell$ (4.20) from the twistor expression for $G_{n,\ell}$. For these, we can construct relatively small ansätze that are easily fixed by numerical comparison to the twistor expression. After obtaining sufficiently many fixed-charge integrands, we can finally reconstruct the full generating function $G_{n,\ell}$.

Below, we explain all of the above steps in more detail, starting with with the projection to the bosonic component $G_{n,\ell}$ (Section 4.2.1), observations on the structure of the integrand and the construction of the ansatz (Section 4.2.2), and finishing with the extraction of fixed-charge integrands (Section 4.2.3) and a note on the separation of parity-even and odd parts (Section 4.2.5).

In Section 3.3.2, we reviewed the twistor Feynman rules Φ for the supercorrelator $\mathbb{G}_{n+\ell}$. These form the basis of the following derivations. Let us introduce an example to which we will apply the twistor Feynman rules, and subsequently use throughout this section

Φ

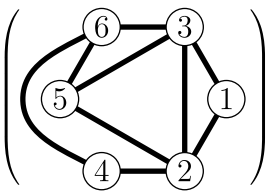

$$
\begin{aligned}
&= D_{12}D_{13}D_{23}D_{24}D_{25}D_{35}D_{36}D_{46}D_{56}V^1_{23}V^2_{4135}V^3_{1652}V^4_{26}V^5_{236}V^6_{345} \\
&= D_{12}D_{13}D_{23}D_{24}D_{25}D_{35}D_{36}D_{46}D_{56}\Delta^2_{413}\Delta^2_{435}\Delta^3_{165}\Delta^3_{152}\Delta^5_{236}\Delta^6_{345}\,.
\end{aligned}
\tag{4.21}
$$

In the last step, we use the representation (3.44) for the vertex factors.

4.2.1. Projection to Loop Integrands

Using the twistor rules explained above, the super-correlator $\mathbb{G}_{n+\ell}$ is written as a sum of products of propagators D_{ij} and vertex factors Δ^i_{jkl}. The resulting expression however has several drawbacks:

- When expanded in terms of R-invariants (3.28), the number of terms grows prohibitively large.
- The super-correlator is not expressed in terms of basic spacetime and internal invariants x_{ij}^2, y_{ij}^2.
- Each R-invariant depends on the reference twistor $Z_\star$, even though the full correlator $\mathbb{G}_{n+\ell}$ is independent of $Z_\star$.

It would be great to resolve these points for the full super-correlator $\mathbb{G}_{n+\ell}$. In this work, we restrict ourselves to the bosonic integrand component $G_{n,\ell}$ (4.17), i. e. the generating function of loop integrands for scalar half-BPS operators $\mathcal{O}(x,y)$, which allows us to find a manifestly invariant closed-form expression. To obtain $G_{n,\ell}$ from $\mathbb{G}_{n+\ell}$, we must perform projections in the Grassmann variables θ and in the internal variables y.

Grassmann Projection. A partial projection in the Grassmann variables can be easily done: The scalar half-BPS operator are the lowest component in the super-multiplet and thus come with Grassmann degree zero. In contrast, the chiral Lagrangians are the top component and thus come with Grassmann degree four. Hence we want to extract the component of $\theta^4_{n+1}\dots\theta^4_{n+\ell}$. Since each R-invariant (3.28) is homogeneous of degree two, we can expand all vertex factors V in terms of R^i_{jkl}, and keep only products of exactly 2ℓ R factors. Moreover, only a subset of R-products will contribute to the component $\theta^4_{n+1}\dots\theta^4_{n+\ell}$. All others can be set to zero. For example, one has

$$R^i_{jkl} = 0 \quad \text{if} \quad i,j,k,l \leq n\,. \tag{4.22}$$

Concretely, we keep only products where each R factor contains at least one of the indices $n+1,\dots,n+\ell$, and the product contains each of those indices at least twice. Among these products, some still vanish although not apparent from their symbolic expression. We thus probe all products numerically and remove any that evaluate to zero.

Lagrangian Projection. After the θ-projection, the super-correlator is projected to $\tilde{G}_{n,\ell}$ (4.16), which still contains all higher KK siblings of the interaction Lagrangian $\mathcal{L}_{\text{int}}(x)$. To project out the higher KK modes, we set $y_i \to 0$ for $i > n$, and thus obtain $G_{n,\ell}$. This projection is slightly more subtle, since individual R-invariants can diverge when taking any y_i to zero. Only the complete products of R-invariants and propagators D_{ij} remain finite or vanish. In order to take the limit, it is necessary to know how products of R-invariants scale with the polarization vectors y_i. We can measure these scalings by dressing the polarization vectors y_i with scalar factors t_i:

$$y^b_{i,a'} \to t_i^{1/2}\, y^b_{i,a'} \qquad \text{for } i > n\,. \tag{4.23}$$

The R-invariants depend on y_i through Y and W, which scale as[4]

$$Y^B_{i,a'} \to t_i^{1/2}\, Y^B_{i,a'} \quad \text{and} \quad W^B_{i,a} \to t_i^{-1/2}\, W^B_{i,a}\,. \tag{4.24}$$

The scaling of a given R-product can in principle be found analytically by explicit expansion. However, we found it much easier to probe the scaling numerically by inserting random numerical values for the spacetime coordinates and polarization vectors, while keeping the scalar factors t_i symbolic.[5]

Moreover, the fat propagators D_{ij} can be expanded in ordinary propagators d_{ij}, which scale as $d_{ij} \to t_i t_j d_{ij}$. Once the scaling behavior of all factors in a given product is known, one can safely take the $t_i \to 0$ limit, thus projecting to the loop integrand $G_{n,\ell}$.

Example. Let us again exemplify this procedure by considering (4.21) and computing which terms survive when projecting to the four-point two-loop integrand

[4] While the scaling of Y_i can be directly inferred from (3.34), the scaling of W_i might seem surprising. SU(4) unitarity conditions (see (2.14)) impose that

$$W^B_{i,a}\overline{Y}^c{}_{i,B} = \delta^c_a \quad \text{with} \quad \overline{Y}^c{}_{i,B} = (\delta^c_b,\, -y^c_{i,b'}) \quad \text{such that} \quad Y^B_{i,a'}\overline{Y}^a{}_{i,B} = 0\,.$$

Since $\overline{Y}_i$ scales with the same power as Y_i, the above condition implies that W_i scales with the inverse power of the respective polarization vector.

[5] Although not immediately apparent from the definition (3.28), after the projection to the $\theta^4_{n+1}\ldots\theta^4_{n+\ell}$ component, each product of R-invariants is a homogeneous function of all t_i. Heuristically, we find that for every $i > n$, every product of R-invariants scales as $t_i^{-2-\#i}$, where $\#i$ is the number of occurrences of i in the upper labels of the R-invariants in the product. See e. g. the examples in (4.26).

$G_{4,2}$. First, we set $\theta_i = 0$ for $i \leq n$ and obtain

$$\begin{aligned}
&\Delta^2_{413}\Delta^2_{435}\Delta^3_{165}\Delta^3_{152}\Delta^5_{236}\Delta^6_{345} \\
&\qquad = 1\,(1+R^2_{435})\,(1+R^3_{165})\,(1+R^3_{152})\,(1+R^5_{236})\,(1+R^6_{345}) \\
&\qquad = R^2_{435}R^3_{165}R^3_{152}R^5_{236} + R^2_{435}R^3_{165}R^3_{152}R^6_{345} + R^2_{435}R^3_{165}R^5_{236}R^6_{345} \\
&\qquad\qquad + R^2_{435}R^3_{152}R^5_{236}R^6_{345} + R^3_{165}R^3_{152}R^5_{236}R^6_{345} + \dots\,. \qquad (4.25)
\end{aligned}$$

The dots indicate terms with fewer or more R factors, which are omitted, since they cannot contribute to the two-loop integrand. We compute the R-charge weights of the five four-products by probing them numerically and obtain

$$\begin{aligned}
R^2_{435}R^3_{165}R^3_{152}R^5_{236} &\sim t_5^{-3} \times t_6^{-2}\,, \\
R^2_{435}R^3_{165}R^3_{152}R^6_{345} &\sim t_5^{-2} \times t_6^{-3}\,, \\
R^2_{435}R^3_{165}R^5_{236}R^6_{345}\,, R^2_{435}R^3_{152}R^5_{236}R^6_{345}\,, R^3_{165}R^3_{152}R^5_{236}R^6_{345} &\sim t_5^{-3} \times t_6^{-3}\,. \qquad (4.26)
\end{aligned}$$

On the other side, the product of propagators scales as

$$D_{12}D_{13}D_{23}D_{24}D_{25}D_{35}D_{36}D_{46}D_{56} \sim t_5^3 \times t_6^3 + \text{higher powers in } t_5, t_6\,. \qquad (4.27)$$

We conclude that in the limit $t_5, t_6 \to 0$, only the terms in the last line of (4.26) survive, while the others only contribute to higher KK siblings of the Lagrangian, and are thus set to zero. Furthermore, in the fat propagators D_{ij} that involve one of the Lagrangian insertion points, only the leading terms contribute. All in all, we obtain

$$\begin{aligned}
(4.21)\big|_{G_{4,2}} &= D_{12}D_{13}D_{23}D_{24} \times d_{25}d_{35}d_{36}d_{46}d_{56} \\
&\quad \times \Big(R^2_{435}R^3_{165}R^5_{236}R^6_{345} + R^2_{435}R^3_{152}R^5_{236}R^6_{345} + R^3_{165}R^3_{152}R^5_{236}R^6_{345}\Big)\,. \qquad (4.28)
\end{aligned}$$

4.2.2. Structure of the Integrand

We have explained how to extract the generating function $G_{n,\ell}$ from the supercorrelator $\mathbb{G}_{n+\ell}$ using the twistor Feynman rules. What remains is to translate the resulting expression from twistor space to coordinate space, i. e. to rewrite it in terms of the basic Lorentz and internal invariants x_{ij}^2 and y_{ij}^2. This step is highly non-trivial, in particular due to the explicit dependence of intermediate expressions on the reference twistor $Z_\star$.

Singularities. To circumvent this difficulty, we construct an ansatz for $G_{n,\ell}$ whose coefficients are fixed by matching to the twistor expression numerically, following the strategy of [59,60]. The structure of this ansatz is strongly constrained by the twistor rules, as well as by the interpretation of $G_{n,\ell}$ as a generating function for fixed-charge loop integrands (4.20). In particular, it takes the form of a finite polynomial $P_{n,\ell}$ in d_{ij} and x_{ij}^2, multiplied by an overall factor that captures all singularities:

$$G_{n,\ell} = \left[\prod_{1 \leq i<j \leq n} \left(\frac{x_{ij}^2}{X_{ij}^2} \right)^{n-3+\delta_{\ell,0}} \right] \left[\prod_{\substack{1 \leq i<j \leq n+\ell \\ n<j}} \frac{1}{x_{ij}^2} \right] P_{n,\ell} \, . \tag{4.29}$$

The polynomial dependence on the fat propagators $D_{ij} \sim 1/X_{ij}^2$ for $i, j \leq n$ follows directly from the twistor rules. For indices involving Lagrangian insertion points ($i > n$ or $j > n$), the propagators reduce to powers of the ordinary propagators d_{ij}, since we project these points to their lowest component ($y_i \to 0$ for $i > n$).

Restricting to graphs of sphere topology (the leading contribution in the planar limit), the maximal power of any D_{ij} is $n-2$.[6] However, this maximal power only occurs at tree level ($\ell = 0$). Indeed, the only n-point graph with $n-2$ propagators D_{ij} and all vertices of valency at least two has the topology illustrated below (shown for $n = 5$):

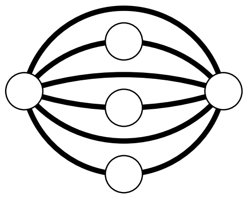 . (4.30)

This graph does not receive loop corrections. Inserting Lagrangian operators into its faces yields zero, since all external operators are BPS and all faces are triangular, and therefore protected.[7] Non-trivial loop corrections arise only for graphs that contain at least one face with four or more vertices. For such graphs, the maximal power of any D_{ij} is reduced to $n-3$, explaining the factor $\delta_{\ell,0}$ in (4.29). Using the

[6] This corresponds to the maximal number of homotopically distinct lines connecting two punctures on an n-punctured sphere. It relies on the fact that fat propagators cannot be separated by Lagrangian insertions.

[7] Otherwise, three-point functions of BPS operators would receive loop corrections. Since such correlators are tree-level exact, triangular faces must not contribute at loop level [52, 95]. While this argument strictly applies to integrated correlators, we find that it also holds at the level of the integrand.

relation $D_{ij} = d_{ij}/(1 - d_{ij}) = d_{ij}\, x_{ij}^2/X_{ij}^2$, it follows that the first factor in (4.29) absorbs all singularities in X_{ij}^2, while preserving polynomial dependence on d_{ij}.
The second factor in (4.29), involving inverse powers of x_{ij}^2, accounts for all divergences in the limits $x_{ij}^2 \to 0$. The corresponding exponents are fixed by the OPEs of the operators $\mathcal{O}$ and $\mathcal{L}_{\text{int}}$, together with our choice of expressing $P_{n,\ell}$ as a polynomial in d_{ij} rather than y_{ij}^2. The conformal weights of the operators in $G_{n,\ell}$ (4.3) imply that $P_{n,\ell}$ carries weight $+\ell$ in each external point $x_{i\leq n}$, and weight $\ell + n - 5$ in each Lagrangian insertion point $x_{n<i}$. The degree in d_{ij} is likewise bounded and increases with the loop order ℓ.

Divide and Conquer. In principle, all coefficients in the polynomial $P_{n,\ell}$ can be determined by matching the ansatz to the twistor expression evaluated at sufficiently many kinematic points. However, the size of the ansatz grows rapidly with n and ℓ, making this approach impractical beyond very low orders.[8]
This issue can be alleviated by refining the ansatz (4.29). Since not all powers of D_{ij} can appear simultaneously (the maximal number of edges in a planar graph with n vertices is $3n - 6$) one can decompose $P_{n,\ell}$ into contributions with fixed monomials in the D_{ij}. Each such contribution involves a much smaller ansatz, which can be determined independently.
In practice, we adopt an equivalent but more efficient "divide and conquer" strategy. Rather than working directly with $G_{n,\ell}$, we extract fixed-charge component correlators $\langle k_1 \dots k_n \rangle_\ell$ from the twistor expression. For these objects, compact ansätze can be constructed and matched numerically to the twistor result, which is independent of the reference twistor.
Once a sufficient set of fixed-charge correlators has been determined, the full generating function $G_{n,\ell}$ is reconstructed by matching (4.29) to the expansion (4.19). In this way, the original problem is reduced to a sequence of smaller and more tractable computations.

4.2.3. Fixed-R-Charge Projection

Twistor Projection. To extract fixed-charge components $\langle k_1 \dots k_n \rangle_\ell$ from the twistor expression for $G_{n,\ell}$, we use (4.20) by applying the scaling (4.23), but this time for

[8] The main limitation arises from solving large systems of linear equations. In practice, we use Mathematica 's `NSolve`, which is efficient up to roughly 10 000 unknowns. A direct ansatz for the full generating function would exceed this limit, necessitating a more refined approach.

the first n points:

$$y^b_{i,a'} \to t_i^{1/2}\, y^b_{i,a'} \qquad \text{for } i \le n\,. \tag{4.31}$$

Expanding both the products of R-invariants and the fat propagators D_{ij} to sufficiently high powers in the scaling parameters t_i, we can collect all terms proportional to $t_1^{k_1} \dots t_n^{k_n}$ that contribute to $\langle k_1 \dots k_n \rangle_\ell$.

Example. Let us again turn to the example in (4.28) and derive what terms contribute to the two-loop integrand $\langle 2442 \rangle_2$ of operators with charges 2, 4, 4, and 2, see (4.20) for the relation to $G_{4,2}$. Introducing scale factors t_i via (4.31), using (4.24), and numerically probing the remaining three R-products in (4.28) yields

$$R^2_{435} R^3_{165} R^5_{236} R^6_{345}\,,\; R^2_{435} R^3_{152} R^5_{236} R^6_{345} \;\sim\; t_2^{-1} \times t_3^{-1}\,, \tag{4.32}$$

$$R^3_{165} R^3_{152} R^5_{236} R^6_{345} \;\sim\; t_3^{-2}\,, \tag{4.33}$$

while the propagator factors scale as

$$D_{12} D_{13} D_{23} D_{24} \times d_{25} d_{35} d_{36} d_{46} d_{56} \;\sim\; t_1^2 \times t_2^4 \times t_3^4 \times t_4^2 + \text{higher powers in } t_i\,. \tag{4.34}$$

One can see that the only terms proportional to $t_1^2 t_2^4 t_3^4 t_4^2$ are the two products in (4.32) dressed with ordinary propagators as follows:

$$\begin{aligned}(4.28)\big|_{\langle 2442 \rangle_2} = {} & d_{12} d_{13} d_{23}^2 d_{24}\, d_{25} d_{35} d_{36} d_{46} d_{56} \times \\ & \Big(R^2_{435} R^3_{165} R^5_{236} R^6_{345} + R^2_{435} R^3_{152} R^5_{236} R^6_{345} \Big)\,.\end{aligned} \tag{4.35}$$

4.2.4. Fixed-R-Charged Ansatz

Finally, let us briefly explain how to construct the coordinate-space ansatz for the fixed-charge correlators $\langle k_1 \dots k_n \rangle_\ell$, following [60]. Due to Lorentz and R-symmetry invariance, it must be a function of the basic invariants $x_{ij}^2 = (x_i - x_j)^2$ and $y_{ij}^2 = (y_i - y_j)^2 = -2\, y_i \cdot y_j$. Considering the various OPE limits among the fixed-charge BPS operators and Lagrangian insertions, the correlator can be written as

$$\langle k_1 \dots k_n \rangle_\ell = \frac{N_{\mathrm{c}}^{2-n-\ell}}{\prod_{i=1}^{n+l} \prod_{i<j=n+1}^{n+l} x_{ij}^2} \sum_{\mathbf{a}} \Big(\prod_{i<j=1}^{n} d_{ij}^{a_{ij}} \Big) P^\ell_{\mathbf{a}}(x_{ij}^2)\,, \tag{4.36}$$

The sum runs over all possible propagator y-structures $\mathbf{a} = \{a_{ij}\}$ that are compatible with the operator charges, i. e. that satisfy

$$k_i = \sum_{j \neq i}^{n} a_{ij} \quad \text{for all} \quad i = 1, \ldots, n\,. \tag{4.37}$$

Finally, $P^\ell_{\mathbf{a}}(x^2_{ij})$ is a polynomial in x^2_{ij} whose conformal weights in x_i is fixed by the conformal weights of the operators: The BPS operators have weights k_i, whereas the Lagrangian insertions have weight four. Taking into account the powers of d_{ij} as well as the denominator in (4.36), the total degree of $P^\ell_{\mathbf{a}}$ in the external points $i \leq n$ must be $+\ell$, and $(n + \ell - 5)$ in the internal points $i > n$. Moreover, the polynomial is constrained by the permutation symmetries of the correlator $\langle k_1 \ldots k_n \rangle_\ell$ and the respective y-structure.

The coefficients of the polynomials $P^\ell_{\mathbf{a}}$ are numerically fitted against the twistor expression. There are a few further constraints one can impose on the polynomials beforehand. Let us discuss these by considering a concrete example for the ansatz construction in the following.

We demonstrate the explicit construction of the fixed-charge ansatz (4.36) by considering integrand of the five-point correlator $\langle 33222 \rangle$ at one and two loops. This component is $\mathrm{S}_2 \times \mathrm{S}_3$ symmetric, which leaves seven different y-structures that needs to be summed over in (4.36), up to those permutations (see Table 4.1).

The maximal number of independent terms of each polynomial $P^\ell_{\mathbf{a}}(x^2_{ij})$ does not depend on the specific charges of the operators, but on the number of points n and the loop order ℓ. At one-loop order, $P^1_{\mathbf{a}}$ has maximally 15 different terms. At two loops, the number of terms can be reduced by identifying terms that are related under the permutations of the two internal Lagrangian insertions, which leaves 442 different terms for each polynomial $P^2_{\mathbf{a}}$. In general, the ℓ-loop polynomials exhibit an S_ℓ symmetry in the internal points, which reflects the permutation symmetry of the integration points.

This number can be lowered further by using the seven-point conformal Gram identity

$$0 = \det\{x^2_{ij}\}_{i,j=1,\ldots,7}\,, \tag{4.38}$$

which relates products of the squared distances x^2_{ij}. It can be used to exclude the integrands of certain conformal integrals from the $\langle 33222 \rangle_2$ ansatz. We choose to

y-structure	# of coeff. in $P^1_{\mathbf{a}}$	# of coeff. in $P^2_{\mathbf{a}}$
$d_{12}^3 d_{34} d_{35} d_{45}$	1	22
$d_{12}^2 d_{13} d_{23} d_{45}^2$	2	48
$d_{13} d_{14} d_{15} d_{23} d_{24} d_{25}$	3	59
$d_{12}^2 d_{13} d_{24} d_{35} d_{45}$	9	228
$d_{12} d_{13} d_{14} d_{23} d_{25} d_{45}$	9	228
$d_{13}^2 d_{14} d_{24} d_{25}^2$	9	228
$d_{12} d_{13}^2 d_{24} d_{25} d_{45}$	9	231
# of coeff. in the ansatz	42	1044

Table 4.1.: Numbers of coefficients that enter the one- and two-loop integrands of the $\langle 33222 \rangle$ component via the polynomials $P^{\ell}_{\mathbf{a}}$. The number of coefficients is reduced by the respective permutation symmetry of the corresponding y-structure. Also, the leading OPE behavior of disconnected y-structures is used to lower the number of independent coefficients.

remove terms in the polynomials $P^2_{\mathbf{a}}$ that have factors $(x^2_{67})^2$. This reduces the number of different terms to 420.

Each polynomial $P^{\ell}_{\mathbf{a}}(x^2_{ij})$ does not exhibit the full permutation symmetry of the correlator, but rather a subgroup thereof that is leaving the respective y-structure invariant. By demanding this invariance for each polynomial, the number of independent coefficients can be further reduced.

Finally, certain terms in the polynomials can be excluded by considering the Euclidean OPE limit of two operators. At leading order, it holds for $x_i \to x_j$ that

$$\begin{aligned} \mathcal{O}_{k_i}(x_i)\mathcal{O}_{k_j}(x_j) \;\longrightarrow\; & (d_{ij})^{\min\{k_i,k_j\}}\, \mathcal{O}_{|k_i-k_j|}(x_j) \\ & + \Big(\text{terms in } (d_{ij})^k \text{ with } k < \min\{k_i,k_j\}\Big) \,, \end{aligned} \tag{4.39}$$

thus reducing an n-point correlator to an $(n-1)$-point correlator. Applying this relation to two operators with identical charge yields the identity operator at leading order. For five points, this implies that we are left with a three-point function that does not obtain loop corrections. Hence, terms in the ansatz contributing to that limit cannot appear in the ultimate expression of the loop integrand. Specifically, for y-structures that contain two operators i and j whose polarization vectors only contract with each other (this can happen e. g. for the first two lines in Table 4.1), one can infer that every term in the corresponding polynomials must contain a factor x^2_{ij}. This further reduces the amount of independent coefficients in these polynomials.

After taking all these reductions into account, the remaining number of coefficients for the different y-structures of the $\langle 33222\rangle$ ansatz at one and two loops is listed in Table 4.1.

At one loop, the total number of coefficients that needs to be fixed via solving a linear equation system by matching against the numerical twistor answer is 42. In fact, for a large class of one-loop integrands this number of coefficients stays reasonably small, such that fixing those coefficients is possible and even sufficiently fast. At two loops, however, that number of independent coefficient is much larger, as can already be seen from this example. Ansätze of specific R-charge components with charges that are invariant under fewer permutations or even exhibit no permutation symmetry are much less constrained, so that the number of independent coefficients is too large to be solved in a linear equation system. For example, the ansatz of the two-loop integrand of the component $\langle 65432\rangle_2$ has 28 980 coefficients.

One way to still obtain a final expression for the components is to sequentially probe those ansätze by choosing different polarizations such that some $d_{ij} = 0$. This effectively sets a part of the y-structures to zero, thus reducing the amount of coefficients. In that way, the coefficients can be fixed step by step, such that the equation systems can be solved numerically. This works very effectively for specific R-charge components of $G_{5,2}$.

4.2.5. A Note on Parity

The correlator $G_{n,\ell}$ can be decomposed into parity-even and parity-odd parts. The ansätze for the parity-even part are (4.29) and (4.36), where in both cases the space-time dependence enters only through parity-symmetric distances x_{ij}^2. The ansätze for the parity-odd part are identical, only that now every term in the polynomials $P_{n,\ell}$, $P_{\mathbf{a}}^{\ell}$ must contain a parity-odd factor

$$\varepsilon_{\mu\nu\rho\sigma} x_i^{\mu} x_j^{\nu} x_k^{\rho} x_l^{\sigma} \,. \tag{4.40}$$

In order to properly build the ansätze, it is useful to write these parity-odd factors into a conformally covariant object that has well-defined conformal weights in each point. To this end, we transform the four-dimensional Minkowski spacetime points to six-dimensional projective vectors X^I upon which the conformal symmetry $\mathrm{SO}(4,2)$

acts linearly. For example, a suitable representation for these vectors is[9]

$$X^I = \left(\frac{1-x^2}{2},\, x^\mu,\, \frac{1+x^2}{2} \right) . \tag{4.41}$$

Starting from six points, it is possible to write down a parity-odd covariant object by contracting all indices with the Levi-Civita tensor

$$X^{\text{anti}}_{123456} = \varepsilon_{IJKLMP} X_1^I X_2^J X_3^K X_4^L X_5^M X_6^P . \tag{4.42}$$

With the representation (4.41) at hand, one can readily relate this covariant to the four-dimensional notation by

$$\begin{aligned} X^{\text{anti}}_{123456} &= \frac{1}{2}\frac{1}{4!} \sum_{\sigma \in \mathrm{S}_5} \operatorname{sign}(\sigma)\, x^2_{\sigma_5 6}\, \varepsilon_{\mu\nu\rho\tau} x^\mu_{\sigma_1 6} x^\nu_{\sigma_2 6} x^\rho_{\sigma_3 6} x^\tau_{\sigma_4 6} \\ &= \frac{1}{2}\, x^2_{56}\, \varepsilon_{\mu\nu\rho\tau} x^\mu_{16} x^\nu_{26} x^\rho_{36} x^\tau_{46} + (\mathrm{C}_5 \text{ perms}) . \end{aligned} \tag{4.43}$$

Here, the point 6 is not special in any fundamental way. We simply choose to shift by x_6^μ in order to obtain a translationally invariant expression. For a more detailed discussion, we refer to Appendix B of [54].

In the numerical twistor computation, even and odd parts are easily separated: Since we work in Lorentzian signature, the parity-odd terms appear as imaginary parts, whereas parity-even parts are real. Thus it is easy to isolate even and odd parts, and they can be separately matched against the respective ansatz.

4.3. Tree-Level Correlators

In this section, we present the tree-level connected correlators at leading order in the planar limit. They are obtained from Wick contractions represented by planar graphs, with each edge weighted by the effective ten-dimensional propagator D_{ij} (4.13). As discussed in Section 3.3.2, the graphs of $G_{n,0}$ serve as seeds for the twistor construction of the supercorrelator $\mathbb{G}_n$, from which one extracts the loop integrands $G_{n-\ell,\ell}$ with loop orders $\ell = 1, \ldots, n-4$. The ten-dimensional poles of these integrands can in part be traced back to those of $G_{n,0}$.

[9] This X^I, with $I = 1, \ldots, 6$, is a six-dimensional vector, which should not be confused with the ten-dimensional vector $X = (x, y)$ used ubiquitously in our results. We only use the 6d vector X^I to write the antisymmetric invariant X^{anti} that enters the odd part of the five-point function (4.60).

Four Points. The four-point generating function (4.12) reads

$$G_{4,0} = \frac{1}{N_c^2}\Bigg(\prod_{i<j=1}^{4} D_{ij}\Bigg)\left[\frac{D_{12}}{4D_{34}} + \frac{1}{12} + \frac{1}{2D_{24}} + \frac{1}{8D_{13}D_{24}} + (\mathrm{S}_4 \text{ perms})\right], \quad (4.44)$$

where $+(\mathrm{S}_4$ perms) stands for 23 repetitions of all previous terms with S_4-permuted point labels. We will use this notation everywhere below.

Five Points. Summing the 21 different single-particle five-point graphs (see figure 6 in [65]) and summing over inequivalent permutations, we find the five-point tree-level generating function

$$\begin{aligned} G_{5,0} = \frac{1}{N_c^3}\Bigg(\prod_{i<j=1}^{5} D_{ij}\Bigg)\Bigg[&\frac{1}{6D_{34}D_{35}D_{45}}D_{12}^2 + \frac{1}{2D_{24}D_{35}D_{45}}\left(1+\frac{1}{D_{23}}\right)D_{12}D_{13} \\ &+ \frac{1}{2D_{35}D_{45}}\left(1+\left(4+\frac{1}{D_{13}}+\frac{2}{D_{23}}\right)\frac{1}{D_{24}}+\frac{1}{D_{34}}\right)D_{12} \\ &+ \frac{1}{60D_{45}}\Bigg(10+15\left(\frac{1}{D_{12}}+\frac{4}{D_{14}}\right)+30\frac{1}{D_{14}}\left(\frac{1}{D_{15}}+\frac{1}{D_{23}}+\frac{4}{D_{25}}\right) \\ &\qquad + \frac{10}{D_{14}}\left(\frac{1}{D_{15}D_{23}}+\frac{3}{D_{12}D_{25}}+\frac{6}{D_{13}D_{25}}\right)+\frac{6}{D_{13}D_{14}D_{23}D_{25}}\Bigg) \\ &+ (\mathrm{S}_5 \text{ perms})\Bigg], \end{aligned} \quad (4.45)$$

Note that there are only 18 terms in the sum (4.45), whereas there are 21 different tree-level graphs. The reason is that some tree-level graphs have different topologies, but lead to the same products of D_{ij} propagators (which thus get extra symmetry factors). For example, the three ribbon graphs

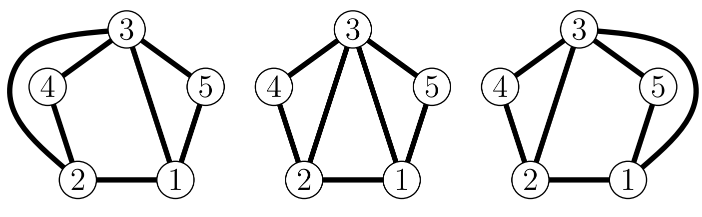

(4.46)

represent non-identical contractions, but all contribute the same term $1/D_{45}D_{14}D_{25}$ to the square bracket in (4.45). On the middle graph, the vertex labels can be permuted in 120 inequivalent ways, whereas the left and right graphs have only 60 permutations each. This leads to the overall term $2/D_{45}D_{14}D_{25}$ in the square bracket.

Six Points. The six-point generating function at tree level can be written as a sum of 127 terms, plus S_6 permutations. We only quote the terms with the largest number of repeating propagators (4 in this case):

$$
\begin{aligned}
G_{6,0} = \frac{1}{N_{\mathrm{c}}^4}\Bigg(\prod_{i<j=1}^{6} D_{ij}\Bigg)\Bigg[&\frac{D_{12}^3}{8D_{34}D_{35}D_{36}D_{45}D_{46}D_{56}} \\
&+\left(1+\frac{1}{D_{23}}\right)\frac{D_{12}^2 D_{13}}{D_{24}D_{35}D_{36}D_{45}D_{46}D_{56}} + \frac{D_{12}D_{13}D_{14}}{2D_{23}D_{25}D_{36}D_{45}D_{46}D_{56}} \\
&+\frac{D_{12}D_{13}D_{15}}{D_{23}D_{24}D_{35}D_{36}D_{45}D_{46}D_{56}} + \frac{D_{12}D_{13}D_{23}}{6D_{14}D_{25}D_{36}D_{45}D_{46}D_{56}} \\
&+\left(1+\frac{2}{D_{23}}+\frac{1}{D_{14}D_{23}}\right)\frac{D_{12}D_{13}D_{34}}{2D_{15}D_{24}D_{25}D_{36}D_{46}D_{56}} \\
&+(\text{lower-order terms}) + (\mathrm{S}_6\ \text{perms})\Bigg]\,,
\end{aligned}
\tag{4.47}
$$

where "lower-order terms" stands for terms with fewer factors D_{ij} in the numerator. This correlator is provided in the ancillary files of [1]. See Appendix A for a guide to these files.

Higher Points. At more than six points, the twistor computation becomes very demanding due to the large number of contributing terms, and the increasingly large ansatz. Beyond six points, we only computed the leading-order generating function $G_{7,0}$. As expected, it displays ten-dimensional poles of degree up to five. This correlator is provided in the ancillary files of [1]. See Appendix A for a guide to these files.

4.4. Review of Four-Point Integrands

The four-point loop integrand was discussed in Section 2.5.3 in the context of the ten-dimensional symmetr. As reviewed there, planar four-point correlators with arbitrary R-charge have been computed up to three loops [50], and subsequently extended to five loops [51]. These results show that all such correlators can be expressed in terms of a finite basis of fixed-charge correlators $\langle k_1,\ldots,k_4\rangle_\ell$ with bounded charges ($k_i < \ell+2$), where the size of the basis grows with the loop order. It was later observed that resumming all fixed-charge correlators leads to a compact generating function [65], which we denote by $G_{4,\ell}$. This resummation makes a hidden ten-dimensional symmetry manifest. In particular, the generating function can be obtained directly from the reduced stress-tensor integrand by performing the uplift

$$x_{ij}^2 \;\to\; X_{ij}^2 \equiv x_{ij}^2 + y_{ij}^2\,,$$

as indicated in (2.66).

In the following, we review the known results for the four-point generating function $G_{4,\ell}$ up to three loops. As will be seen in Section 4.5 and Section 4.6, these functions also appear in our higher-point results as coefficients of higher-order ten-dimensional poles.

The one-loop four-point integrand can be obtained from the NMHV component of the five-point supercorrelator, given in [69] as:

$$\mathbb{G}_5^{\text{NMHV}} = \frac{-2\,\mathcal{I}^{(5)}_{12345}}{N_c^3} \prod_{i<j}^{5} \frac{y_{ij}^2}{X_{ij}^2}\,, \tag{4.48}$$

where the superconformal invariant can be expressed as a degree-two polynomial on the fermionic delta function R, defined in (3.28), as:

$$\mathcal{I}^{(5)}_{12345} = \sum_{10} \frac{R^1_{345} R^2_{345}}{d_{12} d_{34} d_{45} d_{35}} + \sum_{60} \frac{R^1_{234} R^2_{135}}{d_{15} d_{24} d_{34} d_{35}} + \sum_{15} \frac{R^1_{234} R^1_{345}}{d_{23} d_{34} d_{45} d_{52}} \tag{4.49}$$

This combination of R^i_{jkl} with d_{ij} coefficients has permutation invariance on the five points. The numbers on the sums count the S_5 inequivalent permutations, where the identity $R^1_{234}R^1_{345} = R^1_{245}R^1_{345}$ needs to be taken into account. Most importantly, it is independent of the reference twistor $Z_\star$, used in defining the spinors of (3.37), and hence superconformally invariant. For an alternative representation of this same invariant see eq. (5.22) of [105]. In order to extract the loop integrand $G_{4,1}$, here we specialize to the Grassmann projection (4.16) of this invariant:

$$R^{(5)}_{1234;5} \equiv \mathcal{I}^{(5)}_{12345}\Big|_{\theta_5^4} \times \prod_{i<j}^{5} d_{ij} = -\frac{\mathcal{R}_{1234}}{x_{15}^2 x_{25}^2 x_{35}^2 x_{45}^2} \tag{4.50}$$

with the four-point polynomial defined in (2.48).

Finally, by doing the R-charge projection on the last point $y_5 \to 0$ to obtain the Lagrangian operator $\mathcal{L}_{\text{int}}(x_6)$, we can extract the one-loop integrand $G_{4,1}$. By repeating this computation for other supercorrelators of the form $\mathbb{G}_{4+\ell}^{\text{N}^\ell\text{MHV}}$, we can extract the loop integrands $G_{4,\ell}$. Here we present the first three loop orders:

$$\mathbb{G}_5^{\text{NMHV}} \longrightarrow G_{4,1} = \frac{2\mathcal{R}_{1234}}{N_c^2} \prod_{i<j}^{4} x_{ij}^2 \times \frac{1}{\prod\limits_{1\leq i<j\leq 5} X_{ij}^2} \Bigg|_{y_5\to 0} \tag{4.51}$$

$$\mathbb{G}_6^{\text{N}^2\text{MHV}} \longrightarrow G_{4,2} = \frac{2\mathcal{R}_{1234}}{N_c^2} \prod_{i<j}^{4} x_{ij}^2 \times \frac{X_{12}^2 X_{34}^2 X_{56}^2 + 14 \text{ perm.}}{\prod\limits_{1\leq i<j\leq 6} X_{ij}^2} \Bigg|_{y_5,y_6\to 0} \tag{4.52}$$

$$\mathbb{G}_7^{\text{N}^3\text{MHV}} \longrightarrow G_{4,3} = \frac{2\mathcal{R}_{1234}}{N_c^2} \prod_{i<j}^{4} x_{ij}^2$$
$$\times \frac{(X_{12}^2)^2 (X_{34}^2 X_{45}^2 X_{56}^2 X_{67}^2 X_{73}^2) + 251 \text{ perm.}}{\prod\limits_{1\leq i<j\leq 7} X_{ij}^2} \Bigg|_{y_5,y_6,y_7\to 0} \tag{4.53}$$

They all have the polynomial $\mathcal{R}_{1234}$ as a prefactor. The coefficient of $\mathcal{R}_{1234}$, the reduced correlator $F^{(\ell)}(X_i)$, displays ten-dimensional conformal invariance, made explicit by its exclusive dependence on the 10d distances X_{ij}^2. Furthermore, the form of the reduced integrand is the same as for the lightest operator by (2.66). This means that, in principle, the current knowledge of the stress tensor integrand up to twelve loops, see [57, 58], also gives the generating function for all KK modes by doing this 10d uplift.[10] There are other approaches based on positive geometry, see [111–113], which construct the loop integrand of the stress-tensor correlator and could be generalized to our 10d generating functions.

At the integrand level, this 10d symmetry presents spacetime and R-charge kinematics on the same footing, however, this is explicitly broken at the integrated level, since we only integrate the Lagrangian positions on 4d spacetime. Moreover, this integration can be expressed on a basis of conformal integrals, see eq. (4.52) below, which depend on 4d conformal cross-ratios and are known analytically in general kinematics up to three-loop order [42]. At higher-loop orders, there is recent progress on computing the relevant basis of conformal integrals, see [114] and [115].

[10]This statement has a caveat pertaining to the existence of 4d Gram identities. These are polynomials in X_{ij}^2 which vanish when reduced to four-dimensional x_{ij}^2, due to the lower dimensionality of the vector space. If present, such terms will be missed by the uplift of the stress-tensor correlator. So far, however, Gram identities have not been observed for the planar integrand [57] and might not exist at all in this limit.

4.5. Five-Point Integrands

In this section we report on the five-point integrands $G_{5,1}$ and $G_{5,2}$ that we obtained following the method of Section 4.2.

4.5.1. Some General Properties: Zeros and Poles

The loop integrands are rational functions of the variables d_{ij} and x_{ij}^2, and as such are characterized by their zeros and poles in these variables.

Zeros. The integrands $G_{n,\ell}$ vanish on the topological twist introduced by Drukker and Pfleka [116], which effectively enforces the spacetime and R-charge alignment: $y_{ij}^2 = x_{ij}^2$. Written in a $\mathrm{SO}(4,2) \times \mathrm{SO}(6)_R$ covariant form, these zeroes are located at the alignment of the spacetime and R-charge cross ratios:

$$\frac{x_{ij}^2 x_{kl}^2}{x_{ik}^2 x_{jl}^2} = \frac{y_{ij}^2 y_{kl}^2}{y_{ik}^2 y_{jl}^2} \quad \text{or} \quad \frac{d_{ij} d_{kl}}{d_{ik} d_{jl}} = 1\,. \tag{4.54}$$

This property is made manifest in our results by the presence of a two-by-two determinant denoted as:

$$V_{kl}^{ij} \equiv d_{ij}\, d_{kl} - d_{ik}\, d_{jl}\,. \tag{4.55}$$

Furthermore, our results also depend on higher-rank d-determinants, see for instance (4.63).

Poles. The generating functions $G_{n,\ell}$ exhibit two distinct types of poles. On the one hand, there are poles in the four-dimensional distances x_{ij}^2, which are associated with ordinary propagators d_{ij} (4.9). On the other hand, there are poles in the ten-dimensional distances $X_{ij}^2 = x_{ij}^2 + y_{ij}^2$, which arise from the effective ("fat") propagators D_{ij}.

The appearance of poles in x_{ij}^2 can be traced back to the projection of the super-operators $\mathbb{O}$ onto the interaction Lagrangian $\mathcal{L}_{\text{int}}$ at the insertion points $n{+}1, \ldots, n{+}\ell$. This projection truncates the geometric series $D_{ij} = d_{ij} + d_{ij}^2 + \ldots$ to ordinary propagators d_{ij}, thereby producing poles only in x_{ij}^2.

For convenience, it is useful to introduce the variables w_{ij}, which relate the different quantities d_{ij}, D_{ij}, x_{ij}^2, y_{ij}^2, and X_{ij}^2 as follows:

$$w_{ij} \equiv 1 - d_{ij} = \frac{1}{1 + D_{ij}} = \frac{d_{ij}}{D_{ij}} = \frac{x_{ij}^2 + y_{ij}^2}{x_{ij}^2} = \frac{X_{ij}^2}{x_{ij}^2}\,. \tag{4.56}$$

In this parametrization, the ten-dimensional poles can be expressed compactly as poles in w_{ij}. Higher-point functions also display higher-order ten-dimensional poles, whose coefficients are given by lower-point functions. We will see this exemplified in (4.71) and (4.73) below, and provide a general analysis of the higher-order poles in Section 4.7.

4.5.2. One-Loop Integrand $G_{5,1}$

The integrand $G_{5,1}$ can be extracted from the six-point super-correlator $\mathbb{G}_6^{\text{NMHV}}$ computed in [69]. This was given by a combination of two six-point superconformal invariants $\mathcal{I}^{(6a)}$ and $\mathcal{I}^{(6b)}$, and the five-point invariant $\mathcal{I}^{(5)}$ defined in (4.49):

$$N_{\text{c}}^4 \times \mathbb{G}_6^{\text{NMHV}} = \Big(2\,\mathcal{I}_{123456}^{(6a)} - 2\,\mathcal{I}_{123456}^{(6b)}\Big) \prod_{i<j}^{6} D_{ij} + \left[\tilde{C}_{12345,6}^{(5)}\,\mathcal{I}_{12345}^{(5)} \prod_{i<j}^{5} D_{ij} + (\text{C}_6 \text{ perms})\right]. \tag{4.57}$$

Here, C_6 is the cyclic group on six points, that is the last term is summed over six cyclic permutations.

The coefficient of the five-point invariant $\mathcal{I}^{(5)}$, defined in (4.49), is a polynomial in the effective 10d propagator D_{ij}:

$$\begin{aligned} \tilde{C}_{12345,6}^{(5)} &= 4 D_{16} D_{26} D_{36} D_{46} D_{56} + 2 \sum_{5} D_{16} D_{26} D_{36} D_{46} \\ &\quad - 2 \sum_{10} D_{16} D_{26} (1 + D_{12})\,. \end{aligned} \tag{4.58}$$

It has permutation invariance on the labels before the comma, and the numbers on the sums count the S_5 inequivalent permutations.

The simplest of the six-point invariants is given by:

$$\mathcal{I}_{123456}^{(6b)} = \sum_{90} \frac{R_{234}^1 R_{561}^4}{d_{23} d_{56}} \, \frac{\det\,[d_{ij}]_{j=4,5,6}^{i=1,2,3}}{\prod_{\substack{i=1,2,3\\ j=4,5,6}} d_{ij}}$$

$$
\begin{aligned}
&+\sum_{360} \frac{R^1_{234}R^2_{135}}{d_{34}d_{35}d_{36}d_{12}d_{24}d_{45}d_{51}}\left[\frac{d_{12}}{d_{16}d_{26}}-\frac{d_{15}}{d_{16}d_{56}}-\frac{d_{24}}{d_{26}d_{46}}+\frac{d_{45}}{d_{46}d_{56}}\right]\\
&+\sum_{90} \frac{R^1_{234}R^2_{134}}{d_{12}d_{34}d_{35}d_{36}d_{45}d_{46}}\left[\frac{1}{d_{15}d_{26}}+\frac{1}{d_{16}d_{25}}\right]\\
&-\sum_{180} \frac{R^1_{234}R^1_{235}}{d_{16}d_{23}d_{24}d_{25}d_{34}d_{35}d_{46}d_{56}}\,.
\end{aligned}
\tag{4.59}
$$

It is independent of the reference twistor $Z_\star$, and it is proportional to the stress-tensor supercorrelator, see eq. (3.20) of [117]. An expression for the invariant $\mathcal{I}^{(6a)}$ can be found in eq. (6.36) of [69]. This invariant has a higher degree on y_6, and it does not survive the R-charge projection that extracts the Lagrangian operator.

In order to extract the integrand $G_{5,1}$ we consider the Grassmann and R-charge projections:

Grassmann Projection of Super-Invariants. By following the method described in Section 4.2.1, we obtain the Grassmann projections of the six-point invariants:[11]

$$
R^{(6b)}_{12345;6} \equiv \mathcal{I}^{(6b)}_{123456}\Big|_{\theta_6^4} \times \prod_{i<j=1}^{6} d_{ij} \tag{4.60}
$$

$$
= \frac{1}{4}\left[\frac{x_{12}^2x_{34}^2\, d_{15}\, V^{12}_{34}\, V^{23}_{54}}{x_{16}^2x_{26}^2x_{36}^2x_{46}^2} + (\mathrm{S}_5 \text{ perms})\right] + 4i\,\frac{X^{\text{anti}}_{123456}\times d^{\text{anti}}_{12345}}{x_{16}^2x_{26}^2x_{36}^2x_{46}^2x_{56}^2}\,,
$$

$$
R^{(6a)}_{12345;6} \equiv \mathcal{I}^{(6a)}_{123456}\Big|_{\theta_6^4} \times \prod_{i<j=1}^{6} d_{ij} \tag{4.61}
$$

$$
\begin{aligned}
&= \frac{1}{4}\left[\frac{d_{12}d_{23}d_{34}d_{45}d_{51}d_{56}}{x_{16}^2x_{26}^2x_{36}^2x_{46}^2}\left(x_{12}^2x_{34}^2V^{12}_{34}+x_{14}^2x_{23}^2V^{13}_{42}\right) + (\mathrm{S}_5 \text{ perms})\right]\\
&\quad + 4i\,\frac{Y^{\text{anti}}_{123456}\times d^{\text{anti}}_{12345}}{x_{16}^2x_{26}^2x_{36}^2x_{46}^2x_{56}^2},
\end{aligned}
\tag{4.62}
$$

where the V-factors are defined in (4.55) and the function d^{anti}_{12345} is given by:

$$
d^{\text{anti}}_{12345} = \frac{1}{10}\sum_{\sigma\in \mathrm{S}_5} \operatorname{sign}(\sigma) d_{\sigma_1\sigma_2}d_{\sigma_2\sigma_3}d_{\sigma_3\sigma_4}d_{\sigma_4\sigma_5}d_{\sigma_5\sigma_1}\,. \tag{4.63}
$$

[11] The parity-odd parts that involve X^{anti} and Y^{anti} suggest that the invariants $R^{(6b)}$ and $R^{(6a)}$ should combine symmetrically, such that X^{anti} and Y^{anti} join into a larger ten-dimensional invariant. And in fact they do combine symmetrically in (4.57), (4.65). A lesson to be drawn from this is that higher-point correlators with ten-dimensional invariance may contain larger invariants besides the simple ten-dimensional distances X_{ij}^2.

In $R^{(6b)}_{12345;6}$, the unique parity-odd conformal covariant $X^{\rm anti}_{123456}$ at six points appears, which was discussed before around (4.42). Analogously, we define an antisymmetric Y-structure using the projective six-dimensional null-vectors Y^I that transform under the fundamental representation of the internal group SO(6):[12]

$$Y^{\rm anti}_{123456} = \varepsilon_{IJKLMP} Y_1^I Y_2^J Y_3^K Y_4^L Y_5^M Y_6^P \,. \tag{4.64}$$

Notice that, when choosing the polarization matrices $y^{ab'}$ to be real, $Y^{\rm anti}_{123456}$ will in general be imaginary, yielding a real contribution in (4.61). This is consistent, since the term is parity-even and thus should be real. In contrast, the $X^{\rm anti}_{123456}$ term in (4.60) is parity-odd and thus imaginary. Putting these projections together, we obtain the correlator:

$$\tilde{G}_{5,1} = \frac{1}{N_c^3}\frac{2R^{(6a)}_{12345;6} - 2R^{(6b)}_{12345;6}}{\prod_{i<j}^6 w_{ij}} + \left[\frac{1}{N_c^3}\frac{\tilde{C}^{(5)}_{12346,5}\, R^{(5)}_{1234;6}}{\prod_{i<j}^4 w_{ij}\prod_{i=1}^4 w_{i6}} + (\mathrm{C}_5 \text{ perms.})\right], \tag{4.65}$$

where $R^{(5)}_{1234;6}$ was defined in (4.50). This tree-level correlator includes all the higher-R-charge partners of the Lagrangian operator (KK modes in the bulk dual dictionary). In order to obtain the loop integrand $G_{n,\ell}$, we project out these KK modes.

R-charge Projection Down to Loop Integrand. Taking the final projection $y_6 \to 0$, we obtain the loop integrand $G_{5,1}$. Notice that the susy invariant $\mathcal{I}^{(6a)}$ will only contribute to correlators that include higher KK modes of the chiral Lagrangian. The coefficient of the five-point invariant becomes

$$C^{(5)}_{1234,5} \equiv \prod_{i=1}^4 w_{i5} \times \tilde{C}^{(5)}_{12346,5}\Big|_{y_6\to 0} = \frac{1}{2}\left(\frac{d_{15}d_{25}d_{35}d_{45}}{6} - \frac{d_{15}d_{25}\, w_{35}w_{45}}{w_{12}} + (\mathrm{S}_4 \text{ perms})\right). \tag{4.66}$$

[12] Starting from the twistor-like decomposition of the polarization vectors

$$y_i^{AB} = \epsilon^{ab} Y^A_{i,a} Y^B_{i,b} \quad \text{and choosing:} \quad \begin{pmatrix} Y_{i,1} \\ Y_{i,2}\end{pmatrix} = \begin{pmatrix} 1 & 0 & y_i^{11} & y_i^{12} \\ 0 & 1 & y_i^{21} & y_i^{22}\end{pmatrix},$$

one can obtain the six-dimensional projective polarization vectors by using appropriate sigma matrices Σ^I_{AB} that relate the antisymmetric representation of SU(4) to the fundamental of SO(6) by $Y_i^I = \Sigma^I_{AB}\, y_i^{AB}$. As a representation for Σ^I_{AB} we choose $2\,\Sigma^I = (\sigma_{12},\, i\,\sigma_{23},\, -\sigma_{20},\, -i\,\sigma_{21},\, -\sigma_{32},\, i\,\sigma_{21})$, with $\sigma_{\mu\nu} = \sigma_\mu \otimes \sigma_\nu$, and σ_μ being the Pauli matrices.

Since $R^{(6b)}_{12345;6}$ and $R^{(5)}_{1234;6}$ do not depend on y_6, they remain unchanged by this projection and the one-loop integrand can be expressed as

$$G_{5,1} = \frac{1}{N_c^3} \frac{-2R^{(6b)}_{12345;6} + \left[C^{(5)}_{1234,5} R^{(5)}_{1234;6} + (\mathrm{C}_5 \text{ perms.})\right]}{\prod_{i<j}^5 w_{ij}} \,. \tag{4.67}$$

The one-loop integrand can also be expressed as a sum over one-loop box integrals. To achieve this, we introduce the five-point polynomial $\mathcal{R}_{1234,5}$, defined as the even part of the numerator of (4.60):

$$\begin{aligned} \mathcal{R}_{1234,5} &\equiv -\tfrac{1}{2}\, x_{12}^2 x_{34}^2\, d_{15} V_{34}^{12} V_{54}^{23} + (\mathrm{S}_4 \text{ perms}) \\ &= x_{12}^2 x_{34}^2 \Big(d_{45} V_{35}^{12} V_{43}^{12} + d_{35} V_{34}^{12} V_{45}^{12} - d_{15} V_{34}^{12} V_{54}^{23} - d_{15} V_{43}^{12} V_{53}^{24} \Big) \\ &\quad + (1 \leftrightarrow 3) + (1 \leftrightarrow 4) \,, \end{aligned} \tag{4.68}$$

which is independent of the Lagrangian insertion point (6), symmetric on the points $1, \ldots, 4$, and has y-weight 2 in all five points $1, \ldots, 5$. It satisfies a simple OPE-like relation to the four-point polynomial (2.48) as:

$$\lim_{y_5 \to y_4} \frac{\mathcal{R}_{1234,5}}{2\, d_{45}} = \mathcal{R}_{1234} \tag{4.69}$$

Finally, we can rewrite the one-loop integrand as a sum over box diagrams, with numerators given by the polynomials in (2.48) and (4.68) as:

$$\begin{aligned} G_{5,1} = \frac{1}{N_\mathrm{c}^3} \prod_{i<j=1}^{5} \frac{1}{w_{ij}} \Bigg(& \frac{\mathcal{R}_{1234,5} - C^{(5)}_{1234;5}\, \mathcal{R}_{1234} - 4i\, d^{\mathrm{anti}}_{12345}\, \varepsilon_{\kappa\lambda\mu\nu} x_{16}^{\kappa} x_{26}^{\lambda} x_{36}^{\mu} x_{46}^{\nu}}{x_{16}^2 x_{26}^2 x_{36}^2 x_{46}^2} \\ & + (\mathrm{C}_5 \text{ perms}) \Bigg) \,, \end{aligned} \tag{4.70}$$

where we have separated off the parity-odd part and written it using (4.43).

4.5.3. Two-Loop Integrand $G_{5,2}$

In this section we present results on the five-point two-loop integrand $G_{5,2}$, which we extract as a Grassmann and R-charge projection of the seven-point supercorrelator $\mathbb{G}_7^{\mathrm{N^2MHV}}$. After performing this projection, we resort to the "divide and conquer" strategy, described in Section 4.2.2, to fix the numerator that multiplies the ten-dimensional poles of the generating function $G_{5,2}$. We present this numerator in terms of a finite basis of correlators with fixed R-charge, starting with the stress-tensor correlator.

We present the generating function in a finite basis of correlators with fixed R-charge, with coefficients containing simple and double poles on the 10d distances X_{ij}^2. For convenience, we use the variables w_{ij} introduced earlier (4.56) to express these 10d poles.

For the one-loop integrand, this representation follows straightforwardly from (4.70) and reads as:

$$G_{5,1} = \frac{\langle 22222\rangle_1}{\prod\limits_{1\leq i<j\leq 5} w_{ij}} - \frac{1}{2N_\mathrm{c}}\left(\frac{C^{(5)}_{1234;5}}{w_{15}w_{25}w_{35}w_{45}}\, G_{4,1} + (\mathrm{C}_5 \text{ perms.})\right), \tag{4.71}$$

The first term only contains simple poles on each pair w_{ij}, and the numerator is given by the $\mathbf{20'}$ or stress-tensor integrand, see (4.20) for the notation. This correlator can be identified by the terms in (4.70) which depend on the polynomial $\mathcal{R}_{1234,5}$, defined in (4.68). More explicitly, this is given by:

$$\langle 22222\rangle_1 = -\frac{2R^{(6b)}_{12345;6}}{N_\mathrm{c}^3} = \frac{1}{N_\mathrm{c}^3}\,\frac{\mathcal{R}_{1234,5} - 4i\, d^{\mathrm{anti}}_{12345}\,\varepsilon_{\kappa\lambda\mu\nu}x^\kappa_{16}x^\lambda_{26}x^\mu_{36}x^\nu_{46}}{x^2_{16}x^2_{26}x^2_{36}x^2_{46}} + (\mathrm{C}_5 \text{ perms.})\,. \tag{4.72}$$

The second term in (4.71) is given by terms in (4.70) controlled by the polynomial $\mathcal{R}_{1234}$. It can be identified with the four-point generating function $G_{4,1}$ ($\sim N_\mathrm{c}^{-2}$) in (4.51), dressed with a coefficient which contains all the double poles of the five-point integrand. See (4.66) for the explicit definition of the coefficient.

Inspired by the one-loop results above, we searched for a similar representation of the two-loop integrand. Indeed, we found that the double-pole terms are accounted for by the same coefficient in (4.71), now dressed by the two-loop four-point integrand $G_{4,2}$ in (4.52). On the other hand, the simple-pole numerator is slightly more complicated, and is given by a finite basis of fixed-charge correlators with small R-charge, in addition to the $\mathbf{20'}$ correlator. In detail, the parity-even part of the generating function reads as follows:

$$G_{5,2} = \frac{1}{\prod\limits_{1\leq i<j\leq 5} w_{ij}}\Big(\langle 22222\rangle_2 + \langle 42222\rangle_2 + \langle 33222\rangle_2^\star + \langle 33332\rangle_2^\star$$

$$
\begin{aligned}
&\qquad\qquad + \langle 33334\rangle_2^\star + \langle 44444\rangle_2^\star + (\text{ineq perm.})\Big) \\
&- \frac{1}{2N_\mathrm{c}}\left(\frac{C^{(5)}_{1234;5}}{w_{15}w_{25}w_{35}w_{45}}\, G_{4,2} + (\mathrm{C}_5 \text{ perms})\right) .
\end{aligned}
\tag{4.73}
$$

Again, the angled brackets denote fixed-weight correlators (4.20), and the star indicates a modification to the respective correlator. In the first line, each (modified) correlator in the numerator must be permuted over all inequivalent configurations such that the expression becomes S_5-symmetric. In particular, the contributions are defined as

$$
\begin{aligned}
\langle 33222\rangle_2^\star &= \langle 33222\rangle_2 - d_{12}\langle 22222\rangle_2 - \left(\frac{d_{15}d_{25}}{2}\langle 2222\rangle_2 + (\mathrm{C}_3 \text{ perms})\right) , \\
\langle 33332\rangle_2^\star &= \langle 33332\rangle_2 - \Big(\frac{d_{34}}{4}\langle 33222\rangle_2^\star + \frac{d_{12}d_{34}}{8}\langle 22222\rangle_2 + \frac{d_{35}d_{45}}{4}\langle 3322\rangle_2 \\
&\qquad + (\mathrm{C}_4 \text{ perms})\Big) , \\
\langle 33334\rangle_2^\star &= \langle 33334\rangle_2 - \Big(\frac{d_{15}}{6}\langle 23333\rangle_2^\star + \frac{d_{35}d_{45}}{4}\langle 33222\rangle_2^\star + \frac{d_{12}d_{35}}{2}\langle 22233\rangle_2^\star \\
&\qquad + \frac{d_{12}d_{34}}{8}\langle 22224\rangle_2 + \frac{d_{15}d_{25}d_{34}}{4}\langle 22222\rangle_2 \\
&\qquad + \frac{d_{35}d_{45}^2}{2}\langle 3322\rangle_2^{[1,2,3,5]} - \frac{d_{15}d_{25}d_{35}d_{45}}{24}\langle 2222\rangle_2 \\
&\qquad + (\mathrm{C}_4 \text{ perms})\Big), \\
\langle 44444\rangle_2^\star &= \frac{(d_{14}d_{23}x_{14}^2x_{23}^2 + d_{13}d_{24}x_{13}^2x_{24}^2 + d_{12}d_{34}x_{12}^2x_{34}^2)d_{15}d_{25}d_{35}d_{45}}{12N_c^3\; x_{16}^2x_{26}^2x_{36}^2x_{46}^2x_{17}^2x_{27}^2x_{37}^2x_{47}^2}\mathcal{R}_{1234} \\
&\quad + (\mathrm{C}_5 \text{ perms}) .
\end{aligned}
\tag{4.74}
$$

The modifications are such that they preserve the permutation symmetries of the unstarred correlators $\langle\ldots\rangle_2$. Since, the contribution $\langle 44444\rangle_2^\star$ contains only few terms, we refrained from formulating it in terms of the full correlator, but simply state it directly. This basis of R-charge correlators in terms of conformal integrals is provided in the ancillary files of [1]. See Appendix A for a guide to this file. Our result for the lightest correlator $\langle 22222\rangle_2$ matches with [60], and the correlator $\langle 44444\rangle_2$, extracted from (4.73) via (4.20), is consistent with the decagon correlator of [76, 77].

This representation in a finite basis of R-charge correlators is expected based on the "saturation of bridges" in the planar limit at weak coupling [50], see for instance Figure 1 in [65]. When the number of free propagators between two single-trace BPS operators becomes larger than the loop order, to stay in the planar topology, this bridge of propagators becomes uncrossable by loop corrections. Based on this argument, we can expect that at ℓ-loop order the basis of R-charge correlators, sufficient to get the full generating function, starts with $\langle 22\cdots 2\rangle$ and ends with $\langle pp\cdots p\rangle$ with $p = 2\ell$ (or slightly larger). This latter R-charge correlator corresponds to the "simplest correlators", at ℓ-loop order, such as the so-called octagon [71] and decagon [76] in the four- and five-point cases.[13] We are concerned with generalizing these simplest correlators to higher points in Chapter 5. While this representation can become handy in the absence of another organizational principle, it can also obscure the symmetries of the generating function. For instance the generating functions $G_{4,\ell}$ have a ten-dimensional symmetry as shown in eqs. (4.51)-(4.53), however this is not at all evident in the R-charge basis representation of [50, 51]. The presence of the four-point correlator sitting on the double-poles of the five-point correlator can be explained by the same principle, combined with an analysis of the graphs that contribute to the twistor computation. Moreover, we expect this nesting structure of lower-point functions controlling the higher-order poles to be more general. In Section 4.6.1, we present another example of this nesting for the six-point correlator, which contains the five-point and four-point correlators controlling the double and triple poles respectively. A more detailed argument as well as concrete formulas are presented in Section 4.7.

4.6. Six-Point Integrand

We present results on the six-point one-loop integrand extracted from the supercorrelator $\mathbb{G}_7^{\mathrm{NMHV}}$. Besides simple 10d poles, this correlator presents nested five-point integrands sitting at double poles and four-point integrands sitting at third-order 10d poles.

4.6.1. One-Loop Integrand $G_{6,1}$

The six-point one-loop integrand, at leading planar order, is given by

$$G_{6,1} = \prod_{i<j=1}^{6} \frac{1}{w_{ij}} \times \Big(\langle 222222\rangle_1 + \langle 333333\rangle_1^\star + \frac{1}{N_\mathrm{c}} \Big[C^{(6,1)}_{12345,6} \langle 22222\rangle_1 + (5 \text{ perm.}) \Big]$$

[13] The same principle applies at subleading orders in $1/N_\mathrm{c}^2$ (i. e. higher-genus corrections), and was used in [109, 118, 119] to factorize higher-genus large-charge correlators into patches of disk topology that can be computed individually from integrability/hexagonalization.

$$+\frac{1}{N_c^2}\left[C^{(6,2)}_{1234,56}\,\langle 2222\rangle_1 + (14\text{ perm.})\right]\Bigg)\,. \quad (4.75)$$

Here, $\langle 222222\rangle_1$, $\langle 22222\rangle_1$, $\langle 2222\rangle_1$ denote the one-loop $\mathbf{20'}$ integrands at six, five, and four points. In each case, the operators are understood to be labeled by 1 through 6, 5, and 4, respectively. For convenience, we repeat the expressions for the latter two integrands in terms of the invariants discussed in Section 4.5.2:

$$\langle 22222\rangle_1 = -2R^{(6b)}_{12345;7}/N_c^3 \quad \text{and} \quad \langle 2222\rangle_1 = -2R^{(5)}_{1234;7}/N_c^2\,. \quad (4.76)$$

$\langle 333333\rangle_1^\star$ appears as an additional structure, and has an R-charge weight of 3 in each of the six points. As a result, in the charge-expansion (4.19), the six-point correlator that contains only operators of weight 3 is the first correlator in which this structure appears. More explicitly we have:

$$\langle 333333\rangle_1 = \langle 333333\rangle_1^\star + \left(\frac{d_{12}d_{34}d_{56}}{48}\langle 222222\rangle_1 + \frac{d_{12}d_{35}d_{46}d_{56}^2}{4\,N_c^2}\langle 2222\rangle_1 \right.$$
$$\left. + (\mathrm{S}_6\text{ perms})\right)\,. \quad (4.77)$$

Correlators that contain this structure cannot be written as linear combinations of $\mathbf{20'}$ correlators. The new invariant $\langle 333333\rangle_1^\star$ and the $\mathbf{20'}$ six-point correlator $\langle 222222\rangle_1$ are given in terms of V^{ij}_{kl} (4.55) by

$$\langle 222222\rangle_1 = \frac{1}{N_c^4}\frac{d_{26}V^{14}_{32}}{4}\left(2d_{56}V^{14}_{53} + d_{45}V^{15}_{63}\right)\frac{x_{14}x_{23}}{x_{17}x_{27}x_{37}x_{47}} + (\mathrm{S}_6\text{ perms})\,, \quad (4.78)$$

$$\langle 333333\rangle_1^\star = \frac{1}{N_c^4}\frac{d_{26}d_{45}V^{14}_{32}}{4}\frac{x_{14}x_{23}}{x_{17}x_{27}x_{37}x_{47}}\Big(2d_{16}d_{35}d_{56}V^{12}_{43} + 2d_{16}d_{25}d_{36}V^{14}_{53}$$
$$+ d_{12}d_{34}d_{56}V^{15}_{63}\Big) + (\mathrm{S}_6\text{ perms})\,. \quad (4.79)$$

Finally, the coefficient of the five-point invariant in the generating function is:

$$C^{(6,1)}_{12345,6} = d_{16}d_{26}\left(\frac{-d_{36}d_{46}}{24} + \frac{d_{36}d_{46}d_{56}}{40} + \frac{1-3d_{36}+3d_{36}d_{46}-d_{36}d_{46}d_{56}}{12\,w_{12}}\right)$$
$$+ (\mathrm{S}_5\text{ perms.})\,, \quad (4.80)$$

and presents a simple ten-dimensional pole on $w_{ij} = 1 - d_{ij}$ with $i, j \neq 6$, which combined with the overall factor in (4.75) gives a double pole. On the other hand, the four-point coefficient $C^{(6,2)}_{1234,56}$ contains higher-order 10d poles, and can be most compactly written when using the variable $D_{ij} \equiv d_{ij}/(1-d_{ij}) = -y_{ij}^2/X_{ij}^2$. For comparison, here we write both coefficients, $C^{(6,1)}$ and $C^{(6,2)}$, making use of D_{ij}:

$$\begin{aligned}
C^{(6,1)}_{12345,6} = \prod_{i=1}^{5} w_{i6} \times D_{16} D_{26} \Big(1 + D_{12} - \tfrac{1}{2} D_{36} D_{46} - \tfrac{1}{5} D_{36} D_{46} D_{56}\Big) \\
+ (\mathrm{S}_5 \text{ perms.})
\end{aligned} \tag{4.81}$$

$$\begin{aligned}
C^{(6,2)}_{1234,56} = \frac{w_{56}}{24} \prod_{i=1}^{4} w_{i5} w_{i6} \times D_{16} \Big[3 D_{26} D_{35} D_{45} (D_{12}(D_{34}+2)+1) \\
+ 4 D_{56} D_{15}^2 (3 D_{12}(D_{25}+1) + D_{25}(3 - D_{35} D_{45}) + 2) \\
+ D_{15} \Big(4(D_{12}(6 D_{25}+3) + D_{25}(6 - 2 D_{35} D_{45}) + 2) D_{56} \\
+ D_{26}(6(2(D_{12}(D_{13}+2)+1) D_{35} \\
+ (D_{12}+1) D_{25}(D_{12} - D_{35} D_{45} + 1))) \\
+ 2 D_{26} D_{25} D_{56} (3 D_{12} + D_{36} D_{45}(D_{35}(D_{46}+4)+3)+3) \Big) \\
+ 2 D_{25} D_{56} (3(D_{12}+1) - 2 D_{35} D_{45}) \Big] + (\mathrm{S}_4 \times \mathrm{S}_2 \text{ perms.})
\end{aligned} \tag{4.82}$$

We further observe that the five-point coefficient (4.81) reduces to the four-point coefficient in (4.66) by taking the limit:

$$\lim_{y_5 \to 0} C^{(6,1)}_{12345,6} = C^{(5)}_{1234,6} \tag{4.83}$$

while the four-point coefficient in (4.82) vanishes in this same limit. Moreover, we notice that also the four-point coefficient $C^{(5)}_{1234,5}$ vanishes in the limit $y_5 \to 0$, which suggests an iterative structure.

Finally, this one-loop integrand can be easily upgraded to the integrated level by replacing the factors $1/(x_{al}^2 x_{bl}^2 x_{cl}^2 x_{dl}^2)$ by the one-loop scalar box integrals. While the content on arbitrary R-charge correlators remains on the rational coefficients with 10d poles.

4.7. Structure of Higher Poles

Beyond four points, the loop integrand $G_{n,\ell}$ acquires higher ten-dimensional poles. This was anticipated in Section 4.2.2, and in (4.71), (4.73), and (4.75), we observed that double and triple poles can be written in terms of lower-point integrands $G_{m,\ell}$ with $m < n$. Let us now discuss the higher-order poles more systematically.

4.7.1. Factorization Structure of Higher-Order Poles

The nesting structure of higher-order poles can be understood via the "saturation of bridges" property discussed at the end of Section 4.5.3. A ten-dimensional pole (propagator D_{ij}) represents a bundle ("bridge") of arbitrarily many parallel ordinary propagators d_{ij} and therefore cannot be crossed by loop corrections in the planar limit, due to supersymmetry and the BPS nature of the operator insertions. A double pole $D_{ij} \times D_{ij}$ between two operators i and j thus introduces a contour formed by the two ten-dimensional propagators together with the operator insertions, which splits the color sphere into two disc-like regions. Interactions are confined to these separate regions, and the loop corrections factorize along the contour at the double pole.

This general mechanism can be illustrated using the five-point integrand $G_{5,\ell}$. The two propagators D_{ij} must be homotopically distinct, so each of the two regions must contain at least one of the remaining $n-2$ operators. For the five-point function, this leads to a substructure of the form

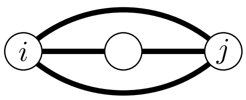

. (4.84)

The sum of all terms surrounding this substructure must reconstruct a part of the generating function $G_{4,\ell}$, namely the contribution containing a bridge $1/w_{ij}$, which is replaced by (4.84). This implies

$G_{5,\ell}\Big[$ 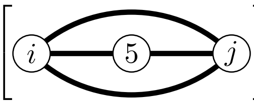

$\Big] = \frac{1}{N_{\mathrm{c}}} \frac{D_{i5} D_{j5}}{w_{ij}} \times G_{4,\ell}\big|_{1/w_{ij}\ \mathrm{term}}\,,$ (4.85)

where the left-hand side denotes all terms in $G_{5,\ell}$ containing the indicated substructure. Terms in $G_{4,\ell}$ without a $1/w_{ij}$ pole do not contribute. This expression matches precisely the double-pole contributions observed at one loop (4.71) and two loops (4.73).

The substructure (4.84) corresponds to a three-point function in which the bridge D_{ij} splits into two. In a spherical representation, this can be interpreted as cutting the sphere along the D_{ij} bridge. Performing the same operation on the four-point function $G_{4,\ell}$ and gluing the resulting pieces produces the double-pole contribution to $G_{5,\ell}$:

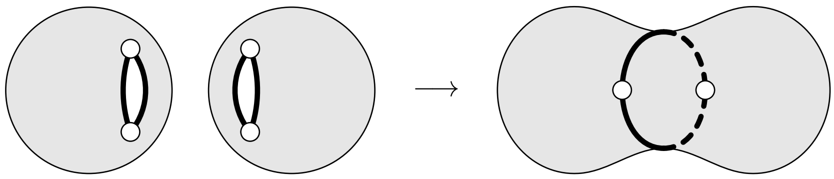

(4.86)

4.7.2. General Decomposition of Higher-Order Poles

At higher points $G_{n,\ell}$ with $n > 5$, both spheres can contain non-trivial lower-point functions G_{m_1,ℓ_1} and G_{m_2,ℓ_2}, with $m_1 + m_2 = n + 2$ and $\ell_1 + \ell_2 = \ell$. Higher-point functions also exhibit poles $1/w_{ij}^p$ of higher order p, with $p \leq n - 3$, which are obtained by gluing together p spheres, i. e. by taking products of p lower-point generating functions. Hence, all double- and higher-pole terms of $G_{n,\ell}$ are given by products of lower-point generating functions. An example of this structure is provided by the six-point integrand (4.75), where the double and triple poles are expressed in terms of five-point and four-point generating functions.

More precisely, the double poles of $G_{n,\ell}$ can be reconstructed entirely from products of single-pole terms of lower-point (and lower-loop) functions $G_{m,k}$ as follows:

$$\hat{W}_{ij}^2[G_{n,\ell}] = \frac{1}{2} \sum_{\mathbf{m}}{}' \sum_{\mathbf{k}} \hat{W}_{ij}^1[G_{\mathbf{m},\mathbf{k}}] \times \hat{W}_{ij}^1[G_{\bar{\mathbf{m}},\bar{\mathbf{k}}}]\,. \tag{4.87}$$

The first sum runs over all subsets $\mathbf{m} \subset \{1, \ldots, n\}$ with $i, j \in \mathbf{m}$ and $3 \leq |\mathbf{m}| \leq n-1$, while $\bar{\mathbf{m}}$ denotes the complement such that $\mathbf{m} \cup \bar{\mathbf{m}} = \{1, \ldots, n\}$ and $\mathbf{m} \cap \bar{\mathbf{m}} = \{i, j\}$. The second sum runs over all bipartitions $\mathbf{k} \,\dot{\cup}\, \bar{\mathbf{k}} = \{n+1, \ldots, n+\ell\}$. We indicate this distinction in the summation by a prime. Here, $G_{\mathbf{m},\mathbf{k}}$ denotes $G_{|\mathbf{m}|,|\mathbf{k}|}$ with operators labeled according to the elements of the sets $\mathbf{m}$ and $\mathbf{k}$.

The operator $\hat{W}_{ij}^p$ extracts the $1/w_{ij}^p$ pole part of a function:

$$\hat{W}_{ij}^p[f(w_{ij})] \equiv \frac{1}{w_{ij}^p} \operatorname*{Res}_{w_{ij}=0}\Big[w_{ij}^{p-1} f(w_{ij})\Big]\,. \tag{4.88}$$

In (4.87), all $G_{n,\ell}$ are assumed to be expressed in terms of w_{ij} variables, i. e. all d_{ij} and D_{ij} are rewritten using (4.56). The overall factor $1/2$ is a symmetry factor compensating the double counting arising from exchanging the two spheres in (4.84).

The formula agrees exactly with the double-pole parts of the five-point functions (4.71) and (4.73).

Similarly, the triple poles of $G_{n,\ell}$ decompose the color sphere into three discs, or equivalently three spheres with a single cut each. Accordingly, the triple pole can be written as a product of three single-pole contributions:

$$\hat{W}^3_{ij}[G_{n,\ell}] = \frac{1}{3} \sum_{\mathbf{m}_1,\mathbf{m}_2,\mathbf{m}_3}{}' \sum_{\mathbf{k}_1,\mathbf{k}_2,\mathbf{k}_3} \prod_{r=1}^{3} \hat{W}^1_{ij}[G_{\mathbf{m}_r,\mathbf{k}_r}]\,, \tag{4.89}$$

where $\mathbf{m}_r \subset \{1,\ldots,n\}$ satisfy $|\mathbf{m}_r| \geq 3$, $\bigcup_r \mathbf{m}_r = \{1,\ldots,n\}$, and $\mathbf{m}_r \cap \mathbf{m}_s = \{i,j\}$. The factor $1/3$ compensates the symmetry under cyclic permutations of the three factors. The second sum runs over all tripartitions $\dot{\bigcup}_r \mathbf{k}_r = \{n+1,\ldots,n+\ell\}$.

Using (4.87), the triple pole can also be written as a product of a single-pole and a double-pole term:

$$\hat{W}^3_{ij}[G_{n,\ell}] = \frac{1}{3} \sum_{\mathbf{m}}{}' \sum_{\mathbf{k}} \hat{W}^1_{ij}[G_{\mathbf{m},\mathbf{k}}] \times 2\, \hat{W}^2_{ij}[G_{\bar{\mathbf{m}},\bar{\mathbf{k}}}]\,. \tag{4.90}$$

These relations generalize straightforwardly to poles of arbitrary order:

$$\hat{W}^p_{ij}[G_{n,\ell}] = \frac{1}{p} \sum_{\mathbf{m}_1,\ldots,\mathbf{m}_p}{}' \sum_{\mathbf{k}_1,\ldots,\mathbf{k}_p} \prod_{r=1}^{p} \hat{W}^1_{ij}[G_{\mathbf{m}_r,\mathbf{k}_r}]\,. \tag{4.91}$$

(4.90) suggests that the complete higher-pole part of $G_{n,\ell}$ may be expressible in terms of products of two lower-point functions, dressed with appropriate symmetry factors.

A caveat is that these relations hold only in the single-trace operator basis, and not in the single-particle basis used elsewhere in this chapter. The reason is that graphs containing operators of valency one can combine into graphs in which all operators have valency at least two, thus contributing to single-particle generating functions. Consequently, in the above decompositions, the lower-point functions on the right-hand side must be taken in the single-trace basis, which then also produces the pole in the single-trace basis on the left-hand side.[14] We have explicitly verified that these relations hold for all higher-order poles of the tree-level functions $G^{\text{st}}_{n,0}$ up

[14] At leading order (without Lagrangian insertions), the relations should remain valid if only the operators i and j on the right-hand side are taken in the single-trace basis, while all other operators remain in the single-particle basis. This, however, does not extend to loop level.

to $n = 6$. Since loop corrections do not modify the ten-dimensional pole structure, we expect them to hold also at loop level in the single-trace basis.
Nevertheless, we find that the relations remain valid in the single-particle basis when restricted to the highest-order poles with $p = n - 3$. This was already verified for the double poles of the five-point function. At six points, the highest poles are of order three. From (4.82), extracting the third-order pole of the one-loop generating function yields

$$\begin{aligned}
\hat{W}_{12}^{3}[G_{6,1}] \;=&\; \prod_{i<j=1}^{6} \frac{1}{w_{ij}} \times \frac{1}{24} D_{16} w_{56} \prod_{i=1}^{4} w_{i5} w_{i6} \times 48 \frac{D_{15} D_{25} D_{26}}{w_{12}^{2}} \frac{\langle 2222 \rangle_{1}}{N_{\mathrm{c}}^{2}} \\
&+ (14 \text{ perm.}) \\
=&\, 2 \frac{D_{15} D_{16} D_{25} D_{26}}{w_{12}^{3}} \times \hat{W}_{12}^{1}[G_{4,1}] + (14 \text{ perm.})\,,
\end{aligned} \tag{4.92}$$

which agrees with (4.89).

5. Ten-Dimensional Null Polygons

In the previous chapter, we introduced generating functions for correlation functions of protected scalar operators in planar $\mathcal{N} = 4$ SYM. Building on this framework, we now turn to a particular class of observables obtained from these generating functions in a specific kinematical regime. In this chapter, we consider higher-point generalizations of the so-called "octagon" [70, 71], namely n-point polygon correlators, which arise as ten-dimensional null limits of the generating functions discussed previously.

The main goal of this chapter is to develop a direct computational approach to the corresponding polygon integrands. To this end, we employ twistor methods and explain how they can be used to efficiently compute these polygon functions. Within this framework, we obtain explicit expressions for the loop integrands and, in particular, determine the two-loop integrands for an arbitrary number of external operators. The final results can be written as linear combinations of conformal integrals, with coefficients given by rational functions of spacetime distances and R-charge polarizations.

We begin by introducing the polygon functions and discussing their main features in Section 5.1. In Section 5.2, we then use the ten-dimensional null limit to extract polygon correlators from the generating functions obtained in the previous chapter. Afterwards, in Section 5.3, we explain how to compute the polygon integrand using the twistor Feynman rules [69], reviewed in Section 3.3.2. Using these ingredients, we determine the polygon integrand for arbitrary multiplicity up to two-loop order in Section 5.4.

This chapter is based on the work presented in [2].

5.1. Ten-Dimensional Null Limit

In this section, we present the higher-point generalizations of the *octagon* function [70, 71] (here renamed as *square*). These higher-point polygons are defined as

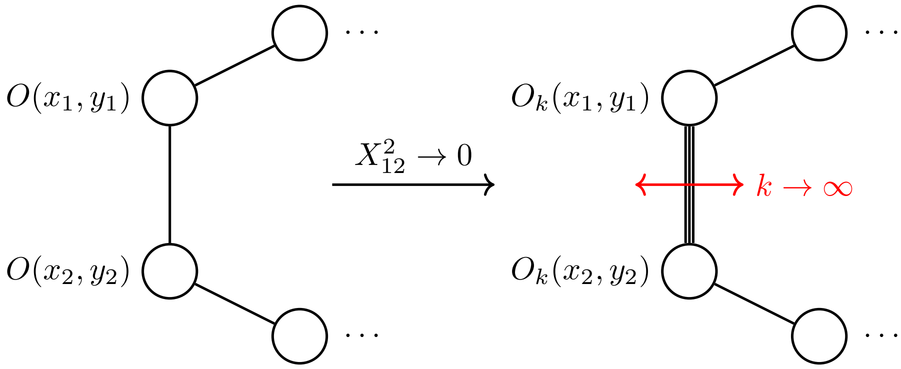

Figure 5.1.: The ten-dimensional null limit of the generating function projects onto an infinite number of four-dimensional propagators between the two operators [2].

the residues of the n-point generating functions on a polygonal set of ten-dimensional poles [65].

5.1.1. Defining the Polygon Function

One notable feature of the generating function (4.3) is that it is expressed in terms of ten-dimensional propagators D_{ij} (4.13). These propagators D_{ij} connect the external operators (4.1).Expanding around $y_{ij}^2 = 0$, they become a geometric sum of arbitrary powers of ordinary four-dimensional propagators d_{ij}:

$$D_{ij} = d_{ij} + d_{ij}^2 + d_{ij}^3 + \dots \,, \qquad d_{ij} = -\frac{y_{ij}^2}{x_{ij}^2} \,. \tag{5.1}$$

The component correlators (4.20) are recovered by performing this expansion and keeping only the appropriate powers of the various y_i polarizations.

Correlators of operators $\mathcal{O}_k$ with small R-charge k receive contributions from the first terms in the series (5.1). Conversely, in the planar limit, correlators of operators with parametrically large R-charge, come from the infinite tail of the geometric series. This can be understood by noting that the Feynman rules only admit propagators D_{ij} that are homotopically distinct from each other on the color sphere [69]. For a finite number of operators, only finitely many such propagators can be drawn on the color sphere. To accomodate for large-charge operators, at least some of the propagators D_{ij} must thus be expanded to large orders. As already noted in [65], one can focus on such large-charge correlators directly at the level of the generating

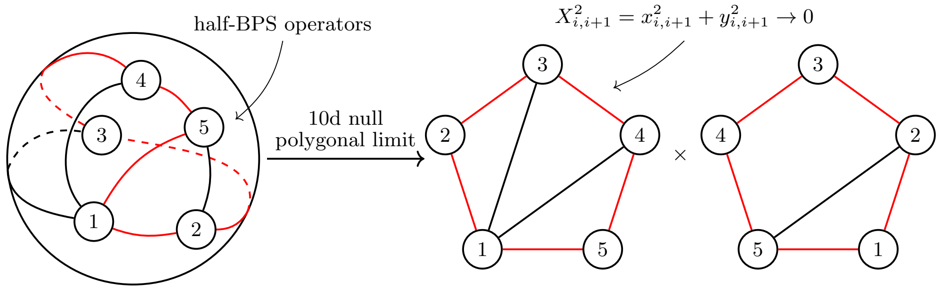

Figure 5.2.: The ten-dimensional null polygon limit cuts the color surface and factorizes the correlator into two polygons with disc topology. Here, schematically depicted in the five-point case, that yields the product of two pentagons.

function (4.19) by taking the ten-dimensional null limit: $X_{ij}^2 \to 0$ (or equivalently $d_{ij} \to 1$). By considering this limit, we project the generating function to correlators where an infinite number of parallel four-dimensional propagators d_{ij} connect the operators at points x_i and x_j, as depicted in Figure 5.1.

A particularly interesting limit is the *ten-dimensional null polygon limit*, in which we simultaneously take $X^2_{i,i+1} \to 0$, $i = 1, \ldots, n$, such that the n operators (4.1) sit at the cusps of an n-sided polygon, where the edges are “thick” propagators of large (essentially infinite) R-charge that connect neighboring operators. This thick propagator perimeter drastically simplifies the correlator, since the “inside” and the “outside” of the perimeter decouple to all orders in perturbation theory. The correlator thus factorizes into the product of two simpler disk-like objects [65], the *polygons* $M_{n,\ell}$:

$$\lim_{\substack{d_{i,i+1}\to 1\\ i=1,\ldots,n}} \prod_{i=1}^{n} (1 - d_{i,i+1}) \times N_{\mathrm{c}}^{n-2}\, G_{n,\ell} = \sum_{\mathbf{k}} M_{n,\mathbf{k}} \times M_{n,\bar{\mathbf{k}}} \tag{5.2}$$

where the factor N_{c}^{n-2} is chosen such that $M_{n,\mathbf{k}} \sim N_{\mathrm{c}}^0$, and the sum on the right-hand side runs over all possible ways of distributing the ℓ Lagrangians onto the two polygons: $\mathbf{k} \,\dot{\cup}\, \bar{\mathbf{k}} = \{n+1, \ldots, n+\ell\}$. Thus, the n-point polygons $M_{n,\mathbf{k}}$ are correlators with disk topology, with n large-charge operators inserted at the boundary of the disk, and the set $\mathbf{k}$ of Lagrangian operators inserted in the interior, see Figure 5.2. In the case where all Lagrangians are inserted in a single polygon, $\mathbf{k} = \{n+1, \ldots, n+\ell\}$, we use the simplified notation $M_{n,\mathbf{k}} \equiv M_{n,\ell}$. These polygons

$M_{n,\ell}$ define the integrands of the n-point interacting polygon correlator

$$\mathbb{M}_n = \sum_{\ell=0}^{\infty} \frac{(-a)^\ell}{\ell!} \int \Big[\prod_{k=1}^{\ell} \frac{\mathrm{d}^4 x_{n+k}}{4\pi^2} \Big] M_{n,\ell} \,. \tag{5.3}$$

Using (4.2), the factorization (5.2) can be written at integrated level as:

$$\lim_{\substack{d_{i,i+1}\to 0 \\ i=1,\dots,n}} \prod_{i=1}^{n} (1-d_{i,i+1}) \times N_{\mathrm{c}}^{n-2} \Big\langle \prod_{i=1}^{n} \mathcal{O}(x_i, y_i) \Big\rangle_{\mathrm{SYM}} = \mathbb{M}_n \times \mathbb{M}_n \,. \tag{5.4}$$

The four-point and five-point polygons $\mathbb{M}_4$ and $\mathbb{M}_5$ have been conventionally called *octagon* and *decagon* in the literature. The origin of these names lies in their integrability-based description in terms of hexagon form factors [22, 23], in which the cusps acquire a non-zero "length". In this work, we will call these objects *square* and *pentagon*, respectively, and consider their higher-point counterparts.

5.1.2. Properties of the Polygons

The polygon correlators $M_{n,\ell}$ and $\mathbb{M}_n$ satisfy several interesting properties:

Factorization. Upon taking additional ten-dimensional null limits on their diagonals, the polygons $M_{n,\ell}$ *factorize* into lower-point polygons:

$$\lim_{d_{ij}\to 0} (1-d_{ij})\, M_{n,\ell} = \sum_{\mathbf{k}} M_{\mathbf{m},\mathbf{k}} \times M_{\bar{\mathbf{m}},\bar{\mathbf{k}}} \,, \tag{5.5}$$

where $\mathbf{m} = \{i,\dots,j \,(\mathrm{mod}\; n)\}$ and $\bar{\mathbf{m}} = \{j,\dots,i \,(\mathrm{mod}\; n)\}$ are the external operators "left" and "right" of the line (i,j), and the sum runs over all bipartitions $\mathbf{k} \,\dot\cup\, \bar{\mathbf{k}} = \{n+1,\dots,n+\ell\}$ of the Lagrangian insertion points onto the two factors. Here, we employ the slight abuse of notation $M_{\mathbf{m},\mathbf{k}} = M_{|\mathbf{m}|,\mathbf{k}}$ with point labels $\mathbf{m}$. For example, the following limit splits the two-loop pentagon $M_{5,2}$ into a square and a triangle:

$$\lim_{d_{14}\to 0} (1-d_{14})\, M_{5,2} = M_{\mathbf{m},\emptyset} M_{\bar{\mathbf{m}},\{6,7\}} + M_{\mathbf{m},\{6\}} M_{\bar{\mathbf{m}},\{7\}} + M_{\mathbf{m},\{7\}} M_{\bar{\mathbf{m}},\{6\}} \\ + M_{\mathbf{m},\{6,7\}} M_{\bar{\mathbf{m}},\emptyset} \tag{5.6}$$

with $\mathbf{m} = \{1,2,3,4\}$ and $\bar{\mathbf{m}} = \{1,4,5\}$. See Figure 5.3 for an illustration. The factorization (5.5) follows by the same reasoning as the factorization of the generating function $G_{n,\ell}$ into two polygon factors (5.2): Taking the $X_{ij}^2 \to 0$

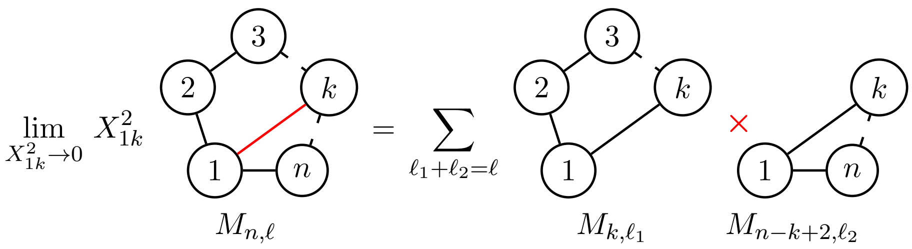

Figure 5.3.: Factorization of the n-gon into lower polygons after taking ten-dimensional null limits on a diagonal.

limit projects to the tail of the geometric series (5.1), thus it limits to terms that include a parametrically large number of parallel propagators d_{ij} that separates the polygon into two subregions that do not interact with each other. The factorization straightforwardly lifts to the integrated polygons:

$$\lim_{d_{ij}=0} (1 - d_{ij})\, \mathbb{M}_n = \mathbb{M}_{\mathbf{m}} \times \mathbb{M}_{\bar{\mathbf{m}}}\,, \tag{5.7}$$

with $\mathbf{m}$ and $\bar{\mathbf{m}}$ as in (5.5).

No Double Poles. The generating function $G_{n,\ell}$ in general contains double and higher poles in the ten-dimensional distances X_{ij}^2. These originate in Feynman graphs where external operators i and j are connected by multiple homotopically distinct propagators D_{ij}. In order to be homotopically distinct, any two such propagators connecting the same two operators must enclose at least one third operator.[1] The polygon disk-topology excludes such diagrams, and thus the polygon correlators $M_{n,\ell}$ only contain at most simple poles in the ten-dimensional distances X_{ij}^2.

Direct Computability. As we will see below in Section 5.3, the polygons $M_{n,\ell}$ can be computed directly from the twistor Feynman rules of [69], avoiding the computation (and subsequent ten-dimensional polygon limit) of the much more complicated generating functions $G_{n,\ell}$ altogether.

[1] Two propagators D_{ij} are also homotopically distinct if they only enclose Lagrangian operators, but no further external operators. Such terms however evaluate to zero, which is in accordance with the fact that two-point functions of scalar BPS operators are protected from quantum corrections.

Massive Amplitudes. As reviewd in Section 2.4.5, there is a well-established duality in $\mathcal{N} = 4$ super Yang–Mills that relates the four-dimensional null polygon limit $x^2_{i,i+1} \to 0$ of the n-point correlation function of the lightest half-BPS operators, $k_i = 2$ in (4.19), with the n-point *massless* MHV gluon scattering amplitude. A less firmly established duality, but with corroborating evidence in the case of four [65] and five points [120, 121], is that something similar also happens in the large R-charge limit. The statement is that the n-point polygons $\mathbb{M}_n$ are dual to *massive* n-point W-boson scattering amplitudes on the Coloumb branch of $\mathcal{N} = 4$ super Yang–Mills theory [65]. Upon additionally taking the *massless* null polygon limit $x^2_{i,i+1} \to 0$, these further reduce to the massless MHV gluon amplitudes. See Figure 5.4 for a diagram of the various limits.

More precisely, the polygons $M_{n,\ell}$ reduce to the ℓ-loop integrands $\mathcal{A}_{n,\ell}$ of the *massless* MHV scattering amplitudes when one sets all internal diagonals d_{ij} to zero and passes to the four-dimensional null limit:

$$M_{n,\ell} \to \mathcal{A}_{n,\ell}/\mathcal{A}_{n,0} \qquad \text{for} \qquad x^2_{i,i+1} \to 0,\ i = 1, \dots, n \quad \text{and} \quad d_{ij} \to 0 \ \forall\, i, j\,, \tag{5.8}$$

where $\mathcal{A}_{n,\ell}$ is the ℓ-loop massless MHV amplitude integrand, and $\mathcal{A}_{n,0}$ its tree-level expression. The relation (5.8) follows by construction when both the amplitude integrands $\mathcal{A}_{n,\ell}$ and the polygons $M_{n,\ell}$ are computed from Lagrangian insertions, see e. g. [102, 103]. The limit can simply be achieved by setting all y^2_{ij} to zero, noticing that $x^2_{i,i+1} = -y^2_{i,i+1} \to 0$ on the perimeter of the polygon, due to the ten-dimensional null limit $0 = X^2_{i,i+1} = x^2_{i,i+1} + y^2_{i,i+1}$.

Integrability. The polygons $\mathbb{M}_n$ are the most natural objects to be computed from integrability via hexagonalization, i. e. decomposition into hexagon form factors [22, 23, 122]. Due to their disk topology, they are free of mirror excitations that wrap operator insertions that require careful treatment [123]. The polygon configurations in fact make hexagonalization conceptionally very similar to the pentagon OPE for massless amplitudes (null polygon Wilson loops) [124–127], and in the four-dimensional null limit, the two should become equivalent. In the case of the square (a. k. a. octagon), the simplifications of the ten-dimensional null limit enabled its bootstrap to all loops [71–73], and

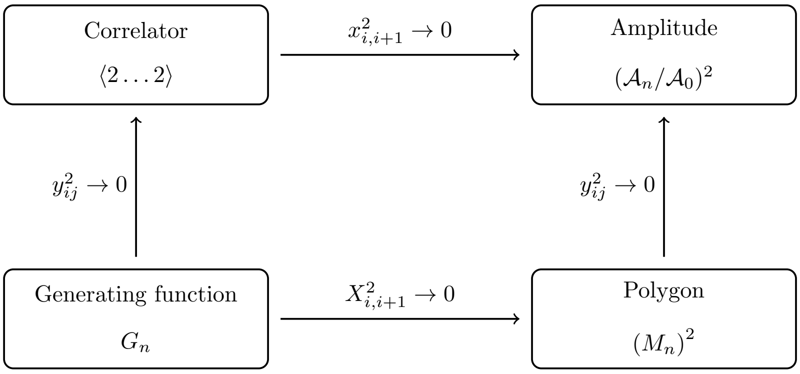

Figure 5.4.: Illustrating of the relation between correlator–amplitude duality (top) and generating functions/polygons (bottom) [2] (adapted from [65]). Arrows denote schematic limits: the left arrow projects to the leading term as $y^2_{ij} \to 0$, yielding the n-point $\mathbf{20'}$ integrand, while top and bottom limits extract the leading divergent contribution in the 4d/10d null limit.

a finite-coupling resummation in terms of a Fredholm determinant [74, 75]. The pentagon (a. k. a. decagon) has been computed to two loops [76]. Also more general correlators become most computable in limits where they can be decomposed into polygons [118], even at subleading non-planar orders of the planar limit expansion [109, 119].

Relation with Fixed-Charge Correlators. The full generating function $G_{n,\ell}$ contains the complete information on all fixed-charge correlators via (4.20). Since the ten-dimensional null polygon limit captures only a specific part of the generating function, it also only contains partial information on any given fixed-charge correlator. Without involving the full generating function, any single generic fixed-charge correlator cannot easily be projected to the part captured by polygons. An exception to this are certain correlators at four, five, and six points, where one can engineer specific operators of large (but fixed) charge, such that the correlator equals the square, pentagon, or hexagon, up to a loop order that is bounded by the operator charges. The operators are R-symmetry descendants of the fixed-charge operators $\mathcal{O}_k$ (4.1), designed so that they form a square/pentagon/hexagon, where only neighboring operators can contract with free propagators. This is how the square was originally defined [70] (see also [118], in particular Figure 11 there).

Since $\mathcal{N} = 4$ SYM has only six scalars that transform in the SO(6) R-symmetry, this procedure only works up to six points. Beyond six points, there is not enough space in the SO(6) to ensure large propagator bundles between neighboring operators. Therefore, any higher-point function with sufficiently large charges will have contributions that factorize into polygons, but will also have other contributions that do not factorize.

Even though there is no one-to-one map between polygons and large-charge correlators beyond six points, these polygons are interesting objects on their own — as corroborated by their properties listed above; in particular their identification as massive amplitudes and their particularly nice integrability representation in terms of hexagon form factors. Computing these objects in perturbation theory is the first step towards better understanding them and it is what we turn to next.

5.2. Polygons from Generating Functions

Before addressing their direct construction from twistor Feynman rules, we will compute the first few one-loop and two-loop polygons by taking the ten-dimensional null limits (5.2) of the generating functions $G_{n,\ell}$. At four points, they were determined in [65] (reviewed in Section 4.4), and for five and six points in the previous chapter. To this end, we first define the null polygon residue

$$R_{n,\ell} \equiv \underset{\substack{d_{i,i+1}=1\\ i=1,\dots,n}}{\operatorname{Res}} N_{\mathrm{c}}^{n-2}\, G_{n,\ell} = \lim_{d_{i,i+1}\to 1} \prod_{i=1}^{n} (1-d_{i,i+1}) \times N_{\mathrm{c}}^{n-2}\, G_{n,\ell} \tag{5.9}$$

Looking at (5.2), one can see that the polygons $M_{n,\ell}$ can be determined from $R_{n,\ell}$ loop order by loop order. Explicitly:

$$M_{n,0} = (R_{n,0})^{1/2}\,, \quad M_{n,1} = \frac{R_{n,1}}{2\,M_{n,0}}\,, \quad M_{n,2} = \frac{R_{n,2} - 2\,(M_{n,1})^2}{2\,M_{n,0}}\,, \quad \dots\,. \tag{5.10}$$

The simplest polygon is the triangle. Since three-point functions of half-BPS scalar operators are protected from quantum corrections, the generating function is simply given by its leading-order term $G_{3,0} = D_{12}D_{13}D_{23}$, and therefore the triangle correlator is trivial:

$$\mathbb{M}_3 = M_{3,0} = 1\,. \tag{5.11}$$

5.2.1. The Square (a. k. a. Octagon)

Both the four-point generating function $G_{n,\ell}$ and its ten-dimensional null polygon limit were computed in [65]. Collecting the results, the square correlator reads

$$
\begin{aligned}
M_{4,0} &= \frac{x_{13}^2 x_{24}^2 - y_{13}^2 y_{24}^2}{X_{13}^2 X_{24}^2}\,, \\
M_{4,1} &= M_{4,0}\, \frac{X_{13}^2 X_{24}^2}{X_{15}^2 X_{25}^2 X_{35}^2 X_{45}^2}\bigg|_{y_5\to 0}\,, \\
M_{4,2} &= M_{4,0}\, \frac{X_{13}^2 X_{24}^4\, X_{15}^2 X_{36}^2 \,+\, X_{13}^4 X_{24}^2\, X_{45}^2 X_{26}^2 + (X_5 \leftrightarrow X_6)}{(X_{15}^2 X_{25}^2 X_{35}^2 X_{45}^2)\, X_{56}^2\, (X_{16}^2 X_{26}^2 X_{36}^2 X_{46}^2)}\bigg|_{y_5,y_6\to 0}
\end{aligned}
\tag{5.12}
$$

Before taking the $y_5, y_6 \to 0$ limits, these functions include the dependence on all higher Kaluza–Klein modes of the Lagrangian operator. Written in this form, the ratios $M_{4,\ell}/M_{4,0}$ display a 10D (dual) conformal symmetry, which only gets broken by taking the $y_i \to 0$ limit to project to the chiral interaction Lagrangian $\mathcal{L}_{\text{int}}(x)$. It corresponds to the loop integrand in higher-dimensional SYM, and by dimensional reduction gives the integrand of a massive amplitude on the Coulomb branch [65].

Performing the $y_5, y_6 \to 0$ projection, the square correlator can alternatively be expanded in a basis of integrands of conformal integrals:

$$
M_{4,0} = \frac{1 - d_{13}d_{24}}{(1-d_{13})(1-d_{24})}\,, \tag{5.13}
$$

$$
M_{4,1} = (1 - d_{13}d_{24})x_{13}^2 x_{24}^2 B^{[1,2,3,4;\,5]}\,, \tag{5.14}
$$

$$
M_{4,2} = (1 - d_{13}d_{24})x_{13}^2 x_{24}^2 \left[\mathcal{I}_4^{[1,3|2,4;\,5,6]}\, X_{13}^2 + \mathcal{I}_4^{[2,4|1,3;\,5,6]}\, X_{24}^2\right]\,, \tag{5.15}
$$

where

$$
B^{[1,2,3,4;\,a]} = \frac{1}{x_{1a}^2 x_{2a}^2 x_{3a}^2 x_{4a}^2}\,, \tag{5.16}
$$

$$
\mathcal{I}_4^{[1,2|3,4;\,a,b]} = \frac{1}{(x_{1a}^2 x_{2a}^2 x_{3a}^2) x_{ab}^2 (x_{1b}^2 x_{2b}^2 x_{4b}^2)} + (a \leftrightarrow b)\,. \tag{5.17}
$$

Note that the square correlators $M_{4,\ell}$, $\ell > 0$ take the form of a universal prefactor $(1 - d_{13}d_{24})x_{13}^2 x_{24}^2$, multiplied by a combination of conformal integrands with ten-dimensional coefficients. This form follows from the ten-dimensional nature of the parent expressions (5.12), and it continues at higher loop orders. The prefactor $(1 - d_{13}d_{24})x_{13}^2 x_{24}^2$ in fact originates from the null polygon limit of the universal four-point supersymmetry invariant $\mathcal{R}_{1234}$ (2.48)

$$\lim_{d_{i,i+1}\to 1} \mathcal{R}_{1234} = (1-d_{13}d_{24})^2 x_{13}^2 x_{24}^2\,. \tag{5.18}$$

5.2.2. The Pentagon

Using the the five-point generating functions provided (4.70) and (4.73), we compute the one-loop and two-loop pentagon by applying (5.9) and (5.10):

$$M_{5,0} = \frac{1}{5} + \frac{d_{13}}{(1-d_{13})(1-d_{14})} + (\mathrm{C}_5 \text{ perms}) \tag{5.19}$$

$$M_{5,1} = \frac{p_{1234}}{2}\, B^{[1,2,3,4;\,6]} - 2i\,\mathcal{I}_{\text{odd}}^{[1,2,3,4;\,6]} + (\mathrm{C}_5 \text{ perms})\,, \tag{5.20}$$

$$\begin{aligned} M_{5,2}^{\text{even}} = {}& \frac{p_{1234}}{2}\Big(\mathcal{I}_4^{[1,3|2,4;\,6,7]}\, X_{13}^2 + \mathcal{I}_4^{[2,4|1,3;\,6,7]}\, X_{24}^2 + \mathcal{I}_{5,1}^{[1,4|2,3|5;\,6,7]}\, X_{14}^2\Big) \\ & + \frac{X_{35}^2\, q_{12345} + X_{13}^2\, q_{54321}}{2}\, \mathcal{I}_{5,2}^{[1,2|4,5|3;\,6,7]} + (\mathrm{C}_5 \text{ perms})\,, \end{aligned} \tag{5.21}$$

The two-loop pentagon is restricted to its parity-even part. The parity-odd part of the one-loop pentagon is written as a sum of four-point parity-odd integrands

$$\mathcal{I}_{\text{odd}}^{[1,2,3,4;\,0]} = \frac{\epsilon_{\mu\nu\rho\sigma} x_{10}^{\mu} x_{30}^{\nu} x_{30}^{\rho} x_{40}^{\sigma}}{x_{10}^2 x_{20}^2 x_{30}^2 x_{40}^2}\,, \tag{5.22}$$

and we introduce the following conformal integrals for the two-loop pentagon

$$\begin{aligned} \mathcal{I}_{5,1}^{[1,2|3,4|5;\,a,b]} &= \frac{x_{5a}^2}{(x_{1a}^2 x_{2a}^2 x_{3a}^2 x_{4a}^2)\, x_{ab}^2\, (x_{1b}^2 x_{2b}^2 x_{5b}^2)} + (a \leftrightarrow b)\,, \\ \mathcal{I}_{5,2}^{[1,2|3,4|5;\,a,b]} &= \frac{1}{(x_{3a}^2 x_{4a}^2 x_{5a}^2)\, x_{ab}^2\, (x_{1b}^2 x_{2b}^2 x_{5b}^2)} + (a \leftrightarrow b)\,. \end{aligned} \tag{5.23}$$

The result (5.21) for the two-loop pentagon $M_{5,2}$ is consistent with the known expressions for the "decagon" function [76, 77].
Similar to the case of the square, one can see that the pentagon expressions at one and two loops are written in terms of four-dimensional structures p and q that multiply linear combinations of conformal integrals with ten-dimensional coefficients. The four-dimensional structures are

$$p_{1234} = x_{12}^2 x_{34}^2 - x_{14}^2 x_{23}^2 + \frac{(1+d_{14}-2d_{13}d_{24})}{1-d_{14}} x_{13}^2 x_{24}^2\,, \tag{5.24}$$

$$q_{12345} = x_{12}^2 x_{34}^2 - x_{14}^2 x_{23}^2 - \frac{d_{35}(1-d_{13}d_{24})}{1-d_{35}} x_{13}^2 x_{24}^2\,. \tag{5.25}$$

The interpretation of these structures is that they are polygon limits of components of superconformal invariants that occur in the five-point generating functions, similar to (5.18) at four points. This picture is further supported by the fact that p can be traced back to the invariants $\mathcal{R}_{1234}$ (2.48) and $\mathcal{R}_{1234,5}$ (4.68) that appear in the five-point generating function as follows:

$$\operatorname*{Res}_{d_{i,i+1}=1} \frac{\mathcal{R}_{1234,5} - C^{(5)}_{1234;5}\,\mathcal{R}_{1234}}{\prod_{i<j=1}^{5} w_{ij}} = M_{5,0} \times p_{1234}\,, \tag{5.26}$$

with $C^{(5)}_{1234;5}$ given in (4.66).

While the four-point generating functions $G_{4,\ell}$ are purely parity-even, the higher-point generating functions develop parity-odd parts, which also induce parity-odd parts for the respective polygons. Since the parity-odd parts integrate to zero, one might be tempted to ignore them. However, when one takes products of polygons to re-construct the null polygon correlators as in (5.2), products of parity-odd parts are essential, as they contribute to the parity-even part of the correlator. In other words, the factorization (5.2) is only consistent if one includes the parity-odd parts of both the generating functions $G_{n,\ell}$ and the polygons $M_{n,\ell}$. The parity-odd parts are similarly essential for the factorization formula (5.5).

With the expressions above, we can explicitly verify the factorization formula (5.5): Taking the ten-dimensional null limit of the diagonal $X^2_{14} \to 0$ (or equivalently $d_{14} \to 1$ in terms of the four-dimensional propagator), the pentagon factorizes into a square and a (trivial) triangle

$$\operatorname*{Res}_{d_{14}=1} M_{5,\ell} = M_{4,\ell} \times M_{3,0} = M_{4,\ell} \times 1\,, \qquad \ell = 0, 1, 2\,, \tag{5.27}$$

at leading order, one-loop, and two-loop order. Consistently, the parity-odd part of the one-loop pentagon vanishes in this limit. Notice that the poles in p and q in the two-loop pentagon are canceled by the factors X^2_{ij} dressing the penta-box integral $\mathcal{I}_{5,1}$ and the five-point double-box $\mathcal{I}_{5,2}$, whereas the poles of p are still present for the four-point box $\mathcal{I}_4$, thus one can see that $\mathcal{I}_{5,1}$, $\mathcal{I}_{5,2}$, and q do not contribute to the limit (5.27).

Before moving on to the hexagon, in the following we provide some more details on the derivation of the pentagon from the generating function.

One Loop. At one-loop order, we also computed the five-point generating function $\tilde{G}_{5,1}$ that also includes all higher-R-charge components of the chiral Lagrangian operator (4.65). Applying the 10d null polygonal limit (5.9), the generating function factorizes according to (5.2) and (5.9), $\tilde{R}_{5,1} = 2M_{5,0}\tilde{M}_{5,1}$, where $\tilde{M}_{5,1}$ is a generalized one-loop pentagon that includes all higher-R-charge components of the chiral Lagrangian:

$$\tilde{M}_{5,1} = \frac{X_{56}^2\, p_{1234} + d_{56}x_{56}^2\big((1-d_{13}d_{24})x_{13}^2x_{24}^2 - (1-d_{14})x_{14}^2x_{23}^2\big) + (\mathrm{C}_5 \text{ perms})}{2\, X_{16}^2X_{26}^2X_{36}^2X_{46}^2X_{56}^2} \\ - \frac{4i\big[X^{\text{anti}}_{123456} - Y^{\text{anti}}_{123456}\big]_{\text{10d null}}}{X_{16}^2X_{26}^2X_{36}^2X_{46}^2X_{56}^2}\,, \tag{5.28}$$

with p_{1234} given in (5.24). X^{anti} and Y^{anti} are antisymmetric scalars defined in (4.42) and (4.64), respectively The subscript "10d null" in the above equation indicates that the X^I and Y^I vectors are not independent, but satisfy the 10d null constraint on the boundary of the pentagon: $X_i^I X_{i+1}^I - Y_i^I Y_{i+1}^I = 0$.
By setting $y_6 = 0$, we project out all higher-R-charge partners of the Lagrangian, and thus, obtain the loop-integrand of the pentagon at one-loop order (5.20). The scalar Y^{anti}_{12345} projects to zero, and the antisymmetric X-scalar becomes the parity-odd integral (5.22) according to (4.43).

Two Loops. Obtaining the two-loop pentagon using the last equation in (5.10) requires a careful treatment of the parity-even and -odd parts in the one-loop pentagon. Starting from the parity-even part of five-point two-loop generating function, we compute the parity-even two-loop pentagon via

$$M^{\text{even}}_{5,2} = \frac{R^{\text{even}}_{5,2} - 2\,(M^{\text{even}}_{5,1})^2 + 2\,(M^{\text{odd}}_{5,1})^2}{2\,M_{5,0}}\,. \tag{5.29}$$

The parity-odd part of the one-loop pentagon squared yields an even contribution to the residue $R^{\text{even}}_{5,2}$ that needs to be subtracted in order to obtain the two-loop pentagon. Since $M^{\text{odd}}_{5,1}$ vanishes upon integration of x_6, its contribution to (5.29) can also be omitted after lifting the expression to the integrated level. In this case, however, an integral identity has to be applied, which is exactly given by $(M^{\text{odd}}_{5,1})^2 = 0$ (after integration). In fact, this integral identity is a generalization of (6.23) in [38], where it was found in the context of the correlator/amplitude duality in the 4d null limit, where $x^2_{i,i+1} = 0$.

Plugging the generating function $G_{5,2}$, provided in (4.73), into (5.29), we obtain the parity-even two-loop pentagon (5.21).

5.2.3. The Hexagon

Taking the parity-even part of one-loop six-point generating function (4.75), we consider its 10d null hexagon limit and apply (5.10) to find the parity-even part of the one-loop hexagon[2]

$$
\begin{aligned}
M_{6,1}^{\text{even}} = & \frac{(1-d_{15}d_{24})}{4\,(1-d_{15})(1-d_{24})} B^{[1,2,4,5;\,7]} \times \\
& \qquad \left(x_{12}^2 x_{45}^2 - x_{15}^2 x_{24}^2 + \frac{(1+d_{15}d_{24}-2d_{14}d_{25})}{1-d_{15}d_{24}} x_{14}^2 x_{25}^2 \right) \\
& - \frac{(d_{15}-d_{35})}{2\,(1-d_{15})(1-d_{35})} B^{[1,2,3,5;\,7]} \times \\
& \qquad \left(x_{12}^2 x_{35}^2 - x_{15}^2 x_{23}^2 - \frac{(d_{15}+d_{35}-2d_{13}d_{25})}{d_{15}-d_{35}} x_{13}^2 x_{25}^2 \right) \\
& + \frac{(1-d_{15}d_{46})}{2\,(1-d_{15})(1-d_{46})}\, p_{1234}\, B^{[1,2,3,4;\,7]} + (\mathrm{C}_6 \text{ perms})\,.
\end{aligned} \tag{5.30}
$$

We present the hexagon in terms of one-loop box integrals (5.16), and notice the appearance of p_{1234} that we already encountered previously in the one- and two-loop pentagon.
We verify the factorization of the hexagon into lower-point polygons by taking the following residues:

$$
\begin{aligned}
& \operatorname*{Res}_{d_{15}=1} M_{6,1}^{\text{even}} = M_{5,1}^{\text{even}} \times 1\,, \\
& \operatorname*{Res}_{d_{36}=1} M_{6,1}^{\text{even}} = M_{\{1236\},0} \times M_{\{3456\},1} + M_{\{1236\},1} \times M_{\{3456\},0}\,,
\end{aligned} \tag{5.31}
$$

where we recover the one-loop pentagon (5.20) (multiplying the trivial triangle) and products of the one-loop square (5.14) (with different point labels).

The explicit computations carried out in this section verify the two types of factorizations we considered: The factorization of the generating function into a product of polygons (5.2), (5.4), and the factorization of polygons into products of smaller polygons (5.5), (5.7). Although straightforward, first evaluating the full generating function to then take its ten-dimensional null polygon limit to factorize it into

[2]For the full expressions of all one-loop polygons, that include both the parity-even as well as the parity-odd parts, we refer to Section 5.4.2.

polygons appears like a long detour. The generating function contains much more information than the polygons, and its computation is accordingly demanding. The polygons have disk topology and contain much less information, hence there should be an easier way to compute them. Indeed it turns out there is a way to compute them directly, which is what we turn to next.

5.3. Twistor Rules for 10d Null Polygons

So far, we computed polygons $M_{n,\ell}$ by taking the square root of a 10d null polygonal limit $X^2_{i,i+1} \to 0$, $i = 1, \ldots, n$, of the corresponding generating function $G_{n,\ell}$. Deriving the generating function using the twistor formulation, however, is computationally quite demanding as both the number of graphs as well as the size of the ansatz grows quickly for higher points and/or higher loops.
The full generating function $G_{n,\ell}$ contains information of all underlying fixed-weight correlators, whereas the polygons only correspond to a specifically polarized large-charge limit. Hence, computing the polygons directly – without having to take a detour deriving the generating function – should be significantly more efficient. In fact, it is possible to compute the polygons directly in the twistor formalism, using the same Feynman rules as for the generating function, but restricting to graphs with disk topology and applying ten-dimensional null kinematics.

Prescription. To compute the full generating function $G_{n,\ell}$ in twistor space, one has to sum over all planar diagrams, i. e. graphs with sphere topology. Once we take the ten-dimensional null polygon limit, the generating function gets projected to a configuration of large-charge operators that factorizes into two polygons — in color space, the sphere factorizes to two disks, and accordingly the polygons have disk topology. It turns out that this can be directly implemented at the level of the twistor Feynman rules: The polygons $M_{n,\ell}$ can be computed directly by only considering a much smaller set of graphs $\Gamma^{\text{disk}}_{n,\ell}$, which consists of all planar graphs with disk topology whose perimeter is formed by n external operators (4.1), with two adjacent operators being connected by a single fat propagator. On the inside of the disk, ℓ Lagrangian insertions are placed that are connected by edges to each other and the external operators while preserving planarity. We list the counting of these graphs in Table 5.1. This should be contrasted with Table 3.1. For example at seven points and two loops, 1 323 096 graphs contribute to the sphere generating function $G_{7,2}$, whereas the polygon $M_{7,2}$ can be computed from only 23 273 graphs. After

$\ell\backslash n$	4	5	6	7	8	9	10	11
0	2	3	11	29	122	479	2 113	9 369
1	9	36	176	830	4 125	20 632	104 924	538 746
2	135	740	4 203	23 273	130 113	726 250	4 069 167	22 838 831
3	2 683	17 210	106 904					
4	61 395	425 819						

Table 5.1.: Counting of single-particle twistor graphs with disk topology for various number of external points n and internal insertions ℓ [2]. These are ribbon (or fat) graphs with n external vertices forming the perimeter of an n-sided polygon, and ℓ internal vertices located inside the disk. The perimeter consists of simple edges, and only graphs that are inequivalent under $\mathrm{C}_n \times \mathrm{S}_\ell$ permutations of the vertices are counted as distinct. The first line ($\ell = 0$) counts the number of dissections of the n-gon by diagonals, see OEIS Sequence A003455.

applying the twistor Feynman rules Φ, reviewed in Section 3.3.2, to all disk-topology graphs, one obtains the polygon $M_{n,\ell}$:

$$M_{n,\ell} = \lim_{d_{i,i+1}\to 1} \prod_{i=1}^{n}(1-d_{i,i+1}) \sum_{\gamma\in\Gamma^{\mathrm{disc}}_{n,\ell}} \Phi(\gamma)\Big|_{\substack{\theta^4_{n+1}\cdots\theta^4_{n+\ell} \\ y_{n+1},\ldots,y_{n+\ell}\to 0}} . \tag{5.32}$$

The limit manifests the 10d null polygonal kinematics that defines the polygons in the first place. It can be readily implemented when evaluating the twistor expression numerically by choosing 10d null kinematics with $X^2_{i,i+1} = 0$. In addition, the internal operators must be projected onto the chiral Lagrangian. This is achieved by first isolating the Grassmann component proportional to $\theta^4_{n+1}\ldots\theta^4_{n+\ell}$ and subsequently sending the polarization vectors $y_{n+1},\ldots,y_{n+\ell}$ to zero, thereby projecting onto the top component of the stress-tensor multiplet according to (4.17).

Derivation. The reasoning for considering only graphs with disk topology is as follows: On the level of graphs, the generating function $G_{n,\ell}$ can be understood as a sum of planar ribbon graphs whose $(n+\ell)$ vertices are at least of valency two. Furthermore, multiple edges between a single pair of vertices are allowed if these edges are homotopically distinct (preserving planarity). After permuting over all distinct labels of the vertices, we partition the set of graphs into three groups (cf. Figure 5.5):

(i) Graphs in which the operators $1,\ldots,n$ are connected by simple edges, such that they form a polygon (i. e. an n-cycle),

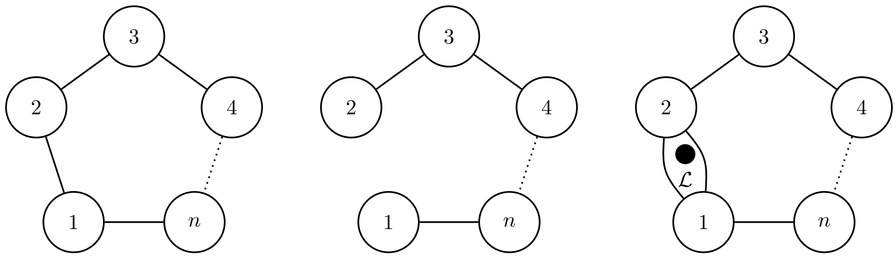

Figure 5.5.: Depicted are exemplary graphs that contribute to an n-point generating function. In the first set of graphs on the left, adjacent external operators are connected by a simple fat propagator. Not depicted are the Lagrangians or propagators connecting them to each other or to external operators, or propagators connecting non-adjacent operators. In the second set of graphs, at least one pair of non-adjacent operators is not connected – here, the operators 1 and 2. And finally on the right, at least one propagator on the perimeter is split into two edges, which is only possible if they enclose at least one Lagrangian insertion.

(ii) graphs in which at least one pair of adjacent operators $(i, i+1)$ is not connected by a propagator, and

(iii) graphs in which the operators $1, \ldots, n$ form an n-cycle, and at least one pair of adjacent operators $(i, i+1)$ is connected by two or more propagators.

We argue that only the first set of graphs (i) reveals a non-zero contribution after taking the 10d null polygonal limit of the generating function. Consider, the second set of graphs (ii). These graphs miss at least one edge on the perimeter of the polygon, and thus, do not obtain a factor $D_{i,i+1} = x^2_{i,i+1}/X^2_{i,i+1}$ for at least one $i = 1, \ldots, n$, after applying the twistor Feynman rules. Consequently, taking the residue (5.32) at $X^2_{i,i+1} \to 0$ eliminates any contribution obtained from such graphs. Summing up the third set of graphs (iii) will inherently lead to a zero contribution. Since all external operators form the boundary of the disk, two adjacent external operators can only be connected by two or more propagators if these propagators enclose Lagrangian insertions. This will effectively lead to an isolated loop integrand of a two-point function which is zero.

Now that we have restricted the graphs to group (i), we can reduce the set further by considering that the polygons are the square roots of the residues (5.4), (5.10). The square root has a natural interpretation in terms of these graphs. The external operators form a polygon that cuts the color surface into two regions with disk topology (an "inside" and an "outside"). Depending on whether the Lagrangian insertions are located on the inside or outside of the polygon, or split between the two regions, different contributions of products of polygon expressions are obtained. At two loops, for example, the residue can be written schematically as follows

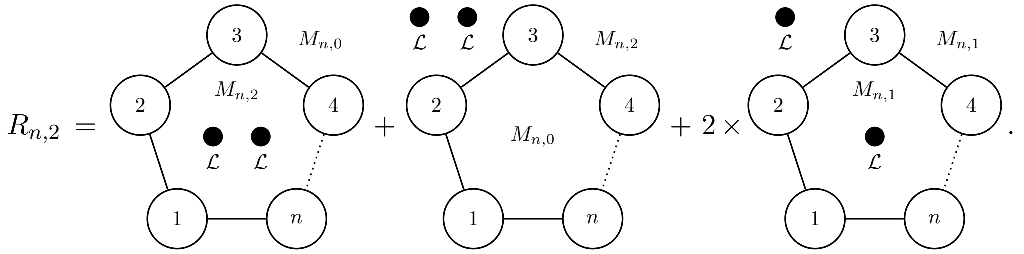

(5.33)

As can be seen from this equation, all Lagrangian insertions have to be gathered inside (or outside) of the polygon to obtain the relevant loop correction, while the propagators on the outside (or inside) will form the tree-level polygon result. Products of lower loop polygons are obtained if the Lagrangians are distributed in both regions. The polygon $M_{n,\ell}$ can thus be isolated by restricting the graphs to disk topology with the perimeter being single edged propagators connecting adjacent operators.[3]

Hence, the polygons are obtained by applying the twistor Feynman rules to the graphs with disk topology $\Gamma^{\text{disk}}_{n,\ell}$ and taking the 10d null polygonal limit as formulated in (5.32).

By exactly the same reasoning, the factorization (5.5) of polygons into smaller polygons upon taking further ten-dimensional null limits directly follows.

Ansatz. We have found a way to compute the polygons directly from twistors, but the general drawback of the twistor formulation still applies: The result contains the (arbitrary but fixed) reference twistor. While the final expression is ultimately independent of this reference twistor, it is virtually impossible to remove the reference twistor from it to write it in terms of basic invariants (i. e. square distances). As usual, we therefore resort to writing a suitable manifestly invariant ansatz, and match it against the twistor result by numerical evaluation.

[3] While the propagators naturally split between the inside and outside of the polygon, one might have to worry about the dressing factors of the vertices $V^i_{j_1\dots j_k}$ when applying the Feynman rules. (Here, i denotes the respective vertex and the lower indices reflect the cyclic ordering of the edges around i.) Since the dressing factor can be written as a product of factors depending only on neighboring edges (3.42), they also factorize along the perimeter of the polygon.

The ansatz has the general form

$$M_{n,\ell} = \sum_a f_a(x_{ij}^2, y_{ij}^2)\, \mathcal{J}_a(x_{ij}^2)\,, \tag{5.34}$$

where the $\mathcal{J}_a$ form a basis of rational functions that are the integrands of conformal integrals planarly embedded inside the polygon, and $f_a(x_{ij}^2, y_{ij}^2)$ are polynomial coefficient functions. An obstacle in the computation is that there appears to be no way to bound the coefficients f_a from first principles, so we have to partially resort to educated guesses to formulate ansätze that are both sufficiently general and not too big to constrain.

5.4. All 10d Null Polygons to Two Loops

Using the twistor Feynman rules on graphs with disk topology enables us to compute the polygons $M_{n,\ell}$ directly, without having to find the full n-point ℓ-loop generating function first. At one-loop order, the explicit expression of the square (5.14), the pentagon (5.20), and the hexagon (5.30) are sufficient to state a formula for all one-loop polygons that includes both the parity-even and parity-odd parts. We have verified this proposal numerically up to nine points by matching against the respective twistor expressions.

At two loops, we focus on the parity-even part of the polygons, by numerically matching appropriate ansätze against the twistor computation, as described above. In this way, we successively compute two-loop polygons starting from six points. We find systematics in their expressions that further constrain the ansatz for respective higher-point polygons. Reaching the ten-sided polygon, we could fix all patterns in the expression, and thus conjecture a formula for the parity-even part of all polygons $M_{n,2}$ at two loops. We checked that proposal explicitly at eleven points, and find agreement with the twistor result.

The final results for all polygons $M_{n,\ell}$, for arbitrary n and up to $\ell = 2$ loops, can be found in the ancillary files of [2]. See Appendix A for a guide to these files.

Before presenting the formulae for all one-loop and two-loop polygons in (5.35), (5.45), and (5.47) below, let us describe how the factorization property of the polygons can be used to organize them systematically.

5.4.1. Factorization Channels

The polygon integrands are rational functions of ten-dimensional distances X_{ij}^2 as well as four-dimensional distances x_{ij}^2 (four-dimensional propagators $d_{i,j}$ appear only polynomially). In particular, they display ten-dimensional poles. Like all rational functions, they are fixed by the residues at their poles, and their behavior at infinity. The poles are precisely the factorization channels, on which the polygons factorize into products of lower polygons (5.7). After taking these residues into account, what remains are terms that are free of ten-dimensional propagators $D_{ij} = x_{ij}^2/X_{ij}^2$ on the diagonals of the polygon (the "empty" polygon).
The factorization property (5.7) as well as the above picture inspire the following natural decomposition of the polygons $\mathbb{M}_n$ into more basic building blocks $\mathbb{F}_f$ that we call *faces*:

$$\mathbb{M}_n = \mathbb{F}_{1,\dots,n} + \sum_{\substack{\Gamma\in \text{tree} \\ \text{graphs}}} \prod_{\substack{\text{edges} \\ (ij)\in\Gamma}} D_{ij} \times \prod_{\substack{\text{faces} \\ f\in\Gamma}} \mathbb{F}_f \,. \tag{5.35}$$

Here, the sum runs over all tree graphs that contribute to $M_{n,0}$, excluding the empty polygon graph (whose contribution is captured by the first term).[4] The formula (5.35)

- defines the faces $\mathbb{F}_{1,\dots,n}$ recursively in terms of the polygons $\mathbb{M}_n$ as well as the lower-point and lower-loop faces,
- makes the polygon factorization property (5.7) manifest,[5]
- and it reduces the polygon functions $\mathbb{M}_n$ to yet simpler functions, the faces $\mathbb{F}_{1,\dots,n}$.

In order to apply (5.35) perturbatively, we expand both the polygons $\mathbb{M}_n$ (cf. (5.3)) and the faces $\mathbb{F}_{1,\dots,n}$ in the coupling,

$$\mathbb{F}_{1,\dots,n} = 1 + \sum_{\ell=1}^{\infty} \frac{(-a)^\ell}{\ell!} \int \Bigg[\prod_k \frac{\mathrm{d}^4 x_k}{4\pi^2} \Bigg] F^{(\ell)}_{1,\dots,n} \,, \tag{5.36}$$

[4] These graphs are exactly the planar graphs one can draw on the disk with n punctures on the boundary (and no internal vertices), i. e. all graphs that tessellate the n-gon by diagonals. See the first line of Table 5.1, as well as [128] for their counting modulo dihedral permutations.

[5] Starting with the factorization property of the polygons $\mathbb{M}_n$, there is some freedom in the definition of the faces $\mathbb{F}$, in the sense that one could write variations of the formula (5.35), that would differ by re-arrangements of the geometric series in the fat propagators, e.g. $D_{ij}/d_{ij} = 1+D_{ij}$. We find that our choice (5.35) yields the most natural definition.

where the product over k is taken over all ℓ loop variables. We wrote the decomposition (5.35) in terms of the integrated objects $\mathbb{M}_n$ and $\mathbb{F}_{1,\ldots,n}$, but we emphasize that they hold at the level of the *integrands*, i. e. the integrations can be removed from the equation. At integrand level, one must symmetrize each term over all distributions of integration points (Lagrangian insertions) on the factors F_f, exactly as it happens in (5.2) and (5.5).

Notably, the leading order $F^{(0)}_{1,\ldots,n}$ of the faces are trivial by construction, and the triangles receive no loop corrections:

$$\mathbb{F}_{i_1,i_2,i_3} = 1\,. \tag{5.37}$$

Let us exemplify the decomposition (5.35) by explicitly writing the expressions for the square, pentagon and hexagon. The former two are expressed as

$$\mathbb{M}_4 = \mathbb{F}_{1,2,3,4} + D_{13} \times \mathbb{F}_{1,2,3}\,\mathbb{F}_{1,3,4} + D_{24} \times \mathbb{F}_{1,2,4}\,\mathbb{F}_{2,3,4}\,, \tag{5.38}$$

$$\begin{aligned} \mathbb{M}_5 = \mathbb{F}_{1,2,3,4,5} + \Big[&\frac{1}{2} D_{14} \times \mathbb{F}_{1,2,3,4}\,\mathbb{F}_{1,4,5} \\ &+ \frac{1}{2} D_{14}\,D_{13} \times \mathbb{F}_{1,2,3}\,\mathbb{F}_{1,3,4}\,\mathbb{F}_{1,4,5} + (\mathrm{D}_5 \text{ perms})\Big]\,, \end{aligned} \tag{5.39}$$

while the hexagon is split into tree-level faces as follows:

$$\mathbb{M}_6 = \mathbb{F}_{1,2,3,4,5,6}$$

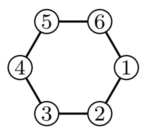

$$+ \Big[\frac{1}{2} D_{13} \times \mathbb{F}_{1,2,3}\,\mathbb{F}_{3,4,5,6,1}$$

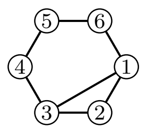

$$+ \frac{1}{4} D_{14} \times \mathbb{F}_{1,2,3,4}\,\mathbb{F}_{4,5,6,1}$$

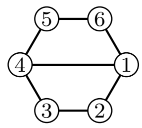

$$+ D_{13} D_{14} \times \mathbb{F}_{1,2,3}\,\mathbb{F}_{3,4,1}\,\mathbb{F}_{4,5,6,1}$$

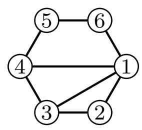

$$+ \frac{1}{2} D_{13} D_{15} \times \mathbb{F}_{1,2,3}\,\mathbb{F}_{5,6,1}\,\mathbb{F}_{3,4,5,1}$$

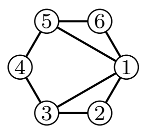

$$+\frac{1}{4}D_{15}D_{24}\times\mathbb{F}_{2,3,4}\,\mathbb{F}_{5,6,1}\,\mathbb{F}_{1,2,4,5}$$

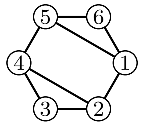

$$+\frac{1}{2}D_{13}D_{14}D_{15}\times\mathbb{F}_{1,2,3}\,\mathbb{F}_{1,3,4}\,\mathbb{F}_{1,4,5}\,\mathbb{F}_{1,5,6}+\ldots$$

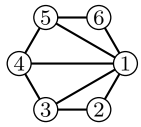

$$+\,(\mathrm{D}_6\text{ perms})\Big]\,, \tag{5.40}$$

where the dots stand for two more terms that are products of three propagators D_{ij} and four triangle faces $\mathbb{F}_{i_1,i_2,i_3}$. Expanding these expressions at one-loop order using (5.36), and passing to the integrands yields

$$M_{4,1}=F^{(1)}_{1,2,3,4}\,, \tag{5.41}$$

$$M_{5,1}=F^{(1)}_{1,2,3,4,5}+\Big[\frac{1}{2}D_{14}\times F^{(1)}_{1,2,3,4}+(\mathrm{D}_5\text{ perms})\Big]\,, \tag{5.42}$$

$$\begin{aligned}M_{6,1}=F^{(1)}_{1,2,3,4,5,6}+\Big[&\frac{1}{2}D_{13}\times F^{(1)}_{3,4,5,6,1}+\frac{1}{4}D_{14}\times(F^{(1)}_{1,2,3,4}+F^{(1)}_{4,5,6,1})\\&+D_{13}D_{14}\times F^{(1)}_{4,5,6,1}+\frac{1}{2}D_{13}D_{15}\times F^{(1)}_{3,4,5,1}\\&+\frac{1}{4}D_{15}D_{24}\times F^{(1)}_{1,2,4,5}+(\mathrm{D}_6\text{ perms})\Big]\,.\end{aligned} \tag{5.43}$$

At two-loop order, these expressions almost stay the same, up to the substitution $F^{(1)}\to F^{(2)}$. Only the two-loop hexagon receives an extra term that is a product of two one-loop squares (from the third line of (5.40)):

$$M_{6,2}=(5.43)\big|_{F^{(1)}\to F^{(2)}}+\Big[\frac{1}{2}D_{14}\times F^{(1)}_{1,2,3,4}F^{(1)}_{1,4,5,6}+(\mathrm{D}_6\text{ perms})\Big]\,. \tag{5.44}$$

Importantly, terms of this type can contain products of parity-odd terms that contribute to the parity-even part of $M_{n,2}$. The four-point faces $F^{(\ell)}_{1,2,3,4}$ are free of parity-odd parts, but $F^{(1)}_{i_1,\ldots,i_{n\geq 5}}$ does contain parity-odd terms, and thus starting from $M_{8,2}$, products of such terms do contribute to the decomposition (5.35). This highlights that it is important to include both parity-even and parity-odd parts in the definition of the polygons M_n and the faces $F_{1,\ldots,n}$ in order to make the decomposition (5.35) consistent. The same happens for massless amplitudes, where parity-odd terms have to be included in order to consistently establish the super-correlator/super-amplitude duality [80, 103].

5.4.2. One-Loop Result

The expressions for the square (5.14), the pentagon (5.20), and the hexagon (5.30) suffice to conjecture the general structure of both the even and odd part of all one-loop polygons. The corresponding one-loop faces that dress the tree-level graphs for any $n \geq 4$ are

$$F^{(1)}_{i_1,i_2,\cdots,i_n} = \sum_{\substack{[i_m,i_{m+1}],[i_l,i_{l+1}] \\ \text{non-adjacent}}} \frac{P_{i_m i_{l+1},i_{m+1}i_l} - 4i\,\epsilon_{\mu\nu\rho\sigma} x^\mu_{i_m 0} x^\nu_{i_{m+1}0} x^\rho_{i_l 0} x^\sigma_{i_{l+1}0}}{2\,x^2_{i_m 0} x^2_{i_{m+1}0} x^2_{i_l 0} x^2_{i_{l+1}0}} - \sum_{1\leq j<k<l<m\leq n} \frac{y^2_{i_j i_l} y^2_{i_k i_m}}{x^2_{i_j 0} x^2_{i_k 0} x^2_{i_l 0} x^2_{i_m 0}}\,, \tag{5.45}$$

where the first sum runs over all pairs of non-adjacent edges at the perimeter of the polygon. The imaginary term proportional to $\epsilon_{\mu\nu\rho\sigma}$ is parity-odd, all other terms are parity-even, x_0 is the coordinate of the Lagrangian insertion, and we defined the combination

$$P_{ij,kl} = -x^2_{ij}x^2_{kl} + x^2_{ik}x^2_{jl} + x^2_{il}x^2_{jk}\,. \tag{5.46}$$

We have verified this proposal by numerically comparing it to the respective twistor expressions (5.32) up to nine points.

5.4.3. Two-Loop Result

The formula for the two-loop faces $F^{(2)}_{1,\dots,n}$ is more intricate, and we only computed its parity-even part. Hence also the two-loop polygons M_n are restricted to their parity-even parts. We will not indicate the superscript "even", with the understanding that all two-loop expressions refer to their parity-even parts only.

Result. We decompose the two-loop n-point faces in exactly the same way as was done for the integrand of the two-loop n-point massless gluon amplitude [129]:[6]

$$F^{(2)}_{1,\dots,n} = \sum_{k,\mathbf{e}} f_{k,\mathbf{e},a,b}(x^2_{ij}, y^2_{ij})\,\mathcal{J}^{\mathbf{e},a,b}_k + (a \leftrightarrow b)\,. \tag{5.47}$$

[6]The two-loop faces (5.47) as well as the resulting two-loop polygons (5.35) are constructed in the ancillary files of [2]. See Appendix A for a guide to these files.

Here, the sum over k runs over three different propagator topologies $\mathcal{J}_k^{\mathbf{e},a,b}$, the sum over $\mathbf{e}$ runs over their planar embeddings in the face $F_{1,\ldots,n}$, and the coefficients $f_{k,\mathbf{e},a,b}$ are polynomials in the basic scalar invariants x_{ij}^2 and y_{ij}^2.

The following three propagator topologies occur in the decomposition:

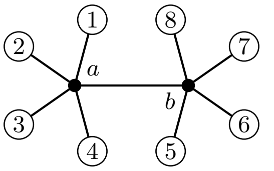

$$\mathcal{J}_1^{1,\ldots,8,a,b} = \frac{1}{x_{1a}^2 x_{2a}^2 x_{3a}^2 x_{4a}^2\, x_{ab}^2\, x_{5b}^2 x_{6b}^2 x_{7b}^2 x_{8b}^2}\,, \tag{5.48}$$

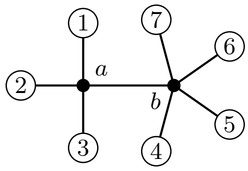

$$\mathcal{J}_2^{1,\ldots,7,a,b} = \frac{1}{x_{1a}^2 x_{2a}^2 x_{3a}^2\, x_{ab}^2\, x_{4b}^2 x_{5b}^2 x_{6b}^2 x_{7b}^2}\,, \tag{5.49}$$

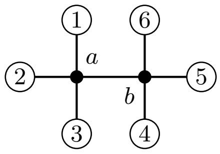

$$\mathcal{J}_3^{1,\ldots,6,a,b} = \frac{1}{x_{1a}^2 x_{2a}^2 x_{3a}^2\, x_{ab}^2\, x_{4b}^2 x_{5b}^2 x_{6b}^2}\,. \tag{5.50}$$

Note that the structures $\mathcal{J}_1$, $\mathcal{J}_2$, $\mathcal{J}_3$ do not include numerator factors, which means that they do not absorb all dependence on the Lagrangian points a, b.

Therefore, the coefficients $f_{k,\mathbf{e},a,b}$ must not only contain factors x_{ij}^2 between external points $i, j \leq n$, but also among external points $i \leq n$ and Lagrangian points $j \in \{a, b\}$. However, they may not contain factors that cancel any of the denominator factors in the definitions of the integrands $\mathcal{J}_1$, $\mathcal{J}_2$, $\mathcal{J}_3$. The only exception to this is the coefficient $f_{1,\mathbf{e},a,b}$ of the double-penta integrand, which may include terms with a factor x_{ab}^2 that turns $\mathcal{J}_1$ into the product of two one-loop box integrands.

The sum over $\mathbf{e}$ runs over all planar embeddings of the integrands $\mathcal{J}_1$, $\mathcal{J}_2$, $\mathcal{J}_3$ into the polygonal face $F_{1,\ldots,n}$. For example, the double-penta integrand $\mathcal{J}_3^{\mathbf{e}}$ is summed over embeddings

$$\mathbf{e} = (i_1, \ldots, i_8)\,, \qquad i_1 < i_2 < i_3 < i_4 \leq i_5 < i_6 < i_7 < i_8 \leq i_1 \ (\mathrm{mod}\, n)\,. \tag{5.51}$$

Making use of the dihedral D_n symmetry, we can fix $i_1 = 1$. Due to the planar embedding, we can equally sum over the distances ℓ_k of neighboring points that attach to the integrand:

$$\tilde{\mathbf{e}} = [\ell_1, \ldots, \ell_8]\,, \qquad \ell_k = i_k - i_{k-1} \;\; (i_0 \equiv i_8)\,, \qquad \ell_k \geq \begin{cases} 1 & k = 2,3,4,6,7,8, \\ 0 & k = 1,5\,. \end{cases} \tag{5.52}$$

We use round/square brackets to distinguish the two notations. The coefficient functions $f_{k,\mathbf{e},a,b}$ are polynomials in x_{ij}^2, $i,j \in \{1,\ldots,n,a,b\}$, and y_{ij}^2, $i,j \in \{1,\ldots,n\}$. For $y_{ij}^2 = 0$, they reduce to the coefficients of the massless gluon amplitude integrand (5.8), which was determined in [129].[7] The coefficient $f_{1,\mathbf{e},a,b}$ of the double-penta integrand $\mathcal{J}_1$ can be written in a relatively compact way:[8]

$$\begin{aligned} 4\, f_{1,i_1,\ldots,i_8,a,b} &= x_{ab}^2 \big(\delta_{\ell_2,1}\delta_{\ell_4,1} P_{i_1 i_4, i_2 i_3} - 2 y_{i_1 i_3}^2 y_{i_2 i_4}^2\big)\big(\delta_{\ell_6,1}\delta_{\ell_8,1} P_{i_5 i_8, i_6 i_7} - 2 y_{i_5 i_7}^2 y_{i_6 i_8}^2\big) \\ &\quad - \delta_{\ell_2,1}\delta_{\ell_4,1}\delta_{\ell_6,1}\delta_{\ell_8,1} \begin{bmatrix} i_1 & i_2 & i_3 & i_4 & a \\ i_5 & i_6 & i_7 & i_8 & b \end{bmatrix} + \delta_{\ell_1,0}\delta_{\ell_3,1}\delta_{\ell_5,0}\delta_{\ell_7,1}\, y_{i_1 i_4}^2\, h_{\mathrm{DP}}\,, \end{aligned} \tag{5.53}$$

with the factor h_{DP} given by

$$\begin{aligned} h_{\mathrm{DP}} = \begin{bmatrix} i_1 & i_2 & i_3 & a \\ i_4 & i_6 & i_7 & b \end{bmatrix} + \begin{bmatrix} i_2 & i_3 & i_4 & a \\ i_6 & i_7 & i_1 & b \end{bmatrix} - x_{i_1 i_4}^2 \begin{bmatrix} i_2 & i_3 & a \\ i_6 & i_7 & b \end{bmatrix} \\ - x_{ab}^2 \left(x_{i_2 i_3}^2 P_{i_1 i_7, i_4 i_6} + x_{i_6 i_7}^2 P_{i_1 i_2, i_3 i_4} - x_{i_1 i_4}^2 x_{i_2 i_3}^2 x_{i_6 i_7}^2 \right)\,, \end{aligned} \tag{5.54}$$

and where the square brackets denote determinants:

$$\begin{bmatrix} i_1 & i_2 & \cdots \\ j_1 & j_2 & \cdots \end{bmatrix} = \det\,\{x_{ij}^2\}_{\substack{i=i_1,i_2,\ldots \\ j=j_1,j_2,\ldots}}\,. \tag{5.55}$$

The numerator functions $f_{k,\mathbf{e}}$ encode all two-loop faces $F^{(2)}_{1,\ldots,n}$, and thereby all two-loop polygons $M_{n,2}$. Through the dependence on the embedding $\mathbf{e}$, one could imagine that the number of functions $f_{k,\mathbf{e}}$ proliferates as n increases. However, we see in the example of f_1 (5.53) that the dependence on the embedding is relatively moderate, in the sense that the expression stabilizes once all ℓ_j are sufficiently large. We observe that the same saturation property also holds for the other coefficients: In general,

[7] Setting $y_{i,j}^2 = 0$ for all i,j in particular includes passing to the four-dimensional null limit $x_{i,i+1}^2 = 0$ at the perimeter of the polygon, due to the ten-dimensional null condition $0 = X_{i,i+1}^2 = x_{i,i+1}^2 + y_{i,i+1}^2$.

[8] For compactness, we use both the i_k and the ℓ_k labels in this formula.

the coefficients cease to depend on the distances ℓ_j once $\ell_j \geq 2$:[9]

$$f_{k,[\dots,\ell_j,\dots]} = f_{k,[\dots,2,\dots]} \quad \text{for} \quad \ell_j \geq 2\,. \tag{5.56}$$

The only exception to this pattern are the distances $\ell_1 = i_1 - i_6$ and $\ell_4 = i_4 - i_3$ of the coefficients $f_{3,\tilde{\mathbf{e}}}$, where this saturation only occurs at $\ell_{1,4} \geq 3$. This is also the case for the integrand of the massless gluon amplitude [129]. Furthermore, the coefficient functions display the following label symmetries that are inherited from the symmetries of the respective propagator topologies $\mathcal{J}_1$, $\mathcal{J}_2$ and $\mathcal{J}_3$:

$$\begin{aligned}
&f_{1,[\ell_1,\ell_2,\ell_3,\ell_4,\ell_5,\ell_6,\ell_7,\ell_8],a,b} && f_{2,[\ell_1,\ell_2,\ell_3,\ell_4,\ell_5,\ell_6,\ell_7],a,b} && f_{3,[\ell_1,\ell_2,\ell_3,\ell_4,\ell_5,\ell_6],a,b}\\
&= f_{1,[\ell_1,\ell_8,\ell_7,\ell_6,\ell_5,\ell_4,\ell_3,\ell_2],b,a} && = f_{2,[\ell_4,\ell_3,\ell_2,\ell_1,\ell_7,\ell_6,\ell_5],a,b}\,, && = f_{3,[\ell_1,\ell_6,\ell_5,\ell_4,\ell_3,\ell_2],b,a}\\
&= f_{1,[\ell_5,\ell_6,\ell_7,\ell_8,\ell_1,\ell_2,\ell_3,\ell_4],b,a} && && = f_{3,[\ell_4,\ell_5,\ell_6,\ell_1,\ell_2,\ell_3],b,a}\\
&= f_{1,[\ell_5,\ell_4,\ell_3,\ell_2,\ell_1,\ell_8,\ell_7,\ell_6],a,b}\,, && && = f_{3,[\ell_4,\ell_3,\ell_2,\ell_1,\ell_6,\ell_5],a,b}\,.
\end{aligned} \tag{5.57}$$

Assuming the saturation property as well as the label symmetries, we can list all potentially different coefficient functions $f_{k,\mathbf{e}}$. In this way, we find that there are a priori 180 different coefficients $f_{1,\tilde{\mathbf{e}}}$, 156 different coefficients $f_{2,\tilde{\mathbf{e}}}$, and 88 different coefficients $f_{3,\tilde{\mathbf{e}}}$ corresponding to the three propagator topologies.
As seen above, the coefficients $f_{1,\mathbf{e}}$ of the double-penta topology combine elegantly into (5.53). In contrast, the other two families $f_{2,\mathbf{e}}$ and $f_{3,\mathbf{e}}$ exhibit a considerably more intricate structure, with a subtler dependence on the embeddings. Their explicit forms can be found in the ancillary files of [2]. See Appendix A for a guide to these files.

Two-Loop Ansatz Construction. Having laid out the structure of the result, we now step back to outline how it was obtained. In order to match the twistor expression of the polygons to a manifestly Lorentz-invariant representation, it is necessary to formulate a compact ansatz. This ansatz is provided by the functions $f_{k,\mathbf{e}}$, but with a priori undetermined numerical coefficients. Combining these functions with

[9] In a strict sense, the saturation means the following:
Given two planar embeddings $\mathbf{e} = (i_1, \dots, i_j, i_{j+1}, \dots, i_{n_k})$ and $\hat{\mathbf{e}} = (i_1, \dots, i_j, i_{j+1}+1, \dots, i_{n_k}+1)$ that only differ by increasing the distance between a single pair of indices by one, then

$$f_{k,\hat{\mathbf{e}},a,b}\big|_{\hat{\mathbf{e}}\to\mathbf{e}} = f_{k,\mathbf{e},a,b} \quad \text{if} \quad i_{j+1} - i_j \geq 2\,.$$

the denominators in (5.47), and using the factorization decomposition (5.35) yields an ansatz for the respective two-loop polygon.

Due to conformal symmetry, the coefficients $f_{k,\boldsymbol{a}}$ are polynomials in x_{ij}^2 and d_{ij}, constructed such that each term becomes conformally invariant in x_{ij}^2 when combined with the corresponding denominator $\mathcal{J}_k$.[10] This property is directly inherited from the generating function $G_{n,\ell}$, which is itself conformal in the variables x_{ij}^2 when expressed as a function of d_{ij} and x_{ij}^2. Consequently, this symmetry constrains the possible monomials in x_{ij}^2 that can appear in the polynomials $f_{k,\boldsymbol{a}}$. Heuristically, we also observe that the appearance of the factors d_{ij} is similarly restricted: Each factor d_{ij} must be accompanied by a corresponding factor x_{ij}^2, ensuring that $f_{k,\boldsymbol{a}}$ remains a polynomial in the combined variables $(x_{ij}^2, y_{ij}^2 = x_{ij}^2 d_{ij})$. In other words, the functions $f_{k,\mathbf{e}}$ are polynomials in x_{ij}^2 and y_{ij}^2 such that the conformal and R-charge weights of the products $f_{k,\mathbf{e}}\mathcal{J}_k^{\mathbf{e}}$ match those of the polygon correlator:

$$f_{k,\mathbf{e},a,b}(\lambda_i\lambda_j x_{ij}^2, \lambda_i\lambda_j y_{ij}^2)\,\mathcal{J}_k^{\mathbf{e},a,b}(\lambda_i\lambda_j x_{ij}^2) = \frac{f_{k,\mathbf{e},a,b}(x_{ij}^2, y_{ij}^2)\,\mathcal{J}_k^{\mathbf{e},a,b}(x_{ij}^2)}{\lambda_a^4\lambda_b^4}\,. \tag{5.58}$$

Moreover, the functions $f_{k,\mathbf{e}}$ do not contain distances x_{ij}^2 that cancel factors in the denominator of $\mathcal{J}_k^{\mathbf{e}}$, with the exception of $f_{1,\mathbf{e}}$, that may contain factors x_{ab}^2, as was already mentioned above. Finally, the functions $f_{k,\mathbf{e}}$ must obey the label symmetries (5.57), which further restricts the size of the ansätze. In this way, we find the number of unknown coefficients to be 1242, 240, and 50 for the functions $f_{1,\mathbf{e}}$, $f_{2,\mathbf{e}}$, and $f_{3,\mathbf{e}}$, respectively (for fixed embeddings $\mathbf{e}$). However, when inserting the ansätze into a specific face function F in an n-sided polygon $M_{n,2}$, the number of coefficients typically reduces, for three reasons: First, factors y_{ij}^2 are identified with x_{ij}^2 for $j = i+1$. Second, part of the ansatz collapses if points in the embedding $\mathbf{e}$ are equal to another. Third, there might be identifications in the ansatz due to the dihedral symmetry D_n of the respective polygon.

The functions $f_{k,\mathbf{e}}$ can now be probed in order of their appearance, beginning from the square $M_{4,2}$, and successively increasing the size of the polygons by one. At each step, the coefficients in the polynomials $f_{k,\mathbf{e}}$ are fixed by comparison to the twistor expression, and subsequently fed into the succeeding ansatz. In this process, we can make use of the saturation property (5.56). To probe all degrees of freedom of the coefficient functions f_k, we would in principle have to push this process all the

[10]The terms become conformally invariant after integration, so the integrands are of conformal weight zero in the external points and of weight 4 in the integration variables a and b.

way to the two-loop hexadecagon $M_{16,2}$, such that all distances ℓ_j become saturated according to (5.56). However, the pattern of the various embeddings often becomes apparent much earlier. This is most notable for the double-penta functions $f_{1,\mathbf{e}}$, which neatly combine into (5.53). In practice, we find the complete forms of all functions $f_{k,\mathbf{e}}$ by matching the respective ansätze to polygons $M_{n,2}$ up to the decagon with $n = 10$. This yields a complete formula for all two-loop polygons. We have checked the resulting formula for the hendecagon $M_{11,2}$ by matching against the twistor computation, and found complete agreement. This verifies the correctness of the result for general n beyond reasonable doubt.

Examples: Square, Pentagon, and Hexagon. To exemplify the decomposition into different propagator topologies (5.35), we explicitly apply this formula up to six points. For the square and pentagon, the two-loop faces read:

$$F^{(2)}_{1,2,3,4} = \frac{1}{4} f_{3,[0,1,1,0,1,1]} \mathcal{J}^{\mathbf{e}}_3 + (\mathrm{D}_4 \text{ perms}) \,, \tag{5.59}$$

$$\begin{aligned} F^{(2)}_{1,2,3,4,5} &= f_{3,[0,1,1,0,1,2]} \mathcal{J}^{\mathbf{e}}_3 + \frac{1}{2} f_{3,[0,1,1,1,1,1]} \mathcal{J}^{\mathbf{e}}_3 \\ &\quad + \frac{1}{2} f_{2,[0,1,1,0,1,1,1]} \mathcal{J}^{\mathbf{e}}_2 + (\mathrm{D}_5 \text{ perms}) \,, \end{aligned} \tag{5.60}$$

with the coefficient functions given by

$$\begin{aligned} f_{3,[0,1,1,0,1,1]} &= (x^2_{13} - y^2_{13}) \, (x^2_{13} x^2_{24} - y^2_{13} y^2_{24}) \,, \\ f_{3,[0,1,1,0,1,2]} &= \frac{1}{2} (x^2_{13} - y^2_{13}) \, (P_{15,23} - 2 y^2_{13} y^2_{24}) \,, \\ f_{3,[0,1,1,1,1,1]} &= -\frac{1}{2} P_{12,45} \, x^2_{13} + \frac{1}{2} P_{12,35} \, (x^2_{14} - y^2_{14}) - \frac{1}{2} y^2_{13} (P_{15,24} - 2 y^2_{14} y^2_{25}) \,, \\ f_{2,[0,1,1,0,1,1,1]} &= \frac{1}{2} x^2_{2b} \Big(P_{16,35} \, y^2_{13} + x^2_{13} (P_{13,56} - 2 y^2_{14} y^2_{35}) \Big) \,, \end{aligned} \tag{5.61}$$

where $P_{ij,kl}$ is defined in (5.46). In the above equations, the coefficients $f_{k,\tilde{\mathbf{e}}}$ are labeled by the distances ℓ_j between neighboring points in the embedding, as in (5.52). It is implied that the corresponding point labels start with point one, that is $\mathbf{e} = (1, 1 + \ell_2, \dots)$, and that the respective factors $\mathcal{J}^{\mathbf{e}}_k$ are defined with this embedding $\mathbf{e}$.

According to (5.41), the two-loop square $M_{4,2}$ equals the two-loop four-point face, and (5.59) consistently matches the expression (5.15) for $M_{4,2}$ obtained from the generating function. In order to obtain the two-loop pentagon $M_{5,2}$, the five-point face (5.60) must be combined with the four-point face as in (5.42). Once more, the expression (5.21) derived from the generating function is correctly reproduced.

The six-point face at two-loop order already consists of a much larger number of propagator topologies:

$$\begin{aligned}
F^{(2)}_{1,2,3,4,5,6} = {} & f_{3,[0,1,1,0,1,3]}\mathcal{J}_3^{\mathbf{e}} + \frac{1}{2} f_{3,[0,1,1,0,2,2]}\mathcal{J}_3^{\mathbf{e}} + f_{3,[0,1,1,1,1,2]}\mathcal{J}_3^{\mathbf{e}} \\
& + f_{3,[0,1,1,1,2,1]}\mathcal{J}_3^{\mathbf{e}} + \frac{1}{2} f_{3,[0,1,1,2,1,1]}\mathcal{J}_3^{\mathbf{e}} + \frac{1}{2} f_{3,[0,1,2,0,1,2]}\mathcal{J}_3^{\mathbf{e}} \\
& + \frac{1}{2} f_{3,[0,1,2,0,2,1]}\mathcal{J}_3^{\mathbf{e}} + \frac{1}{4} f_{3,[1,1,1,1,1,1]}\mathcal{J}_3^{\mathbf{e}} + f_{2,[0,1,1,0,1,1,2]}\mathcal{J}_2^{\mathbf{e}} \\
& + \frac{1}{2} f_{2,[0,1,1,0,1,2,1]}\mathcal{J}_2^{\mathbf{e}} + f_{2,[0,1,1,1,1,1,1]}\mathcal{J}_2^{\mathbf{e}} + f_{2,[0,1,2,0,1,1,1]}\mathcal{J}_2^{\mathbf{e}} \\
& + \frac{1}{4} f_{1,[0,1,1,1,0,1,1,1]}\mathcal{J}_1^{\mathbf{e}} + (\mathrm{D}_6 \text{ perms})\,.
\end{aligned} \tag{5.62}$$

In particular, the double-penta topology $\mathcal{J}_1$ appears for the first time. Again, the coefficients are labeled by to the distances between neighboring points, and are given by

$$\begin{aligned}
f_{3,[0,1,1,0,1,3]} &= \frac{1}{2}(x_{13}^2 - y_{13}^2)\,(P_{15,23} - 2y_{13}^2 y_{24}^2)\,, \\
f_{3,[0,1,1,0,2,2]} &= -\,y_{13}^2\, y_{25}^2\,(x_{13}^2 + y_{13}^2)\,, \\
f_{3,[0,1,1,1,1,2]} &= -\frac{1}{2}x_{15}^2(x_{13}^2 x_{24}^2 - y_{13}^2 y_{24}^2) + \frac{1}{4}P_{12,35}(x_{14}^2 - y_{14}^2) \\
&\quad + \frac{1}{2}y_{13}^2(2y_{14}^2 y_{25}^2 - P_{15,24})\,, \\
f_{3,[0,1,1,1,2,1]} &= -\frac{1}{4}P_{15,23}x_{14}^2 + \frac{1}{2}x_{12}^2 x_{13}^2 x_{46}^2 - \frac{1}{2}x_{16}^2 y_{13}^2 y_{24}^2 \\
&\quad - \frac{1}{4}y_{14}^2(P_{12,35} - 4y_{13}^2 y_{26}^2)\,, \\
f_{3,[0,1,1,2,1,1]} &= -\frac{1}{2}P_{15,24}y_{13}^2 - \frac{1}{2}y_{15}^2(P_{12,35} - 2y_{13}^2 y_{26}^2)\,, \\
f_{3,[0,1,2,0,1,2]} &= \frac{1}{2}(x_{14}^2 - y_{14}^2)\Big(\frac{1}{2}P_{15,23} + x_{12}^2 x_{45}^2 - 2y_{14}^2 y_{25}^2\Big)\,, \\
f_{3,[0,1,2,0,2,1]} &= \frac{1}{4}(x_{14}^2 - y_{14}^2)(P_{15,23} - 2x_{12}^2 x_{46}^2 - 4y_{14}^2 y_{26}^2)\,, \\
f_{3,[1,1,1,1,1,1]} &= \frac{1}{4}\bigg(\begin{bmatrix} 2 & 3 & 4 \\ 5 & 6 & 1 \end{bmatrix} + \begin{bmatrix} 6 & 1 & 2 \\ 3 & 4 & 5 \end{bmatrix} + P_{25,46}x_{13}^2 + P_{13,25}x_{46}^2 \\
&\quad + P_{25,36}y_{14}^2 + P_{14,25}y_{36}^2 - 2x_{56}^2 y_{13}^2 y_{24}^2 - 2x_{45}^2 y_{13}^2 y_{26}^2 \\
&\quad - 2x_{23}^2 y_{15}^2 y_{46}^2 - 2x_{12}^2 y_{35}^2 y_{46}^2 + 4y_{13}^2 y_{25}^2 y_{46}^2\bigg)\,,
\end{aligned}$$

$$
\begin{aligned}
f_{2,[0,1,1,0,1,1,2]} &= \frac{1}{2}x_{2b}^2(P_{16,35}y_{13}^2 - 2x_{13}^2y_{14}^2y_{35}^2)\,, \\
f_{2,[0,1,1,0,1,2,1]} &= \frac{1}{2}x_{13}^2x_{2b}^2(P_{13,56} - 2y_{14}^2y_{36}^2)\,, \\
f_{2,[0,1,1,1,1,1,1]} &= \frac{1}{4}\bigg(- \begin{bmatrix} 1 & 2 & 3 & 4 \\ 5 & 6 & 1 & b \end{bmatrix} - \begin{bmatrix} 1 & 2 & 3 \\ 5 & 6 & b \end{bmatrix} y_{14}^2 \\
&\quad + (x_{13}^2x_{2b}^2 - x_{12}^2x_{3b}^2)(P_{14,56} + x_{56}^2y_{14}^2 - 2y_{15}^2y_{46}^2)\bigg)\,, \\
f_{2,[0,1,2,0,1,1,1]} &= \frac{1}{4}x_{2b}^2(P_{16,35}y_{14}^2 + x_{14}^2(P_{13,56} - 2y_{15}^2y_{46}^2))\,, \\
f_{1,[0,1,1,1,0,1,1,1]} &= \frac{1}{4}x_{ab}^2(P_{14,23} - 2y_{13}^2y_{24}^2)(P_{14,56} - 2y_{15}^2y_{46}^2) \\
&\quad - \frac{1}{4}\begin{bmatrix} 1 & 2 & 3 & 4 & a \\ 4 & 5 & 6 & 1 & b \end{bmatrix} + \frac{1}{4}y_{14}^2\, h_{\mathrm{DP}}\,,
\end{aligned} \tag{5.63}
$$

where again it is understood that $\mathbf{e} = (1, 1+\ell_2, \dots)$ starts with the point label 1. The last (double-penta) coefficient $f_{1,\dots}$ can be obtained from (5.53), with the factor h_{DP} given in (5.54). In accordance with the saturation property (5.56), one can see that $f_{3,[0,1,1,0,1,3]} = f_{3,[0,1,1,0,1,2]}$. The two-loop hexagon $M_{6,2}$ can then be obtained by using (5.44), and plugging in the expressions for the two-loop four-point and five-point faces as well as the product of one-loop squares.

6. Higher-Loop Pentagon Integrand

In the last chapter, we introduced the polygon functions that arise when taking a ten-dimensional null limit on the generating functions. Subsequently, we used their properties to build ansätze and fixed the remaining freedom through a direct twistor-based computation, thereby determining all polygon integrands of arbitrary multiplicity up to two loops. We now turn to the five-point case, the pentagon, with the aim of uncovering its structural features and computing it to high-loop orders. Mimicking the bootstrap program for amplitudes, where massless amplitudes can be determined at four [130] and higher points [131] using soft and collinear constraints, we adapt these ideas to massive amplitudes and bootstrap the pentagon up to five loops.

We begin by reintroducing the pentagon in Section 6.1, now also specifically as a five-point correlator in the large-charge limit. Based on the known one- and two-loop results, we then construct a general ℓ-loop ansatz for the pentagon integrand in Section 6.2. In Section 6.3, we introduce the soft and collinear constraints and explain how they must be modified to apply in off-shell kinematics. Using these constraints, we bootstrap the pentagon integrand in Section 6.4 up to five-loop order and constrain it significantly at six loops. Finally, we perform a twistor-based computation in Section 6.5 up to four loops to verify our results.

This chapter is based on the work presented in [4].

6.1. The Pentagon Correlator

We begin by introducing the pentagon function, which generalizes the octagon [70, 71] to five points. It admits two complementary definitions.

The first construction was already outlined in the previous chapter. Starting from the generating function, one performs a ten-dimensional null limit along a polygonal configuration. In this limit, the correlator factorizes into two identical copies of a polygon function (5.4). This factorization holds already at the level of the integrand.

The Lagrangian insertions are then distributed among the two polygon functions in all possible ways, as described in (5.2).

An alternative approach is to consider an n-point correlator of operators carrying large R-charge. Taking the large-charge limit, together with a suitable choice of polarization, leads to a correlator of polygon type. Since $\mathcal{N} = 4$ SYM contains six scalar fields, this construction is possible for up to six points, and in particular applies to the pentagon case. In the following, we discuss this second approach in more detail.

6.1.1. The Pentagon from the Large-Charge Limit

To define the pentagon, we consider a five-point correlation function of scalar BPS operators with general R-charge,

$$G^{2k}(x_i, y_i) \equiv \langle \mathcal{O}_{2k}(x_1, y_1)\mathcal{O}_{2k}(x_2, y_2)\mathcal{O}_{2k}(x_3, y_3)\mathcal{O}_{2k}(x_4, y_4)\mathcal{O}_{2k}(x_5, y_5)\rangle\,, \quad (6.1)$$

where

$$\mathcal{O}_k(x, y) = \frac{1}{k}\,\mathrm{tr}\,(y \cdot \phi(x))^k\,, \quad (6.2)$$

is the scalar half-BPS operator of general dimension k discussed throughout this thesis. The operators can be taken in either the single-trace or the single-particle basis. In the large-charge limit, and when polarized in a polygonal manner (as we do in the following), the choice of basis does not affect the resulting pentagon.

We aim to construct polarizations such that, in the large-charge limit, each operator contracts only with its neighbors. This produces large R-charge propagator bundles along the edges of a pentagon, effectively cutting the color surface into two halves and drastically simplifying the correlator. A similar construction allows one to recover the octagon from the large-charge four-point function [70, 71], and has also been implemented at five points [76, 77].

For our purposes, we take

$$\begin{aligned}
y_1 &= (1, i, 0, 0, 0, 0)/\sqrt{2}\,,\\
y_2 &= (1, -i, 1, -i, 0, 0)/\sqrt{2}\,,\\
y_3 &= (0, 0, 1, i, 0, 0)/\sqrt{2}\,,\\
y_4 &= (0, 0, 1, -i, 1, -i)/\sqrt{2}\,,
\end{aligned}$$

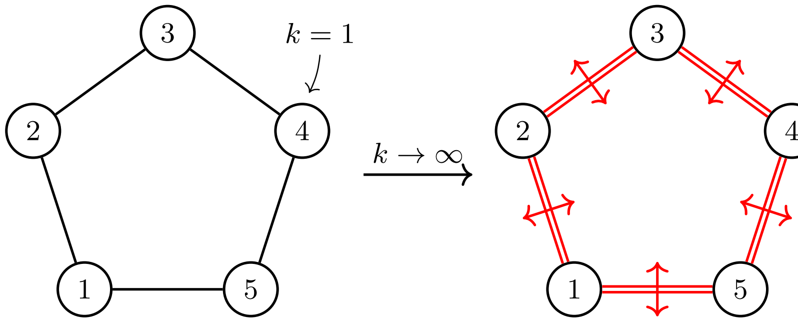

Figure 6.1.: Factorization into the pentagon in the large-charge limit. Each label i denotes an operator $\mathcal{O}_{2k}(x_i, y_i)$ with polarizations given in (6.3). On the left, for $k = 1$, each pair of adjacent operators is connected by a single propagator, and loop corrections can propagate across the perimeter. On the right, in the large-charge limit $k \to \infty$, infinitely many propagators span the perimeter, and the correlator factorizes.

$$y_5 = (1, -i, 0, 0, 1, i)/\sqrt{2}\,. \tag{6.3}$$

With this choice, polarization contractions between non-adjacent operators vanish, while adjacent ones are equal to one,

$$y_{i,i+1}^2 = y_i \cdot y_{i+1} = 1\,, \qquad y_{ij}^2 = y_i \cdot y_j = 0 \tag{6.4}$$

for i and j non-adjacent. Taking the large-charge limit then factorizes the correlator,

$$\lim_{k\to\infty} (x_{12}^2 x_{23}^2 x_{34}^2 x_{45}^2 x_{15}^2)^k \, G^{2k}(x_i, y_i) = \left(\mathbb{M}_5^{\text{empty}}\right)^2, \tag{6.5}$$

where $\mathbb{M}_5^{\text{empty}}$ denotes the empty pentagon, see Figure 6.1 for an illustration. At five points, the large propagator bundles automatically distribute evenly along the perimeter, in contrast to four and six points where derivatives with respect to polarization parameters are required to enforce this. We refer to this configuration as empty since the chosen polarization forbids any R-charge flow between non-adjacent operators by construction. To allow, for instance, a single propagator between operators 1 and 3, we modify

$$y_1 \to (1, i, \beta, -\beta i, 0, 0)/\sqrt{2}\,, \tag{6.6}$$

which yields

$$\lim_{k\to\infty}(x_{12}^2x_{23}^2x_{34}^2x_{45}^2x_{15}^2)^k\frac{\partial}{\partial\beta}G^{2k+1,2k,2k+1,2k,2k}(x_i,y_i)\Big|_{\beta=0}=\mathbb{M}_5^{\text{empty}}\times\mathbb{M}_5^{(1,0,0,0,0)}\,. \tag{6.7}$$

Here the superscript on $\mathbb{M}_5$ indicates the number of R-charge contractions between non-adjacent operators,

$$\mathbb{M}_5^{(\ell_1,\ell_2,\ell_3,\ell_4,\ell_5)}=\text{terms proportional to}\quad(y_{13}^2)^{\ell_1}(y_{14}^2)^{\ell_2}(y_{24}^2)^{\ell_3}(y_{25}^2)^{\ell_4}(y_{35}^2)^{\ell_5}\,. \tag{6.8}$$

In particular, $\mathbb{M}_5^{\text{empty}}=\mathbb{M}_5^{(0,0,0,0,0)}$. To make contact to the pentagon defined via the generating function, one must sum over all possible R-charge flows between non-adjacent operators,

$$\mathbb{M}_5=\sum_{\ell_i\geq 0}\mathbb{M}_5^{(\ell_1,\ell_2,\ell_3,\ell_4,\ell_5)}\,. \tag{6.9}$$

This object then encodes all possible R-charge flows between non-adjacent operators, and it coincides with pentagon defined via (5.4).

6.1.2. One- and Two-Loop Integrands

In Chapter 5, we constructed all polygons up to two-loop order in detail. In particular, we reviewed the integrand of the square as well as the pentagon. We reiterate the results up to two loops here in a slightly different form that already anticipates the construction of a general ℓ-loop ansatz in the next section.

The square integrand up to two loops is given by (cf. (5.14) and (5.15))

$$M_{4,1}\;=\;R_{1234}^{(4)}\,B^{[1,2,3,4;\,5]}\,, \tag{6.10}$$

$$M_{4,2}\;=\;R_{1234}^{(4)}\,\Big[X_{13}^2\,\mathcal{I}_4^{[1,3|2,4;\,5,6]}+X_{24}^2\,\mathcal{I}_4^{[2,4|1,3;\,5,6]}\Big]\,. \tag{6.11}$$

For the integrals, see (5.16) and (5.17), and we introduced the prefactor

$$R_{1234}^{(4)}=(1-d_{13}d_{24})x_{13}^2x_{24}^2\,. \tag{6.12}$$

In contrast, the pentagon integrands up to two loops are given by (cf. (5.20) and (5.21))

$$
\begin{aligned}
M_{5,1} &= \frac{R^{(5,1)}_{1234}}{X^2_{14}}\, B^{[1,2,3,4;\,6]} + (\mathrm{C}_5 \text{ perms}) \\
&= \frac{R^{(5,1)}_{1234}}{X^2_{14} R^{(4)}_{1234}}\, M_{4,1} + (\mathrm{C}_5 \text{ perms})\,,
\end{aligned}
\tag{6.13}
$$

$$
\begin{aligned}
M_{5,2} &= \frac{R^{(5,1)}_{1234}}{X^2_{14}} \left(\mathcal{I}^{[1,3|2,4;\,6,7]}_4\, X^2_{13} + \mathcal{I}^{[2,4|1,3;\,6,7]}_4\, X^2_{24} + \mathcal{I}^{[1,4|2,3|5;\,6,7]}_{5,1}\, X^2_{14}\right) \\
&\quad + R^{(5,2)}_{12345}\, \mathcal{I}^{[1,2|4,5|3;\,6,7]}_{5,2} + (\mathrm{C}_5 \text{ perms}) \\
&= \frac{R^{(5,1)}_{1234}}{X^2_{14} R^{(4)}_{1234}} M_{4,2} + R^{(5,1)}_{1234}\, \mathcal{I}^{[1,4|2,3|5;\,6,7]}_{5,1} + R^{(5,2)}_{12345}\, \mathcal{I}^{[1,2|4,5|3;\,6,7]}_{5,2} \\
&\quad + (\mathrm{C}_5 \text{ perms})\,.
\end{aligned}
\tag{6.14}
$$

Here, we have only displayed the parity-even part of the one-loop pentagon and omitted explicitly indicating this restriction. It is understood that throughout this chapter we consider only the parity-even part. In the above expressions, the prefactors are defined as

$$
R^{(5,1)}_{1234} = \frac{X^2_{14}\, p_{1234}}{2}\,, \qquad R^{(5,2)}_{12345} = \frac{X^2_{35}\, q_{12345} + X^2_{13}\, q_{54321}}{2}\,, \tag{6.15}
$$

with p and q given in (5.24) and (5.25), respectively. For the integrals appearing in the pentagon expression, see (5.23).

In the expressions for the pentagon, we inserted the square integrand of the same loop order to highlight that it is fully contained within the above expressions. Naturally, the loop variables must then be relabeled in the square from $5 \to 5 + \ell$, which is implicitly understood. We will leverage the occurrence of the square within the pentagon in the next section to build a higher-loop ansatz.

The polygon integrands are invariant under dihedral permutations of the external variables and are fully symmetric in the internal ones, i.e. they exhibit $\mathrm{D}_n \times \mathrm{S}_\ell$ symmetry. In the above expressions, we explicitly indicated that C_5 terms must be added. This is equivalent to summing over all inequivalent permutations in D_5. The integrals are already invariant under internal S_ℓ permutations as defined. In this chapter, we slightly modify this convention. The integrals will denote only a representative term, and in the final ℓ-loop pentagon expression we understand each term to be permuted over all inequivalent $\mathrm{D}_5 \times \mathrm{S}_\ell$ permutations. Each term, then, appears with the same numerical coefficient as in the canonicalized version.

6.2. The ℓ-Loop Pentagon Integrand

The explicit one- and two-loop expressions of the pentagon integrand suggest structural features that extend to general ℓ-loop order. Guided by these examples, we formulate a set of assumptions for the higher-loop cases and use them to construct a constrained ansatz for the pentagon integrand. Let us start by summarizing the structure of this ansatz and its main ingredients, before turning to a detailed discussion of its construction and implementation, which we carry out up to six loops.

We begin by presenting the ansatz in compact form. The ℓ-loop pentagon integrand is written as

$$M_{5,\ell} = \frac{R^{(5,1)}_{1234}}{X^2_{14}\, R^{(4)}_{1234}}\, M_{4,\ell} + R^{(5,1)}_{1234} \sum_{k=1}^{K_1^{(\ell)}} c^{(\ell)}_{1,k}\, h^{(\ell)}_{1,k}(X^2_{ij})\, \mathcal{I}^{(\ell)}_{1,k} + R^{(5,2)}_{12345} \sum_{k=1}^{K_2^{(\ell)}} c^{(\ell)}_{2,k}\, h^{(\ell)}_{2,k}(X^2_{ij})\, \mathcal{I}^{(\ell)}_{2,k}\,. \tag{6.16}$$

Let us comment on the various elements entering this expression. First, each term is implicitly summed over all inequivalent permutations of the group $\mathrm{D}_5 \times \mathrm{S}_\ell$, reflecting the dihedral symmetry of the external points and the symmetric symmetry of the integration points.. In particular, this applies to every term appearing in both sums. For the term proportional to $M_{4,\ell}$, the dihedral symmetry effectively reduces to a sum over cyclic permutations C_5. Second, the functions $\mathcal{I}^{(\ell)}_{m,k}$ denote ℓ-loop dual-conformal integrals admitting a planar embedding within the pentagon topology. Third, the functions $h^{(\ell)}_{m,k}$ are monomials in ten-dimensional distances of the form

$$h^{(\ell)}_{m,k}(X^2_{ij}) = (X^2_{13})^{\alpha_1}(X^2_{14})^{\alpha_2}(X^2_{24})^{\alpha_3}(X^2_{25})^{\alpha_4}(X^2_{35})^{\alpha_5} \qquad \text{for some} \qquad \alpha_i \geq 0\,. \tag{6.17}$$

Thus, the $h^{(\ell)}_{m,k}$ encode ten-dimensional structures built from these distances that dress the integrals $\mathcal{I}^{(\ell)}_{m,k}$. Finally, the sums run over all combinations of $h^{(\ell)}_{m,k}$ and $\mathcal{I}^{(\ell)}_{m,k}$ that are invariant under $\mathrm{D}_5 \times \mathrm{S}_\ell$ permutations and satisfy the homogeneity condition

$$R^{(5,m)}\, h^{(\ell)}_{m,k}\, \mathcal{I}^{(\ell)}_{m,k}\Big|_{x^2_{ij} \to t_i t_j x^2_{ij}} = \left(\prod_{i=6}^{5+\ell} t_i^{-4}\right) R^{(5,m)}\, h^{(\ell)}_{m,k}\, \mathcal{I}^{(\ell)}_{m,k}\,. \tag{6.18}$$

This requirement ensures that the conformal weight in the four-dimensional variables x_i is equal to 4 at each integration point and vanishes at the external points. Eventually, this fixes the numbers $K^{(\ell)}_m$ of terms possibly appearing in both sums.

The coefficients $c_{m,k}^{(\ell)}$ are numerical constants that are not fixed by the structural assumptions entering the ansatz and are left undetermined for the time being.

6.2.1. Ansatz Construction

Square contribution. The first observation concerns the contribution of the pentagon that is directly inherited from the corresponding square at ℓ-loop order. All polygons feature a factorization property that arises when a taking a ten-dimensional null limit between two non-adjacent points. The polygon then decomposes into two lower-point polygons (5.5). For the pentagon this implies that

$$\lim_{X_{14}^2 \to 0} \frac{X_{14}^2}{x_{14}^2} M_{5,\ell} \; = \; M_{4,\ell} \, . \tag{6.19}$$

The ansatz (6.16) satisfies this limit by construction. The square appears explicitly in the first term, but multiplied by the factor $R_{1234}^{(5,1)}$ and a pole in a ten-dimensional distance. When taking the null limit only this first time survives, while the sums vanish as they do not contain a pole in X_{14}^2. However, this contribution not only includes the factorization property of the pentagon but also makes further assumptions of several terms within the ansatz.

Integrands with disc topology. The basis of the ansatz at ℓ-loop order consists of planar ℓ-loop integrands $\mathcal{I}_{m,k}^{(\ell)}$ that can be embedded within a disc bounded by the edges of the pentagon. This assumption is not only motivated by the explicit expressions of the pentagon up to two-loop order, but is also supported by the expectation that such a property holds more generally, given that the computation is performed in the planar limit of $\mathcal{N} = 4$ SYM. In the planar theory, the pentagon can in principal be derived by a perturbative Feynman computation, in which each contributing graph exhibits a planar structure. We assume that this still holds term by term after resumming the Feynman graphs to the conformal graphs given by the integrands.

In order to obtain a complete list of canonicalized integrands with disc topology, we start by constructing all planar four- and five-point graphs that are embedded within the pentagon and contain ℓ internal vertices each of which has a valency of at least four[1]. The edges of these graphs correspond to the denominator of the

[1] We omit planar three-point graphs since they are not able to fulfill the homogeneity condition (6.18) although they admit a planar embedding inside the pentagon.

integrand when identifying edges connecting vertices i and j to squared distances x_{ij}^2. If the graph includes internal vertices that are of valency greater or equal five, we add factors in the numerator such that the conformal weight of each internal points is exactly four. In this process, the numerator factor is chosen such that it does not remove any factors in the denominator or introduce a negative conformal weight to any of the external operators. For example, this assignment from graph to integrand looks as follows in the four-loop case

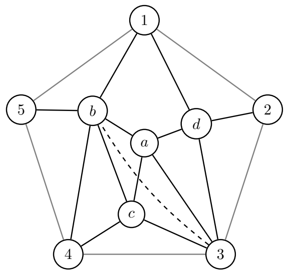

$$\mathcal{I}_{\text{ex}}^{(4)} = \frac{x_{3b}^2}{x_{1b}^2 x_{1d}^2 x_{2d}^2 x_{3a}^2 x_{3c}^2 x_{3d}^2 x_{4b}^2 x_{4c}^2 x_{5b}^2 x_{ab}^2 x_{ac}^2 x_{ad}^2 x_{bc}^2}\,, \tag{6.20}$$

where the dashed line corresponds to the numerator factor.

In practice, we generate the relevant graphs starting from a seed output produced by `plantri` [132], which is able to enumerate non-isomorphic triangulations of planar graphs. As a starting point, we consider all triangulations of a graph with disc topology. Concretely, we construct triangulations of a disc with four and five boundary edges and ℓ internal vertices. The program further allows us to exclude chords, i.e edges connecting non-adjacent boundary vertices, as well as vertices of degree two. Imposing these restrictions removes lower-point integral topologies at the outset. For discs with four and five boundary edges, the numbers of non-isomorphic triangulations up to six internal vertices are

$$\{1,\, 2,\, 8,\, 38,\, 219,\, 1\,404\} \qquad \text{and} \qquad \{1,\, 2,\, 12,\, 73,\, 503,\, 3\,661\},$$

respectively. These sequences coincide with the first entries of OEIS A058786 and A342054. Starting from these triangulations, we systematically generate more general graphs by successively removing edges, subject to the constraint that all internal vertices retain valency greater than or equal to four. Collecting all graphs obtained in this way yields the complete set of admissible denominator topologies. These are then dressed with the allowed numerator factors, as described above, resulting in the full set of integrands with disc topology. Combining the four- and five-point cases provides the complete list of such integrals.

loop-order ℓ	1	2	3	4	5	6
# disc topology integrals	1	3	18	182	2 868	55 517
# different integrals	–	2	10	66	656	8 766
# terms in first sum $K_1^{(\ell)}$	–	1	6	41	413	5 471
# terms in second sum $K_2^{(\ell)}$	–	1	5	41	447	6 184
# prefactor relations	–	–	–	5	65	945
# total coefficients	–	2	11	77	795	10 710

Table 6.1.: Five-point integrands up to five-loop order relevant for the ansatz construction of the pentagon [4]. First row: Total number of integrands with disc topology. Second and third row: Number of terms in the ansatz appearing with $R^{(5,1)}$ and $R^{(5,2)}$, respectively. Fourth row: Number of different integrands appearing in the ansatz.

The total number of integrands with disc topology that are inequivalent under permutations of $\mathrm{D}_5 \times \mathrm{S}_\ell$ is given in the first row of Table 6.1.

Distribution into the sums. After having obtained all possible four- and five-point dual-conformal integrals admitting a planar embedding in the pentagon, we need to specify how they distribute into the sums that multiply the factors $R^{(5,1)}_{1234}$ and $R^{(5,2)}_{12345}$ in (6.16). In general, the pentagon is conformally invariant in the variables x_i for $i = 1, \ldots, 5$, when treated as a function of independent variables x^2_{ij} and d_{ij}. This property is directly inherited from the generating function $G_{n,\ell}$, which is itself conformal in the variables x^2_{ij} when expressed as a function of d_{ij} and x^2_{ij} (see the discussion in Section 5.4.3).

For this to be realized in the ansatz, the integrands need to be dressed by factors x^2_{ij} such that each external point is of conformal weight zero. Following the structure of the ansatz (6.16), these factors are introduced both in the factors $R^{(5,m)}$ and in the functions $h^{(\ell)}_{m,k}$ of ten-dimensional distances $X^2_{ij} = x^2_{ij}(1 - d_{ij})$. Combing these functions with the integrals $\mathcal{I}^{(\ell)}_{m,k}$, we require this combination to satisfy the homogeneity condition (6.18), which yields all admissible integrals that may appear in the ansatz. In practice, we permute all integrands with disc topology over the dihedral group D_5, multiply them by either $R^{(5,1)}_{1234}$ or $R^{(5,2)}_{12345}$, and add factors X^2_{ij} in all different ways under D_5 such that the conformal weight of the external points become zero.

We find that this is not possible to achieve for a large part of the integrals such that they do not appear in the ansatz. Also, more often than less there is only a unique combination of prefactor, ten-dimensional distances and conformal integral that is allowed to appear. We list the number of the total amount of different integrals appearing in the ansatz up to six-loop order in Tab. 6.1. There, we also list the numbers of integrals appearing in both sums $K^{(\ell)}_{m,k}$. The sum of both these numbers is typically larger than the number of overall different integrals, since the same integral may appear in both sums multiple times starting from three loops.

We illustrate this procedure with the four-loop integrand given in the previous example (6.20). The integrand is of conformal weight $\{2,1,2,2,1\}$ in the points $x_1,\ldots,x_5$, whereas the factors $R^{(5,1)}_{1234}$ and $R^{(5,2)}_{12345}$ are of conformal weight $\{-2,-1,-1,-2,0\}$ and $\{-1,-1,-2,-1,-1\}$, respectively. Introducing ten-dimensional distances X^2_{ij}, there are four permutationally invariant ways to saturate the weights of the integral yielding the following contribution to the ansatz of $M_{5,\ell}$

$$\Big(c^{(4)}_{1,1}\,X^2_{35}\,R^{(5,1)}_{1234}+c^{(4)}_{1,2}\,X^2_{24}\,R^{(5,1)}_{1543}+c^{(4)}_{2,1}\,X^2_{14}\,R^{(5,2)}_{12345}+c^{(4)}_{2,2}\,X^2_{13}\,R^{(5,2)}_{15432}\Big)\,\mathcal{I}^{(4)}_{\text{ex}}\,, \tag{6.21}$$

where $c^{(4)}_{1,1}$, $c^{(4)}_{1,2}$, $c^{(4)}_{2,1}$, $c^{(4)}_{2,2}$ are a priori undetermined coefficients.

Prefactor relation. So far, the ansatz consists of all four- and five-point dual-conformal integrals with disc topology that allow to be multiplied by either one of the two factors $R^{5,m}$ and ten-dimensional squared distances X^2_{ij} such that the homogeneity condition (6.18) is satisfied. This yields a preliminary ansatz consisting of the two sums in (6.16) of sizes $K^{(\ell)}_1$ and $K^{(\ell)}_2$ which we list up to six-loop order in Table 6.1.

As it turns out, the description of the ansatz in terms of a decomposition into the two sums is not unique due to the existence of an identity relating both prefactors

$$X^2_{35}\,R^{(5,1)}_{1234}-X^2_{24}\,R^{(5,1)}_{1543}-X^2_{14}\,R^{(5,2)}_{12345}+X^2_{13}\,R^{(5,2)}_{15432}=0\,. \tag{6.22}$$

This identity starts to appear as a prefactor in front of some integrands starting from four-loop order. We use it in order to reduce the number of coefficients by simply removing some terms within the ansatz such that the remaining coefficients posses a unique solution. We list the number of relations appearing in each ℓ-loop order ansatz in Tab. 6.1.

Incidentally, we can also use this identity to remove a contribution from the previous four-loop example (6.21). By choosing, for example,

$$c^{(4)}_{2,2} = 0\,, \tag{6.23}$$

the solution for the remaining three coefficients becomes unique without imposing any actual constraints. In practice, we will use this relation to remove terms in the second sum multiplied by $R^{(5,2)}_{12345}$ in the four-, five- and six-loop ansatz.

6.2.2. Application up to Three Loops

As a first test of the described method of constructing the pentagon integrand, we consider its construction at one- and two-loop order to reproduce the known expressions.

At one loop there is only one conformal integral that exhibits a planar embedding in the pentagon which is the one-loop four-point box integral. It is not possible to multiply this integral to one of the factors $R^{(5,m)}$ such that the homogeneity condition (6.18) is satisfied. Thus, the sums in the ansatz run effectively over zero terms and the pentagon is given by

$$M_{5,1} = \frac{R^{(5,1)}_{1234}}{X^2_{14}\, R^{(4)}_{1234}}\, M_{4,1}\,. \tag{6.24}$$

which precisely matches the result (6.13).

At two loops, we find the construction to yield an ansatz that depends on two unknown coefficients each attached to one of the prefactors

$$M_{5,2} = \frac{R^{(5,1)}_{1234}}{X^2_{14}\, R^{(4)}_{1234}}\, M_{4,2} + R^{(5,1)}_{1234}\, c^{(2)}_{1,1}\, \mathcal{I}^{(2)}_{1,1} + R^{(5,2)}_{12345}\, c^{(2)}_{2,1}\, \mathcal{I}^{(2)}_{2,1}\,. \tag{6.25}$$

Note that functions $h^{(2)}_{m,1}(X^2_{ij}) = 1$, since both terms satisfy the homogeneity condition without introducing any ten-dimensional distances. We relabeled the integrals compared to (6.14) by $\mathcal{I}_{5,1} \to \mathcal{I}_{1,1}$ and $\mathcal{I}_{5,2} \to \mathcal{I}_{2,1}$ as to make it consistent with the integral labeling in the ansatz (6.16). Again, this expression precisely matches the two-loop pentagon (6.14), if one sets

$$c^{(2)}_{1,1} = 1 \quad \text{and} \quad c^{(2)}_{2,1} = 1\,. \tag{6.26}$$

In the next section, we will see how to recover these coefficients via soft-collinear constraints.

Finally, let us present the expression for the ansatz of the pentagon integrand at three loops, when constructed by applying the method described in this section

$$\begin{aligned}
M_{5,3} = &\frac{R^{(5,1)}_{1234}}{X^2_{14}}\, M_{4,3} \\
&+ R^{(5,1)}_{1234}\Big(c^{(3)}_{1,1}\,\mathcal{I}^{(3)}_1 + c^{(3)}_{1,2}\,\mathcal{I}^{(3)}_2 + c^{(3)}_{1,3}\,X^2_{13}\,\mathcal{I}^{(3)}_3 \\
&\qquad + c^{(3)}_{1,4}\,X^2_{35}\mathcal{I}^{(3)}_4 + c^{(3)}_{1,5}\,X^2_{14}\,\mathcal{I}^{(3)}_5 + c^{(3)}_{1,6}\,\mathcal{I}^{(3)}_6\Big) \\
&+ R^{(5,2)}_{12345}\Big(c^{(3)}_{2,1}\,\mathcal{I}^{(3)}_7 + c^{(3)}_{2,2}\,\mathcal{I}^{(3)}_8 + c^{(3)}_{2,3}\,X^2_{13}\,\mathcal{I}^{(3)}_9 \\
&\qquad + c^{(3)}_{2,4}\,X^2_{14}\,\mathcal{I}^{(3)}_4 + c^{(3)}_{2,5}\,\mathcal{I}^{(3)}_{10}\Big)\,,
\end{aligned} \tag{6.27}$$

where the integrals are given by

$$\begin{aligned}
\mathcal{I}^{(3)}_1 &= \frac{1}{x^2_{17}x^2_{18}x^2_{28}x^2_{36}x^2_{46}x^2_{47}x^2_{67}x^2_{68}x^2_{78}}\,,\\
\mathcal{I}^{(3)}_2 &= \frac{(x^2_{56})^2}{x^2_{16}x^2_{18}x^2_{26}x^2_{36}x^2_{46}x^2_{47}x^2_{57}x^2_{58}x^2_{67}x^2_{68}x^2_{78}}\,,\\
\mathcal{I}^{(3)}_3 &= \frac{x^2_{56}}{x^2_{16}x^2_{17}x^2_{18}x^2_{27}x^2_{36}x^2_{37}x^2_{46}x^2_{48}x^2_{58}x^2_{67}x^2_{68}}\,,\\
\mathcal{I}^{(3)}_4 &= \frac{1}{x^2_{17}x^2_{18}x^2_{28}x^2_{36}x^2_{38}x^2_{46}x^2_{47}x^2_{57}x^2_{67}x^2_{68}}\,,\\
\mathcal{I}^{(3)}_5 &= \frac{x^2_{57}}{x^2_{16}x^2_{17}x^2_{18}x^2_{27}x^2_{37}x^2_{46}x^2_{47}x^2_{48}x^2_{58}x^2_{67}x^2_{68}}\,,\\
\mathcal{I}^{(3)}_6 &= \frac{x^2_{27}x^2_{56}}{x^2_{17}x^2_{18}x^2_{26}x^2_{28}x^2_{36}x^2_{46}x^2_{47}x^2_{57}x^2_{67}x^2_{68}x^2_{78}}\,,\\
\mathcal{I}^{(3)}_7 &= \frac{x^2_{26}}{x^2_{17}x^2_{27}x^2_{28}x^2_{36}x^2_{38}x^2_{46}x^2_{56}x^2_{67}x^2_{68}x^2_{78}}\,,\\
\mathcal{I}^{(3)}_8 &= \frac{1}{x^2_{16}x^2_{27}x^2_{37}x^2_{38}x^2_{48}x^2_{56}x^2_{67}x^2_{68}x^2_{78}}\,,\\
\mathcal{I}^{(3)}_9 &= \frac{1}{x^2_{16}x^2_{18}x^2_{28}x^2_{36}x^2_{37}x^2_{38}x^2_{47}x^2_{57}x^2_{67}x^2_{68}}\,,\\
\mathcal{I}^{(3)}_{10} &= \frac{x^2_{17}x^2_{56}}{x^2_{16}x^2_{18}x^2_{26}x^2_{36}x^2_{37}x^2_{47}x^2_{57}x^2_{58}x^2_{67}x^2_{68}x^2_{78}}\,.
\end{aligned} \tag{6.28}$$

In the above expression, we have refrained from assigning labels to the integrals based on the specific sum in which they appear. Rather, we enumerate them in a uniform manner to make explicit that one integral, $\mathcal{I}_4^{(\ell)}$, occurs in both sums. We thus find that the pentagon integrand can be expressed in terms of a remarkably compact ansatz depending on only 11 coefficients. In the next section, we will formulate a set of constraints that allow us to determine these coefficients within a bootstrap procedure.

In Table 6.1, we also listed the sizes of the ansätze for the pentagon integrand at four, five, and six loops. The explicit expressions will be made available with the submission of [4].

6.3. Soft and Collinear Constraints

In order to constrain the integrand, we formulate limits of the external and internal variables under which the integrand exhibits controlled behavior. For massless amplitudes, bootstrapping multi-loop integrands has proven particularly successful by exploiting the *collinear* and *soft* constraints, which relate the n-point ℓ-loop integrand to its lower-loop and lower-point counterparts, respectively [55, 130, 131]. In the section, we formulate the soft and collinear constraints such that they can be applied also for amplitudes with off-shell external momenta.

We begin by defining the empty polygon through the limit in which all internal propagators are set to zero,

$$M_{n,\ell}^{\text{empty}} = M_{n,\ell}\big|_{d_{ij}^2\to 0} \,. \tag{6.29}$$

The empty polygon can be expressed purely in terms of dual momentum variables x_i (with n external and ℓ internal points), that are still subject to the constraints $x_{i,i+1}^2 = y_{i,i+1}^2$ on the external variables. Introducing momentum variables $p_i = x_i - x_{i-1}$, we see that all momenta are off-shell for the moment ($p_i^2 \neq 0$). Upon imposing the on-shell conditions ($p_i^2 \to 0$), the empty polygon reduces to the corresponding massless amplitude integrand.

For a more convenient implementation of the constraints, it is useful to introduce twistor variables [133], which provide an equivalent parametrization of the empty polygon. Since the momenta are off-shell, each point x_i is described by a pair of momentum twistors $\{Z_{2i-1}, Z_{2i}\}$, resulting in a total of $2(n+\ell)$ twistors specifying the kinematics of the empty polygon. We denote the sets of twistors as

$$\text{external:} \quad \{Z_1, Z_2, \ldots, Z_{2n}\}\,,$$

$$\text{internal:} \quad \{Z_{2n+1},\, Z_{2n+2},\, \ldots,\, Z_{2(n+\ell)-1},\, Z_{2(n+\ell)}\}\,. \tag{6.30}$$

In terms of momentum twistors, the spacetime distances take the form

$$x_{ij}^2 = \frac{\langle Z_{2i-1}Z_{2i}Z_{2j-1}Z_{2j}\rangle}{\langle Z_{2i-1}Z_{2i}\rangle\langle Z_{2j-1}Z_{2j}\rangle} \propto \langle Z_{2i-1}Z_{2i}Z_{2j-1}Z_{2j}\rangle\,, \tag{6.31}$$

where the four-bracket denotes the determinant of the four twistors. Since the distances enter only through the dual-conformal integrand, the two-brackets in the denominator can be omitted, as they cancel term by term in the integrand.[2] The main advantage of introducing momentum twistors is that imposing light-like separation of two spacetime points becomes particularly simple. For example, setting $x_{ij}^2 = 0$ amounts to identifying one twistor from each of the pairs describing the points x_i and x_j, e.g. $Z_{2i} \propto Z_{2j-1}$. In this case, the four-bracket in (6.31) vanishes, since two of its arguments become linearly dependent, and hence the determinant is zero.

Soft limit. It is well known that massless amplitude integrands exhibit very simple behavior under the soft limit [134]. In particular, setting one of the external momenta to zero reduces the n-point integrand to the corresponding $(n-1)$-point integrand.

For the massive amplitude (empty polygon), we find that the soft limit can be implemented in a closely analogous manner. One of the off-shell momenta is set to zero, which corresponds to identifying two adjacent points while simultaneously putting one of the neighboring momenta on-shell,

$$x_n \to x_{n-1} \qquad \text{and} \qquad x_{1,n-1}^2 \to 0\,. \tag{6.32}$$

Here we choose $p_n = 0$ and $p_1^2 = 0$, although equivalently one could impose $p_{n-1}^2 = 0$ instead.

In the language of momentum twistors, this limit is realized as

$$Z_{2n-1} \to Z_{2n-2}\,, \qquad Z_{2n} \to Z_1\,, \qquad \text{and} \qquad Z_{2n-2} \to \alpha Z_{2n-3} + \beta Z_1\,, \tag{6.33}$$

[2] As already discussed, the spacetime distance can be computed via twistors as given in (3.35). For twistors that are not chosen with a specific parametrization, the four-bracket is normalized by two two-brackets. These are defined as $\langle Z_1 Z_2\rangle = \epsilon_{\alpha\beta}\lambda_1^\alpha\lambda_2^\beta$, where each twistor is decomposed into two spinors as $Z_i = (\lambda_i^\alpha, \mu_{i,\dot\alpha})$.

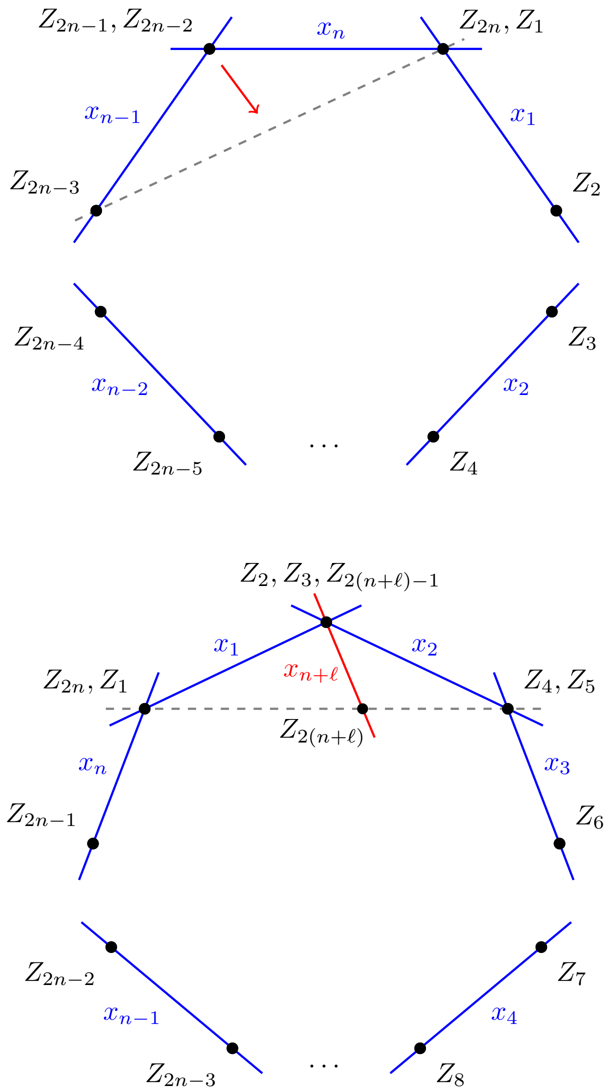

Figure 6.2.: Depiction of the twistor variables in the soft (top) and collinear (bottom) limits [4]. In the soft limit, two adjacent segments of the polygon are made light-like by identifying $Z_{2n-1} = Z_{2n-2}$ and $Z_{2n} = Z_1$. In addition, the momentum $p_n = x_n - x_{n-1}$ is set to zero by constraining the twistor Z_{2n-1} to lie on the hyperplane spanned by $\{Z_1, Z_{2n-3}\}$ (indicated by the dashed gray line). In the collinear limit, three adjacent edges are taken to be light-like by setting $Z_{2n} = Z_1$, $Z_2 = Z_3$, and $Z_4 = Z_5$. The internal point is then taken to lie on the middle light-like segment by identifying one of its twistor variables with Z_3 and constraining the other to lie on the hyperplane spanned by $\{Z_1, Z_5\}$ (again indicated by the dashed gray line).

where the condition $p_n = 0$ is equivalent to identifying $Z_{2n-1} = Z_{2n-2}$ and constraining this twistor to lie on the hyperplane spanned by $\{Z_{2n-3}, Z_{2n}\}$ (see Figure 6.2). Importantly, all momenta not involved in this limit can be kept off-shell. As a consequence, this constraint probes a more terms in the integrand compared to the conventional soft limit of the massless amplitude.

Under this limit, we find that the n-point integrand reduces to the $(n-1)$-point integrand at every loop order,

$$\lim_{(6.33)} \left[M_{n,\ell}^{\text{empty}} - M_{n-1,\ell}^{\text{empty}} \right] \longrightarrow 0 \,. \tag{6.34}$$

We emphasize that we do not have a general proof of this relation. However, we have verified that it holds for all integrands up to two loops, computed in Section 5.4. In the next section, we will see how this limit strongly constrains our ansatz for constructing higher-loop pentagon integrands.

Collinear limit. In the massless case, this constraint is based on the observation that the logarithm of the amplitude exhibits a softer divergence than naively expected, when one of the internal momenta becomes collinear with an external one. To adapt this limit to the polygon integrands, we define its logarithm as $\mathbb{L}_n \equiv \log \mathbb{M}_n$, which in turn admits the following perturbative expansion

$$\mathbb{L}_n = \sum_{\ell=1}^{\infty} \frac{(-a)^\ell}{\ell!} \int \left[\prod_{k=1}^{\ell} \frac{d^4 x_{n+k}}{4\pi^2} \right] L_{n,\ell} \,, \tag{6.35}$$

where the logarithm integrand $L_{n,\ell}$ is given by a sum of the polygon integrand $M_{n,\ell}$ together with products of its lower-loop counterparts.

In terms of dual momentum variables, the collinear limit is realized when one of the internal points approaches a light-like separated segment of an external edge, for instance x_{12}^2. We find that this constraint persists for the massive amplitude provided that not only x_{12}^2 becomes light-like, but also the two adjacent segments x_{n1}^2 and x_{23}^2,

$$x_{n1}^2,\, x_{12}^2,\, x_{23}^2 \to 0 \,, \qquad \text{and} \qquad x_{1,n+\ell}^2,\, x_{2,n+\ell}^2 \to \mathcal{O}(\epsilon) \,. \tag{6.36}$$

Using momentum twistor variables, this limit is easily implemented by identifying three pairs of twistors such that three adjacent edges become light-like separated. Subsequently, one of the internal variables is taken to approach the middle light-like segment by letting one of its twistors approach Z_3 and constraining the other to lie on the hyperplane spanned by $\{Z_1, Z_5\}$ (see Figure 6.2),

$$\begin{aligned} &Z_{2n} \to Z_1\,, \qquad Z_2 \to Z_3\,, \qquad Z_4 \to Z_5\,, \\ &\text{and} \qquad Z_{2(n+\ell)-1} \to Z_3 + \mathcal{O}(\epsilon)\,, \qquad Z_{2(n+\ell)} \to \alpha Z_1 + \beta Z_5\,. \end{aligned} \tag{6.37}$$

Analogously to the massless case, the logarithmic integrand in this limit produces only a $1/\epsilon$ divergence, rather than the naively expected $\mathcal{O}(1/\epsilon^2)$ behavior. This imposes a constraint on the integrand, which can be written as

$$\lim_{(6.37)} \left[x_{1,n+\ell}^2\, x_{2,n+\ell}^2\, L_{n,\ell}^{\text{empty}}\right] \longrightarrow 0 + \mathcal{O}(\epsilon)\,, \tag{6.38}$$

where $L_{n,\ell}^{\text{empty}}$ is defined by setting all internal propagators to zero, analogously to (6.29).

In [131], it was argued that this constraint can equivalently be formulated directly in terms of the massless amplitude integrand, thereby avoiding the explicit expansion of the logarithm. While conceptually equivalent, this formulation is computationally more convenient for multi-loop applications, since it avoids the products of lower-loop integrands that arise in the perturbative expansion of the logarithm. We find that this adaptation extends straightforwardly to the massive case. The collinear constraint can therefore be written equivalently[3]

$$\lim_{(6.37)} \left[x_{1,n+\ell}^2\, x_{2,n+\ell}^2\, M_{n,\ell}^{\text{empty}} + \frac{1}{\alpha\beta}\, M_{n,\ell-1}^{\text{empty}}\right] \longrightarrow 0 + \mathcal{O}(\epsilon)\,. \tag{6.39}$$

Again, we emphasize that this constraint is supported only by empirical evidence. We have verified that it holds for all available one- and two-loop data, computed in Section 5.4. In fact, even in the massless case the corresponding statement has not been proven rigorously, but it has been extensively tested and successfully employed to determine the four-point integrand up to eight loops [55, 130], and higher-point integrands at two and three loops [131].

[3]The difference by a factor of $1/\ell$ compared to eq. (2.12) in [131] is due to a difference in conventions: our definition of the loop integrands differs by an overall factor of $(\ell!)$.

6.4. Bootstrapping the Pentagon Integrand

In this section, we apply the soft and collinear constraints to the pentagon integrand ansatz constructed in Section 6.2. Before presenting in detail how these constraints fix the integrand up to five-loop order and discussing their solutions, we first analyze the constraints that arise from taking massless limits of the pentagon.

6.4.1. Constraints from Massless Amplitudes

In the following, we consider the limit of the pentagon in which it reduces to its five-point massless MHV amplitude counterpart. As discussed in Section 5.1, there exists a well-established duality in $\mathcal{N} = 4$ SYM that relates the four-dimensional null-polygon limit, $x^2_{i,i+1} \to 0$, of the n-point correlation function of $\mathbf{20'}$ operators to the n-point massless MHV gluon scattering amplitude [30, 36–38, 80, 101–103]. The ten-dimensional null polygonal limit of the generating function under which the polygons are defined mimics this duality. Since the correlator of $\mathbf{20'}$ operators is the leading term of the generating function when setting $y^2_{ij} \to 0$, the polygons similarly reduce to the massless MHV amplitudes in this limit, see Figure 5.4. For convenience, let us spell out this relation again

$$M_{n,\ell} \to \mathcal{A}_{n,\ell}/\mathcal{A}_{n,0} \qquad \text{for} \qquad x^2_{i,i+1} \to 0,\ i = 1, \ldots, n \quad \text{and} \quad d_{ij} \to 0\ \forall\, i, j\,, \tag{6.40}$$

Here, $\mathcal{A}_{n,\ell}$ is the ℓ-loop massless MHV amplitude integrand, and $\mathcal{A}_{n,0}$ its tree-level expression.

Since the parity-even integrands of the five-point MHV amplitude have been computed explicitly up to six-loop order [54] using the supersymmetric extension of the correlator/amplitude duality [80,103], we can, in principle, exploit the limit (6.40) to fix the coefficients in the ansatz for the pentagon integrand. In terms of the ansatz construction, we observe the following behavior of the invariants in this limit

$$R^{(1)}_{1234} \to x^2_{13}x^2_{24}x^2_{14} \quad \text{and} \quad R^{(2)}_{12345} \to 0\,. \tag{6.41}$$

By matching the pentagon ansatz to the corresponding MHV amplitude, we obtain constraints on the coefficients of those integrals that are multiplied by the first prefactor, but not on those associated with the second. Consequently, the limit (6.40) constrains at most half of the ansatz.

As it turns out, the collinear constraints are sufficiently powerful to determine all coefficients multiplying $R^{(5,1)}$ (at least up to six loops). For this reason, we refrain from using the massless amplitude to constrain the ansatz. Nevertheless, after deriving the pentagon integrand up to five-loop order and obtaining the partially constrained result at six loops, we employed the results of [54] to test our expressions under the limit (6.40). We find complete agreement.

6.4.2. Soft and Collinear Constraints

With the ansätze of the pentagon integrand constructed up to six loops, the implementation of the soft and collinear constraints becomes straightforward. To impose the soft limit, we make use of the known expressions for the square integrand, which is already embedded in the pentagon ansatz, and evaluate (6.34) in the kinematics (6.33). Repeating this procedure as many times as there are unfixed coefficients yields a numerical linear system, which can then be solved to determine the coefficients. Similarly, the collinear constraint can be implemented loop order by loop order by numerically evaluating (6.38) in the kinematics specified in (6.37).

A natural practical question is which of the two limits provides stronger constraints. This can be understood by examining the behavior of the prefactors $R^{(5,1)}$ and $R^{(5,2)}$ under the respective limits. In the soft limit, we find

$$R^{(5,1)}_{5123} \;\to\; \frac{x_{34}^2}{2}\left(x_{13}^2 x_{24}^2 - x_{12}^2 x_{34}^2\right), \qquad R^{(5,2)}_{12345} \;\to\; -\frac{x_{34}^2}{2}\left(x_{13}^2 x_{24}^2 - x_{12}^2 x_{34}^2\right), \tag{6.42}$$

while all other cyclic permutations vanish. Thus only a small subset of the ansatz survives, and moreover the two sums collapse into one, since the prefactors coincide up to a sign. In practice, the soft limit therefore imposes only linear relations among the coefficients rather than fixing them completely. For instance, already at two loops it merely implies

$$c^{(2)}_{1,1} = c^{(2)}_{2,1}\,, \tag{6.43}$$

and this pattern persists at higher loop orders: the soft constraint restricts the ansatz but does not fully determine it.

The collinear constraint, on the other hand, proves to be significantly more powerful. All cyclic permutations of $R^{(5,1)}$ remain non-vanishing, as well as three out of the five permutations of $R^{(5,2)}$. Consequently, a much larger portion of the ansatz is probed in this limit. Up to four loops, the collinear constraint uniquely determines all coefficients. In particular, it reproduces the two-loop coefficients given in (6.26). At three loops we obtain

$$
\begin{aligned}
&c_{1,1}^{(3)} = -1\,, && c_{1,2}^{(3)} = 1\,, && c_{1,3}^{(3)} = 1\,, && c_{1,4}^{(3)} = -\tfrac{1}{2}\,,\\
&c_{1,5}^{(3)} = 1\,, && c_{1,6}^{(3)} = 1\,, && c_{2,1}^{(3)} = 1\,, && c_{2,2}^{(3)} = -1\,,\\
&c_{2,3}^{(3)} = 1\,, && c_{2,4}^{(3)} = \tfrac{1}{2}\,, && c_{2,5}^{(3)} = 1\,. &&
\end{aligned}
\tag{6.44}
$$

Together with (6.27), this yields the complete three-loop pentagon integrand. At four loops, the collinear constraint fixes all 77 coefficients of the ansatz.

At five loops, the collinear constraint determines all but one of the 795 coefficients. The remaining undetermined parameter multiplies an integral associated with $R_{12345}^{(5,2)}$, namely

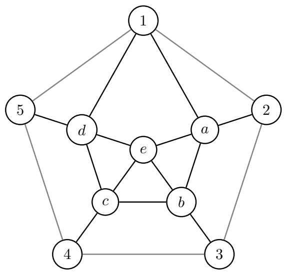

$$
\mathcal{I}^{(5)}_{\text{non-div.}} = \frac{1}{x_{1a}^2 x_{1d}^2 x_{2a}^2 x_{3b}^2 x_{4c}^2 x_{5d}^2 x_{ab}^2 x_{bc}^2 x_{cd}^2 x_{ae}^2 x_{be}^2 x_{ce}^2 x_{de}^2}\,,
\tag{6.45}
$$

which does not develop a divergence in the collinear limit. Imposing the soft constraint in addition fixes the coefficient of this integral to zero, thereby uniquely determining the full five-loop pentagon integrand.

Finally, at six loops, the collinear constraints reduce the original ansatz of 10 710 terms to a 39-parameter family. Imposing the soft constraints further reduces this to a 23-parameter solution, leaving only these coefficients undetermined.

The explicit expressions for all pentagon integrands up to six loops will be made available together with the submission [4].

6.4.3. Statistics of the Coefficients

Let us conclude this section by discussing the structure of the pentagon integrand up to five loops. As described above, the collinear and soft constraints uniquely fixes all coefficients appearing in the respective ansätze up to this loop order. In Table 6.2, we summarize how often each numerical value occurs.

Integer coefficients. As can be seen from Table 6.2, the vast majority of non-vanishing coefficients are either $+1$ or -1. This pattern can be partially understood from the behavior in the massless limit discussed in Section 6.4.1. In that limit, the pentagon integrand reduces to the massless MHV amplitude by setting the internal propagators d_{ij} to zero and taking the four-dimensional polygonal null limit on the external operators, $x_{i,i+1}^2 \to 0$. As emphasized earlier, only the part of the pentagon integrand proportional to the first prefactor $R^{(5,1)}$ survives in this limit. Therefore, however, most of the coefficients entering this part of the ansatz can be inferred from the corresponding MHV amplitude.
One way to construct five-point massless MHV amplitudes is via the supercorrelator/superamplitude duality [80, 103]. According to this duality, the ℓ-loop five-point amplitude can be obtained from the $(\ell+1)$-loop four-point correlator of $\mathbf{20}'$ operators. When expanded in conformal integrals, the numerical coefficients of the amplitude are thus inherited from those of the four-point correlator. The latter has been computed up to twelve loops [41, 53–58], so we can readily read off the corresponding coefficients in the expressions (see, for instance, Table II of [58]). This allows us to anticipate the coefficients appearing in the first sum of the pentagon integrand, i.e. the part proportional to $R^{(5,1)}$.

- Up to three loops, all coefficients multiplying conformal integrals in the four-point correlator are equal to 1. Correspondingly, from Table 6.2, we observe that the two-loop pentagon integrand contains only coefficients equal to 1.
- At four and five loops, the four-point correlator involves both $+1$ and -1 coefficients. Ignoring for the moment the non-integer entries, we see that -1 also appears among the coefficients of the three- and four-loop pentagon integrands.
- At six loops, the value 2 appears for the first time in the four-point correlator. In parallel, a coefficient equal to 2 occurs in the five-loop pentagon integrand.

Altogether, this demonstrates a clear pattern: the integer coefficients of the pentagon integrand appear to be inherited from those of the four-point correlator via the massless limit. Remarkably, this pattern seems to extend even to the part of the pentagon integrand proportional to the second prefactor $R^{(5,2)}$, although this contribution cannot be reconstructed directly from the four-point correlator in the same manner.

Non-integer coefficients. In addition to the integer coefficients, non-integer values first appear starting at three loops. These arise as solutions to the combined collinear and soft constraints. We do not have a structural explanation for their occurrence in terms of intrinsic properties of the corresponding integrals (nor do we have such an explanation for the integer coefficients). Nevertheless, it is worthwhile to record the pattern in which they appear.

The coefficients $\pm 1/2$ always occur in pairs. More precisely, they multiply the same integral, which appears twice in the ansatz, once attached to each of the two prefactors. For example, at three loops we find

$$M_{5,3}\big|_{\mathcal{I}_4^{(3)}\,\text{contr.}} = -\frac{1}{2}\, R^{(5,1)}_{1234}\, X^2_{35}\, \mathcal{I}^{(3)}_4 + \frac{1}{2}\, R^{(5,2)}_{12345}\, X^2_{14}\, \mathcal{I}^{(3)}_4\,. \tag{6.46}$$

The same phenomenon persists at four and five loops: the coefficients $\pm 1/2$ multiply an integral that appears twice in the ansatz, once with each prefactor and accompanied by different ten-dimensional distances. The converse, however, does not hold in general. An integral appearing multiple times in the ansatz does not necessarily come with non-integer coefficients. In many cases, such contributions still carry integer coefficients.

Finally, at five loops, the coefficients $-1/5$ and $2/5$ appear. These again multiply the same integral,

$$M_{5,5}\big|_{\mathcal{I}^{(5)}_{\text{sym}}\,\text{contr.}} = +\frac{2}{5}\, R^{(5,1)}_{1234}\, X^2_{25}\, X^2_{35}\, \mathcal{I}^{(5)}_{\text{sym}} - \frac{1}{5}\, R^{(5,2)}_{12345}\, X^2_{14}\, X^2_{25}\, \mathcal{I}^{(5)}_{\text{sym}}\,, \tag{6.47}$$

where

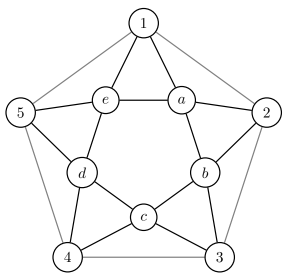

$$\mathcal{I}^{(5)}_{\text{sym}} = \frac{1}{x^2_{1a}x^2_{1e}x^2_{2a}x^2_{2b}x^2_{3b}x^2_{3c}x^2_{4c}x^2_{4d}x^2_{5d}x^2_{5e}x^2_{ab}x^2_{bc}x^2_{cd}x^2_{de}x^2_{ae}}\,. \tag{6.48}$$

	# of integrals with coefficient							
loop-order ℓ	0	1	-1	2	$1/2$	$-1/2$	$-1/5$	$2/5$
2	–	2	–	–	–	–	–	–
3	–	7	2	–	1	1	–	–
4	15	39	21	–	1	1	–	–
5	313	259	210	1	5	5	1	1

Table 6.2.: Statistics of the coefficients dressing the integrals that enter the pentagon integrand ansatz up to five-loop order [4].

As is evident from its structure, this integral possesses a high degree of symmetry. When permuted under $\mathrm{D}_5 \times \mathrm{S}_5$, it generates only 120 distinct terms instead of the possible 1 200. Although this symmetry is partially broken by the accompanying prefactors and ten-dimensional distances in (6.47), the fractional coefficients appear to reflect this enhanced symmetry and compensate for overcounting in the full permutation sum.

6.5. Twistor Computation

So far, we have constructed an ansatz for the pentagon integrand that we conjecture to capture its structure at general ℓ-loop order, leaving only a finite set of undetermined coefficients. This structure was inferred from the explicit one- and two-loop expressions. We then imposed soft and collinear constraints, which are expected to hold more generally also for these integrands with off-shell external kinematics, in order to fix the coefficients as far as possible. Up to five loops, this procedure uniquely determines all coefficients and thus yields explicit expressions for the pentagon integrand. As a first non-trivial check, we compared these results to the known massless MHV amplitudes via the limit (6.40), finding complete agreement. However, this limit probes only a restricted part of the integrand. In particular, the entire $R^{(5,2)}$ contribution vanishes in this limit, so that a large portion of the integrand remains untested.

In this section, we therefore subject our results to a more stringent test by performing a direct computation of the pentagon integrand using the twistor reformulation of $\mathcal{N} = 4$ SYM [29], that was reviewed in Chapter 3. As discussed there, a characteristic feature of the twistor approach is the introduction of an auxiliary reference twistor

loop-order l	1	2	3	4
# twistor graphs	36	740	17 210	425 819
# terms initial	49	2 178	87 775	3 523 496
# terms nonzero	47	1 615	48 456	1 378 656
# terms permuted	167	11 732	1 023 174	111 517 637

Table 6.3.: Number of twistor graphs and resulting terms in the expression for the pentagon integrand up to four loops [4].

$Z_\star$ associated with the axial gauge. Individual twistor Feynman diagrams depend on this reference twistor, but this dependence cancels in the full sum. Since our goal is merely to verify the previously obtained integrand, it suffices to compare our bootstrap results numerically to the twistor expressions, rendering this framework particularly well suited for our purposes.

To derive the pentagon integrand, we make use of the twistor Feynman rules Φ [69], reviewed in Section 3.3.2, in combination with the method outlined in Section 5.3. As discussed there, we apply the Feynman rules to a restricted set of graphs, namely those with disc topology $\Gamma_{5,\ell}^{\text{disc}}$. The pentagon integrand is then given by

$$M_{5,\ell} = \lim_{d_{i,i+1}\to 1} \prod_{i=1}^{5} (1 - d_{i,i+1}) \sum_{\gamma \in \Gamma_{5,\ell}^{\text{disc}}} \Phi(\gamma) \Big|_{\substack{\theta_6^4 \cdots \theta_{5+\ell}^4 \\ y_6,\dots,y_{5+\ell}\to 0}} , \tag{6.49}$$

where the ten-dimensional null limit is taken along the perimeter of the pentagon.

In the following, we provide a practical summary of how to compute the pentagon loop integrand within this framework, without entering technical details. These have been spelled out throughout this thesis previously: for a detailed explanation of the Feynman rules Φ [69] see Section 3.3.2; for an explanation of why restricting to disc-topology graphs yields the polygon integrand, see Section 5.3; and for details on the projection to chiral Lagrangians required to extract the loop integrand, we refer to Section 4.2.

- We begin by constructing all graphs with disc topology. Concretely, these are planar ribbon graphs with $(5+\ell)$ vertices. Hence, the graphs are distinguished not only by their simple structure but also by their embedding on the plane. In addition, they are required to have disc topology: five vertices must form a pentagon whose perimeter consists of simple edges, while the remaining ℓ

vertices lie on one side of this disc and are connected in a planar way. We list the number of such graphs that are inequivalent under $D_5 \times S_\ell$ permutations in the first row of Table 6.3.

- Next, we apply the twistor Feynman rules Φ to each graph. The resulting expressions can be expanded according to their total Grassmann degree. We retain only those terms that produce the required Grassmann degree $\sim \theta^{4\ell}$. Moreover, we discard contributions involving higher KK modes of the Lagrangians. This procedure yields a set of seed terms which, after permutation under $D_5 \times S_\ell$, generate the pentagon integrand. The number of such terms is given in the second row of Table 6.3.
- Before performing the permutations, we further test each term for its ability to produce the desired Grassmann structure $\theta_6^4 \dots \theta_{5+\ell}^4$. This can be implemented straightforwardly in a numerical evaluation by identifying terms that vanish identically. In this way, we obtain a reduced set containing only non-vanishing contributions. The corresponding numbers are displayed in the third row of Table 6.3.
- Finally, we permute the resulting expressions under $D_5 \times S_\ell$. The only subtlety is that each graph contribution must be permuted only over inequivalent permutations. Since this may be obscured by the previous reductions, it is convenient to introduce appropriate symmetry factors for each graph from the outset. With this prescription, the final sum can be fully permuted without overcounting. The total number of terms in the final expression is shown in the fourth row of Table 6.3.

We carried out this procedure up to four-loop order and obtained explicit twistor-space representations of the pentagon integrand at each loop order. These expressions can be evaluated numerically and compared with the known one- and two-loop results, as well as with our bootstrap results at three and four loops. In all cases, we find complete numerical agreement, thereby providing a verification of our construction.

We did not extend this computation to five loops, as the number of disc-topology graphs at that order already reaches 11 001 418, rendering the explicit construction substantially more resource-intensive. Nevertheless, given the perfect agreement observed up to four loops, we consider this derivation to provide substantial evidence for the correctness of our results.

7. The Non-Planar Four-Point Integrand at Five Loops

In this chapter, we shift our focus from higher-charge operators to the lightest ones, namely the $\mathbf{20'}$ operators. As discussed in Section 2.4.4, the four-point function of these operators exhibits remarkable properties and is highly constrained by symmetry alone. In the planar limit, these constraints are sufficiently strong to determine the integrand up to twelve loops [58]. In the non-planar sector, corrections to the planar integrand first appear at four loops. At this order, a constrained ansatz with four undetermined coefficients was constructed in [53]. Using the twistor reformulation, this ansatz was subsequently fixed in [59].

Extending this computation to five loops presents significant challenges. Beyond the increasing number of contributing graphs, the main difficulty arises from the contraction of 20 Grassmann variables appearing in the twistor Feynman rules. These contractions are computationally expensive and render a direct evaluation infeasible on standard hardware. To overcome this, we implement a GPU-based algorithm that significantly accelerates the contraction procedure.

We begin in Section 7.1 by reviewing how the four-point loop integrand is constructed in terms of so-called f-graphs, and then formulate a constrained ansatz for the full five-loop four-point function. In Section 7.2, we continue by discussing how to efficiently determine the loop integrand in twistor space, applying the Feynman rules $\Phi_{\mathbf{20'}}$ [105], reviewed in Section 3.4. The algorithm for evaluating the Grassmann multiplications is descussed in Section 7.3. Finally we present the result of the full five-loop integrand in Section 7.4. As a first application of this result, we extract the anomalous dimension of the Konishi operator in Section 7.5.

In this chapter, we revert to the notation introduced in Section 2.4. In particular, we consider $\mathcal{N} = 4$ SYM with gauge group $\mathrm{SU}(N_\mathrm{c})$, following the conventions commonly used in the literature on four-point correlators.

This chapter is based on the work presented in [3].

7.1. Ansatz Construction

In Section 2.4.4, we reviewed how the loop integrand of the four-point function can be obtained via the Lagrangian insertion procedure and subsequently decomposed into a universal superconformal invariant multiplied by a function that is fully symmetric in the internal and external spacetime points. We briefly recall this structure here. The tree-level correlator of four stress-tensor multiplets with $\ell > 0$ insertions of the chiral on-shell Lagrangian takes the form [53, 66][1]

$$G_4^{(\ell)}(x_i, y_i) = 2\frac{N_{\rm c}^2 - 1}{(4\pi^2)^{4+\ell}}\,\mathcal{R}_{1234}\,\xi_4\,F^{(4+\ell)}(x_i)\,, \tag{7.1}$$

where $\mathcal{R}_{1234}$ (cf. (2.48)) is the unique superconformal invariant of four points and $\xi_4 = x_{12}^2 x_{13}^2 x_{14}^2 x_{23}^2 x_{24}^2 x_{34}^2$. $F^{(n)}$ is a rational function of x_{ij}^2 that is invariant under all permutations of $x_1, \ldots, x_n$, has at most simple poles in x_{ij}^2, and conformal weight $+4$ in each point x_i. This function can be expanded in so-called f-graphs

$$F^{(n)} = \sum_{i=1}^{\mathcal{N}_n} c_i^{(n)} f_i^{(n)}\,, \tag{7.2}$$

where each $f_i^{(n)}$ represents a permutation-invariant sum of terms, normalized such that each term appears with unit coefficient. The total number of f-graphs $\mathcal{N}_n$ is listed in Table 7.1. The color dependence of $G_4^{(\ell)}$ is encoded in the coefficients $c_i^{(n)}$, which are polynomials in $1/N_{\rm c}^2$. Thus we can define the genus expansion of $F^{(n)}$ by

$$F^{(n)} = \sum_{g\geq 0} \frac{1}{N_{\rm c}^{2g}} F^{(g,n)} = \sum_{g\geq 0} \frac{1}{N_{\rm c}^{2g}} \sum_{i=1}^{\mathcal{N}_n} c_i^{(g,n)} f_i^{(n)}\,, \tag{7.3}$$

where $c_i^{(g,n)}$ are now purely numerical coefficients.
It has been conjectured that the integrand $G_4^{(g,\ell\geq 2)}$ only depends on f-graphs up to genus g [53]:

$$c_i^{(g,n)} = 0 \quad \text{if} \quad \text{genus}(f_i^{(n)}) > g\,, \tag{7.4}$$

where the genus of an f-graphs is defined as the minimal genus of the simple, connected graph obtained by associating an edge to each squared distance in the denominator. For planar integrands ($g = 0$), this implies that only the planar f-graphs

[1] In the notation of Section 2.4, this integrand is given by $\mathcal{G}_{4+\ell;\ell}^{(0)}$.

n	$\mathcal{N}_n$	genus 0	genus 1	genus 2	Gram id.
7	4	1	3	–	1
8	32	3	29	–	3
9	930	7	833	90	208

Table 7.1.: Numbers of f-graphs $\mathcal{N}_n$ entering the three-, four-, and five-loop ansatz, their genus distribution, and the number of linearly independent Gram identities [3].

contribute, which has been verified up to twelve loops [58]. In practice, we find the genus by using the algorithm `multi_genus` of [135], see Table 7.1 for the statistics.

In general, not all f-graphs are linearly independent. Since they are functions of squared distances x_{ij}^2, they satisfy conformal Gram identities. These emerge when considering the $(n \times n)$ Gram matrix with elements

$$\mathcal{G}_{ij} = X_i \cdot X_j = x_{ij}^2 \quad \text{for} \quad i, j = 1, \ldots, n\,, \tag{7.5}$$

where X_i are the six-dimensional null vectors on which the conformal symmetry $\mathrm{SO}(2,4)$ acts linearly. This matrix is of rank six, implying that all (7×7)-minors vanish. After dividing by appropriate monomials in x_{ij}^2, such that each point is of conformal weight $+4$, and symmetrizing over all n points, these conditions generate the Gram identities between the f-graphs.

Determining the four-point integrand amounts to finding the numerical coefficients $c_k^{(g,n)}$ in the ansatz (7.3). The freedom in the ansatz can be greatly reduced by imposing null or coincidence limits. At the planar level, such limits in fact uniquely determine the integrand up to twelve loops [41, 53–58]. For the subleading $1/N_c^2$ terms, this is no longer the case: Some free coefficients remain, which have to be fixed by a numerical match with the twistor computation.

In order to constrain $F^{(g\geq 1,9)}$, we impose the light-cone constraint [53]: Setting neighboring external operators to null separation $(x_{12}^2, x_{23}^2, x_{34}^2, x_{41}^2 \to 0)$, the tree-level normalized correlator takes the form

$$\frac{G_4}{G_4^{(0)}} = 1 + 2 \sum_{\ell \geq 1} \frac{a^\ell}{(-4\pi^2)^\ell} \int \left(\prod_{k=5}^{4+\ell} d^4 x_k \right) \mathcal{F}^{(4+\ell)}(x_i)\,, \tag{7.6}$$

where

$$\mathcal{F}^{(n)} = \lim_{x^2_{i,i+1}\to 0} x^2_{13}x^2_{24}\xi_4 F^{(n)}/\ell! \tag{7.7}$$

is the null-square limit of the tree-level normalized sum of f-graphs. While $\mathcal{F}^{(n)}$ is finite, the integrals in (7.6) diverge: Starting from $\ell = 2$, the ℓ-loop contribution to the logarithm of (7.6) exhibits a $\log^{\ell}(x^2_{i,i+1})$ divergence [30]. However, the integrals of individual f-graphs generally produce stronger divergences $\log^k(x^2_{i,i+1})$, $k > \ell$. These divergences arise from integration regions where one of the internal operators approaches one of the light-like segments. To ensure the correct logarithmic divergence of the correlator, we require the *light-cone constraints*:[2] In the limit $x_5 \to \alpha x_1 + (1-\alpha)x_2$, the integrand of the logarithm of (7.6) must vanish order by order in α. For the non-planar five-loop integrand, these conditions are:[3]

$$\lim_{x_5\to\alpha x_1+(1-\alpha)x_2} x^2_{15}x^2_{25}\big(\mathcal{F}^{(1,9)} - 2\mathcal{F}^{(1,8)}\mathcal{F}^{(0,5)}\big) = 0\,, \tag{7.8}$$

$$\lim_{x_5\to\alpha x_1+(1-\alpha)x_2} x^2_{15}x^2_{25}\,\mathcal{F}^{(g\geq 2,\,9)} = 0\,. \tag{7.9}$$

For the genus-one integrand, following (7.4), one can impose that the 90 genus-two f-graphs do not contribute to the final integrand. Then, imposing (7.8) fixes all but 155 coefficients of $F^{(1,9)}$, of which 134 parametrize Gram identities. Hence, only 21 coefficients are left to be determined by the twistor computation.[4] Starting from genus two, all 930 f-graphs contribute, and (7.9) fixes all but 23 coefficients, accompanied by 208 Gram identities, at every order in the genus expansion.

7.2. Twistor Computation

We briefly summarize the steps necessary to compute the integrand of the four-point correlator using the twistor formulation. We explained the relevant rules for computing the tree-level correlator of stress-tensor multiplets in Section 3.4. Here, we focus on the practical steps required to carry out the computation.

[2] For the planar integrand, given by an ansatz in terms of planar f-graphs, this constraint fixes all seven coefficients.

[3] There are no further terms in (7.8) because $\mathcal{F}^{(1,n)} = 0$ for $n < 8$.

[4] We further tested the five-loop ansatz against the cusp-limit constraint of [57]. This constraint turns out to be less restrictive and is already fully captured by the light-cone constraints.

First, all relevant skeleton graphs are generated. At ℓ-loop order, they are specified as all connected $(4+\ell)$-point graphs with $4+2\ell$ edges and a valency of at least 2 at each vertex, and can for example be obtained with the open-source program Sage [136] (see Table 6.3).
Second, starting from each skeleton graph $\mathfrak{g}$, all associated ribbon graphs $\gamma \in \Gamma_{\mathfrak{g}}$ can be formed by permuting over the order of the edges around each vertex. Then, the twistor Feynman rules are applied to these ribbon graphs: Each graph is dressed with a factor $(g^2_{\mathrm{YM}})^{P-V}(4\pi^2)^{-P}$, with P and V denoting the number of edges (propagators) and vertices of the graph. Every edge connecting vertices i and j is dressed with a propagator $d_{ij} = y^2_{ij}/x^2_{ij}$. Each vertex i connected to cyclically ordered vertices $j_1, \ldots, j_k$ produces a vertex factor $V^i_{j_1 \ldots j_k}$ and a color trace $\mathrm{tr}(T^{a_{ij_1}} \ldots T^{a_{ij_k}})$, where T^a denote the $\mathrm{SU}(N_\mathrm{c})$ generators in the fundamental representation. For each ribbon graph γ, the traces can be evaluated to a function in N_c by successively applying the fusion and fission rules

$$\mathrm{tr}(T^a B T^a C) = \mathrm{tr}(B)\,\mathrm{tr}(C) - \mathrm{tr}(BC)/N_\mathrm{c}\,, \tag{7.10}$$

$$\mathrm{tr}(B T^a)\,\mathrm{tr}(C T^a) = \mathrm{tr}(BC) - \mathrm{tr}(B)\,\mathrm{tr}(C)/N_\mathrm{c}\,. \tag{7.11}$$

This yields an overall factor of $(N^2_\mathrm{c}-1)N^\ell_\mathrm{c}$ multiplied by a polynomial $c_\gamma(1/N^2_\mathrm{c})$. Furthermore, the dependence of the vertex factors on the ribbon structure can be canonicalized by pulling out factors $\langle ijk \rangle = \epsilon_{\alpha\beta}\lambda^\alpha_{ij}\lambda^\beta_{ik}$ (cf. (3.37))

$$V^i_{j_{\tau(1)} \cdots j_{\tau(k)}} = V^i_{j_1 \ldots j_k} \frac{\langle i j_1 j_2 \rangle \ldots \langle i j_k j_1 \rangle}{\langle i j_{\tau(1)} j_{\tau(2)} \rangle \ldots \langle i j_{\tau(k)} j_{\tau(1)} \rangle}\,, \tag{7.12}$$

where τ is a permutation. Let us denote the product of these kinematic factors for each canonicalized ribbon graph by $s_\gamma(\langle ijk \rangle)$. In this way, a universal product of propagators and R-factors can be pulled out of the sum over all ribbon graphs $\Gamma_{\mathfrak{g}}$ associated to the same skeleton graph $\mathfrak{g}$, leaving a sum that entails the complete dependency on the color structure $c_\gamma(1/N^2_\mathrm{c})$, and includes some kinematic factors $s_\gamma(\langle ijk \rangle)$. Splitting the vertex factors into basic factors R^i_{jkl} of Grassmann degree two (cf. (3.28)), the sum of ribbon graphs over $\Gamma_{\mathfrak{g}}$ can be schematically written as

$$\begin{aligned} &\sum_{\gamma \in \Gamma_{\mathfrak{g}}} \Phi_{\mathbf{20'}}(\gamma) = a^\ell \, \frac{N^2_\mathrm{c}-1}{(4\pi^2)^{4+\ell}} \, p_{\mathfrak{g}}(1/N^2_\mathrm{c}, \langle ijk \rangle) \prod^{4+2\ell}_{\mathfrak{g}} d_{ij} \times \prod^{2\ell}_{\mathfrak{g}} R^i_{jkl} \\ &\text{with} \quad p_{\mathfrak{g}}(1/N^2_\mathrm{c}, \langle ijk \rangle) = \sum_{\gamma \in \Gamma_{\mathfrak{g}}} c_\gamma(1/N^2_\mathrm{c})\, s_\gamma(\langle ijk \rangle)\,, \end{aligned} \tag{7.13}$$

where $\Phi_{\mathbf{20'}}$ are the twistor Feynman rules as reviewed in Section 3.4. Here, the symbol $\mathfrak{g}$ below the product signs indicate that the products only depend on the skeleton graph, not on the specific ribbon graph, while the number above denotes the number of factors in each product. The prefactors $p_{\mathfrak{g}}$ encode the genus expansion, and can be evaluated for each skeleton graph at this stage. It is known that the full integrand is completely planar up to three loops, and there is a single correction of order $\mathcal{O}(1/N_{\mathrm{c}}^2)$ at four loops. We find that the same is true at five loops: The prefactors $p_{\mathfrak{g}}$ exhibit at most a $\mathcal{O}(1/N_{\mathrm{c}}^2)$ contribution. This implies that $F^{(g\geq 2,\,9)}$ vanishes, leaving only the remaining 21 coefficients of $F^{(1,9)}$ to be determined.

Third and finally, each skeleton graph must be permuted over all inequivalent vertex labelings. This yields a large number of graphs $\mathfrak{G}$, in terms of which the integrand (7.1) can now be schematically expressed as

$$G_4^{(\ell)} = \frac{N_{\mathrm{c}}^2 - 1}{(4\pi^2)^{4+\ell}} \sum_{\mathfrak{g}\in\mathfrak{G}} \left(p_{\mathfrak{g}} \prod_{\mathfrak{g}}^{4+2\ell} d_{ij} \times \prod_{\mathfrak{g}}^{2\ell} R^i_{jkl} \right) . \tag{7.14}$$

To reduce the computational time of evaluating the expression, we aim to reduce the number of permuted graphs $\mathfrak{G}$ to consider. As in [59], we choose a polarization in which all y_{ij}^2 vanish except y_{12}^2 and y_{34}^2, which drastically cuts down the number of contributing graphs. Yet, the complete integrand is still accessible, since the polarizations only appear in the four-point invariant $\mathcal{R}_{1234}$ in (7.1). Moreover, we can eliminate graphs that cannot generate the desired Grassmann monomial $\theta_5^4 \ldots \theta_{4+\ell}^4$. For example, R-factors only depending on the external operators can be set to zero, and products of R-factors in which any internal label appears fewer than twice can also be removed. Listing the permutations, specifying the polarization, and removing non-contributing products of R-factors, we arrive at the second row of Table 7.2. Some remaining graphs still evaluate to zero, despite it not being apparent from their symbolic expression. We remove such graphs by probing all remaining products of R-factors numerically, and keeping only graphs that are indeed non-vanishing. Their counts appear in the third row of Table 7.2.

Let us mention that in four dimensions, the integrand $G_4^{(\ell)}$ has a pseudo-scalar contribution, which is produced by a total derivative term in the twistor-reformulated action of $\mathcal{N} = 4$, and therefore vanishes upon integration. In Lorentzian signature, this contribution is imaginary, and hence can be numerically isolated. However, we perform the calculation in split signature, where the twistor computation remains real, such that we can efficiently employ finite fields. In order to isolate the pseudo-

ℓ	1	2	3	4	5
# skeleton graphs	3	11	63	513	5,553
# permuted graphs	1	73	6,321	732,288	110,732,441
# non-zero graphs	1	73	5,901	627,148	87,757,390

Table 7.2.: Graphs that enter the twistor computation [3]. First row: Number of skeleton graphs generated with Sage. Second row: Number of permuted and polarized graphs, excluding graphs that cannot produce the correct Grassmann monomial. Third row: Final number of graphs that have a non-vanishing contributions to the twistor result.

scalar contribution, we compute each numerical point twice, with kinematics that differ by a parity transformation. Taking their mean removes any pseudo-scalar contribution.

7.3. The Grassmann Contraction at Five Loops

One of the main challenges in evaluating the twistor expression numerically lies in the contraction of the Grassmann numbers that appear in the R-factors. Each term in the five-loop twistor expression (7.14) contains ten R-factors $\{R_1, \ldots, R_{10}\}$, each quadratic in the Grassmann variables $\theta^{a\alpha}$, that must be contracted into the unique product $\theta_5^4 \ldots \theta_9^4$ involving all 20 Grassmann numbers. Splitting each R_a into a list of the $\binom{20}{2} = 190$ products of Grassmann numbers, we find that the most efficient implementation iteratively contracts the R-factors into successively higher-degree products of Grassmann numbers as follows:

$$(S_a)^k = (t_{a-1})^k_{ij} (S_{a-1})^i (R_a)^j \quad \text{with} \quad a \in [2,\, 10]\,, \tag{7.15}$$

with $S_1 = R_1$, and t_a being fixed numerical sparse tensors that contract the vectors at each intermediate step. These successive tensor–vector–vector multiplications can be implemented highly efficiently on a graphics processing unit (GPU).

The algorithm starts by multiplying the first two R-factors to a purely quartic polynomial with $\binom{20}{4} = 4845$ terms corresponding to all ordered products of four Grassmann variables. Then, this intermediate result is multiplied with the next R-factor, arriving at a polynomial of a degree six. In this manner, we successively multiply one R-factor at a time, eventually arriving at the final unique product involving all 20 Grassmann numbers. At each intermediate step, the degree $2a$

a	size	N_a
1	$4845 \times 190 \times 190$	29 070
2	$38760 \times 4845 \times 190$	581 400
3	$125970 \times 38760 \times 190$	3 527 160
4	$184756 \times 125970 \times 190$	8 314 020
5	$125970 \times 184756 \times 190$	8 314 020
6	$38760 \times 125970 \times 190$	3 527 160
7	$4845 \times 38760 \times 190$	581 400
8	$190 \times 4845 \times 190$	29 070
9	$1 \times 190 \times 190$	190

Table 7.3.: Properties of the order-three tensors t_a appearing in the algorithm for the Grassmann contraction [3]. Listed are the respective sizes of the tensors, as well as the number of non-zero entries N_a.

polynomial is represented as a vector of $\binom{20}{2a}$ coefficients, and the multiplication is performed by an order-three tensor t_{a-1} of size $\binom{20}{2a} \times \binom{20}{2a-2} \times \binom{20}{2}$, whose non-zero entries are ± 1. The number of non-zero elements of each tensor can be computed by

$$N_{a-1} = \binom{2a}{2} \times \binom{20}{2a}. \tag{7.16}$$

The first factor counts the number of ways to decompose a degree $2a$ monomial into two monomials of degrees 2 and $2a-2$, while the second factor corresponds to the number of terms in a degree $2a$ polynomial (i. e. the range of the last index of t_{a-1}). As such, the tensors are very sparse, facilitating the computation. We summarize the properties of the tensors in Table 7.3.

Since the numerical computation is highly parallelizable, we opt to run the sequence of ten sparse tensor-vector-vector multiplications on a GPU, which significantly accelerates the computation. We use the `cuda.jit` decorator from the Python package Numba [137], which compiles the function into a custom CUDA kernel for efficient parallel execution. For each $a \in \{2, \dots, 10\}$, the kernel distributes the work of iterating over non-zero entries of the tensor t_{a-1} across CUDA threads, each of which independently multiplies a single non-zero tensor element with the corresponding values in the input vectors S_{a-1} and R_a. The partial product is then atomically accumulated into the output vector S_a to avoid race conditions.

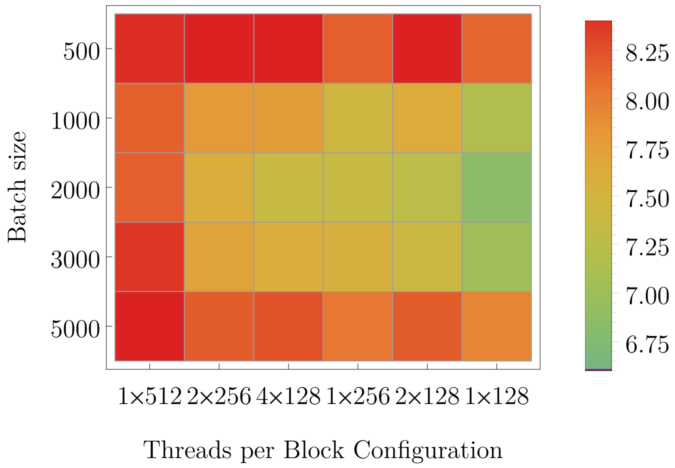

Figure 7.1.: Heat map showing the time (in seconds) to perform 10,000 five-loop contractions on an *Nvidia A100* GPU [3]. The y-axis represents the batch size, and the x-axis corresponds to the threads-per-block configuration.

To achieve high performance, we adopt a batched processing strategy in which multiple tensor-vector-vector multiplications of the same tensor but different R-factors are executed simultaneously. This batch dimension allows us to better utilize GPU resources and increase thread occupancy. For each multiplication, the kernel launch configuration uses a specified number of threads per block and blocks per grid, which control the parallel decomposition of the workload. Over all contractions, we use a fixed number of threads per block, while the number of blocks per grid is computed dynamically based on the number of non-zero elements in each tensor and the batch size. The values of the thread block size and batch dimension were tuned through performance benchmarking to maximize throughput on the GPU (see Figure 7.1). With optimal setting of these parameters, we find that the Grassmann contractions involved when evaluating the twistor expression for one numerical kinematic point takes roughly 17 hours on a single *Nvidia A100* GPU.

The numerical implementation of this contraction entails a significant precision loss, such that not even `float64` numbers are sufficient to ensure accurate results. For this reason, we opt to evaluate both the twistor expression and the ansatz of the integrand using `int32` integers within a finite field $\mathbb{F}_p$. To ensure the intermediate values remain within the bounds of the `int32` format, each tensor contraction must

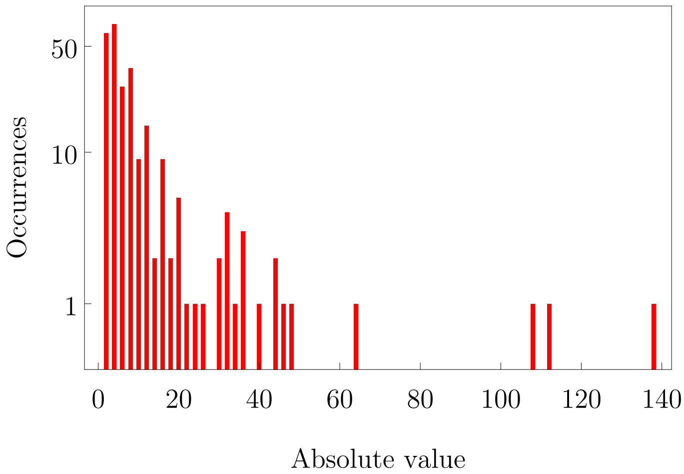

Figure 7.2.: Histogram of absolute values in the particular genus-one five-loop integrand solution provided in the ancillary files, excluding 582 zero coefficients [3].

produce results that do not exceed the 32 bit integer limit. Considering that the tensor multiplications involve at most 190 summands, we require that $190\,p^2 < 2^{31}$, which implies that the largest prime we can safely use is given by $p = 3361$.

In the first instance, the particular solution (match between ansatz and twistor expression) will only be valid over the finite field $\mathbb{F}_{3361}$. However, tuning the result by adding suitable combinations of the 208 Gram identities, we can construct a particular solution where the majority of the 930 f-graph coefficients is zero, and all others attain small integer values (see Figure 7.2). We expect this to be the true solution over the real numbers. As a check, we compare the particular solution against the twistor expression a few times over different finite fields ($\mathbb{F}_{3347}$ and $\mathbb{F}_{3359}$). We find perfect agreement, which proves the validity of the solution beyond reasonable doubt.

Under optimal settings, the Grassmann contractions required to evaluate (7.14) at a single numerical point take approximately 17 hours on a single *Nvidia A100* GPU, rendering the determination of the 21 coefficients (each requiring the evaluation at two numerical points) in the five-loop genus-one ansatz practically feasible.

7.4. The Five-Loop Integrand and Genus Conjecture

As discussed above, the full five-loop integrand only consist of the planar part and the genus-one correction. By numerically matching against the twistor result, we can fix the remaining 21 free parameters in the genus-one ansatz, and find the full five-loop integrand. Of the 930 nine-point f-graphs, we excluded the 90 genus-two graphs, as they do not contribute to the genus-one integrand. By adding an appropriate combination of the 134 Gram identities among the remaining graphs, we obtain a particular solution for the remaining 840 f-graph coefficients that exhibits the following properties: First, 582 coefficients are zero, thus the corresponding f-graphs do not contribute to the genus-one integrand. Second, the remaining 258 non-zero coefficients are of small integer value, as is visualized in Figure 7.2. This solution is provided in the ancillary files of [3]. See Appendix A for a guide to this file.

Furthermore, we notice that a stronger statement than (7.4) might hold, namely the following: *The integrand $G_4^{(g,\ell\geq 2)}$ only depends on f-graphs of exactly genus g*, that is

$$c_i^{(g,n)} = 0 \quad \text{if} \quad \text{genus}(f_i^{(n)}) \neq g\,. \tag{7.17}$$

First, this is consistent with the non-planar integrands found so far. The genus-one correction to the four-loop integrand [53, 59] can be uniquely written in terms of the 29 genus-one eight-point f-graphs, using the three Gram identities to remove the dependency on the planar graphs. At five loops, we can construct a result in terms of only the genus-one f-graphs, reducing the Gram freedom to 127. Second, it immediately rules out $g \geq 2$ and $g \geq 3$ correction to the four- and five-loop integrand, respectively. Regarding the genus-two correction to the five-loop integrand, this statement implies that it is given in terms of the 90 genus-two nine-point f-graphs. Imposing the light-cone constraint (7.9) on this ansatz sets all but one coefficient to zero.

7.5. The Konishi Anomalous Dimension at Five Loops

The four-point correlator contains a variety of interesting observables. Many of these can be extracted without performing the full integration of the integrand by instead taking suitable limits and simplifications, and subsequently integrating only simpler expressions. In the following, we extract the Konishi anomalous dimension at five loops following this strategy.

7.5.1. Extraction from the Four-Point Integrand

One of the immediate observables obtainable from the four-point $\mathbf{20'}$ integrand is the anomalous dimension $\gamma_{\mathcal{K}}(a)$ of the Konishi operator $\mathcal{K}(x) = \mathrm{tr}(\phi(x)\cdot\phi(x))$, which is encoded in its two-point function. The latter can be extracted from the four-point correlator via the operator product expansion (OPE). $\mathcal{K}$ dominates the OPE, thus $\gamma_{\mathcal{K}}(a)$ can be extracted by by double-pinching the integrand ($x_2 \to x_1$ and $x_4 \to x_3$) [138]:

$$\log\left(1 + 6\sum_{\ell\geq 1}\frac{a^\ell}{(-4\pi^2)^\ell}\int\left(\prod_{k=5}^{4+\ell} d^4x_k\right)\hat{F}^{(4+\ell)}(x_i)\right) = \frac{1}{2}\gamma_{\mathcal{K}}(a)\log(u) + \mathcal{O}(u^0)\,, \tag{7.18}$$

with $u = x_{12}^2 x_{34}^2/(x_{13}^2 x_{24}^2)$ being one of the conformal cross-ratios and

$$\hat{F}^{(n)} = \lim_{\substack{x_2\to x_1\\ x_4\to x_3}} x_{13}^4 \xi_4 F^{(n)}/\ell!\,. \tag{7.19}$$

Expanding the above equation to the genus-one five-loop order yields

$$\int\left(\prod_{k=5}^{9} d^4x_k\right) I^{(1,5)} = \frac{1}{2}\gamma_{\mathcal{K}}^{(1,5)}\log(u) + \mathcal{O}(u^0)\,, \tag{7.20}$$

with $\gamma_{\mathcal{K}}^{(1,5)}$ denoting the genus-one five-loop correction to the Konishi anomalous dimension, and the integrand given by

$$I^{(1,5)} = -6(\hat{F}^{(1,5)} - 6\hat{F}^{(0,1)}\hat{F}^{(1,4)})/(4\pi^2)^5\,. \tag{7.21}$$

The log-divergence of the above integral arises when all of the integration points approach one of the external points x_1 or x_3. In order to extract the coefficient $\gamma_{\mathcal{K}}^{(1,5)}$ in front of this divergence, we follow the steps outlined in [138]: First, we take $x_3 \to \infty$, effectively replacing all $x_{3k}^2 \to x_{13}^2$, to single out the divergence that arises when all points approach x_1, and define $\hat{I}^{(1,5)} = \lim_{x_3\to\infty} I^{(1,5)}$. Second, we apply dimensional regularization with $d = 4 - 2\epsilon$ and perform all but one integration

$$2\int\left(\prod_{k=6}^{9} d^{4-2\epsilon}x_k\right)\hat{I}^{(1,5)} = \frac{C^{(1,5)}}{\pi^2}(x_{15}^2)^{-2-4\epsilon}\,, \tag{7.22}$$

where $C^{(1,5)}$ is finite for $\epsilon \to 0$. The factor 2 is included to take into account the contribution of the integration around x_3. Third, comparing with (7.18), a careful analysis on the infrared rearrangement of the remaining integration allows to identify the log-divergence by

$$-2\int \frac{d^{4-2\epsilon}x_5}{\pi^2}(x_{15}^2)^{-2-4\epsilon} = \log u + \mathcal{O}(u^0) + \mathcal{O}(\epsilon)\,, \tag{7.23}$$

in the leading behavior in ϵ. We refer for details on this regularization scheme to App. A in [138]. Finally, we identify $\gamma_{\mathcal{K}}^{(1,5)} = -C^{(1,5)}$, obtaining the correction to the anomalous dimension.

Practically, obtaining the genus-one five-loop anomalous dimension boils down to performing the four-loop propagator-type integration in (7.22). Starting from the obtained genus-one five-loop integrand $G_4^{(1,5)}$ and the known result of $G_4^{(1,4)}$ [53, 59], we construct $\hat{I}^{(1,5)}$ and find that $C^{(1,5)}$ is a linear combination of 2855 two-point four-loop integrals. Applying the integration-by-parts method, we reduce this linear combination of integrals to a small set of master integrals using the program `FIRE6` [139, 140]. In particular, we find that it consists of 24 master integrals, 20 of which are associated to planar graphs, while the remaining integrals are associated to non-planar ones:

$$\gamma_{\mathcal{K}}^{(1,5)} = \left[\sum_{k=1}^{20} v_k\,\mathcal{J}_k + \sum_{k=1}^{4} w_k\,\mathcal{I}_k\right]_{\epsilon\to 0}. \tag{7.24}$$

The coefficient functions v_k and w_k are expressed as expansions in ϵ. In particular, the leading order of each w_k is -1. By introducing dual momenta, the master integrals corresponding to planar graphs can be transformed to four-loop propagator-type integrals in momentum representation. Graphically, these momentum master integrals are represented by the dual graphs of the original planar ones. The latter were explicitly calculated as expansions in ϵ in [141, 142], carried out to sufficiently high orders, such that (7.24) can be evaluated at $\mathcal{O}(\epsilon^0)$. Of the four remaining master integrals associated to non-planar graphs, $\mathcal{I}_1$ and $\mathcal{I}_2$ were derived in [138] (cf. App. B therein). These integrals already appeared in the computation of the planar five-loop correction to the Konishi anomalous dimension.

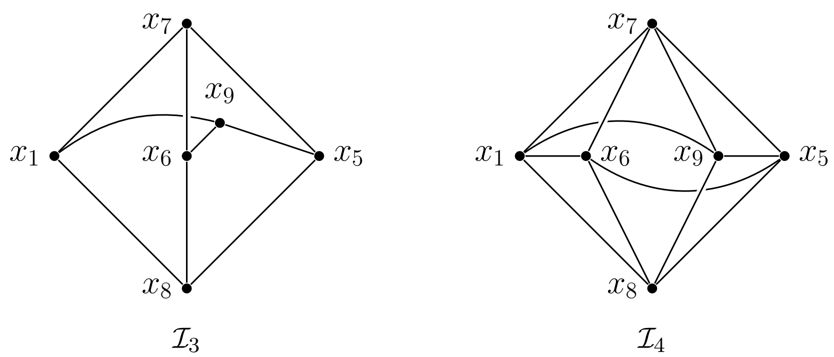

Figure 7.3.: Diagrammatic representation of the two non-planar four-loop master integrals that contribute to the Konishi anomalous dimension [3]. The edges connecting vertices i and j stand for factors $1/x_{ij}^2$.

7.5.2. Evaluation of Two Master Integrals

The final two master integrals $\mathcal{I}_3$ and $\mathcal{I}_4$ were not determined so far to our knowledge. Explicitly, they read (with $D = 4 - 2\epsilon$)

$$
\begin{aligned}
\mathcal{I}_3 &= \frac{1}{(\pi^2)^4} \int \frac{d^D x_6 d^D x_7 d^D x_8 d^D x_9}{x_{17}^2 x_{18}^2 x_{19}^2 x_{57}^2 x_{58}^2 x_{59}^2 x_{67}^2 x_{68}^2 x_{69}^2}\,, \qquad (7.25)\\
\mathcal{I}_4 &= \frac{1}{(\pi^2)^4} \int \frac{d^D x_6 d^D x_7 d^D x_8 d^D x_9}{x_{16}^2 x_{17}^2 x_{18}^2 x_{19}^2 x_{56}^2 x_{57}^2 x_{58}^2 x_{59}^2 x_{67}^2 x_{78}^2 x_{89}^2 x_{69}^2}\,,
\end{aligned}
$$

see Figure 7.3 for their diagrammatic representation. Expanding the integrals to linear order in ϵ with a priori undetermined coefficients yields (setting $x_{15}^2 = 1$)

$$
\begin{aligned}
\mathcal{I}_3 &= \frac{a_3}{\epsilon} + b_3 + c_3\epsilon + \mathcal{O}(\epsilon^2)\,,\\
\mathcal{I}_4 &= \frac{a_4}{\epsilon} + b_4 + c_4\epsilon + \mathcal{O}(\epsilon^2)\,. \qquad (7.26)
\end{aligned}
$$

To constrain the six unknown coefficients, we begin by deriving relations between the 24 master integrals by making use of the Gram identities. As discussed around (7.5), these identities manifest as 208 linear relations among the nine-point f-graphs. By following the same steps that led to (7.24), we can transform these identities to relations among the 24 two-point four-loop master integrals.

First, we normalize the Gram identities among f-graphs in analogy to (7.19). We then take the OPE limit ($x_2 \to x_1$, $x_4 \to x_3$), followed by $x_3 \to \infty$, and finally integrate over points $x_6, \ldots, x_9$ in $D = 4 - 2\epsilon$ dimensions. Thus, we again arrive at four-loop propagator-type integrals, that can be reduced to a set of master integrals using FIRE6. In fact, they reduce to the same set of 24 master integrals that already appear in the computation of $\gamma_{\mathcal{K}}^{(1,5)}$. Thus the Gram identities turn into linear relations among the 24 master integrals, with ϵ-dependent coefficients.

Plugging in the expressions (ϵ expansions) of the 20 known planar integrals [141,142] and the two known non-planar ones [138], we find constraints among the coefficients in (7.26). The constraints can be brought to the following form:

$$
\begin{aligned}
&a_3 = 0\,, \quad b_3 = 36\zeta_3^2\,, \\
&a_4 = -10\zeta_5\,, \quad b_4 = -\tfrac{5\pi^6}{189} + 2\zeta_3^2 + 50\zeta_5\,, \\
&c_4 = -\tfrac{32}{27}c_3 + \tfrac{25\pi^6}{189} + \tfrac{67}{45}\pi^4\zeta_3 + \tfrac{226}{3}\zeta_3^2 + 90\zeta_5 - \tfrac{1143}{2}\zeta_7\,.
\end{aligned}
\tag{7.27}
$$

In total, four of the coefficients are fixed, while the remaining two at linear order in ϵ are related by one equation. Notably, $\mathcal{I}_3$ is finite in ϵ. Let us mention, that this solution is formulated in the G-scheme used also in [141,142].

To determine the final two coefficients c_3 and c_4, we evaluate $\mathcal{I}_3$, which is linearly reducible: The integrations can be performed iteratively in a way that each intermediate integral is a hyperlogarithm. In addition, $\mathcal{I}_3$ involves comparatively few factors $1/x_{ij}^2$, and therefore can be evaluated with HyperInt [143]. We Fourier transform the integral to momentum representation using

$$
\mathcal{F}\left[\frac{1}{x^2}\right] = \frac{1}{\pi^{2-\epsilon}}\int d^{4-2\epsilon}x\,\frac{e^{ipx}}{x^2} = 4^{1-\epsilon}\frac{\Gamma(1-\epsilon)}{(p^2)^{1-\epsilon}}\,,
\tag{7.28}
$$

and evaluate the momentum integrals with non-integer propagator exponents. In this way, we obtain the ϵ-expansion of $\mathcal{I}_3$. The result validates the values of a_3 and b_3 found in (7.27), and determines the value of c_3. Finally, c_4 is obtained from the last equation in (7.27):

$$
\begin{aligned}
&c_3 = \tfrac{6\pi^4}{5}\zeta_3 + 72\zeta_3^2 - 567\zeta_7\,, \\
&c_4 = \tfrac{25\pi^6}{189} + \tfrac{\pi^4}{15}\zeta_3 - 10\zeta_3^2 + 90\zeta_5 + \tfrac{201}{2}\zeta_7\,.
\end{aligned}
\tag{7.29}
$$

We verify the solution of the integrals $\mathcal{I}_3$ and $\mathcal{I}_4$ numerically using FIESTA [144] up to four digits in precision, and find perfect agreement with our exact coefficients.

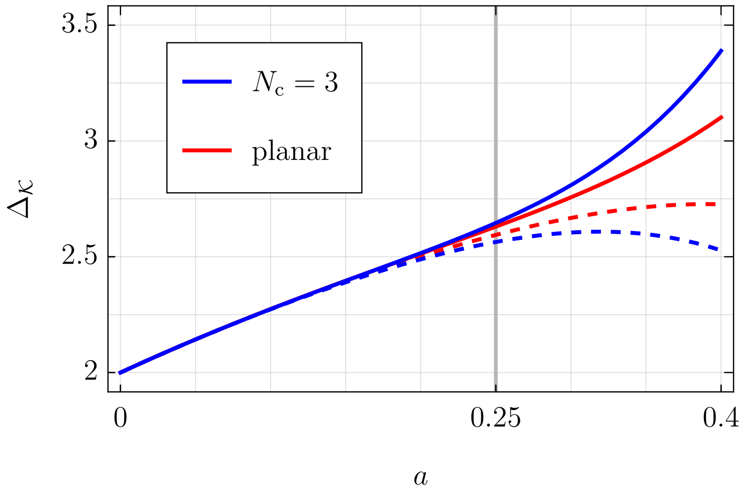

Figure 7.4.: The Konishi Dimension $\Delta_{\mathcal{K}}$ as a function of the coupling a for $N_c = \infty$ (red) and $N_c = 3$ (blue) at four loops (dashed) and five loops (solid) [3]. The radius of convergence of the planar theory is at $a = 1/4$.

7.5.3. Five-Loop Result

Gathering the results of all master integrals and plugging them into (7.24), finally yields the non-planar contribution to the anomalous dimension of the Konishi operator at five loops:

$$\boxed{\gamma_{\mathcal{K}}^{(1,5)} = 135\zeta_5 - \frac{243}{4}\zeta_3^2 + \frac{11907}{32}\zeta_7 \approx 427.406\,.} \tag{7.30}$$

Importantly, all poles in ϵ vanish in the final result of the anomalous dimension, which is a strong consistency check of the derivation. Furthermore, $\gamma_{\mathcal{K}}^{(1,5)}$ does not depend on even Zeta values, which agrees with general expectations [145, 146] as well as existing data [147, 148]. More subtly, there are also no terms with transcendentality weight zero and three. This is also the case for the non-planar correction of the four-loop Konishi anomalous dimension [148].

For reference, we record the complete five-loop scaling dimension of the Konishi operator:

$$\Delta_{\mathcal{K}} = 2 + 3a - 3a^2 + \frac{21}{4}a^3 + \left(-\frac{39}{4} + \frac{9}{4}\zeta_3 - \frac{45}{8}\left[1 + \frac{12}{N_c^2}\right]\zeta_5\right)a^4$$

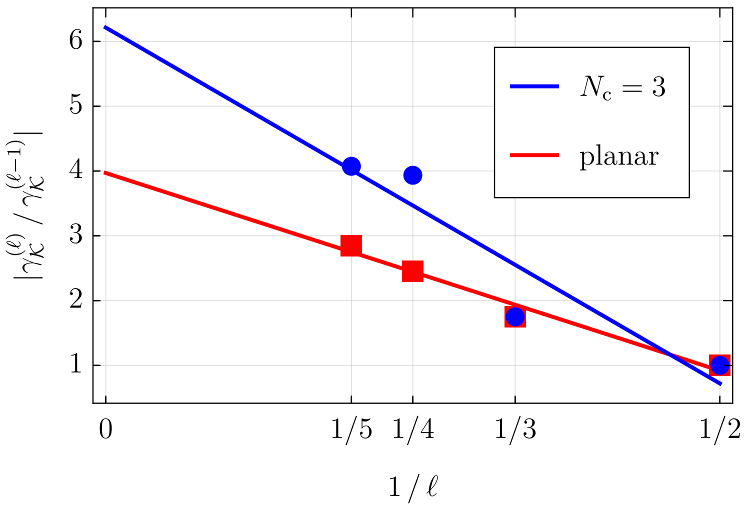

Figure 7.5.: Estimate of the convergence radius of the Konishi dimension weak-coupling expansion, for $N_c = \infty$ (squares, red) and for $N_c = 3$ (circles, blue) [3]. Shown are the ratios $|\gamma_{\mathcal{K}}^{(\ell)}/\gamma_{\mathcal{K}}^{(\ell-1)}|$ as in (7.33), as a function of $1/\ell$, as well as linear fits whose intersections with $1/\ell = 0$ yield the numbers in (7.33).

$$
\begin{aligned}
&+ \left(\frac{237}{16} + \frac{27}{4}\zeta_3 - \frac{135}{16}\left[1 - \frac{16}{N_c^2}\right]\zeta_5 - \frac{81}{16}\left[1 + \frac{12}{N_c^2}\right]\zeta_3^2 \right. \\
&\qquad \left. + \frac{189}{32}\left[5 + \frac{63}{N_c^2}\right]\zeta_7 \right) a^5 + \mathcal{O}(a^6) \\
&\approx 2 + 3a - 3a^2 + 5.25a^3 - \left(12.878 + \frac{69.993}{N_c^2}\right) a^4 \\
&\quad + \left(36.64 + \frac{427.406}{N_c^2}\right) a^5 + \mathcal{O}(a^6)\,.
\end{aligned} \tag{7.31}
$$

The planar parts were found in [149], [150, 151], [152], [153–155], and [156–158] at one, two, three, four, and five loops, respectively. The four-loop $1/N_c^2$ non-planar correction term was found in [148]. The planar parts were re-derived in [138], which also established the method employed in this chapter.

It is known that the weak-coupling expansion of the planar theory in the $N_c \to \infty$ limit converges for $a < 1/4$ [159]. The coefficients in the Konishi dimension (7.31) indicate that the radius of convergence will shrink at finite N_c, as expected in a general Yang–Mills theory. A plot of the Konishi dimension for different values of

N_c is shown in Figure 7.4. Writing the Konishi dimension as

$$\Delta_\mathcal{K} = 2 + \sum_{\ell=0}^{\infty} \gamma_\mathcal{K}^{(\ell)} a^\ell \,, \tag{7.32}$$

we can estimate the radius of convergence as

$$\lim_{\ell\to\infty} \left| \frac{\gamma_\mathcal{K}^{(\ell)}}{\gamma_\mathcal{K}^{(\ell-1)}} \right| \approx \begin{cases} 1/0.25 & N_\mathrm{c} = \infty \,, \\ 1/0.16 & N_\mathrm{c} = 3 \,, \end{cases} \tag{7.33}$$

see Figure 7.5. The number 0.25 for $N_\mathrm{c} = \infty$ is expected, and the lower number 0.16 confirms that the radius of convergence shrinks at finite N_c.

8. Conclusion

In this thesis, we have explored correlation functions of protected half-BPS operators in $\mathcal{N} = 4$ supersymmetric Yang–Mills theory. By leveraging the symmetries of the theory and employing advanced computational methods, most notably the twistor space reformulation, we have extended the range of known perturbative results along several directions: multiplicity, loop order, R-charge, and topology. The core of this work is divided into four results chapters. We now summarize the main findings and discuss open questions.

Generating Functions (Chapter 4). The investigation began with the study of generating functions for planar correlation functions of scalar half-BPS operators with arbitrary R-charge. These objects unify an infinite set of fixed-charge correlators into a single function. Building on the work of [65,69], we explicitly determined the five-point generating function at one and two loops, as well as the six-point generating function at one loop. These generating functions reorganize the dependence on R-charge into geometric series that are poles in ten-dimensional distances

$$X_{ij}^2 = x_{ij}^2 + y_{ij}^2 \,,$$

thereby unifying spacetime and internal R-symmetry coordinates. This representation allows one to systematically extract correlators of fixed R-charge while maintaining a compact formulation.

The generating functions exhibit a nested structure in which higher-point correlators are expressed in terms of lower-point functions, as discussed in Section 4.7. In particular, for the five-point one-loop generating function, contributions localized on simple and double poles in X_{ij}^2 are governed by four- and five-point correlators of the lightest operators, which are reminiscent to earlier recursive constructions [63]. This pattern persists at higher multiplicity and loop order, although it becomes more intricate: higher-order poles are determined by lower-point generating functions, while the leading contributions proportional to simple poles are given by linear combinations of fixed-charge correlators. Importantly, these structures are not artifacts of perturbation theory, but can already be traced back to the combinatorics of free-theory Wick contractions.

At two loops, we extended the known $\mathbf{20'}$ two-loop five-point integrand [60] by determining the corresponding generating function at the integrand level. The resulting expressions can be written in the same basis of conformal integrals as in the $\mathbf{20'}$ case. Naturally, the coefficients dressing these integrals are promoted to rational functions featuring ten-dimensional poles. The explicit evaluation of these integrals had been largely restricted to special limits [77, 121], but recent work has enabled their complete computation [160], thereby providing access to the full generating function.

A structural feature of the generating functions is the emergence of ten-dimensional conformal symmetry at the level of the integrand. This symmetry, which combines spacetime and R-symmetry transformations into an $SO(10,2)$ group, is well established in the four-point case, where it is conjectured to hold to all loop order [65]. At four points, the manifestation of this symmetry relies on separating the unique superconformal invariant from the reduced correlator, which exhibits this symmetry. To make the ten-dimensional symmetry visible at higher points, it is therefore natural to expect that one must first decompose the higher-point functions into superconformal invariants. The construction of such higher-point invariants is still under investigation, see [68, 117, 161] for developments. We hope that the data obtained here will help to draw further conclusions in this direction.

Furthermore, by means of light-ray transforms, correlators of local operators can be reformulated as correlators of detectors, such as the three-point energy correlator (EEEC) [40, 162, 163]. Since our generating function provides access to arbitrary R-charges, it offers a natural framework to extend EEEC analyses to heavy states created by operators with large or unrestricted R-charge [164].

Ten-Dimensional Null Polygons (Chapter 5). Building on the notion of generating functions, we turned to the study of n-point polygon correlators, which arise in the ten-dimensional null polygonal limit. These objects generalize the well-known octagon [70, 71] to arbitrary multiplicity and are conjectured to be dual to massive scattering amplitudes on the Coulomb branch [65]. We established a direct twistor-space prescription for computing these polygons by restricting the sum over Feynman graphs to those with disk topology. This approach significantly reduces computational complexity, as the number of disk graphs is orders of magnitude smaller than the full set of planar graphs. Using this prescription, we determined the one-loop and parity-even two-loop integrands for polygons of arbitrary multiplicity. In the case of massless scattering amplitudes, the determination of the two-loop MHV amplitude for any number of points [129, 165] was an important milestone for many later developments and discoveries. One may hope that many features of these massless amplitudes extend to the polygons.

In this context, it would be interesting to investigate whether polygon functions admit a geometric representation. For massless MHV amplitudes, such a description is provided by the amplituhedron [166], and proposals for its deformation have been put forward [120]. A natural question is how these ideas can be extended to incorporate polygon functions and establish a connection to massive amplitudes on the Coulomb branch. This direction appears particularly promising in light of the increasing amount of perturbative data available for massive amplitudes, see for instance [167].

The construction of polygon functions via a ten-dimensional null limit of generating functions closely parallels the correlator/amplitude duality in $\mathcal{N} = 4$ SYM [38, 101] (see Figure 5.4). This duality admits an extension that incorporates the full supermultiplets on both sides [80, 103]. In this context, it is natural to ask to what extent the generating function/polygon framework persists once supersymmetric degrees of freedom are included. In particular, this may provide insight into whether, and in what form, Yangian symmetry continues to hold for polygon functions [18]. A promising approach is to employ the twistor formulation of the theory and construct additional objects with Grassmann degrees of freedom that could reveal an extended version of the duality.

Higher-Loop Pentagon Integrand (Chapter 6). The third major direction focused on pushing the loop order for a higher-point observable, namely the five-point pentagon function. Drawing inspiration from the bootstrap program for massless amplitudes, we adapted soft and collinear constraints [130, 131] to the case of massive, off-shell kinematics. We demonstrated that these constraints are remarkably powerful: up to five loops, they uniquely fix all coefficients in a constrained ansatz built from planar dual-conformal integrals with disc topology. Moreover, applying these constraints at six loops reduces the pentagon integrand to a solution parameterized by only 23 remaining unknowns. The results were verified through an independent twistor computation using the methods developed in the preceding chapters up to four-loop order.

The results exhibit what is likely the most striking appearance of ten-dimensional symmetry in a five-point function in perturbation theory. The loop integrand appears to decompose into two contributions multiplied by the factors $R^{(5,1)}_{1234}$ and $R^{(5,2)}_{12345}$ (see (6.16)). It seems likely that these factors are descendants of five-point superconformal invariants that survive the ten-dimensional null limit. The coefficients dressing these invariants display intriguing features suggestive of ten-dimensional conformal symmetry $\mathrm{SO}(10,2)$. They are given by dual-conformal integrals dressed with ten-dimensional distances X^2_{ij}. More definitive conclusions could be drawn by including higher-KK modes of the Lagrangian insertions. In that case, the coefficients may be promoted to exhibit full ten-dimensional symmetry, and additional invariants could emerge.

In any case, the perturbative data obtained here provide valuable guidance for further investigations into the emergence of ten-dimensional symmetry in the weak-coupling expansion of $\mathcal{N}=4$ SYM.

Non-Planar Four-Point Integrand (Chapter 7). Finally, we moved beyond the planar limit and considered non-planar corrections in the theory. We focused on the four-point correlation function of the lightest protected scalar operators ($\mathbf{20'}$). The first non-planar corrections appear at four loops, and the corresponding integrand was ultimately computed in [59]. We extended this analysis to five loops, observing that there is again only a single non-planar correction at order $1/N_\mathrm{c}^2$. To overcome the computational bottleneck associated with Grassmann contractions involving 20 variables, we developed and implemented a GPU-accelerated algorithm based on finite fields. As a first application, we extracted the genus-one five-loop contribution to the Konishi anomalous dimension. Our result,

$$\gamma_{\mathcal{K}}^{(1,5)} = 135\zeta_5 - \frac{243}{4}\zeta_3^2 + \frac{11907}{32}\zeta_7 \approx 427.406\,,$$

satisfies all expected consistency checks, including the absence of even zeta values and the reduction of the radius of convergence for the Konishi dimension at finite N_c. Moreover, the anomalous dimension lacks a purely rational term and a contribution of transcendental weight 3, as was already observed for the genus-one contribution at four loops [154]. This points to structural features of non-planar corrections that persist at higher-loop orders.

An interesting open question is whether the non-planar integrand can be fully determined from analytic constraints alone. For instance, the non-planar part of the

logarithm of $G_4^{(\ell)}/G_4^{(0)}$ is expected to exhibit at most $\log^{\ell-1}$ singularities at ℓ loops in the light-cone limit [53]. This property is not necessarily fully captured by the constraints (7.8) and (7.9). Additional constraints may be obtained by matching the f-graph periods [168] to the known fully integrated correlator [169, 170].
The objects we have constructed also allow access to a lot of additional dynamical data. In the non-planar sector, very little is known about scaling dimensions and structure constants in $\mathcal{N} = 4$ SYM. Extracting these from our five-loop result requires state-of-the-art integral-reduction techniques and the evaluation of complicated master integrals. Particular interesting observables include the Konishi OPE coefficient [171], the twist-two spin-J anomalous dimensions and OPE coefficients [59, 138, 148], and the cusp anomalous dimension [172]. Extracting some of this data would provide valuable insight, particularly also because of their relevance to the respective QCD counterparts.

In summary, this work has developed new methods and produced explicit results for correlation functions of half-BPS operators in $\mathcal{N} = 4$ SYM across a range of regimes, including higher multiplicity, higher-loop order, and non-planar corrections. By combining twistor-space techniques, bootstrap constraints, and numerical methods, we have obtained new data for generating functions, polygon observables, and non-planar integrands, and uncovered structural features such as recursive pole behavior and indications of ten-dimensional symmetry. While many aspects remain to be understood in greater depth, these results provide a set of concrete benchmarks that may help guide future investigations. We hope that the approaches and data presented here will contribute to a more complete understanding of the perturbative structure of $\mathcal{N} = 4$ SYM and its underlying symmetries, and that they may also help guide future non-perturbative explorations by providing useful boundary data.

A. Guide to Ancillary Files

In this thesis, we study loop integrands of correlation functions of scalar half-BPS operators at higher charge, loop order, and multiplicity. Many of the expressions obtained in this context are too large to be presented explicitly. Moreover, writing them out in full would obscure, rather than clarify, their underlying structure. For this reason, we do not display these expressions explicitly, following the presentation adopted in the publications on which this thesis is based. Instead, all relevant results are provided in the form of ancillary data files, which were released together with the corresponding manuscripts on the arXiv.

In this appendix, we summarize the available files, thereby making the results presented in this thesis fully accessible.

Chapter 4: Generating Functions
The following files are provided at https://arxiv.org/src/2509.14332/anc:

- `G52CorrelatorBasis.m`: The file constructs the parity-even two-loop five-point generating function $G_{5,2}$ from the basis of (modified) R-charge correlators given in the first line of (4.73) The R-charge correlators are given as explicit expressions of d_{ij} and x_{ij}^2, which are fully symmetrized over the permutation group that respects the charge configuration of the respective R-charge correlator.

- `G60.m`: The file generates the expression for the leading-order six-point generating function $G_{6,0}$. It is computed from a minimal expression $G_{6,0}^{\text{seed}}$ by summing over S_6 permutations.

- `G70.m`: The file generates the expression for the leading-order seven-point generating function $G_{7,0}$. It is computed from a minimal expression $G_{7,0}^{\text{seed}}$ by summing over S_7 permutations.

Chapter 5: Ten-Dimensional Null Polygons

The following files are provided at https://arxiv.org/src/2512.19780/anc:

- `polygons.m`: The file produces the expression for the polygons of any number of up to two loops. Specifically, it includes the decomposition of the polygons into faces (5.35), and the full one-loop faces (5.45) and parity-even two-loop faces (5.47).
- `twoLoopCoefficients.m`: The file contains a list of all coefficients $f_{k,\mathtt{e},a,b}$ as functions of x_{ij}^2 adn y_{ij}^2 that dress the different denominator topologies of the two-loop faces (5.47).

Chapter 6: Higher-Loop Pentagon Integrand

The manuscript is to be published, and the ancillary files will be made available with the corresponding arXiv submission.

Chapter 7: The Non-Planar Four-Point Integrand at Five Loops

The following file is provided at https://arxiv.org/src/2511.21807/anc:

- `solution.m`: The file guides through the production of the genus-one five-loop four-point integrand. Together with data files contained in `solution/`, it contains a list of all relevant f-graphs, the particular solution displayed in Figure 7.2, and the set of all 208 Gram identities parameterizing the solution.

Bibliography

[1] T. Bargheer, A. Bekov, C. Bercini and F. Coronado, *Higher-point correlators in $\mathcal{N} = 4$ SYM: generating functions*, *JHEP* **02** (2026) 161 [2509.14332].

[2] T. Bargheer, A. Bekov, C. Bercini and F. Coronado, *Higher-Point Correlators in N=4 SYM: Ten-Dimensional Null Polygons*, 2512.19780.

[3] T. Bargheer and A. Bekov, *The Non-Planar Four-Point Integrand and Konishi Dimension in N=4 Super Yang-Mills Theory at Five Loops*, 2511.21807.

[4] T. Bargheer and A. Bekov, *The Higher-Loop Pentagon Integrand in N=4 SYM*, *To appear* (2026) .

[5] F. Gliozzi, J. Scherk and D. I. Olive, *Supersymmetry, supergravity theories and the dual spinor model*, *Nucl. Phys.* **B122** (1977) 253.

[6] L. Brink, J. H. Schwarz and J. Scherk, *Supersymmetric Yang–Mills theories*, *Nucl. Phys.* **B121** (1977) 77.

[7] L. Susskind, *The world as a hologram*, *J. Math. Phys.* **36** (1995) 6377 [hep-th/9409089].

[8] J. M. Maldacena, *The large n limit of superconformal field theories and supergravity*, *Adv. Theor. Math. Phys.* **2** (1998) 231 [hep-th/9711200].

[9] E. Witten, *Anti de Sitter space and holography*, *Adv. Theor. Math. Phys.* **2** (1998) 253 [hep-th/9802150].

[10] S. S. Gubser, I. R. Klebanov and A. M. Polyakov, *Gauge theory correlators from noncritical string theory*, *Phys. Lett. B* **428** (1998) 105 [hep-th/9802109].

[11] G. 't Hooft, *A planar diagram theory for strong interactions*, *Nucl. Phys.* **B72** (1974) 461.

[12] N. Beisert, C. Ahn, L. F. Alday, Z. Bajnok, J. M. Drummond, L. Freyhult et al., *Review of AdS/CFT integrability: An overview*, *Lett. Math. Phys.* **99** (2012) 3 [1012.3982].

[13] J. A. Minahan and K. Zarembo, *The Bethe ansatz for N=4 superYang-Mills*, *JHEP* **03** (2003) 013 [hep-th/0212208].

[14] N. Beisert and M. Staudacher, *Long-range psu(2,2|4) Bethe Ansatze for gauge theory and strings*, *Nucl. Phys. B* **727** (2005) 1 [hep-th/0504190].

[15] N. Gromov, V. Kazakov, S. Leurent and D. Volin, *Quantum spectral curve for planar $\mathcal{N} = 4$ super-Yang–Mills theory*, *Phys. Rev. Lett.* **112** (2014) 011602 [1305.1939].

[16] N. Gromov, V. Kazakov, S. Leurent and D. Volin, *Quantum spectral curve for arbitrary state/operator in AdS_5/CFT_4*, *JHEP* **09** (2015) 187 [1405.4857].

[17] J. M. Drummond, J. Henn, G. P. Korchemsky and E. Sokatchev, *Dual superconformal symmetry of scattering amplitudes in $\mathcal{N} = 4$ super-Yang–Mills theory*, *Nucl. Phys.* **B828** (2010) 317 [0807.1095].

[18] J. M. Drummond, J. M. Henn and J. Plefka, *Yangian symmetry of scattering amplitudes in N=4 super Yang-Mills theory*, *JHEP* **05** (2009) 046 [0902.2987].

[19] R. Britto, F. Cachazo, B. Feng and E. Witten, *Direct proof of tree-level recursion relation in Yang–Mills theory*, *Phys. Rev. Lett.* **94** (2005) 181602 [hep-th/0501052].

[20] N. Arkani-Hamed, J. L. Bourjaily, F. Cachazo, S. Caron-Huot and J. Trnka, *The All-Loop Integrand For Scattering Amplitudes in Planar N=4 SYM*, *JHEP* **01** (2011) 041 [1008.2958].

[21] N. Arkani-Hamed, J. L. Bourjaily, F. Cachazo and J. Trnka, *Local Integrals for Planar Scattering Amplitudes*, *JHEP* **06** (2012) 125 [1012.6032].

[22] B. Basso, S. Komatsu and P. Vieira, *Structure constants and integrable bootstrap in planar $\mathcal{N} = 4$ SYM theory*, 1505.06745.

[23] T. Fleury and S. Komatsu, *Hexagonalization of correlation functions*, *JHEP* **01** (2017) 130 [1611.05577].

[24] R. Penrose, *Twistor Algebra*, *Journal of Mathematical Physics* **8** (1967) 345.

[25] R. Penrose, *Solutions of the zero-rest-mass equations*, *J. Math. Phys.* **10** (1969) 38.

[26] R. S. Ward, *On Selfdual gauge fields*, *Phys. Lett. A* **61** (1977) 81.

[27] E. Witten, *Perturbative gauge theory as a string theory in twistor space*, *Commun. Math. Phys.* **252** (2004) 189 [hep-th/0312171].

[28] L. J. Mason, *Twistor actions for non-self-dual fields: A Derivation of twistor-string theory*, *JHEP* **10** (2005) 009 [hep-th/0507269].

[29] R. Boels, L. J. Mason and D. Skinner, *Supersymmetric gauge theories in twistor space*, *JHEP* **02** (2007) 014 [hep-th/0604040].

[30] L. F. Alday, B. Eden, G. P. Korchemsky, J. Maldacena and E. Sokatchev, *From correlation functions to Wilson loops*, *JHEP* **1109** (2011) 123 [1007.3243].

[31] L. F. Alday and J. M. Maldacena, *Gluon scattering amplitudes at strong coupling*, *JHEP* **06** (2007) 064 [0705.0303].

[32] N. Berkovits and J. Maldacena, *Fermionic T-duality, dual superconformal symmetry, and the amplitude/Wilson loop connection*, *JHEP* **09** (2008) 062 [0807.3196].

[33] N. Beisert, R. Ricci, A. A. Tseytlin and M. Wolf, *Dual superconformal symmetry from $AdS_5 \times S^5$ superstring integrability*, *Phys. Rev.* **D78** (2008) 126004 [0807.3228].

[34] Z. Bern, L. J. Dixon, D. A. Kosower, R. Roiban, M. Spradlin, C. Vergu et al., *The two-loop six-gluon MHV amplitude in maximally supersymmetric Yang–Mills theory*, *Phys. Rev.* **D78** (2008) 045007 [0803.1465].

[35] J. M. Drummond, J. Henn, G. P. Korchemsky and E. Sokatchev, *Hexagon Wilson loop = six-gluon MHV amplitude*, *Nucl. Phys.* **B815** (2009) 142 [0803.1466].

[36] L. Mason and D. Skinner, *The complete planar S-matrix of $\mathcal{N} = 4$ SYM as a Wilson loop in twistor space*, *JHEP* **12** (2010) 018 [1009.2225].

[37] S. Caron-Huot, *Notes on the scattering amplitude / Wilson loop duality*, *JHEP* **07** (2011) 058 [1010.1167].

[38] B. Eden, G. P. Korchemsky and E. Sokatchev, *From correlation functions to scattering amplitudes*, *JHEP* **1112** (2011) 002 [1007.3246].

[39] A. V. Belitsky, S. Hohenegger, G. P. Korchemsky, E. Sokatchev and A. Zhiboedov, *Energy-energy correlations in $\mathcal{N} = 4$ supersymmetric Yang–Mills theory*, *Phys. Rev. Lett.* **112** (2014) 071601 [1311.6800].

[40] I. Moult and H. X. Zhu, *Energy correlators: A journey from theory to experiment*, 2506.09119.

[41] B. Eden, P. Heslop, G. P. Korchemsky and E. Sokatchev, *Hidden symmetry of four-point correlation functions and amplitudes in $\mathcal{N} = 4$ SYM*, *Nucl. Phys. B* **862** (2012) 193 [1108.3557].

[42] J. Drummond, C. Duhr, B. Eden, P. Heslop, J. Pennington and V. A. Smirnov, *Leading singularities and off-shell conformal integrals*, *JHEP* **1308** (2013) 133 [1303.6909].

[43] G. Arutyunov and S. Frolov, *Four point functions of lowest weight cpos in $\mathcal{N} = 4$ SYM(4) in supergravity approximation*, *Phys. Rev.* **D62** (2000) 064016 [hep-th/0002170].

[44] V. Gonçalves, *Four point function of $\mathcal{N} = 4$ stress-tensor multiplet at strong coupling*, *JHEP* **1504** (2015) 150 [1411.1675].

[45] L. F. Alday and T. Hansen, *The ads Virasoro-Shapiro amplitude*, *JHEP* **10** (2023) 023 [2306.12786].

[46] C. Beem, L. Rastelli and B. C. van Rees, *More $\mathcal{N} = 4$ superconformal bootstrap*, *Phys. Rev. D* **96** (2017) 046014 [1612.02363].

[47] S. M. Chester, R. Dempsey and S. S. Pufu, *Level repulsion in $\mathcal{N} = 4$ super-Yang–Mills via integrability, holography, and the bootstrap*, *JHEP* **07** (2024) 059 [2312.12576].

[48] S. Caron-Huot, F. Coronado, A.-K. Trinh and Z. Zahraee, *Bootstrapping $\mathcal{N} = 4$ sym correlators using integrability*, *JHEP* **02** (2023) 083 [2207.01615].

[49] S. Caron-Huot, F. Coronado and Z. Zahraee, *Bootstrapping $\mathcal{N} = 4$ sym correlators using integrability and localization*, *JHEP* **05** (2025) 220 [2412.00249].

[50] D. Chicherin, J. Drummond, P. Heslop and E. Sokatchev, *All three-loop four-point correlators of half-BPS operators in planar $\mathcal{N} = 4$ SYM*, *JHEP* **08** (2016) 053 [1512.02926].

[51] D. Chicherin, A. Georgoudis, V. Gonçalves and R. Pereira, *All five-loop planar four-point functions of half-BPS operators in $\mathcal{N} = 4$ SYM*, *JHEP* **11** (2018) 069 [1809.00551].

[52] K. A. Intriligator and W. Skiba, *Bonus symmetry and the operator product expansion of $\mathcal{N} = 4$ super-Yang–Mills*, *Nucl. Phys.* **B559** (1999) 165 [hep-th/9905020].

[53] B. Eden, P. Heslop, G. P. Korchemsky and E. Sokatchev, *Constructing the correlation function of four stress-tensor multiplets and the four-particle amplitude in $\mathcal{N} = 4$ SYM*, *Nucl. Phys.* **B862** (2012) 450 [1201.5329].

[54] R. G. Ambrosio, B. Eden, T. Goddard, P. Heslop and C. Taylor, *Local integrands for the five-point amplitude in planar $\mathcal{N} = 4$ SYM up to five loops*, *JHEP* **01** (2015) 116 [1312.1163].

[55] J. L. Bourjaily, P. Heslop and V.-V. Tran, *Perturbation Theory at Eight Loops: Novel Structures and the Breakdown of Manifest Conformality in N=4 Supersymmetric Yang-Mills Theory*, *Phys. Rev. Lett.* **116** (2016) 191602 [1512.07912].

[56] J. L. Bourjaily, P. Heslop and V.-V. Tran, *Amplitudes and correlators to ten loops using simple, graphical bootstraps*, *JHEP* **11** (2016) 125 [1609.00007].

[57] S. He, C. Shi, Y. Tang and Y.-Q. Zhang, *The cusp limit of correlators and a new graphical bootstrap for correlators/amplitudes to eleven loops*, *JHEP* **03** (2025) 192 [2410.09859].

[58] J. L. Bourjaily, S. He, C. Shi and Y. Tang, *The four-point correlator of planar sym at twelve loops*, 2503.15593.

[59] T. Fleury and R. Pereira, *Non-planar data of $\mathcal{N} = 4$ SYM*, *JHEP* **03** (2020) 003 [1910.09428].

[60] T. Bargheer, T. Fleury and V. Gonçalves, *Higher-point integrands in $\mathcal{N} = 4$ super Yang–Mills theory*, *SciPost Phys.* **15** (2023) 059 [2212.03773].

[61] V. Gonçalves, R. Pereira and X. Zhou, $20'$ *five-point function from* $ads_5 \times s^5$ *supergravity*, *JHEP* **10** (2019) 247 [1906.05305].

[62] V. Gonçalves, M. Nocchi and X. Zhou, *Dissecting supergraviton six-point function with lightcone limits and chiral algebra*, *JHEP* **06** (2025) 173 [2502.10269].

[63] N. Drukker and J. Plefka, *The structure of n-point functions of chiral primary operators in $\mathcal{N} = 4$ super Yang–Mills at one-loop*, *JHEP* **0904** (2009) 001 [0812.3341].

[64] S. Caron-Huot and A.-K. Trinh, *All tree-level correlators in* $ads_5 \times s_5$ *supergravity: hidden ten-dimensional conformal symmetry*, *JHEP* **01** (2019) 196 [1809.09173].

[65] S. Caron-Huot and F. Coronado, *Ten dimensional symmetry of $\mathcal{N} = 4$ SYM correlators*, *JHEP* **03** (2022) 151 [2106.03892].

[66] B. Eden, A. C. Petkou, C. Schubert and E. Sokatchev, *Partial non-renormalisation of the stress-tensor four-point function in $\mathcal{N} = 4$ SYM$_4$ and AdS/CFT*, *Nucl. Phys.* **B607** (2001) 191 [hep-th/0009106].

[67] P. Heslop, *The SAGEX review on scattering amplitudes, chapter 8: Half BPS correlators*, *J. Phys. A* **55** (2022) 443009 [2203.13019].

[68] B. Fernandes, V. Gonçalves, Z. Huang, Y. Tang, J. Vilas Boas and E. Y. Yuan, *Ads×s mellin bootstrap, hidden 10d symmetry and five-point Kaluza-Klein functions in $\mathcal{N} = 4$ SYM*, 2507.14124.

[69] S. Caron-Huot, F. Coronado and B. Mühlmann, *Determinants in self-dual $\mathcal{N} = 4$ SYM and twistor space*, *JHEP* **08** (2023) 008 [2304.12341].

[70] F. Coronado, *Perturbative four-point functions in planar $\mathcal{N} = 4$ SYM from hexagonalization*, *JHEP* **01** (2019) 056 [1811.00467].

[71] F. Coronado, *Bootstrapping the simplest correlator in planar $\mathcal{N} = 4$ SYM at all loops*, *Phys. Rev. Lett.* **124** (2020) 171601 [1811.03282].

[72] I. Kostov, V. B. Petkova and D. Serban, *Determinant formula for the octagon form factor in $\mathcal{N} = 4$ SYM*, Phys. Rev. Lett. **122** (2019) 231601 [1903.05038].

[73] I. Kostov, V. B. Petkova and D. Serban, *The octagon as a determinant*, *JHEP* **11** (2019) 178 [1905.11467].

[74] A. V. Belitsky and G. P. Korchemsky, *Exact null octagon*, *JHEP* **05** (2020) 070 [1907.13131].

[75] A. V. Belitsky and G. P. Korchemsky, *Octagon at finite coupling*, *JHEP* **07** (2020) 219 [2003.01121].

[76] T. Fleury and V. Gonçalves, *Decagon at two loops*, *JHEP* **07** (2020) 030 [2004.10867].

[77] C. Bercini, B. Fernandes and V. Gonçalves, *Two-loop five-point integrals: light, heavy and large-spin correlators*, *JHEP* **10** (2024) 242 [2401.06099].

[78] F. A. Dolan and H. Osborn, *Superconformal symmetry, correlation functions and the operator product expansion*, Nucl. Phys. B **629** (2002) 3 [hep-th/0112251].

[79] E. D'Hoker and D. Z. Freedman, *Supersymmetric gauge theories and the AdS / CFT correspondence*, in *Theoretical Advanced Study Institute in Elementary Particle Physics (TASI 2001): Strings, Branes and EXTRA Dimensions*, pp. 3–158, 1, 2002, hep-th/0201253.

[80] B. Eden, P. Heslop, G. P. Korchemsky and E. Sokatchev, *The super-correlator/super-amplitude duality: Part i*, Nucl. Phys. **B869** (2013) 329 [1103.3714].

[81] R. Grimm, M. Sohnius and J. Wess, *Extended supersymmetry and gauge theories*, *Nuclear Physics B* **133** (1978) 275.

[82] J. Polchinski, *Scale and Conformal Invariance in Quantum Field Theory*, Nucl. Phys. B **303** (1988) 226.

[83] Y. Nakayama, *Scale invariance vs conformal invariance*, Phys. Rept. **569** (2015) 1 [1302.0884].

[84] K. Konishi, *Anomalous Supersymmetry Transformation of Some Composite Operators in SQCD*, *Phys. Lett. B* **135** (1984) 439.

[85] S. Penati, A. Santambrogio and D. Zanon, *Two point functions of chiral operators in N=4 SYM at order g**4*, *JHEP* **12** (1999) 006 [hep-th/9910197].

[86] S. Penati, A. Santambrogio and D. Zanon, *More on correlators and contact terms in N=4 SYM at order g**4*, *Nucl. Phys. B* **593** (2001) 651 [hep-th/0005223].

[87] A. Galperin, E. Ivanov, S. Kalitzin, V. Ogievetsky and E. Sokatchev, *Unconstrained N=2 Matter, Yang-Mills and Supergravity Theories in Harmonic Superspace*, *Class. Quant. Grav.* **1** (1984) 469.

[88] P. S. Howe and P. C. West, *AdS/SCFT in superspace*, *Class. Quant. Grav.* **18** (2001) 3143 [hep-th/0105218].

[89] P. J. Heslop and P. S. Howe, *A note on composite operators in N=4 SYM*, *Phys. Lett. B* **516** (2001) 367 [hep-th/0106238].

[90] P. J. Heslop and P. S. Howe, *OPEs and 3-point correlators of protected operators in N=4 SYM*, *Nucl. Phys. B* **626** (2002) 265 [hep-th/0107212].

[91] P. J. Heslop, *Superconformal field theories in analytic superspace*, *Class. Quant. Grav.* **19** (2002) 303 [hep-th/0108235].

[92] P. J. Heslop and P. S. Howe, *Four-point functions in N=4 SYM*, *JHEP* **01** (2003) 043 [hep-th/0211252].

[93] P. J. Heslop and P. S. Howe, *Aspects of N=4 SYM*, *JHEP* **01** (2004) 058 [hep-th/0307210].

[94] G. Arutyunov, F. A. Dolan, H. Osborn and E. Sokatchev, *Correlation functions and massive Kaluza-Klein modes in the AdS / CFT correspondence*, *Nucl. Phys. B* **665** (2003) 273 [hep-th/0212116].

[95] K. A. Intriligator, *Bonus symmetries of $\mathcal{N} = 4$ super-Yang–Mills correlation functions via AdS duality*, *Nucl. Phys.* **B551** (1999) 575 [hep-th/9811047].

[96] E. D'Hoker, D. Z. Freedman and W. Skiba, *Field theory tests for correlators in the AdS / CFT correspondence*, Phys. Rev. D **59** (1999) 045008 [hep-th/9807098].

[97] S. Lee, S. Minwalla, M. Rangamani and N. Seiberg, *Three point functions of chiral operators in D = 4, N=4 SYM at large N*, Adv. Theor. Math. Phys. **2** (1998) 697 [hep-th/9806074].

[98] P. S. Howe, E. Sokatchev and P. C. West, *Three point functions in N=4 Yang-Mills*, Phys. Lett. B **444** (1998) 341 [hep-th/9808162].

[99] J. M. Drummond, G. P. Korchemsky and E. Sokatchev, *Conformal properties of four-gluon planar amplitudes and Wilson loops*, Nucl. Phys. **B795** (2008) 385 [0707.0243].

[100] A. Brandhuber, P. Heslop and G. Travaglini, *MHV amplitudes in $\mathcal{N} = 4$ super Yang–Mills and Wilson loops*, Nucl. Phys. **B794** (2008) 231 [0707.1153].

[101] B. Eden, G. P. Korchemsky and E. Sokatchev, *More on the duality correlators/amplitudes*, Phys. Lett. B **709** (2012) 247 [1009.2488].

[102] T. Adamo, M. Bullimore, L. Mason and D. Skinner, *A proof of the supersymmetric correlation function / Wilson loop correspondence*, JHEP **08** (2011) 076 [1103.4119].

[103] B. Eden, P. Heslop, G. P. Korchemsky and E. Sokatchev, *The super-correlator/super-amplitude duality: Part II*, Nucl. Phys. **B869** (2013) 378 [1103.4353].

[104] F. Aprile, J. M. Drummond, P. Heslop, H. Paul, F. Sanfilippo, M. Santagata et al., *Single particle operators and their correlators in free $\mathcal{N} = 4$ SYM*, JHEP **11** (2020) 072 [2007.09395].

[105] D. Chicherin, R. Doobary, B. Eden, P. Heslop, G. P. Korchemsky, L. Mason et al., *Correlation functions of the chiral stress-tensor multiplet in $\mathcal{N} = 4$ SYM*, JHEP **06** (2015) 198 [1412.8718].

[106] T. Adamo, *Twistor actions for gauge theory and gravity*, 1308.2820.

[107] G. Chalmers and W. Siegel, *Self-dual sector of qcd amplitudes*, *Phys. Rev. D* **54** (1996) 7628 [hep-th/9606061].

[108] F. Cachazo, P. Svrcek and E. Witten, *MHV vertices and tree amplitudes in gauge theory*, *JHEP* **09** (2004) 006 [hep-th/0403047].

[109] T. Bargheer, J. Caetano, T. Fleury, S. Komatsu and P. Vieira, *Handling handles. part II. stratification and data analysis*, *JHEP* **11** (2018) 095 [1809.09145].

[110] G. Arutyunov and S. Frolov, *Some cubic couplings in type iib supergravity on ads(5) x s**5 and three point functions in SYM(4) at large n*, *Phys. Rev. D* **61** (2000) 064009 [hep-th/9907085].

[111] B. Eden, P. Heslop and L. Mason, *The correlahedron*, *JHEP* **09** (2017) 156 [1701.00453].

[112] S. He, Y.-t. Huang and C.-K. Kuo, *All-loop geometry for four-point correlation functions*, *Phys. Rev. D* **110** (2024) L081701 [2405.20292].

[113] S. He, Y.-t. Huang and C.-K. Kuo, *Leading singularities and chambers of correlahedron*, 2505.09808.

[114] S. He, X. Jiang, J. Liu and Y.-Q. Zhang, *Notes on conformal integrals: Coulomb branch amplitudes, magic identities and bootstrap*, 2502.08871.

[115] S. He and X. Jiang, *Solving infinite families of dual conformal integrals and periods*, 2506.20095.

[116] N. Drukker and J. Plefka, *Superprotected n-point correlation functions of local operators in $\mathcal{N} = 4$ super Yang–Mills*, *JHEP* **0904** (2009) 052 [0901.3653].

[117] D. Chicherin, R. Doobary, B. Eden, P. Heslop, G. P. Korchemsky and E. Sokatchev, *Bootstrapping correlation functions in $\mathcal{N} = 4$ SYM*, *JHEP* **03** (2016) 031 [1506.04983].

[118] T. Bargheer, F. Coronado and P. Vieira, *Octagons i: Combinatorics and non-planar resummations*, *JHEP* **08** (2019) 162 [1904.00965].

[119] T. Bargheer, J. Caetano, T. Fleury, S. Komatsu and P. Vieira, *Handling handles: Nonplanar integrability in $\mathcal{N} = 4$ supersymmetric Yang–Mills theory*, *Phys. Rev. Lett.* **121** (2018) 231602 [1711.05326].

[120] A. V. Belitsky, L. V. Bork, R. N. Lee, A. I. Onishchenko and V. A. Smirnov, *Five w-boson amplitude = near-null decagon*, 2510.16471.

[121] L. V. Bork, N. B. Muzhichkov and E. S. Sozinov, *Infrared properties of five-point massive amplitudes in $\mathcal{N} = 4$ SYM on the coulomb branch*, *JHEP* **08** (2022) 173 [2201.08762].

[122] B. Eden and A. Sfondrini, *Tessellating cushions: four-point functions in $\mathcal{N} = 4$ SYM*, *JHEP* **10** (2017) 098 [1611.05436].

[123] B. Basso, V. Gonçalves, S. Komatsu and P. Vieira, *Gluing hexagons at three loops*, *Nucl. Phys.* **B907** (2016) 695 [1510.01683].

[124] B. Basso, A. Sever and P. Vieira, *Spacetime and flux tube S-matrices at finite coupling for $\mathcal{N} = 4$ supersymmetric Yang–Mills theory*, *Phys. Rev. Lett.* **111** (2013) 091602 [1303.1396].

[125] B. Basso, A. Sever and P. Vieira, *Space-time S-matrix and flux tube S-matrix II. extracting and matching data*, *JHEP* **1401** (2014) 008 [1306.2058].

[126] B. Basso, A. Sever and P. Vieira, *Space-time S-matrix and flux-tube S-matrix III. the two-particle contributions*, *JHEP* **1408** (2014) 085 [1402.3307].

[127] B. Basso, A. Sever and P. Vieira, *Space-time S-matrix and flux-tube S-matrix IV. gluons and fusion*, *JHEP* **1409** (2014) 149 [1407.1736].

[128] E. Krasko and A. Omelchenko, *Brown's theorem and its application for enumeration of dissections and planar trees*, *The Electronic Journal of Combinatorics* **22** (2015) 1.17.

[129] C. Vergu, *The two-loop mhv amplitudes in $\mathcal{N} = 4$ supersymmetric Yang–Mills theory*, *Phys. Rev. D* **80** (2009) 125025 [0908.2394].

[130] J. L. Bourjaily, A. DiRe, A. Shaikh, M. Spradlin and A. Volovich, *The Soft-Collinear Bootstrap: N=4 Yang-Mills Amplitudes at Six and Seven Loops*, *JHEP* **03** (2012) 032 [1112.6432].

[131] J. Golden and M. Spradlin, *Collinear and Soft Limits of Multi-Loop Integrands in N=4 Yang-Mills*, *JHEP* **05** (2012) 027 [1203.1915].

[132] G. Brinkmann and B. McKay, *Fast generation of planar graphs*, *Match* **58** (2007) 323.

[133] A. Hodges, *Eliminating spurious poles from gauge-theoretic amplitudes*, *JHEP* **05** (2013) 135 [0905.1473].

[134] J. M. Drummond and J. M. Henn, *Simple loop integrals and amplitudes in N=4 SYM*, *JHEP* **05** (2011) 105 [1008.2965].

[135] G. Brinkmann, *A practical algorithm for the computation of the genus*, *Ars Mathematica Contemporanea* **22** (2022) .

[136] The Sage Developers, *SageMath, the Sage Mathematics Software System (Version 10.7)*, 2025.

[137] S. K. Lam, A. Pitrou and S. Seibert, *Numba: a LLVM-based python JIT compiler*, in *Proceedings of the Second Workshop on the LLVM Compiler Infrastructure in HPC*, LLVM '15, (New York, NY, USA), Association for Computing Machinery, 2015, DOI.

[138] B. Eden, P. Heslop, G. P. Korchemsky, V. A. Smirnov and E. Sokatchev, *Five-loop Konishi in $\mathcal{N} = 4$ SYM*, *Nucl. Phys. B* **862** (2012) 123 [1202.5733].

[139] A. V. Smirnov and F. S. Chukharev, *FIRE6: Feynman Integral REduction with modular arithmetic*, *Comput. Phys. Commun.* **247** (2020) 106877 [1901.07808].

[140] A. V. Smirnov and M. Zeng, *FIRE 6.5: Feynman integral reduction with new simplification library*, *Comput. Phys. Commun.* **302** (2024) 109261 [2311.02370].

[141] P. A. Baikov and K. G. Chetyrkin, *Four loop massless propagators: An algebraic evaluation of all master integrals*, *Nucl. Phys. B* **837** (2010) 186 [1004.1153].

[142] R. N. Lee, A. V. Smirnov and V. A. Smirnov, *Master integrals for four-loop massless propagators up to transcendentality weight twelve*, *Nucl. Phys. B* **856** (2012) 95 [1108.0732].

[143] E. Panzer, *Algorithms for the symbolic integration of hyperlogarithms with applications to Feynman integrals*, Comput. Phys. Commun. **188** (2015) 148 [1403.3385].

[144] A. V. Smirnov, N. D. Shapurov and L. I. Vysotsky, *FIESTA5: Numerical high-performance Feynman integral evaluation*, Comput. Phys. Commun. **277** (2022) 108386 [2110.11660].

[145] D. J. Broadhurst and D. Kreimer, *Knots and numbers in phi**4 theory to 7 loops and beyond*, Int. J. Mod. Phys. C **6** (1995) 519 [hep-ph/9504352].

[146] F. Brown and O. Schnetz, *Proof of the zig-zag conjecture*, 1208.1890.

[147] S. Leurent and D. Volin, *Multiple zeta functions and double wrapping in planar $\mathcal{N} = 4$ SYM*, Nucl. Phys. B **875** (2013) 757 [1302.1135].

[148] V. N. Velizhanin, *The non-planar contribution to the four-loop universal anomalous dimension in $\mathcal{N} = 4$ supersymmetric Yang–Mills theory*, JETP Lett. **89** (2009) 593 [0902.4646].

[149] D. Anselmi, M. T. Grisaru and A. Johansen, *A critical behavior of anomalous currents, electric - magnetic universality and CFT in four-dimensions*, Nucl. Phys. B **491** (1997) 221 [hep-th/9601023].

[150] B. Eden, C. Schubert and E. Sokatchev, *Three loop four point correlator in $\mathcal{N} = 4$ SYM*, Phys. Lett. B **482** (2000) 309 [hep-th/0003096].

[151] M. Bianchi, S. Kovacs, G. Rossi and Y. S. Stanev, *Anomalous dimensions in $\mathcal{N} = 4$ SYM theory at order g**4*, Nucl. Phys. B **584** (2000) 216 [hep-th/0003203].

[152] A. V. Kotikov, L. N. Lipatov, A. I. Onishchenko and V. N. Velizhanin, *Three-loop universal anomalous dimension of the Wilson operators in $\mathcal{N} = 4$ SUSY Yang–Mills model*, Phys. Lett. **B595** (2004) 521 [hep-th/0404092].

[153] F. Fiamberti, A. Santambrogio, C. Sieg and D. Zanon, *Anomalous dimension with wrapping at four loops in $\mathcal{N} = 4$ SYM*, Nucl. Phys. **B805** (2008) 231 [0806.2095].

[154] V. N. Velizhanin, *The four-loop anomalous dimension of the Konishi operator in $\mathcal{N} = 4$ supersymmetric Yang–Mills theory*, JETP Lett. **89** (2009) 6 [0808.3832].

[155] Z. Bajnok and R. A. Janik, *Four-loop perturbative konishi from strings and finite size effects for multiparticle states*, Nucl. Phys. **B807** (2009) 625 [0807.0399].

[156] Z. Bajnok, A. Hegedus, R. A. Janik and T. Lukowski, *Five loop Konishi from AdS/CFT*, Nucl. Phys. B **827** (2010) 426 [0906.4062].

[157] G. Arutyunov, S. Frolov and R. Suzuki, *Five-loop konishi from the mirror TBA*, JHEP **04** (2010) 069 [1002.1711].

[158] J. Balog and A. Hegedus, *5-loop Konishi from linearized TBA and the xxx magnet*, JHEP **06** (2010) 080 [1002.4142].

[159] N. Beisert, B. Eden and M. Staudacher, *Transcendentality and crossing*, J. Stat. Mech. **07** (2007) P01021 [hep-th/0610251].

[160] C.-K. Kuo and Q. Yang, *Notes on off-shell conformal integrals and correlation functions at five points*, 2512.21947.

[161] P. Heslop, *The SAGEX review on scattering amplitudes, chapter 8: Half BPS correlators*, 2203.13019.

[162] H. Chen, I. Moult, J. Sandor and H. X. Zhu, *Celestial blocks and transverse spin in the three-point energy correlator*, JHEP **09** (2022) 199 [2202.04085].

[163] C.-H. Chang and D. Simmons-Duffin, *Three-point energy correlators and the celestial block expansion*, JHEP **02** (2023) 126 [2202.04090].

[164] D. Chicherin, G. P. Korchemsky, E. Sokatchev and A. Zhiboedov, *Energy correlations in heavy states*, JHEP **11** (2023) 134 [2306.14330].

[165] S. Caron-Huot, *Superconformal symmetry and two-loop amplitudes in planar $\mathcal{N} = 4$ super Yang–Mills*, JHEP **1112** (2011) 066 [1105.5606].

[166] N. Arkani-Hamed and J. Trnka, *The amplituhedron*, JHEP **1410** (2014) 30 [1312.2007].

[167] A. V. Belitsky, *Towards six W-boson amplitude at two loops*, 2511.20828.

[168] S.-Q. Zhang, *Nonplanar integrated correlator in $\mathcal{N} = 4$ SYM*, Phys. Rev. D **110** (2024) 025003 [2404.18900].

[169] D. Dorigoni, M. B. Green and C. Wen, *Novel representation of an integrated correlator in $\mathcal{N} = 4$ supersymmetric Yang–Mills theory*, Phys. Rev. Lett. **126** (2021) 161601 [2102.08305].

[170] D. Dorigoni, M. B. Green and C. Wen, *Exact properties of an integrated correlator in $\mathcal{N} = 4$ su(n) SYM*, JHEP **05** (2021) 089 [2102.09537].

[171] A. Georgoudis, V. Gonçalves and R. Pereira, *Konishi ope coefficient at the five loop order*, JHEP **11** (2018) 184 [1710.06419].

[172] J. M. Henn, G. P. Korchemsky and B. Mistlberger, *The full four-loop cusp anomalous dimension in $\mathcal{N} = 4$ super Yang–Mills and QCD*, JHEP **04** (2020) 018 [1911.10174].

Acknowledgments

First of all, I would like to thank my supervisor, Till Bargheer, for his guidance and support throughout my whole PhD journey. I particularly appreciate his availability and openness to discussion, which made it easy to seek advice whenever needed, as well as his deep intuition for physics and his ability to explain even the most complex concepts, which greatly shaped my understanding of the subject. His kind and thoughtful feedback, both on technical aspects and on the broader direction of the work, was essential in shaping this thesis. I especially want to thank him for all the times that he let me complain about bugs in my code and his excitement when I finally found them after a few weeks.

I would also like to thank my coauthors, Carlos Bercini and Frank Coronado, for the collaboration on our joint work and for the insightful discussions that led to the publications.

Finally, I am grateful to the whole research group at DESY for providing a supportive environment throughout the last years.

Eidesstattliche Versicherung

Hiermit versichere ich an Eides statt, die vorliegende Dissertationsschrift selbst verfasst und keine anderen als die angegebenen Hilfsmittel und Quellen benutzt zu haben.

Sofern im Zuge der Erstellung der vorliegenden Dissertationsschrift generative Künstliche Intelligenz (gKI) basierte elektronische Hilfsmittel verwendet wurden, versichere ich, dass meine eigene Leistung im Vordergrund stand und dass eine vollständige Dokumentation aller verwendeten Hilfsmittel gemäß der Guten wissenschaftlichen Praxis vorliegt. Ich trage die Verantwortung für eventuell durch die gKI generierte fehlerhafte oder verzerrte Inhalte, fehlerhafte Referenzen, Verstöße gegen das Datenschutz- und Urheberrecht oder Plagiate.

Hamburg, den 19. April 2026